Acoustic reciprocity and Green's theorem in imaging across the scales

Kees Wapenaar

With many contributions from
Joeri Brackenhoff, Jan Thorbecke,
Joost van der Neut, Evert Slob, Deyan Draganov,
Elmer Ruigrok, Myrna Staring, Giovanni Meles,
Christian Reinicke, Lele Zhang, Huub Douma,
Johno van IJsseldijk, Aydin Shoja…..

Cargèse International School 2019
Imaging in Wave Physics
Multi-Wave and Large Sensor Networks

Course material:

Solid Earth, 10, 517–536, 2019
https://doi.org/10.5194/se-10-517-2019

Solid Earth | Open Access | EGU

Green's theorem in seismic imaging across the scales

Kees Wapenaar, Joeri Brackenhoff, and Jan Thorbecke

Department of Geoscience and Engineering, Delft University of Technology, Stevinweg 1, 2628 CN Delft, the Netherlands

plus on-line material connected to this paper

Acoustic reciprocity

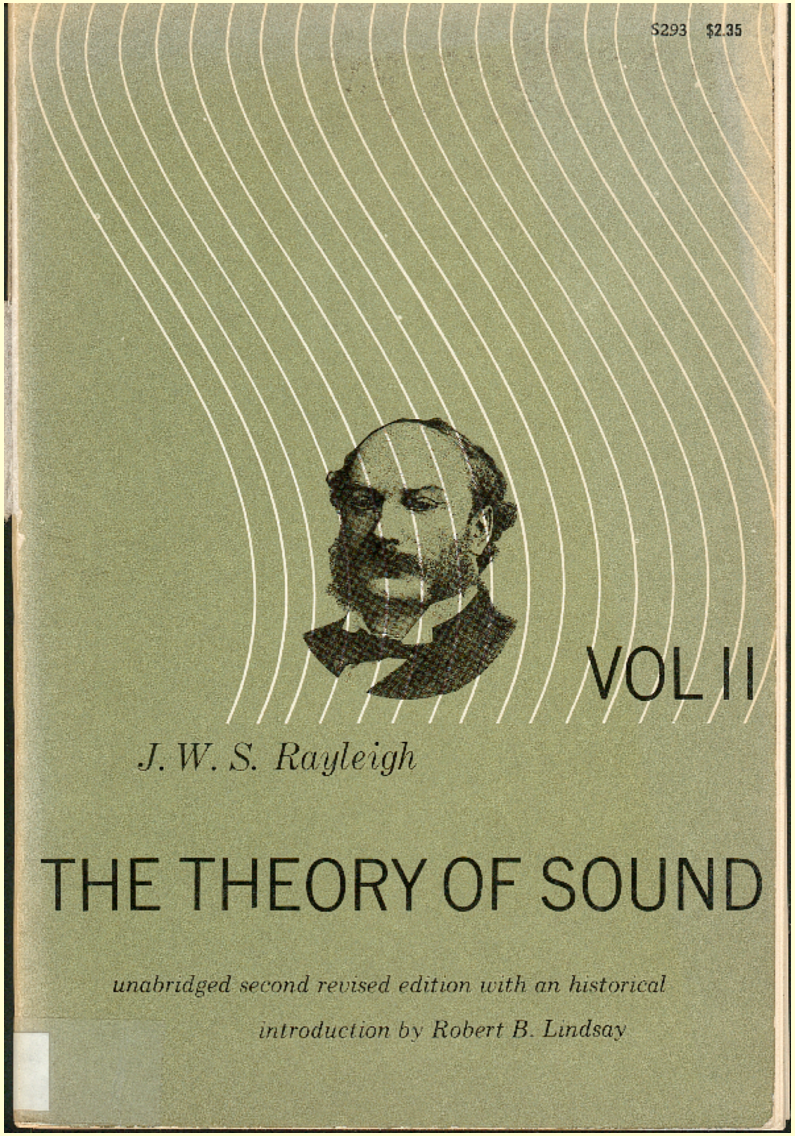

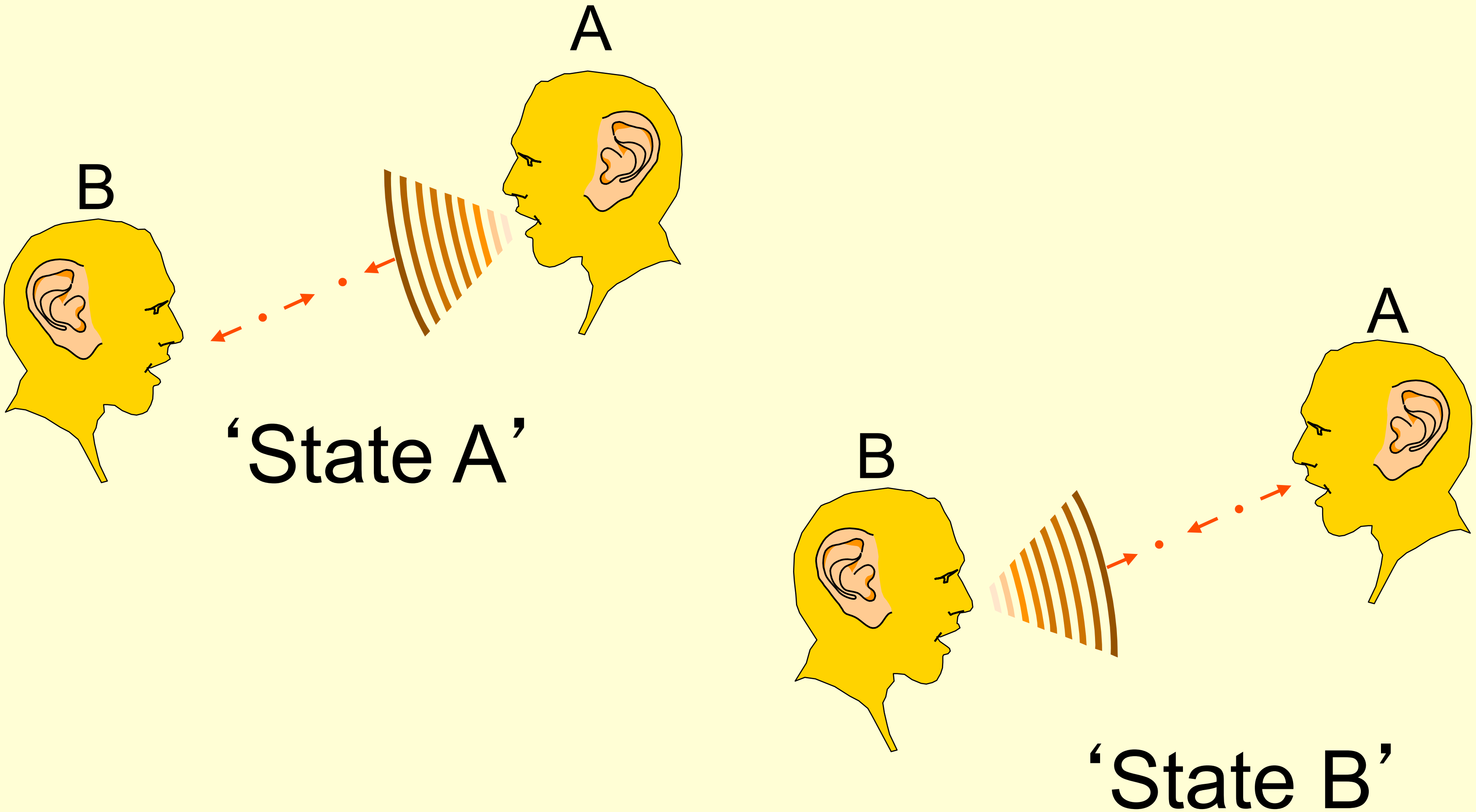

$$p_A(\mathbf{x}_B, t) = p_B(\mathbf{x}_A, t)$$

Reciprocity interrelates states A and B

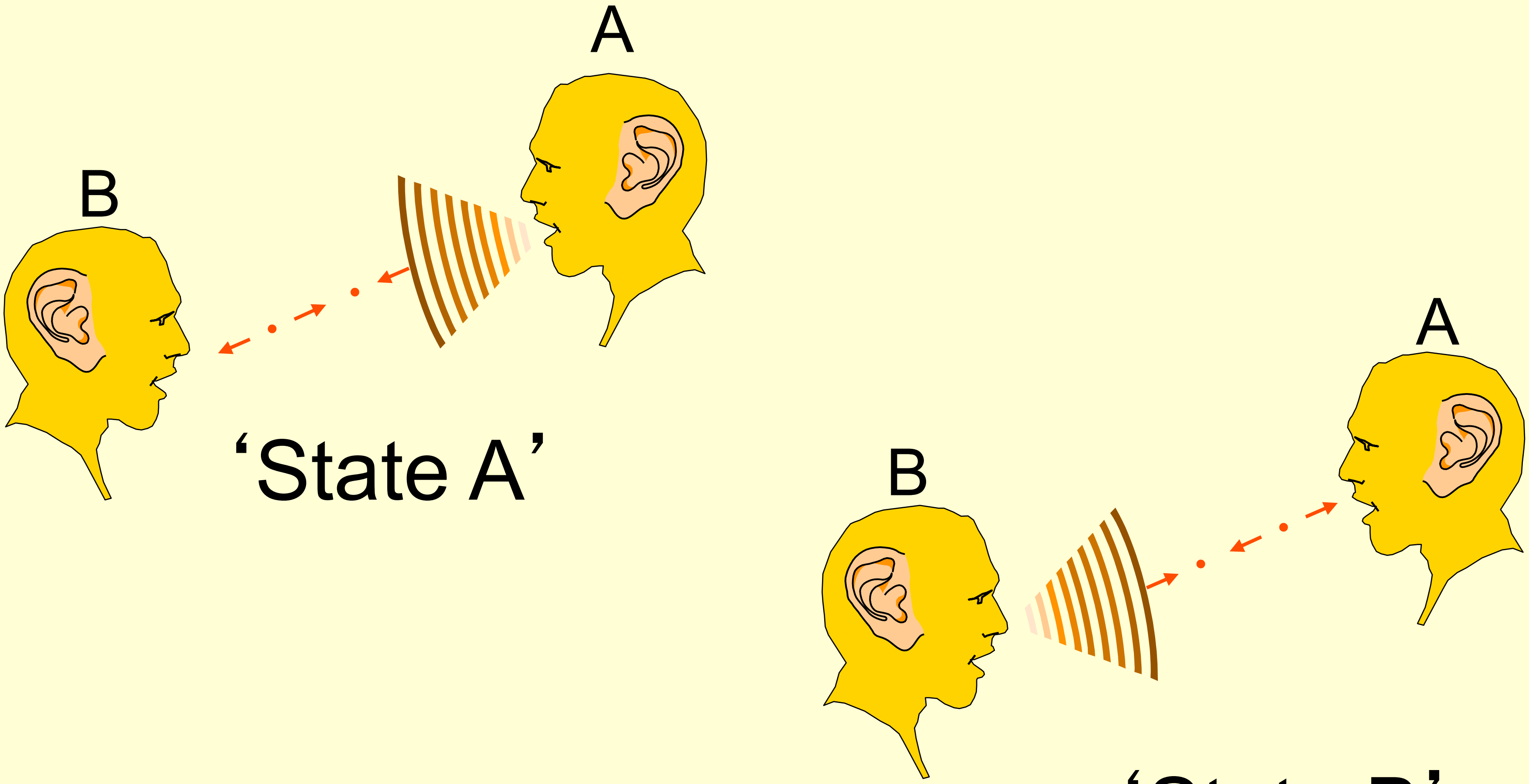

$$P_A(\mathbf{x}_B,\omega) = P_B(\mathbf{x}_A,\omega)$$

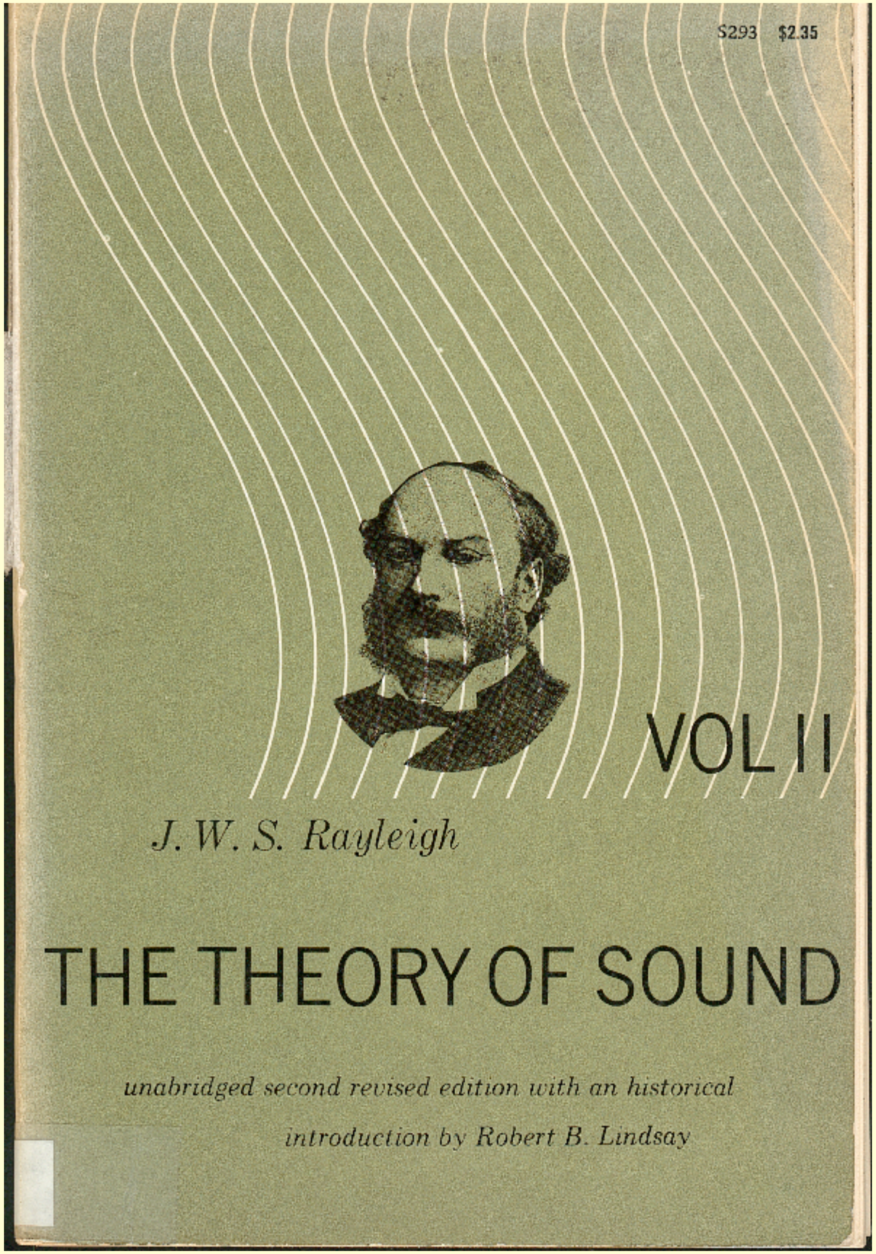

If the dimensions of the space S be very small in comparison with $\lambda (= 2\pi/k)$, e^{-ikr} may be replaced by unity; and we learn that ψ differs but little from a function which satisfies throughout S the equation $\nabla^2\phi = 0$.

294. On his extension of Green's theorem (1) Helmholtz founds his proof of the important theorem contained in the following statement: *If in a space filled with air which is partly bounded by finitely extended fixed bodies and is partly unbounded, sound waves be excited at any point A, the resulting velocity-potential at a second point B is the same both in magnitude and phase, as it would have been at A, had B been the source of the sound.*

If the equation

$$a^2 \iint \left(\phi \frac{d\psi}{dn} - \psi \frac{d\phi}{dn}\right) dS = \iiint (\psi\Phi - \phi\Psi)\, dV \ldots\ldots(1),$$

in which ϕ and ψ are arbitrary functions, and

$$\Phi = -a^2(\nabla^2\phi + k^2\phi), \qquad \Psi = -a^2(\nabla^2\psi + k^2\psi),$$

be applied to a space completely enclosed by a rigid boundary and containing any number of detached rigid fixed bodies, and if ϕ, ψ be velocity-potentials due to sources within S, we get

$$\iiint (\psi\Phi - \phi\Psi)\, dV = 0 \ldots\ldots\ldots\ldots\ldots(2).$$

Thus, if ϕ be due to a source concentrated in one point A, $\Phi = 0$ except at that point, and

$$\iiint \psi\Phi\, dV = \psi_A \iiint \Phi\, dV,$$

where $\iiint \Phi\, dV$ represents the intensity of the source. Similarly, if ψ be due to a source situated at B,

$$\iiint \phi\Psi\, dV = \phi_B \iiint \Psi\, dV.$$

Accordingly, if the sources be finite and equal, so that

$$\iiint \Phi\, dV = \iiint \Psi\, dV \ldots\ldots\ldots\ldots\ldots(3),$$

it follows that

$$\psi_A = \phi_B \ldots\ldots\ldots\ldots\ldots\ldots\ldots(4),$$

which is the symbolical statement of Helmholtz's theorem.

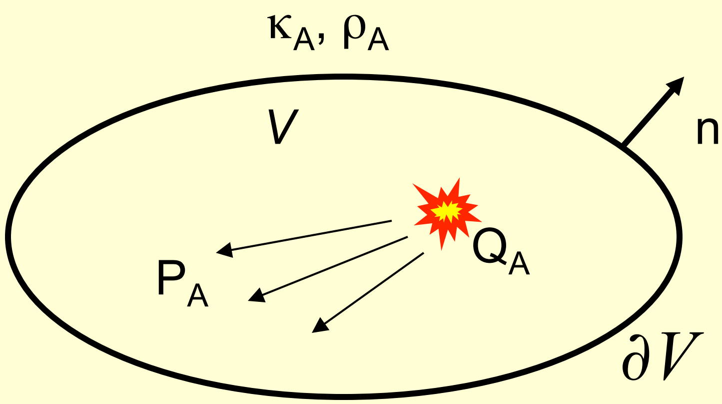

'State A'

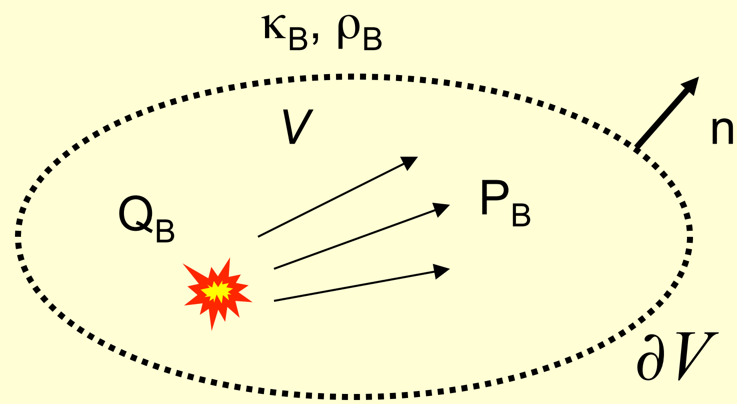

'State B'

	State A	State B
Wave fields	P_A, $V_{k,A}$	P_B, $V_{k,B}$
Sources	Q_A,$F_{k,A}$	Q_B,$F_{k,B}$
Medium	κ_A, ρ_A	κ_B, ρ_B

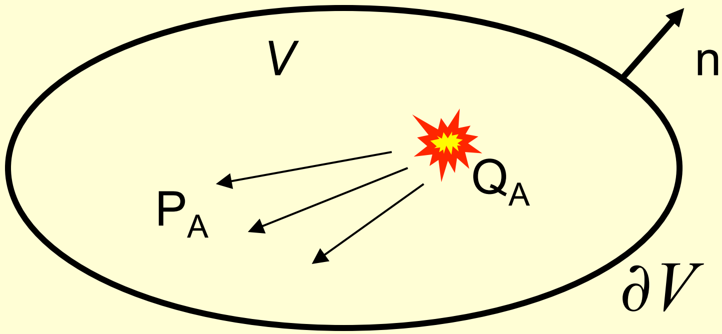

‘State A’

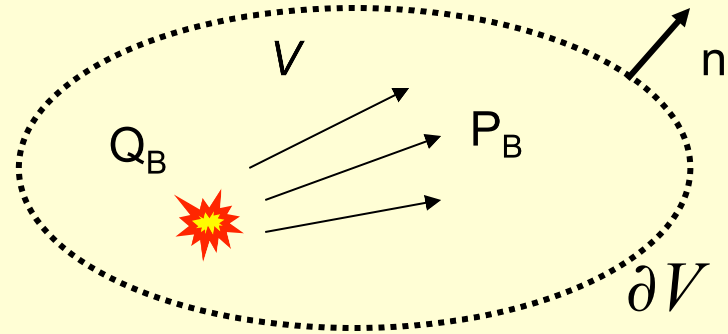

‘State B’

$$\int_{\partial V} \{P_A V_{k,B} - V_{k,A} P_B\} n_k \mathrm{d}^2\mathbf{x} = -j\omega \int_V \{P_A P_B \Delta\kappa - V_{k,A} V_{k,B} \Delta\rho\} \mathrm{d}^3\mathbf{x}$$

$$+ \int_V \{P_A Q_B - V_{k,A} F_{k,B} + F_{k,A} V_{k,B} - Q_A P_B\} \mathrm{d}^3\mathbf{x}$$

Note: The medium is arbitrarily inhomogeneous

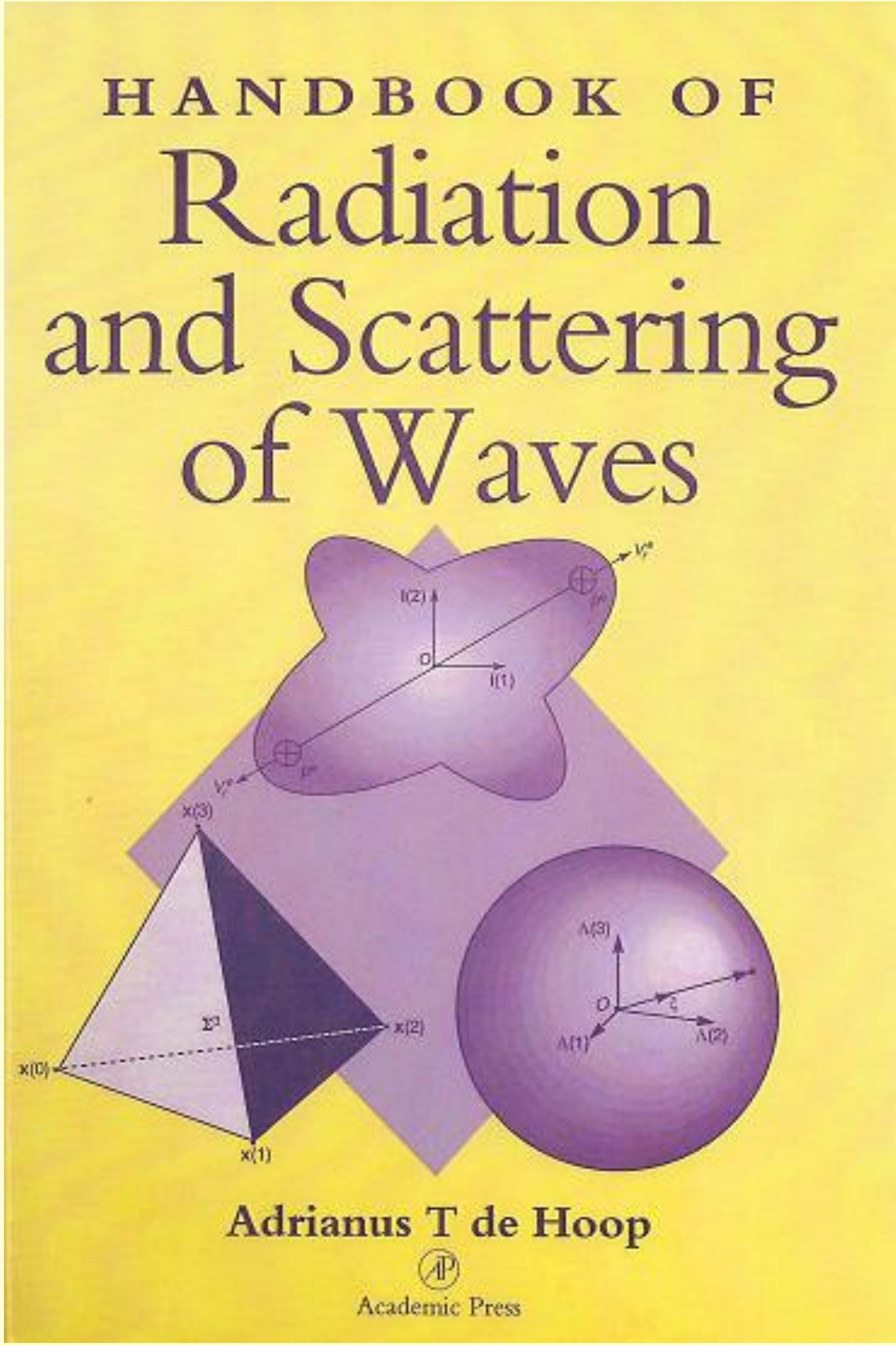

From the pertaining acoustic wave equations, first the *local form* of a reciprocity theorem will be derived, which form applies to each point of any subdomain of $\mathcal{D}$ where the acoustic wave-field quantities are continuously differentiable. By integrating the local form over such subdomains and adding the results, the *global form* of the reciprocity theorem is arrived at. In it, a boundary integral over $\partial\mathcal{D}$ occurs, the integrand of which always contains the unit vector ν_m along the normal to $\partial\mathcal{D}$, oriented away from $\mathcal{D}$ (Figure 7.1-1).

The two states will be denoted by the superscripts A and B. The construction of the time-domain reciprocity theorems will be based on the acoustic wave equations (see Equations (2.7-22), (2.7-23), (2.7-26) and (2.7-27))

$$\partial_k p^{A} + \partial_t C_t(\mu^{A}_{k,r}, v^{A}_r; \boldsymbol{x}, t) = f^{A}_k , \qquad (7.1\text{-}1)$$

$$\partial_r v^{A}_r + \partial_t C_t(\chi^{A}, p^{A}; \boldsymbol{x}, t) = q^{A} , \qquad (7.1\text{-}2)$$

for state A, and

$$\partial_k p^{B} + \partial_t C_t(\mu^{B}_{k,r}, v^{B}_r; \boldsymbol{x}, t) = f^{B}_k , \qquad (7.1\text{-}3)$$

$$\partial_r v^{B}_r + \partial_t C_t(\chi^{B}, p^{B}; \boldsymbol{x}, t) = q^{B} , \qquad (7.1\text{-}4)$$

for state B, where C_t denotes the time convolution operator (see Equation (B.1-11)) (Figure 7.1-2).

If, in $\mathcal{D}$, either surfaces of discontinuity in acoustic properties or acoustically impenetrable objects are present, Equations (7.1-1)–(7.1-4) are supplemented by boundary conditions of the type discussed in Section 2.6, both for state A and for state B. These are either (see Equations (2.6-2) and (2.6-3))

$$p^{A,B} \quad \text{is continuous across any interface ,} \qquad (7.1\text{-}5)$$

and

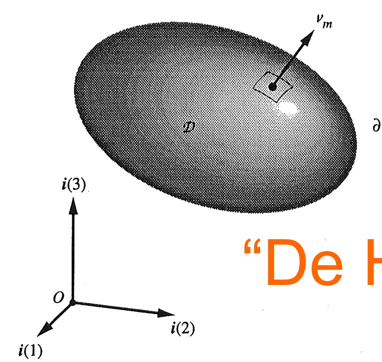

“De Hoop egg”

7.1-1 Bounded domain $\mathcal{D}$ with boundary surface $\partial\mathcal{D}$ and unit vector ν_m along the normal to $\partial\mathcal{D}$, pointing away from $\mathcal{D}$, to which the reciprocity theorems apply.

1958-1995

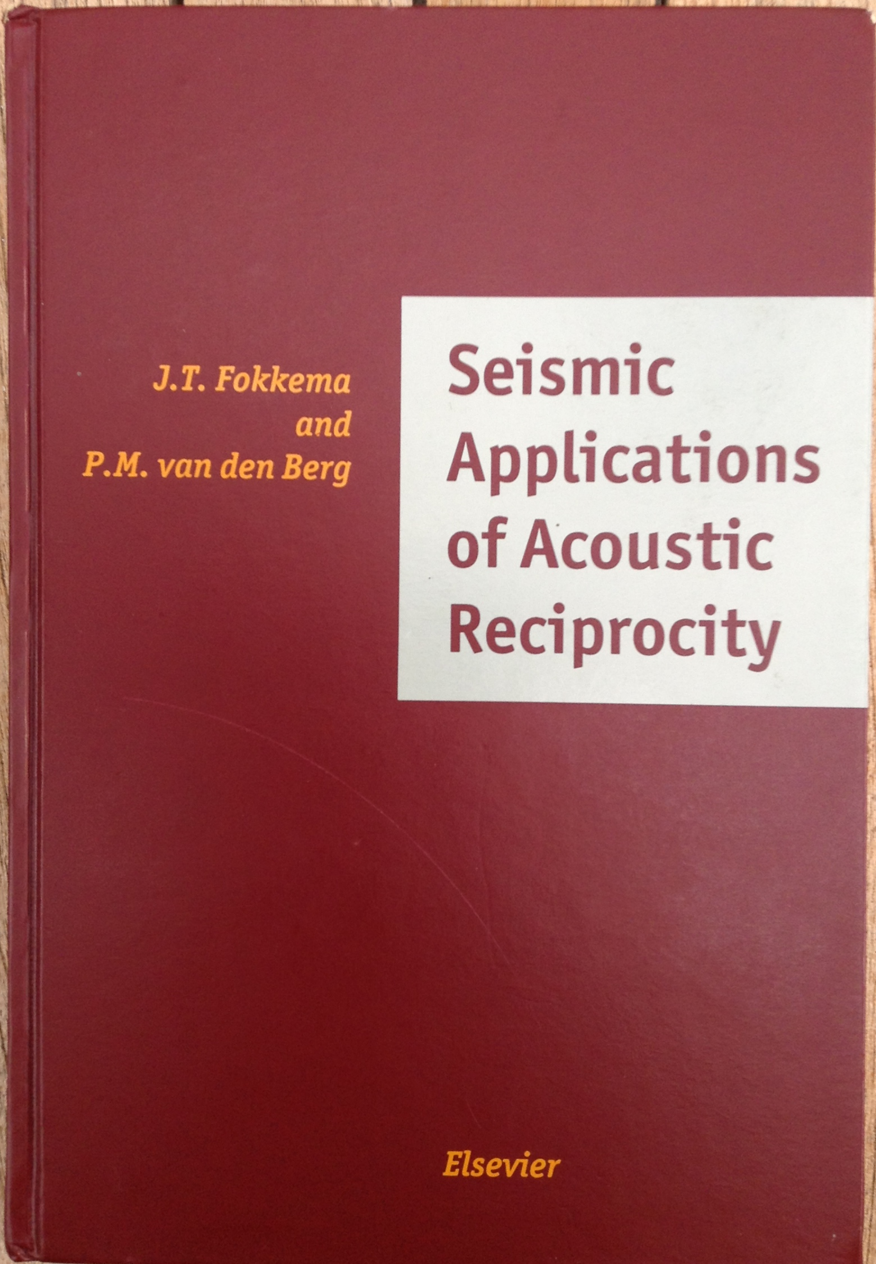

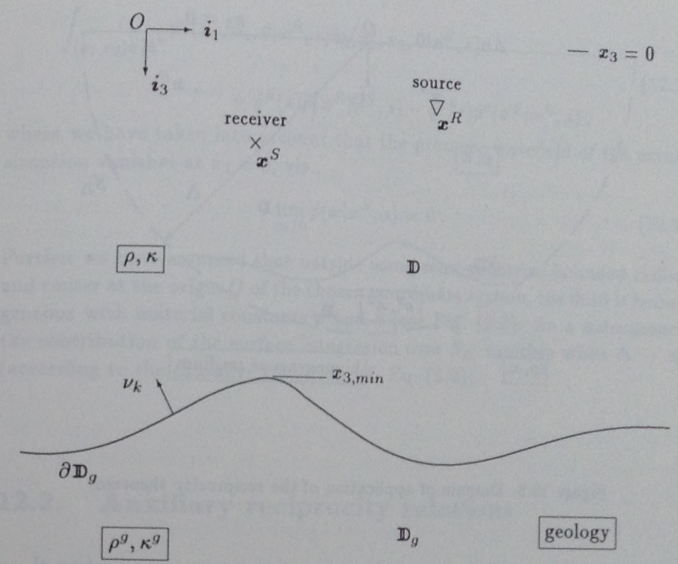

Figure 12.2. State B in the desired configuration.

case $x_3 = 0$ is just an artificial boundary Further, in State B we choose a point source with the spectrum $\hat{q}^S(s)$ identical to the one of the real situation, however the source is now located at the receiver location $x^R \in \mathbb{D}$. Let this wavefield be denoted as $\{\hat{p}^B, \hat{v}_k^B\} = \{\hat{p}^d, \hat{v}_k^d\}(x|x^R, s)$ with sources $\{\hat{q}^B, \hat{f}_k^B\}$ $= \{\hat{q}^S(s)\delta(x - x^R), 0\}$ (see Table 12.1).

With the above mentioned states, we apply the reciprocity theorem to the domain $\mathbb{D} \cup \mathbb{D}_g$ enclosed by a semi-infinite sphere S_Δ of radius Δ and center O of the chosen coordinate system (see Fig. 12.3). Taking the limit $\Delta \to \infty$ we arrive at

1993

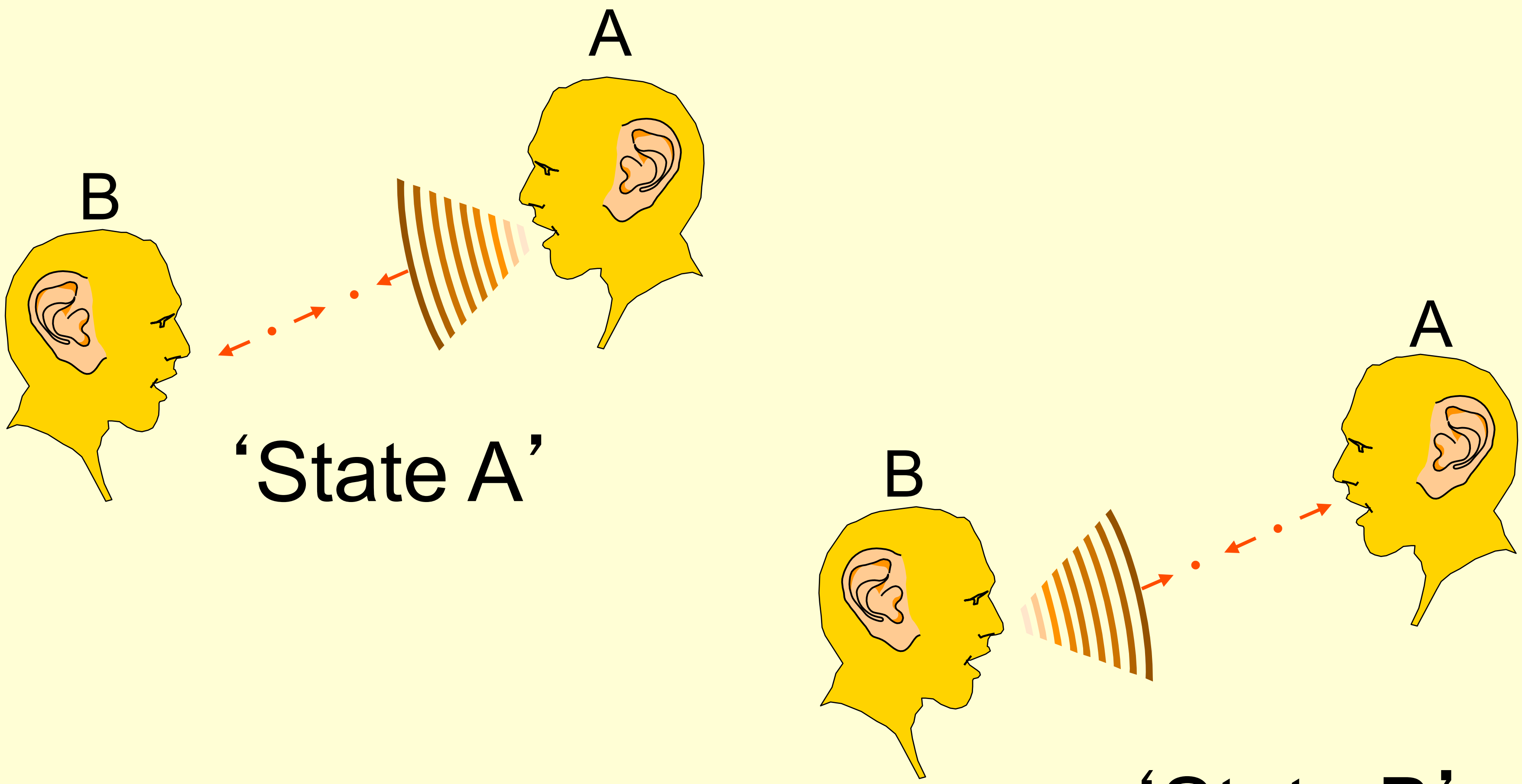
A
B
'State A'
A
B
'State B'

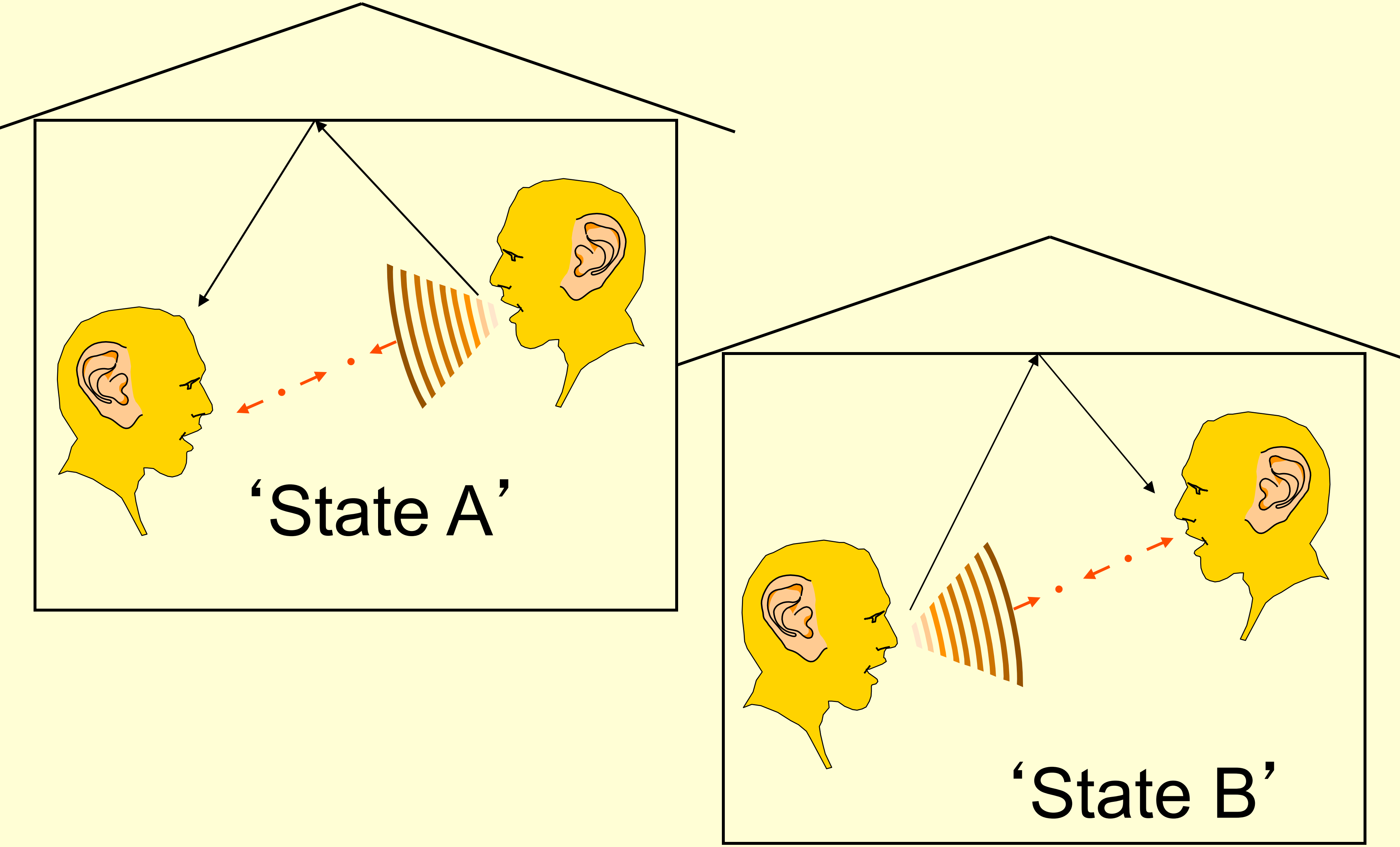

$$P_A(\mathbf{x}_B, \omega) = P_B(\mathbf{x}_A, \omega)$$

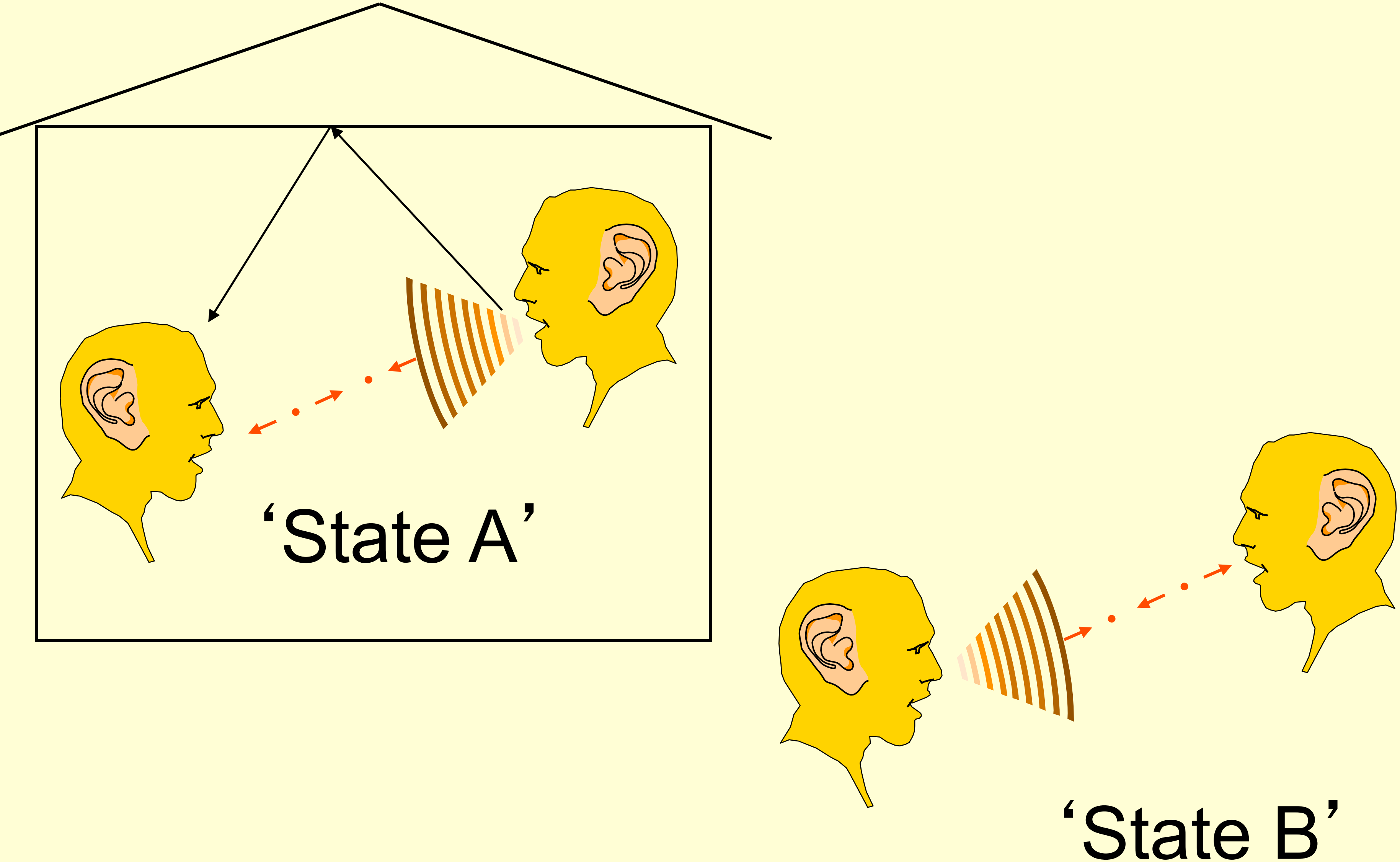

$$P_A(\mathbf{x}_B,\omega) \neq P_B(\mathbf{x}_A,\omega)$$

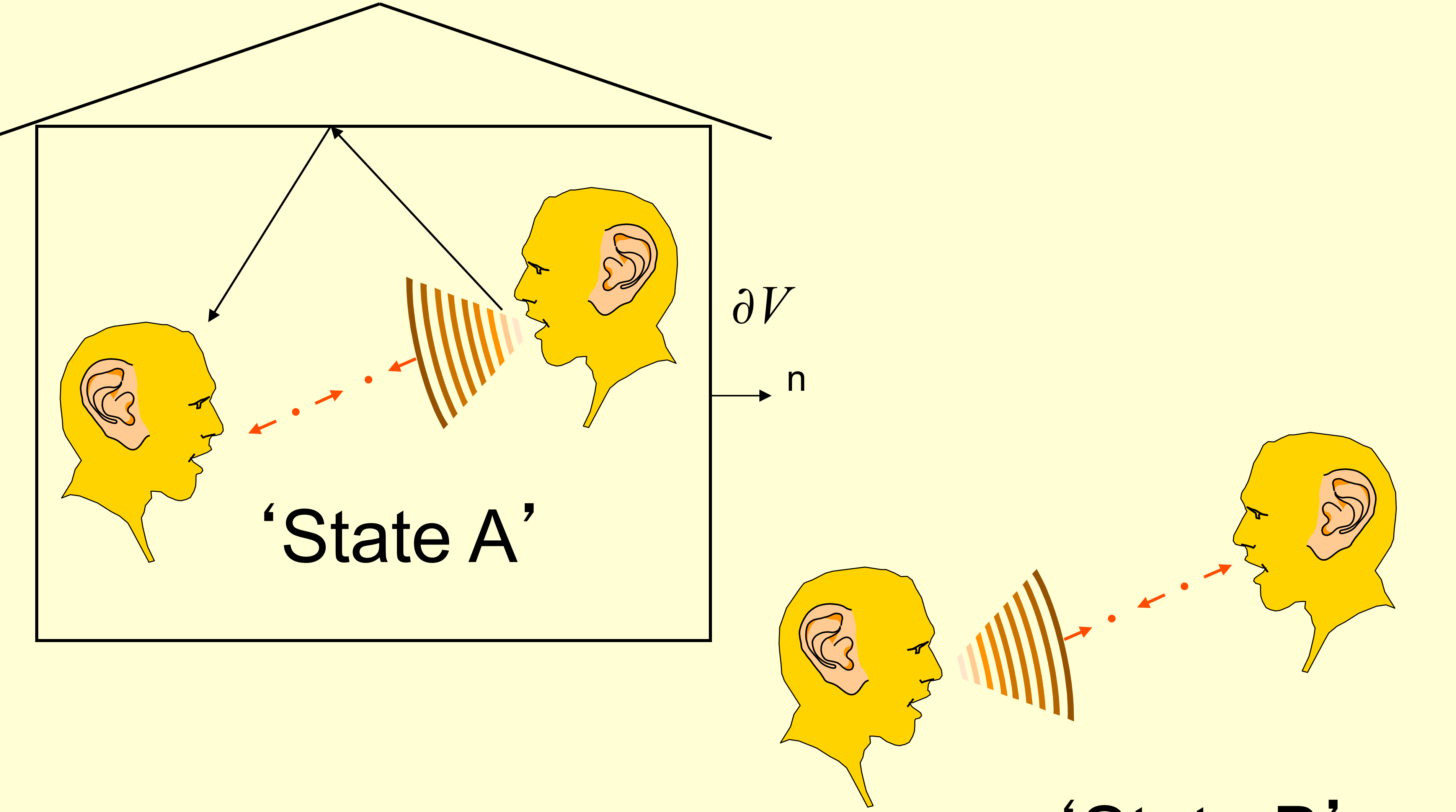

$$P_A(\mathbf{x}_B,\omega) = P_B(\mathbf{x}_A,\omega) + \int_{\partial V}\{P_A V_{k,B} - V_{k,A} P_B\} n_k \mathrm{d}^2\mathbf{x}$$

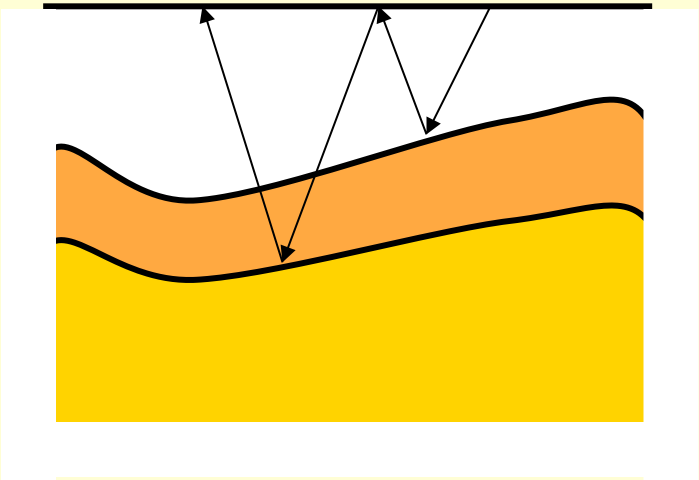

'State A'

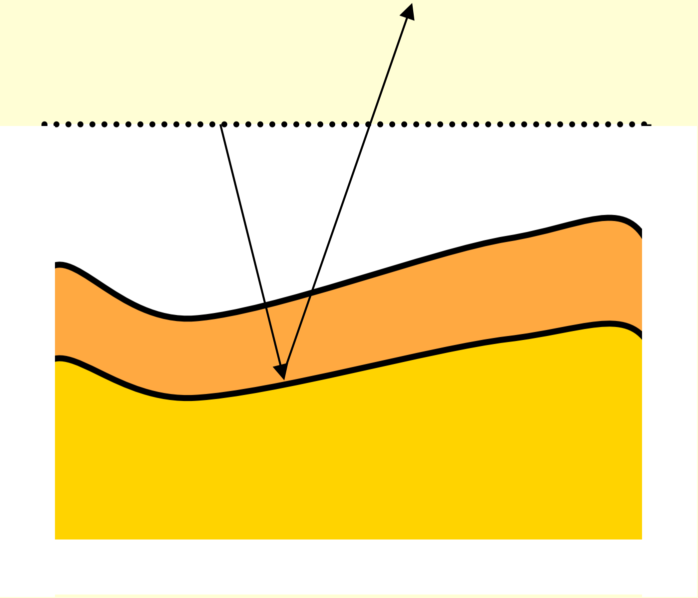

'State B'

$$P_A(\mathbf{x}_B,\omega) = P_B(\mathbf{x}_A,\omega) + \int_{\partial V} \{P_A V_{k,B} - V_{k,A} P_B\} n_k \mathrm{d}^2\mathbf{x}$$

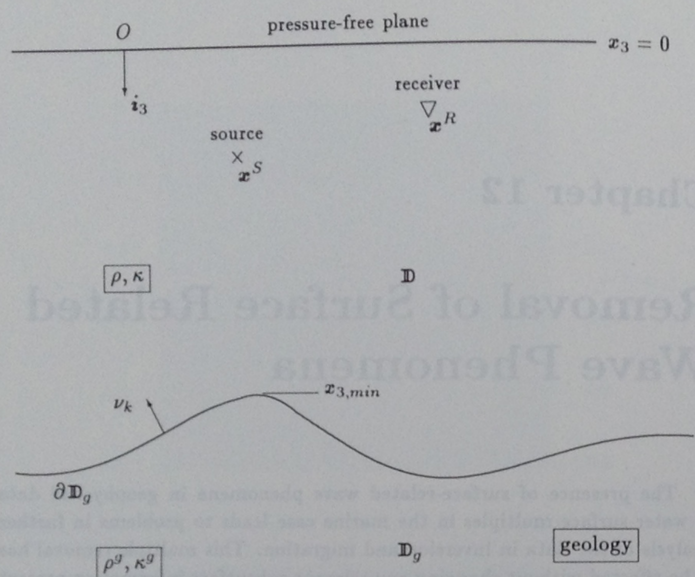

Figure 12.1. State A in the actual configuration.

water surface $x_3 = 0$ is zero. The material constants in $\mathbb{D}$ are ρ and κ, and the material constants in $\mathbb{D}_g$ are ρ^g and κ^g. A monopole source of the volume injection type is used and is located at $\boldsymbol{x}^S$. The seismic response, the acoustic pressure, is measured at $\boldsymbol{x}^R$ below the water surface. In order to remove the effect of the water surface, we apply the reciprocity theorem of Section 5.1 to the domain $\mathbb{D} \cup \mathbb{D}_g$. State A is the actual state resulting from the real seismic experiment (see Fig. 12.1). Let this wavefield be denoted as $\{\hat{p}^A, \hat{v}_k^A\} = \{\hat{p}, \hat{v}_k\}(\boldsymbol{x}|\boldsymbol{x}^S, s)$ with sources $\{\hat{q}^A, \hat{f}_k^A\} = \{\hat{q}^S(s)\delta(\boldsymbol{x}-\boldsymbol{x}^S), 0\}$, where $\hat{q}^S(s)$ is the spectrum of the volume injection source. In State B, the desired state, the water layer extends to $x_3 \to -\infty$ (see Fig. 12.2). In this

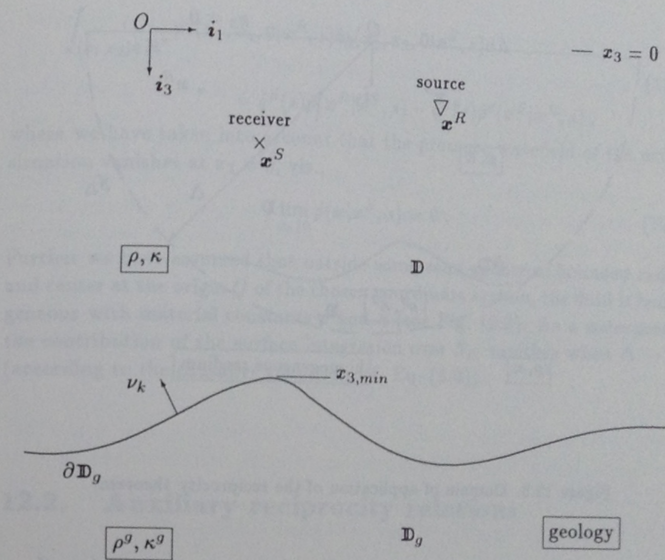

Figure 12.2. State B in the desired configuration.

case $x_3 = 0$ is just an artificial boundary Further, in State B we choose a point source with the spectrum $\hat{q}^S(s)$ identical to the one of the real situation, however the source is now located at the receiver location $\boldsymbol{x}^R \in \mathbb{D}$. Let this wavefield be denoted as $\{\hat{p}^B, \hat{v}_k^B\} = \{\hat{p}^d, \hat{v}_k^d\}(\boldsymbol{x}|\boldsymbol{x}^R, s)$ with sources $\{\hat{q}^B, \hat{f}_k^B\}$ $= \{\hat{q}^S(s)\delta(\boldsymbol{x}-\boldsymbol{x}^R), 0\}$ (see Table 12.1).

With the above mentioned states, we apply the reciprocity theorem to the domain $\mathbb{D} \cup \mathbb{D}_g$ enclosed by a semi-infinite sphere S_Δ of radius Δ and center O of the chosen coordinate system (see Fig. 12.3). Taking the limit $\Delta \to \infty$ we arrive at

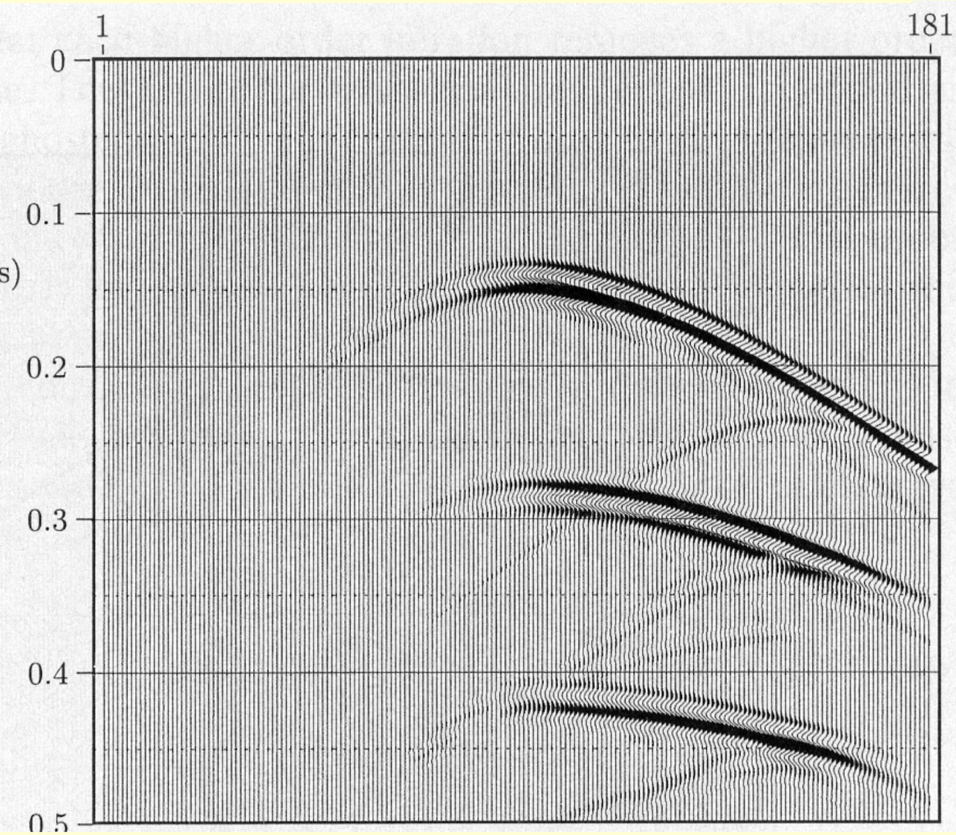

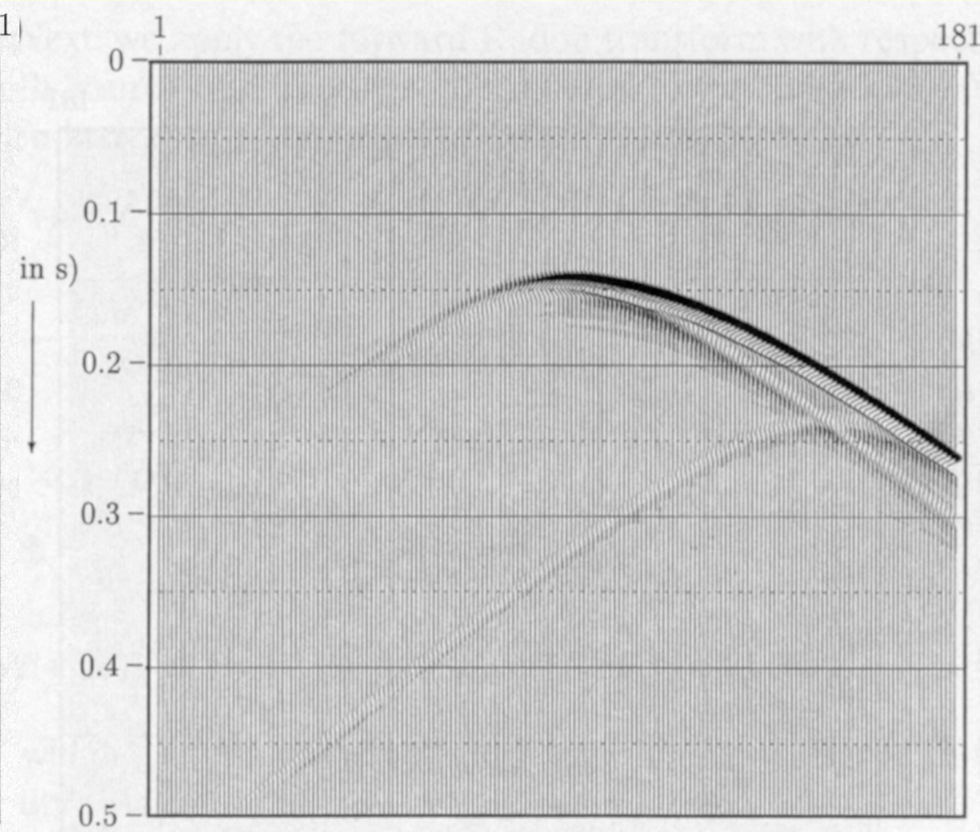

‘State A’ ‘State B’

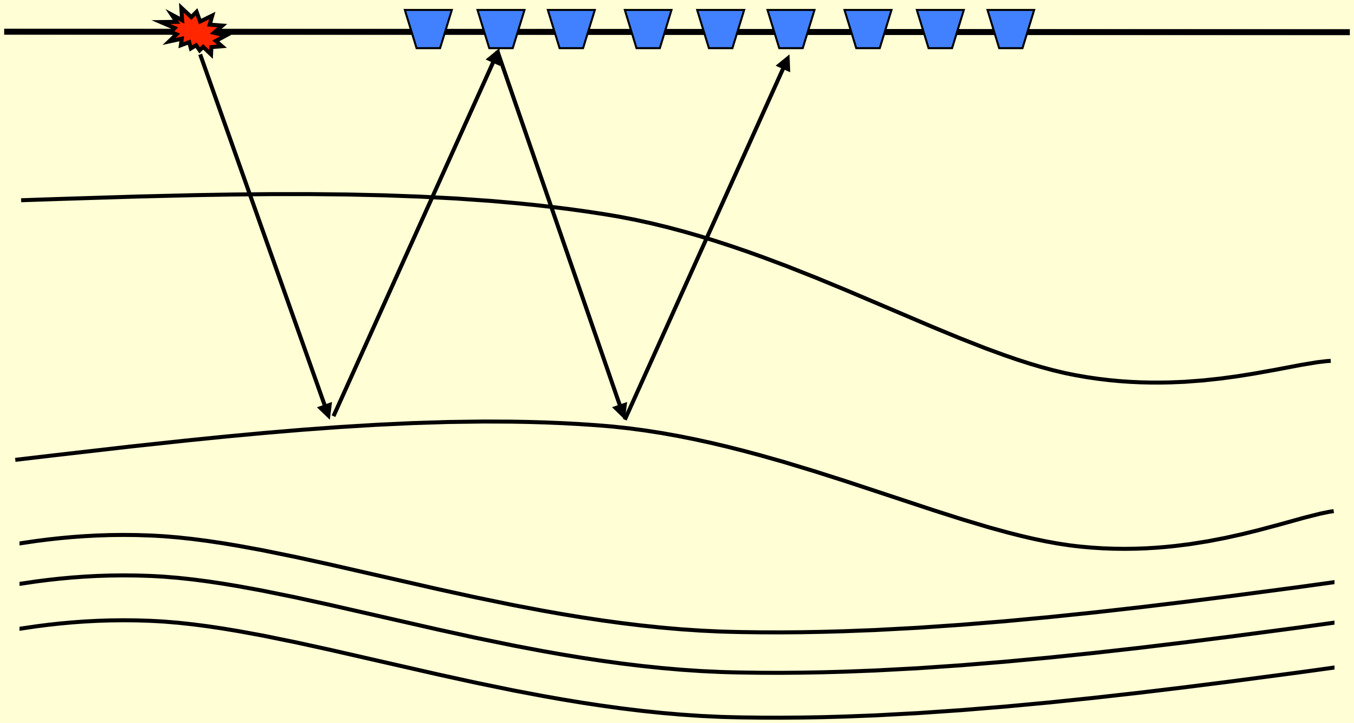

Surface-related multiples

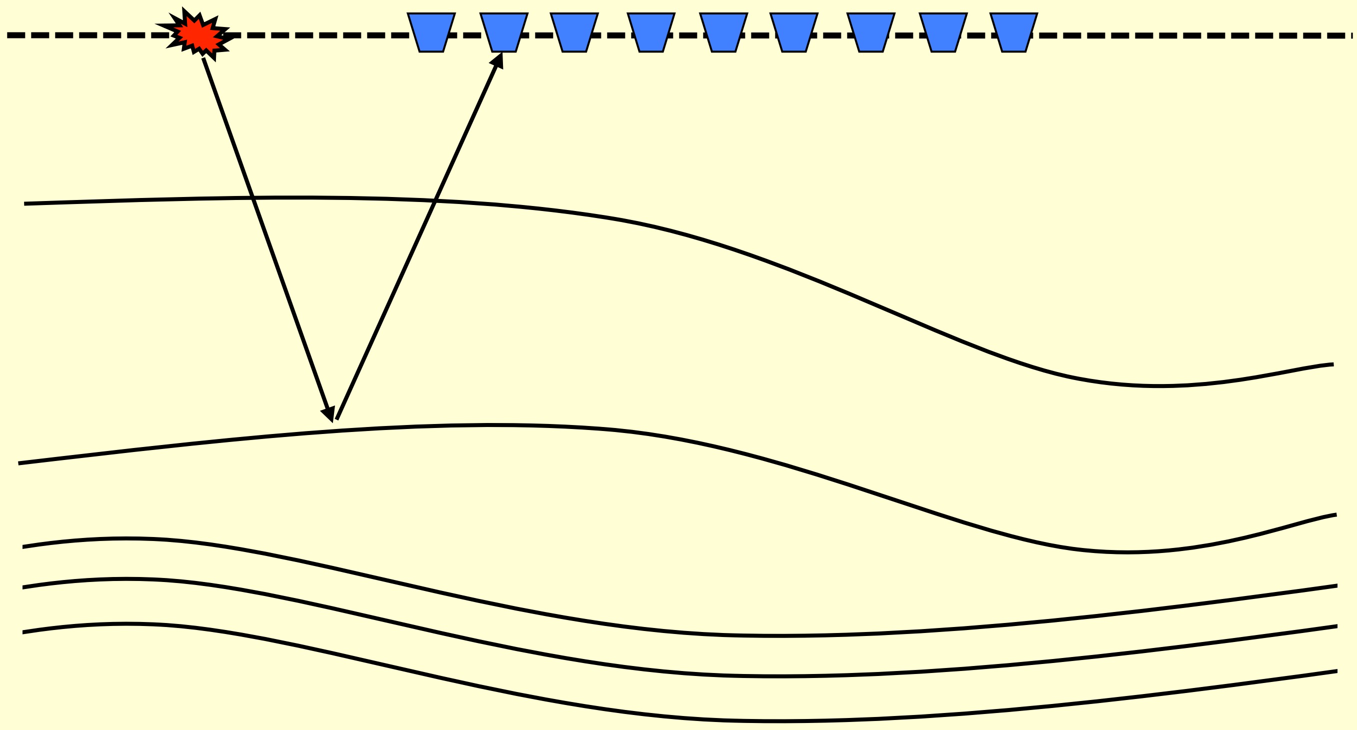

Surface-related multiples

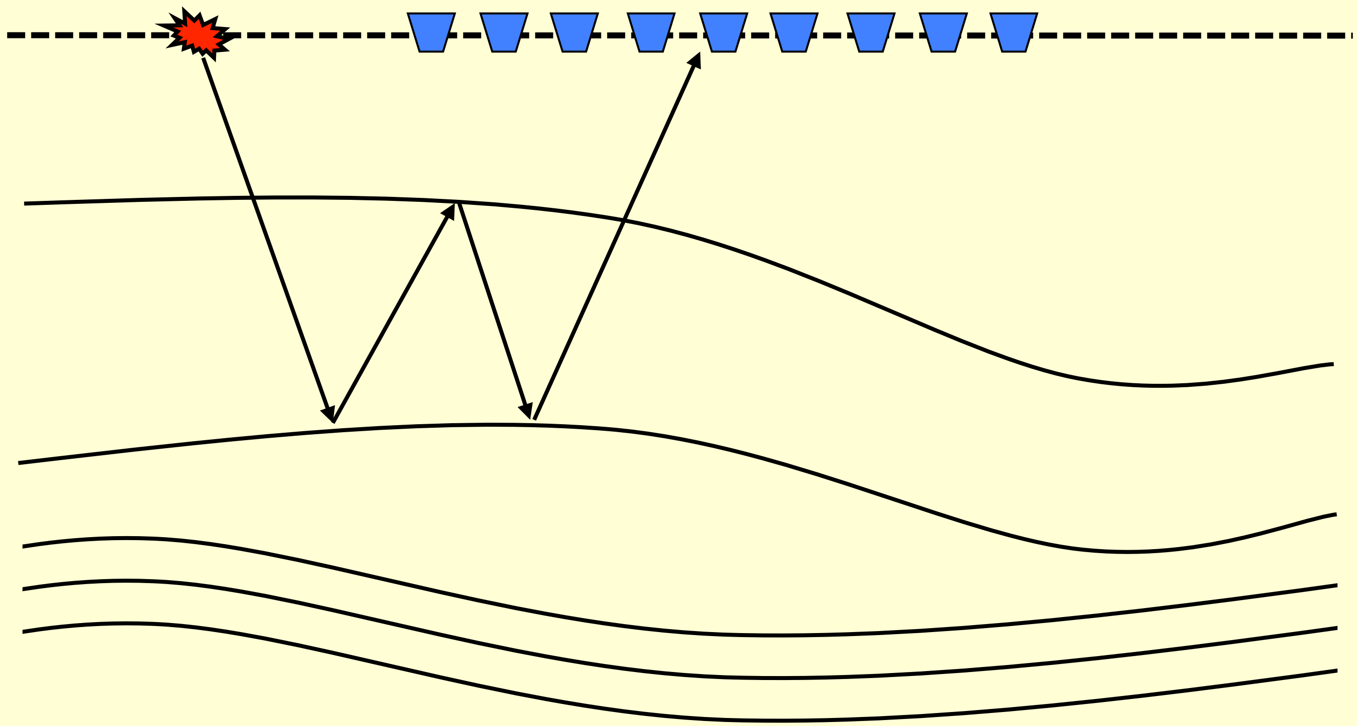

Internal multiples: much more difficult

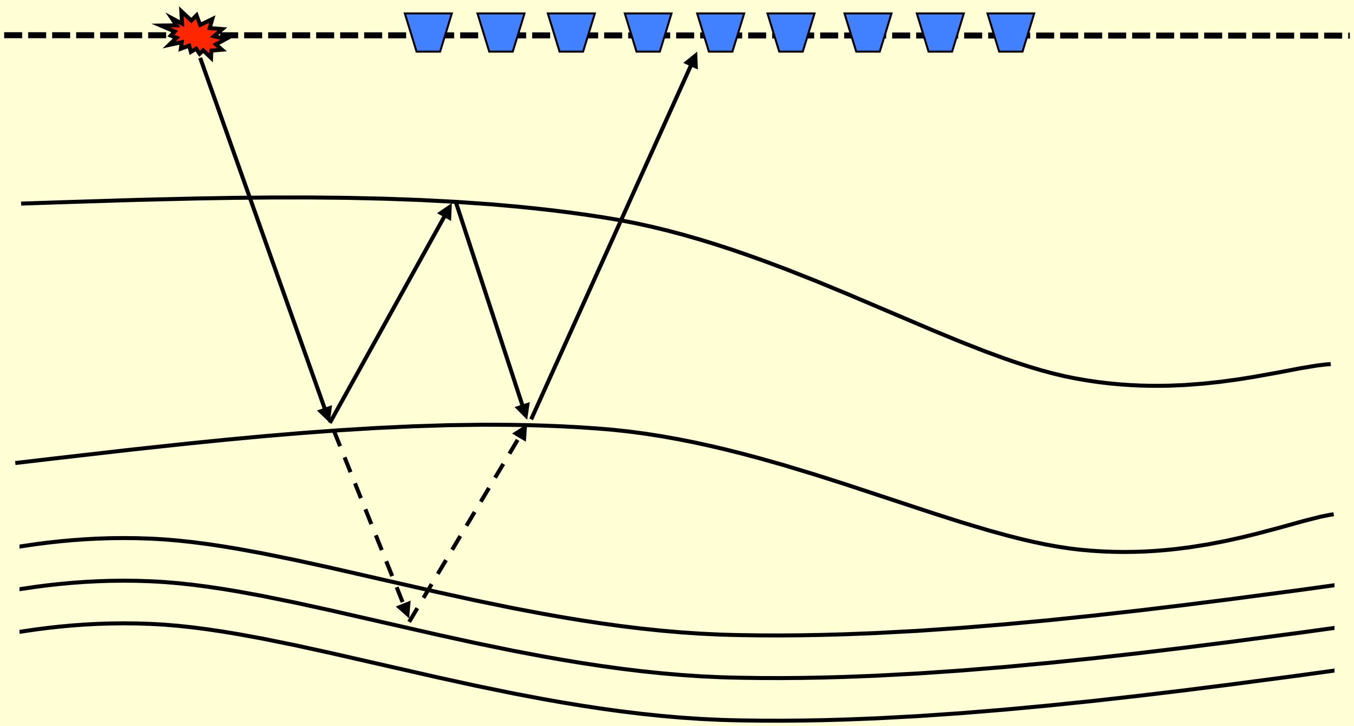

False images of internal multiples

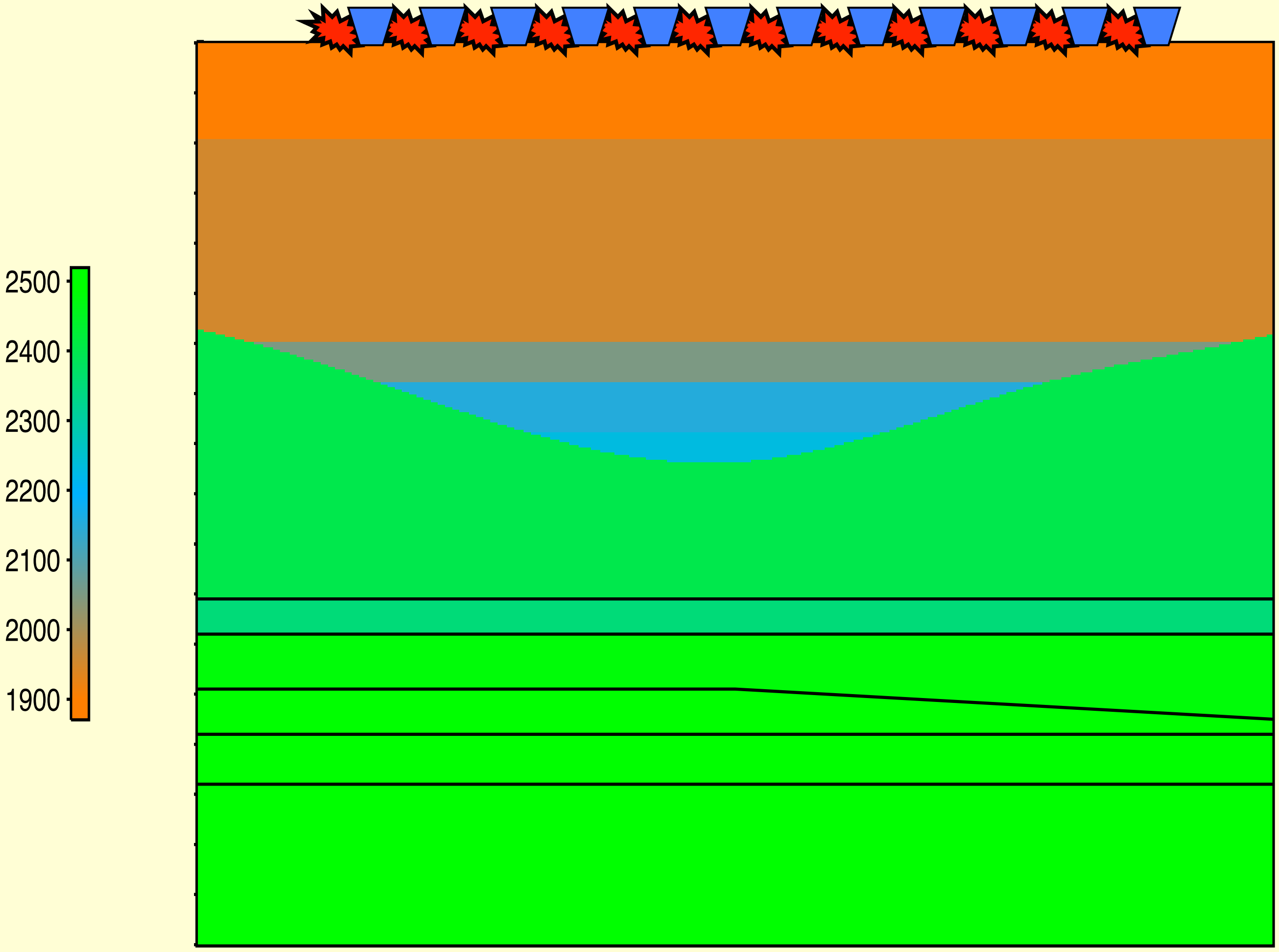
2500
2400
2300
2200
2100
2000
1900

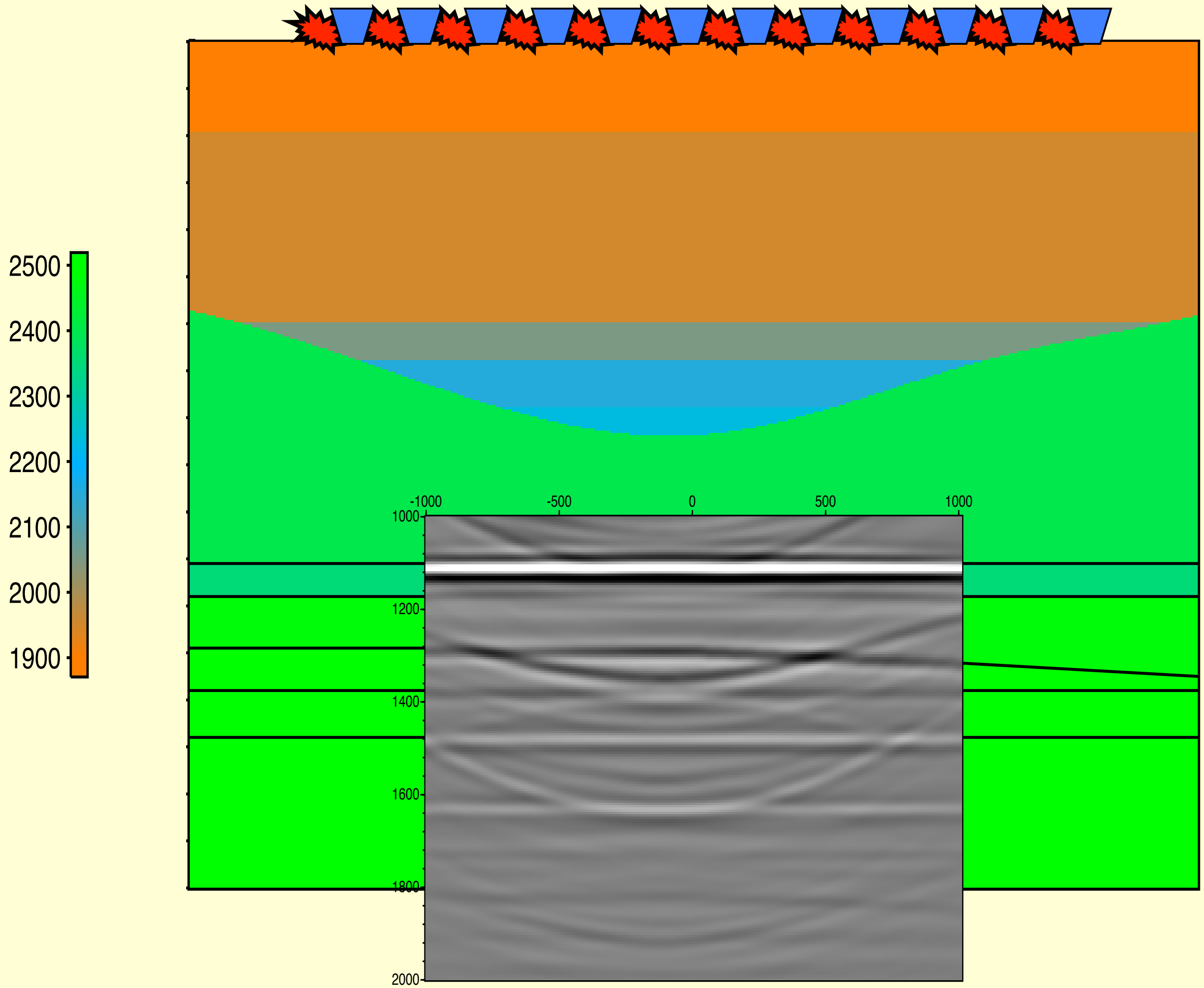

False images of internal multiples

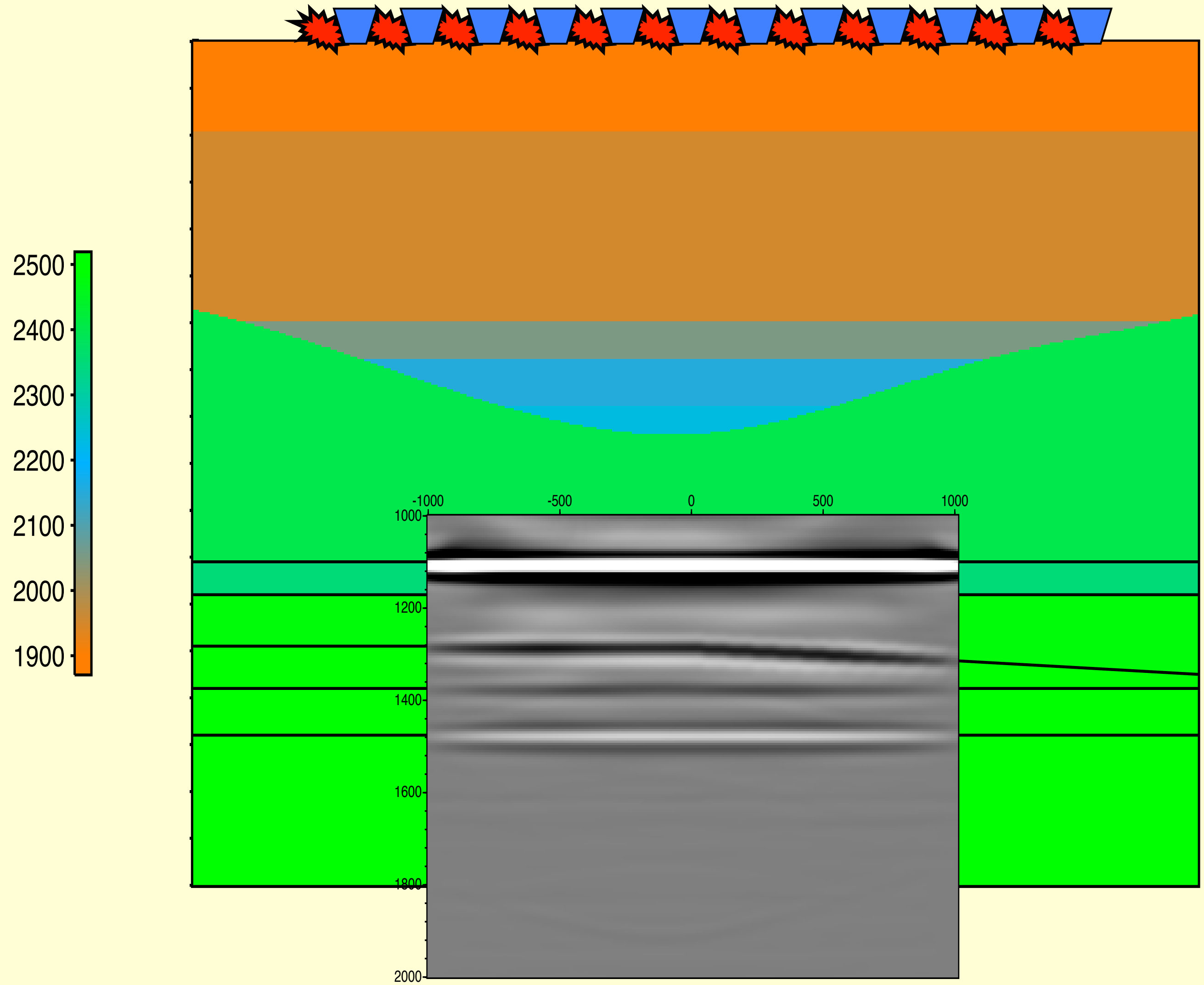

Marchenko imaging

Representations for the homogeneous Green's function

AN ESSAY

ON THE

APPLICATION

OF

MATHEMATICAL ANALYSIS TO THE THEORIES OF ELECTRICITY AND MAGNETISM.

BY

GEORGE GREEN.

Nottingham:

PRINTED FOR THE AUTHOR, BY T. WHEELHOUSE.

SOLD BY HAMILTON, ADAMS & Co. 33, PATERNOSTER ROW; LONGMAN & Co.; AND W. JOY, LONDON; J. DEIGHTON, CAMBRIDGE;

AND S. BENNETT, H. BARNETT, AND W. DEARDEN, NOTTINGHAM.

1828.

JOURNAL OF THE OPTICAL SOCIETY OF AMERICA VOLUME 60, NUMBER 8 AUGUST 1970

Diffraction-Limited, Scalar Image Formation with Holograms of Arbitrary Shape*

ROBERT P. PORTER†

The MITRE Corporation, Box 208, Bedford, Massachusetts 01730

(Received 12 September 1969)

A theory of image formation is presented for a large-angle, point reference hologram, whose recording arrangement consists of a surface of arbitrary shape, a point reference source, and the object. The hologram is illuminated by a spherical wave during reconstruction. The resulting image field is similar to that of a Fourier-transform hologram. An exact, integral formulation of monochromatic, scalar diffraction theory is used to find the image field. The hologram is modeled by surface sources determined from the irradiance of the recorded field. The image field produced by the holographic system approximates the field produced by the ideal system, which forms the image of a point object by launching a converging, spherical wave.

INDEX HEADINGS: Holography; Image formation; Diffraction; Resolution; Microwaves.

Resolution in diffraction-limited holographic image systems can be improved by using large-angle, curved holograms, which intercept a large sector of the field radiating from the object; therefore, a theory of image formation with large curved holograms is required. These holograms are useful in acoustic and radio-wave systems because their resolving power is constrained by the wavelength and by the angle subtended by the aperture, unlike most optical systems whose performance is limited by film or source properties. Specifically, the diffraction-limited resolution of a small circular aperture is $0.61\ \lambda R/b$ (according to Rayleigh's criterion[1]) for a disk of diameter b at a distance R from the object, radiating at the wavelength λ, where the subtended cone angle is $b/2R \ll 1$. For example, the resolution is about 0.2 m for an aperture subtending a 5° cone angle of X-band radiation (3×10^{-2}-m wavelength) diverging from an object consisting of two nearby point sources. Thus, small-angle microwave and acoustic systems cannot resolve much object detail. Recent experiments with microwave and acoustic holographic systems have used large-angle holograms to overcome the diffraction limit.[2–6]

The images formed by these systems must be analyzed by a theory of large-angle holograms to ascertain the increased resolving power. With the exception of the work of Mittra and Ransom[7] and Wolf,[8] who have considered the infinite planar aperture, present theories of holography are restricted to apertures that intercept only a small sector of the radiation diverging from the object.[9–12] Related image theories for the infinite planar aperture have been developed. Montgomery has considered self-imaging planar objects[13]; Sherman,[14] Wolf and Shewell,[15,16] and Lalor[17] have considered inversion of the field recorded on a planar aperture. More generally, a theory of curved holograms can show that resolution depends on subtended angle, not on aperture shape. As indicated by Jeong,[18] curved holograms, such as cylindrical films, have potential applications in practical image systems. In this paper the theory of holography is extended to include large-angle, nonplanar holograms. Specifically, the image field of a point reference hologram is found and compared to the image field of an ideal system.

It is shown that the image field of a point reference hologram, whose recording arrangement consists of a surface of arbitrary shape, a point reference source, and the object, only approximates the field of an ideal system denoted as the basic image system. The basic image system is the collection of sources on a surface surrounding the object that form an image of a point object by launching a converging, spherical wave. The system is ideal, in the sense defined by Born and Wolf,[19] because the trajectories orthogonal to the converging wave fronts intersect at a single point. The image field of the basic image system is concentrated at the image point in the geometric-optics limit.

An exact, integral formulation of diffraction theory is used to find the image field produced by the hologram. The point reference hologram, whose recording arrangement is shown in Fig. 1, is modeled by a collection of

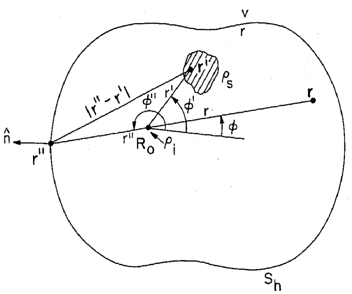

FIG. 1. Geometry for a holographic surface S_h of arbitrary shape. The r and v spaces are, as indicated, inside and outside S_h. The unit normal $\hat{n}$ points into the v space. During the reconstruction step, the inside sources are removed and reconstruction sources are placed either inside or outside. The coordinate system for the two-dimensional problem, where S_h is a cylinder of arbitrary cross section, is shown.

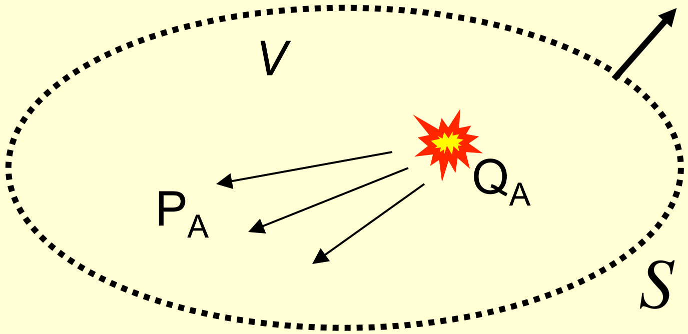

‘State A’

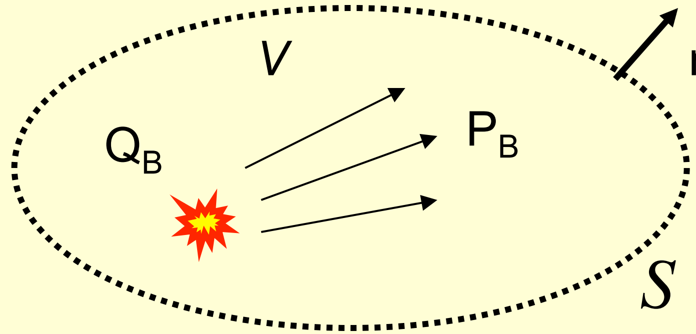

‘State B’

$$
\begin{aligned}
\int_{\mathbb{V}} \{P_A Q_B - V_{k,A} F_{k,B} + F_{k,A} V_{k,B} - Q_A P_B\} \mathrm{d}^3\mathbf{x} &= \\
\oint_{\mathbb{S}} \{P_A V_{k,B} - V_{k,A} P_B\} n_k \mathrm{d}^2\mathbf{x} \\
-i\omega \int_{\mathbb{V}} \{P_A P_B \Delta\kappa - V_{k,A} V_{k,B} \Delta\rho\} \mathrm{d}^3\mathbf{x}
\end{aligned}
$$

Note: The medium is arbitrarily inhomogeneous

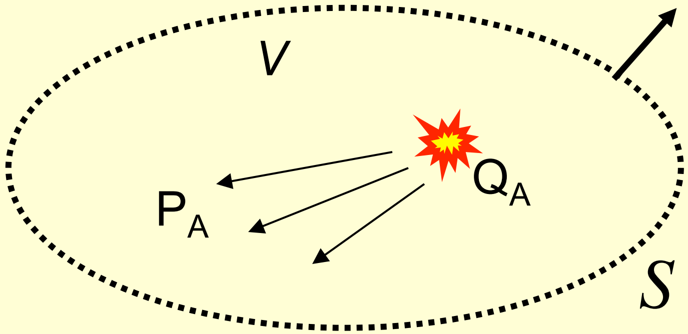

‘State A’

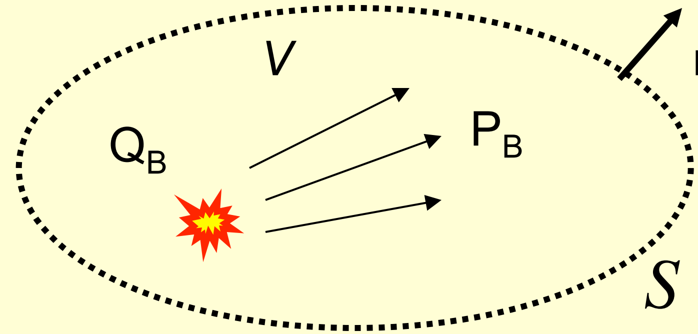

‘State B’

$$\int_{\mathbb{V}} \{P_A Q_B - V_{k,A} F_{k,B} + F_{k,A} V_{k,B} - Q_A P_B\} \mathrm{d}^3\mathbf{x} = \oint_{\mathbb{S}} \{P_A V_{k,B} - V_{k,A} P_B\} n_k \mathrm{d}^2\mathbf{x} - i\omega \int_{\mathbb{V}} \{P_A P_B \Delta\kappa - V_{k,A} V_{k,B} \Delta\rho\} \mathrm{d}^3\mathbf{x}$$

$$\Delta\kappa = 0$$

$$\Delta\rho = 0$$

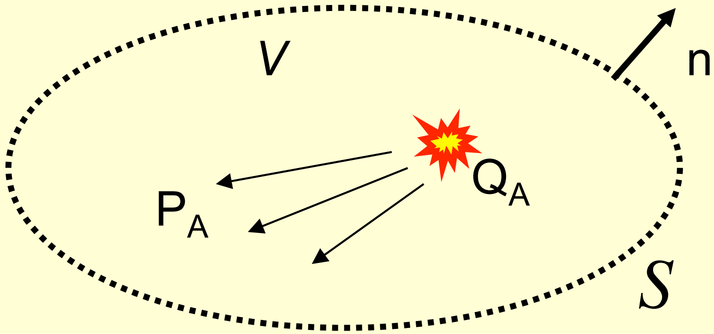

'State A'

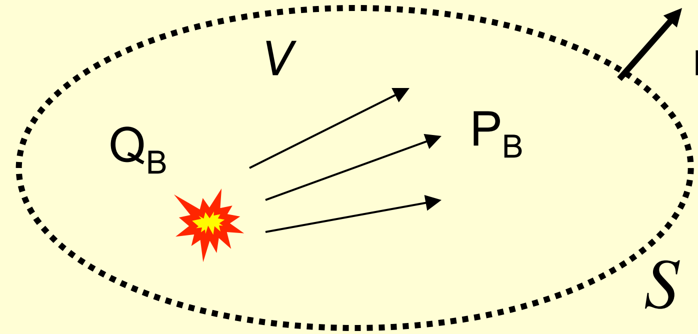

'State B'

$$\int_{\mathbb{V}} \{P_A Q_B - V_{k,A} F_{k,B} + F_{k,A} V_{k,B} - Q_A P_B\} \mathrm{d}^3\mathbf{x} = \oint_{\mathbb{S}} \{P_A V_{k,B} - V_{k,A} P_B\} n_k \mathrm{d}^2\mathbf{x}$$

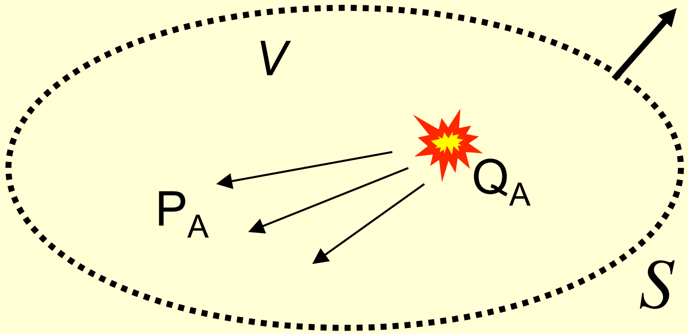

‘State A’

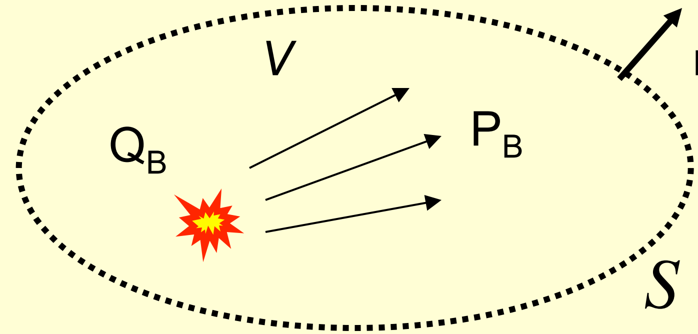

‘State B’

$$\int_{\mathbb{V}} \{P_A Q_B - V_{k,A} F_{k,B} + F_{k,A} V_{k,B} - Q_A P_B\} \mathrm{d}^3\mathbf{x} = \oint_{\mathbb{S}} \{P_A V_{k,B} - V_{k,A} P_B\} n_k \mathrm{d}^2\mathbf{x}$$

$$F_{k,A} = 0$$

$$F_{k,B} = 0$$

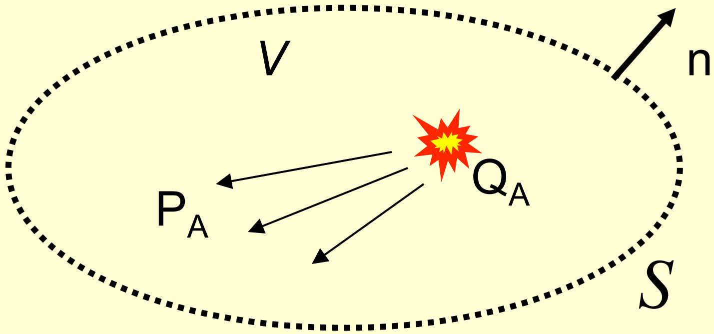

‘State A’

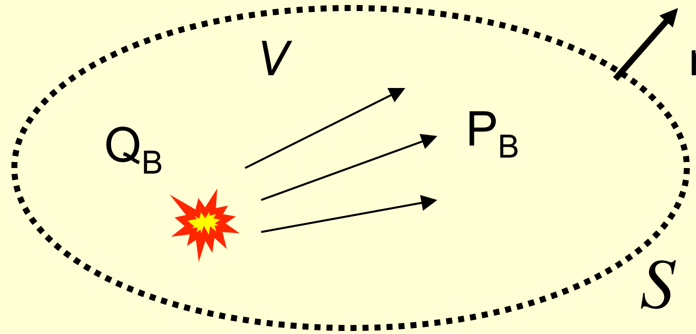

‘State B’

$$\int_{\mathbb{V}} \{P_A Q_B - Q_A P_B\} \mathrm{d}^3\mathbf{x} = \oint_{\mathbb{S}} \{P_A V_{k,B} - V_{k,A} P_B\} n_k \mathrm{d}^2\mathbf{x}$$

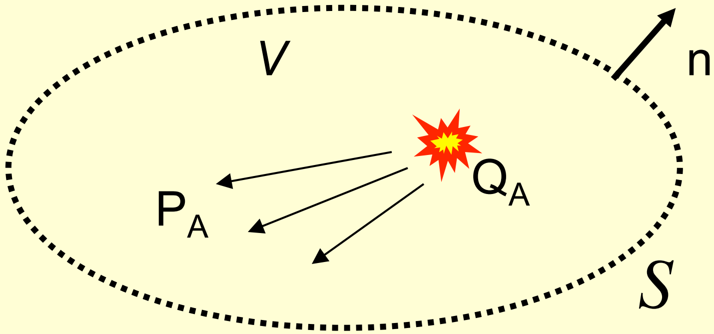

‘State A’

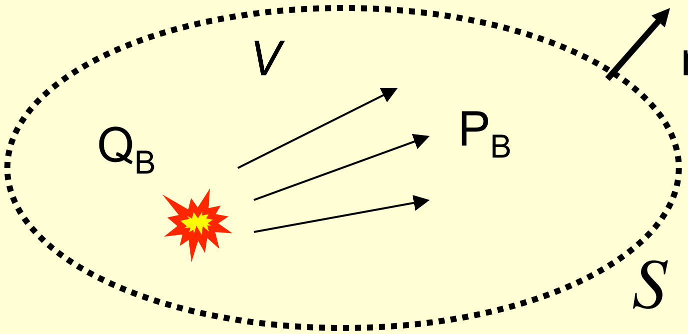

‘State B’

$$\int_{\mathbb{V}} \{P_A Q_B - Q_A P_B\} \mathrm{d}^3\mathbf{x} = \oint_{\mathbb{S}} \{P_A V_{k,B} - V_{k,A} P_B\} n_k \mathrm{d}^2\mathbf{x}$$

Time-reversal State A (assuming a lossless inhomogeneous medium):

$$P_A \rightarrow P_A^*$$

$$V_{k,A} \rightarrow -V_{k,A}^*$$

$$Q_A \rightarrow -Q_A^*$$

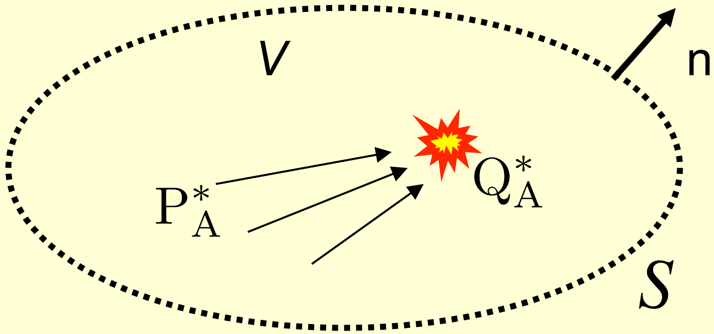

‘State A’

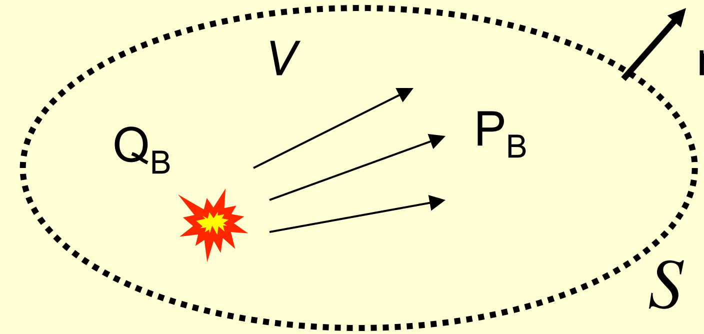

‘State B’

$$\int_{\mathbb{V}} \{P_A^* Q_B + Q_A^* P_B\} \mathrm{d}^3\mathbf{x} = \oint_{\mathbb{S}} \{P_A^* V_{k,B} + V_{k,A}^* P_B\} n_k \mathrm{d}^2\mathbf{x}$$

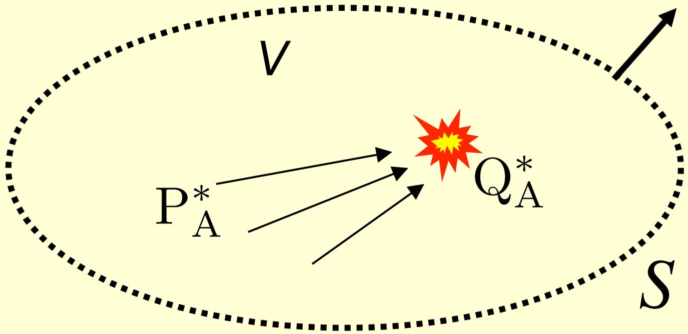

'State A'

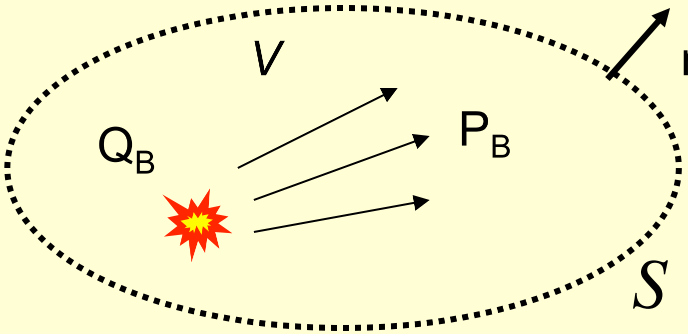

'State B'

$$\int_{\mathbb{V}} \{P_A^* Q_B + Q_A^* P_B\} \mathrm{d}^3\mathbf{x} = \oint_{\mathbb{S}} \{P_A^* V_{k,B} + V_{k,A}^* P_B\} n_k \mathrm{d}^2\mathbf{x}$$

$$Q_A^* \to \delta(\mathbf{x} - \mathbf{x}_A) \qquad Q_B \to \delta(\mathbf{x} - \mathbf{x}_B)$$

$$P_A^* \to G^*(\mathbf{x}, \mathbf{x}_A, \omega) \qquad P_B \to G(\mathbf{x}, \mathbf{x}_B, \omega)$$

$$V_{k,A}^* \to \frac{-1}{i\omega\rho} \partial_k G^*(\mathbf{x}, \mathbf{x}_A, \omega) \qquad V_{k,B} \to \frac{1}{i\omega\rho} \partial_k G(\mathbf{x}, \mathbf{x}_B, \omega)$$

$G^*(\mathbf{x}_B, \mathbf{x}_A, \omega)$

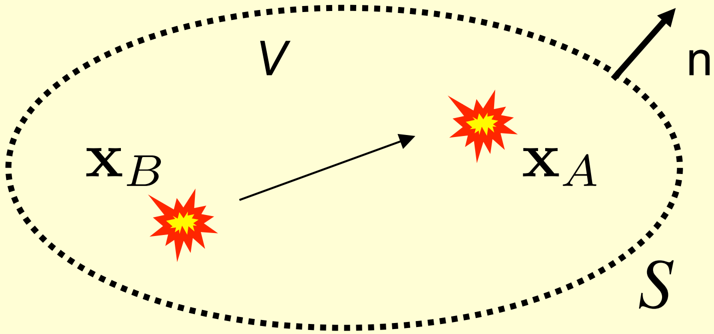

'State A'

$G(\mathbf{x}_A, \mathbf{x}_B, \omega)$

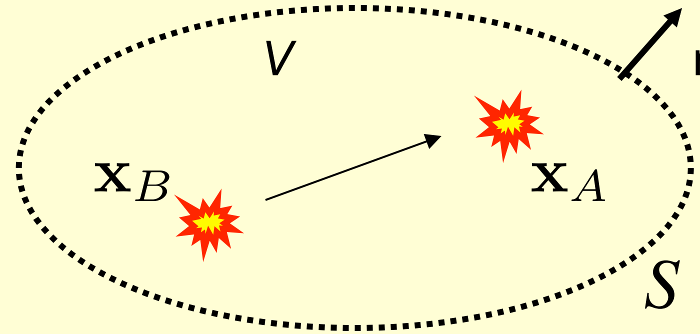

'State B'

$$G^*(\mathbf{x}_B, \mathbf{x}_A, \omega) + G(\mathbf{x}_A, \mathbf{x}_B, \omega) =$$

$$\frac{1}{i\omega\rho} \oint_{\mathbb{S}} \Big(G^*(\mathbf{x}, \mathbf{x}_A, \omega) \partial_k G(\mathbf{x}, \mathbf{x}_B, \omega) - \partial_k G^*(\mathbf{x}, \mathbf{x}_A, \omega) G(\mathbf{x}, \mathbf{x}_B, \omega) \Big) n_k \mathrm{d}^2\mathbf{x}$$

(Porter, 1970, JOSA; Oristaglio, 1989, Inverse Problems)

$G^*(\mathbf{x}_B, \mathbf{x}_A, \omega)$

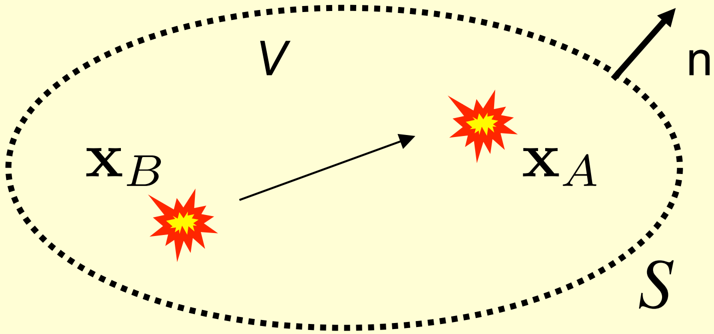

'State A'

$G(\mathbf{x}_B, \mathbf{x}_A, \omega)$

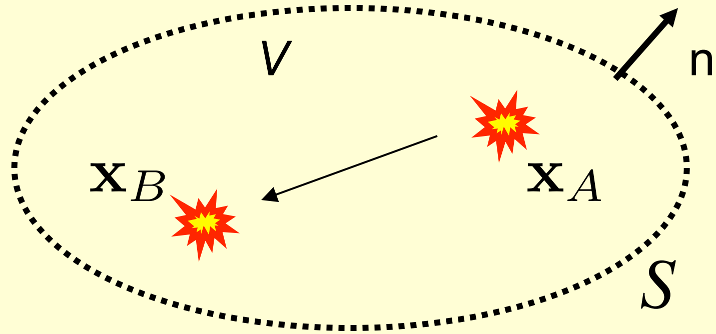

'State B'

$$G^*(\mathbf{x}_B, \mathbf{x}_A, \omega) + G(\mathbf{x}_B, \mathbf{x}_A, \omega) =$$

$$\frac{-2}{i\omega\rho} \oint_{\mathbb{S}} \Big(\partial_k G^*(\mathbf{x}, \mathbf{x}_A, \omega) G(\mathbf{x}, \mathbf{x}_B, \omega) \Big) n_k \mathrm{d}^2\mathbf{x}$$

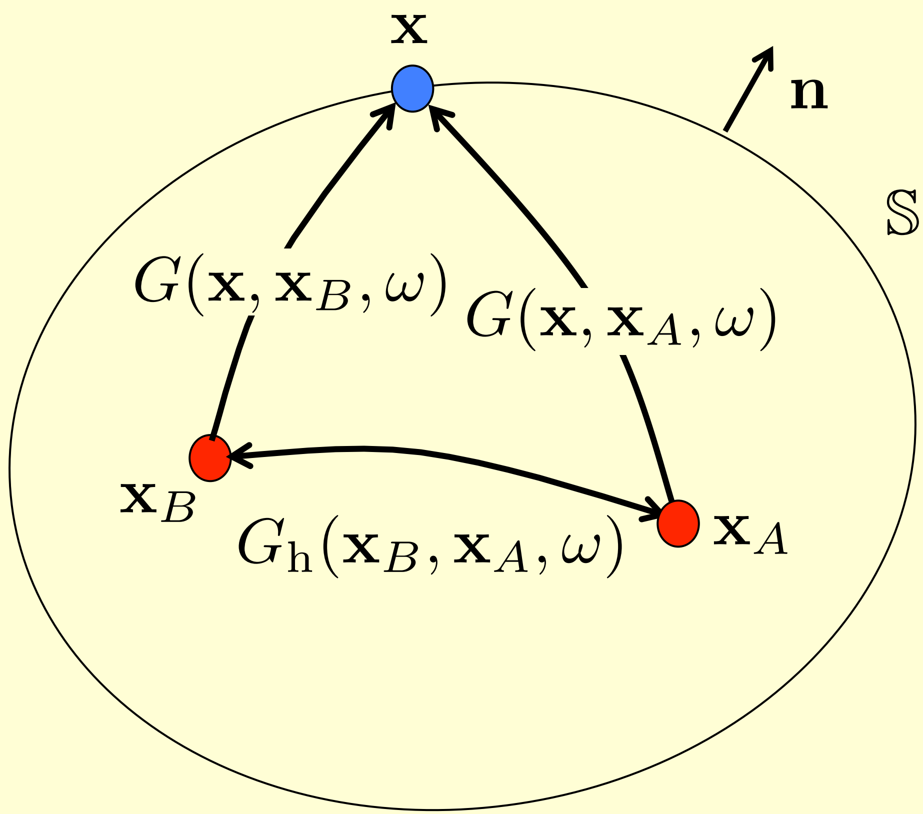

$$\overbrace{G(\mathbf{x}_B,\mathbf{x}_A,\omega)+G^*(\mathbf{x}_B,\mathbf{x}_A,\omega)}^{G_\mathrm{h}(\mathbf{x}_B,\mathbf{x}_A,\omega)} \propto \oint_{\mathbb{S}} G(\mathbf{x},\mathbf{x}_B,\omega)\partial_i G^*(\mathbf{x},\mathbf{x}_A,\omega)n_i\mathrm{d}\mathbf{x}$$

Fundamental basis for:

- Time-reversal acoustics
- Seismic interferometry
  (=Green's function retrieval)
- Imaging by double focusing
- Monitoring of induced seismicity
- Etc.

$$\overbrace{G(\mathbf{x}_B,\mathbf{x}_A,\omega)+G^*(\mathbf{x}_B,\mathbf{x}_A,\omega)}^{G_{\rm h}(\mathbf{x}_B,\mathbf{x}_A,\omega)} \propto \oint_{\mathbb{S}} G(\mathbf{x},\mathbf{x}_B,\omega)\partial_i G^*(\mathbf{x},\mathbf{x}_A,\omega)n_i{\rm d}\mathbf{x}$$

Fundamental basis for:

- Time-reversal acoustics
- Seismic interferometry
  (=Green's function retrieval)
- Imaging by double focusing
- Monitoring of induced seismicity
- Etc.

However:

- Requires data at a closed boundary

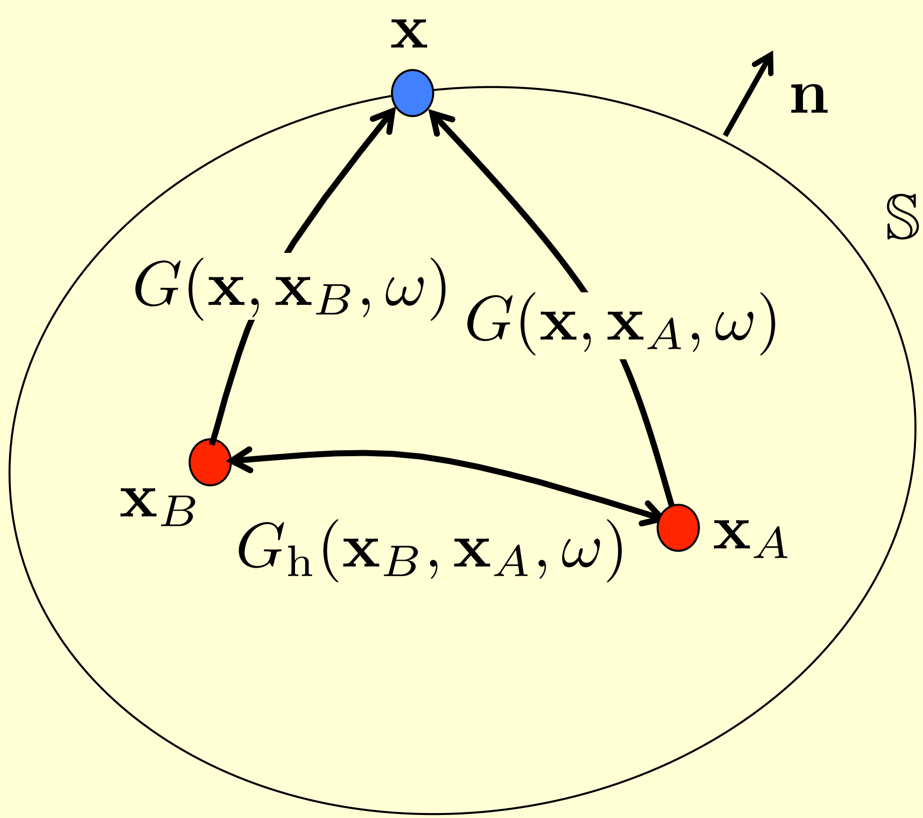

$$\overbrace{G(\mathbf{x}_B,\mathbf{x}_A,\omega)+G^*(\mathbf{x}_B,\mathbf{x}_A,\omega)}^{G_\mathrm{h}(\mathbf{x}_B,\mathbf{x}_A,\omega)} \propto \oint_{\mathbb{S}} G(\mathbf{x},\mathbf{x}_B,\omega)\partial_i G^*(\mathbf{x},\mathbf{x}_A,\omega)n_i \mathrm{d}\mathbf{x}$$

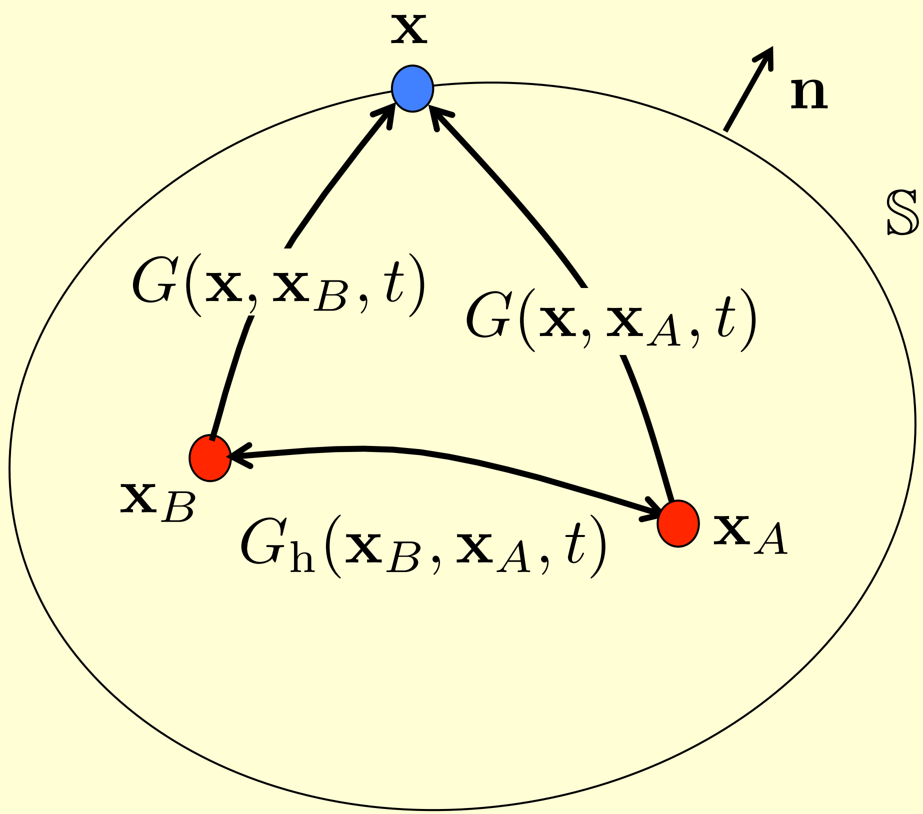

$$\overbrace{G(\mathbf{x}_B,\mathbf{x}_A,t)+G(\mathbf{x}_B,\mathbf{x}_A,-t)}^{G_\mathrm{h}(\mathbf{x}_B,\mathbf{x}_A,t)} \propto \oint_{\mathbb{S}} G(\mathbf{x},\mathbf{x}_B,t) * \partial_i G(\mathbf{x},\mathbf{x}_A,-t) n_i \mathrm{d}\mathbf{x}$$

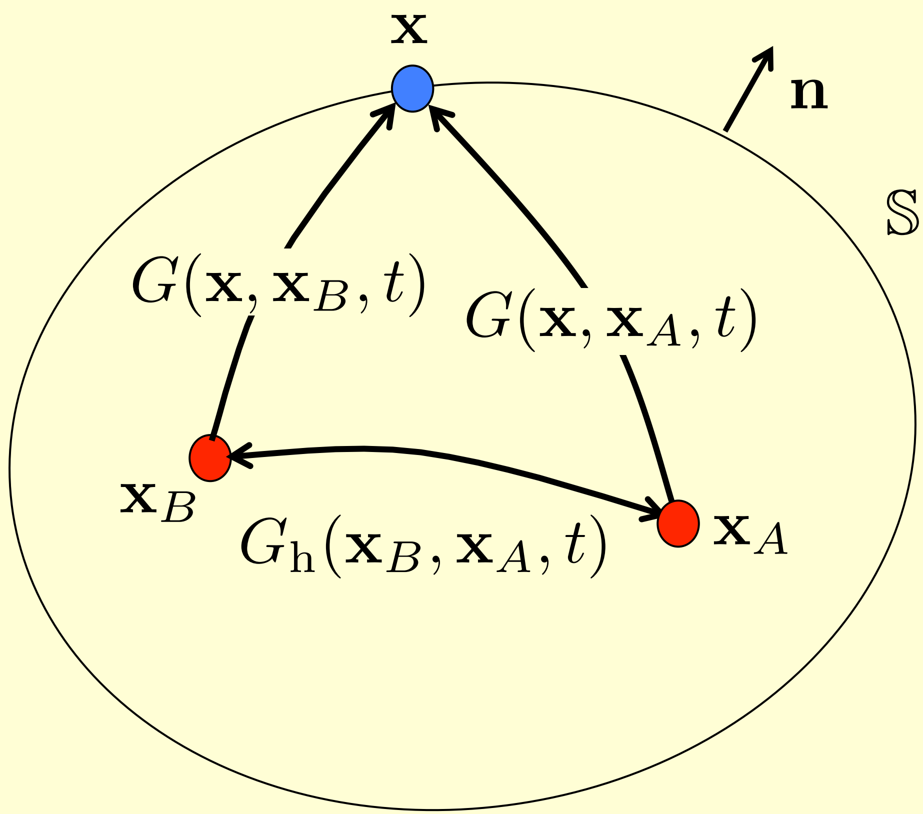

$$\overbrace{G(\mathbf{x}_B,\mathbf{x}_A,t)+G(\mathbf{x}_B,\mathbf{x}_A,-t)}^{G_{\mathrm{h}}(\mathbf{x}_B,\mathbf{x}_A,t)} \propto \oint_{\mathbb{S}} G(\mathbf{x},\mathbf{x}_B,t) * \overbrace{\partial_i G(\mathbf{x},\mathbf{x}_A,-t)n_i}^{v_n(\mathbf{x},\mathbf{x}_A,-t)}\,\mathrm{d}\mathbf{x}$$

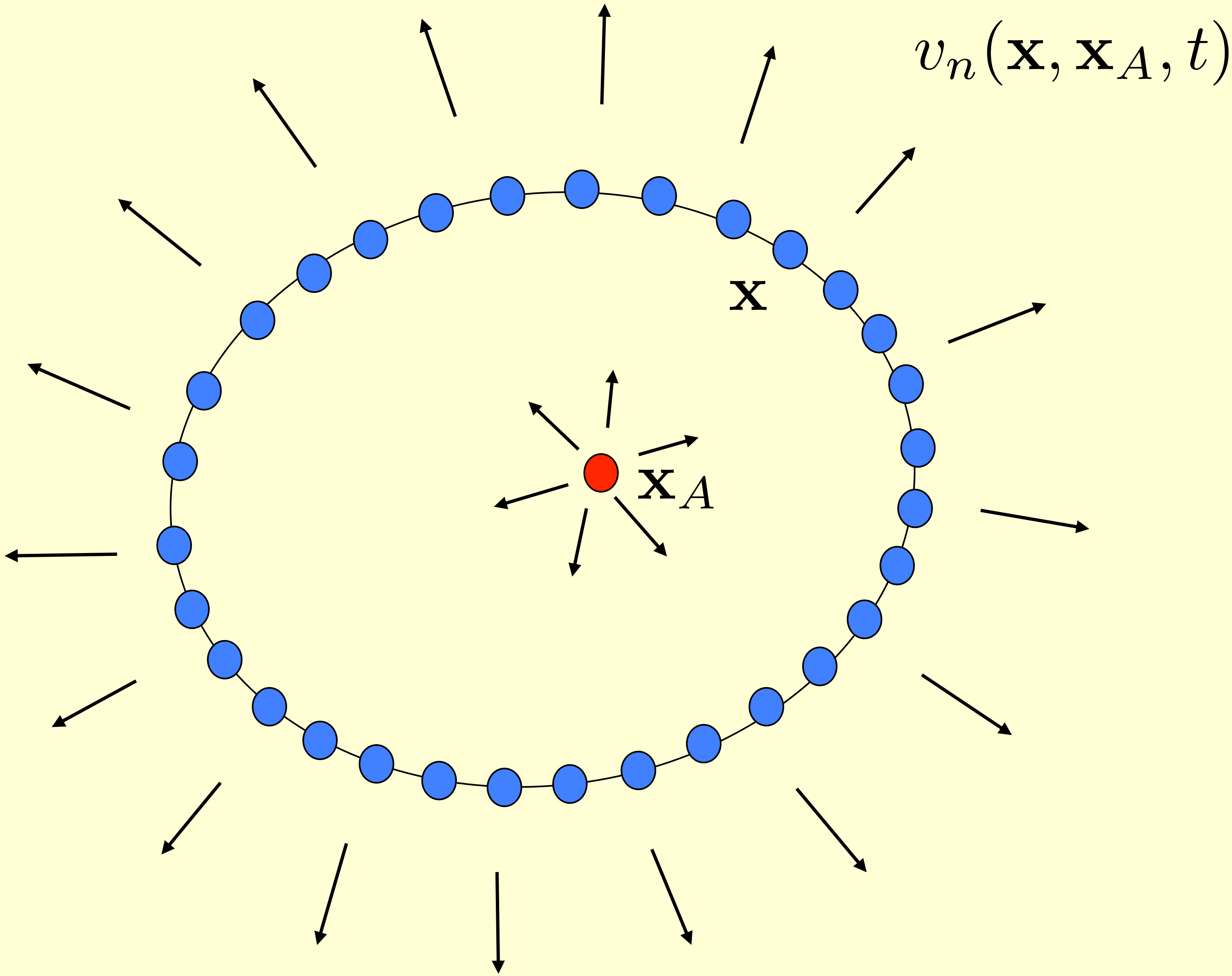

$v_n(\mathbf{x}, \mathbf{x}_A, t)$
$\mathbf{x}$
$\mathbf{x}_A$

Time-reversal

$$v_n(\mathbf{x}, \mathbf{x}_A, -t)$$

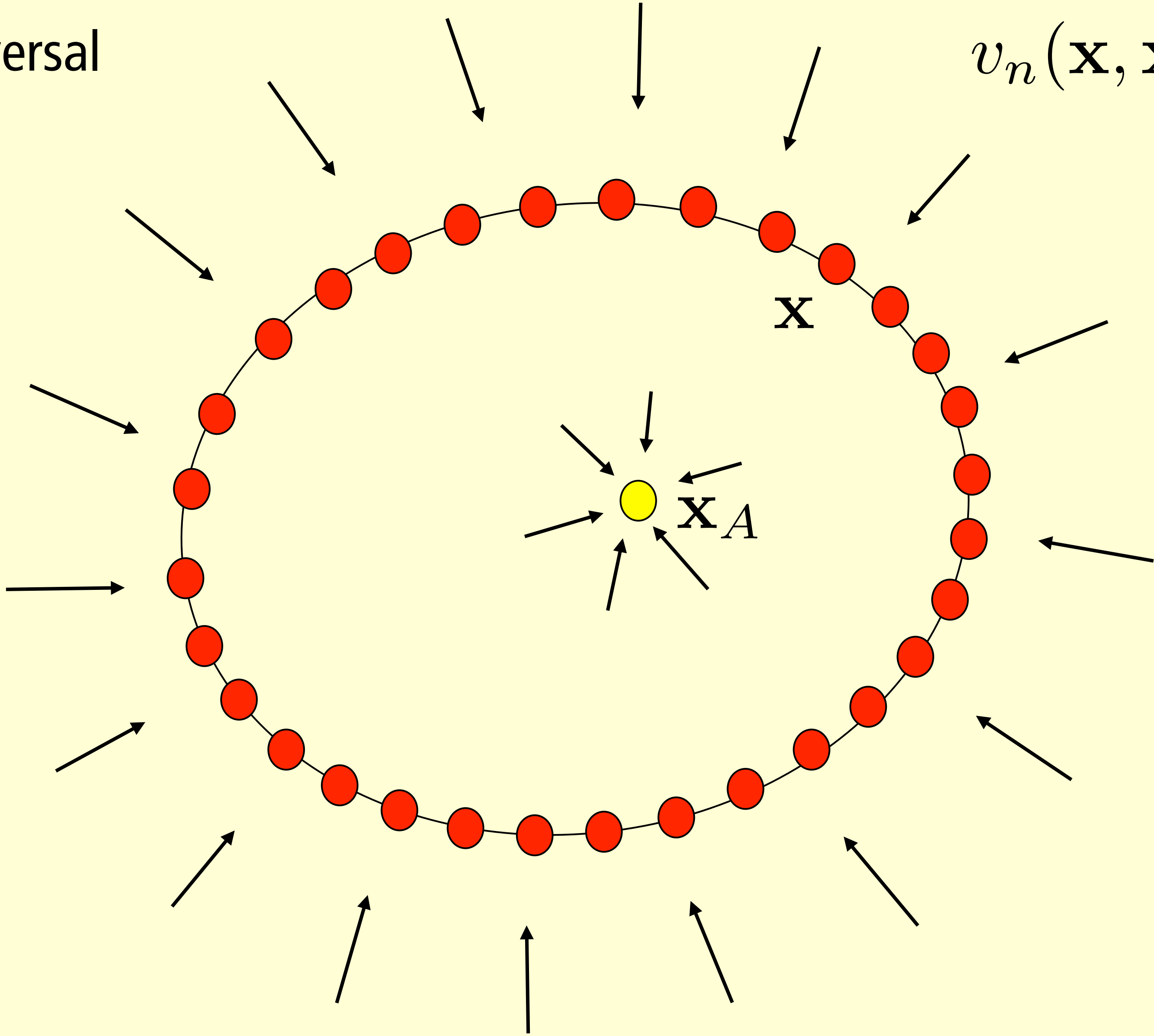

$$\oint_{\mathbb{S}} G(\mathbf{x}_A, \mathbf{x}, t) * v_n(\mathbf{x}, \mathbf{x}_A, -t)\mathrm{d}\mathbf{x}$$

Time-reversal

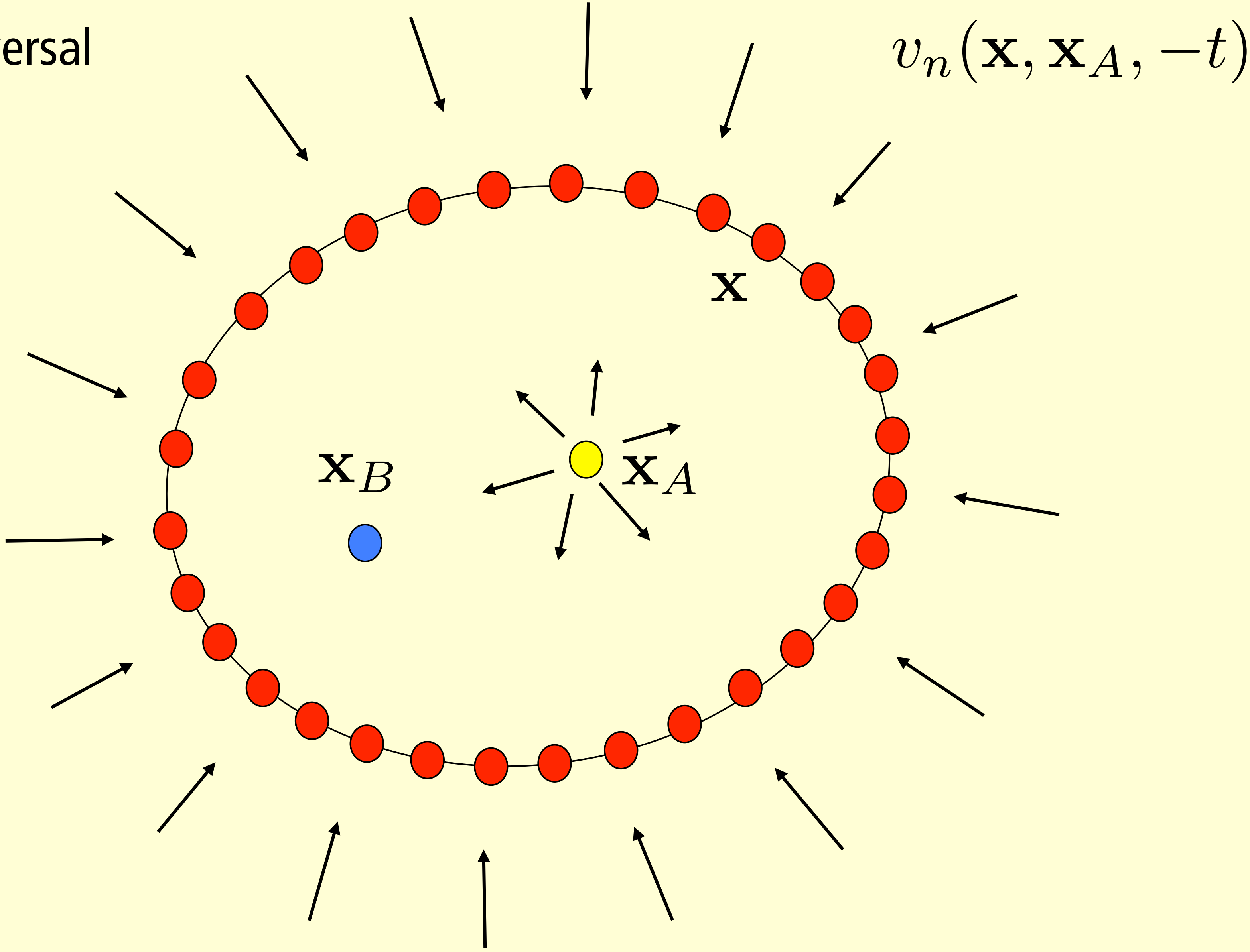

$$G(\mathbf{x}_B, \mathbf{x}_A, t) + G(\mathbf{x}_B, \mathbf{x}_A, -t) = 2 \oint_{\mathbb{S}} G(\mathbf{x}_B, \mathbf{x}, t) * v_n(\mathbf{x}, \mathbf{x}_A, -t) \mathrm{d}\mathbf{x}$$

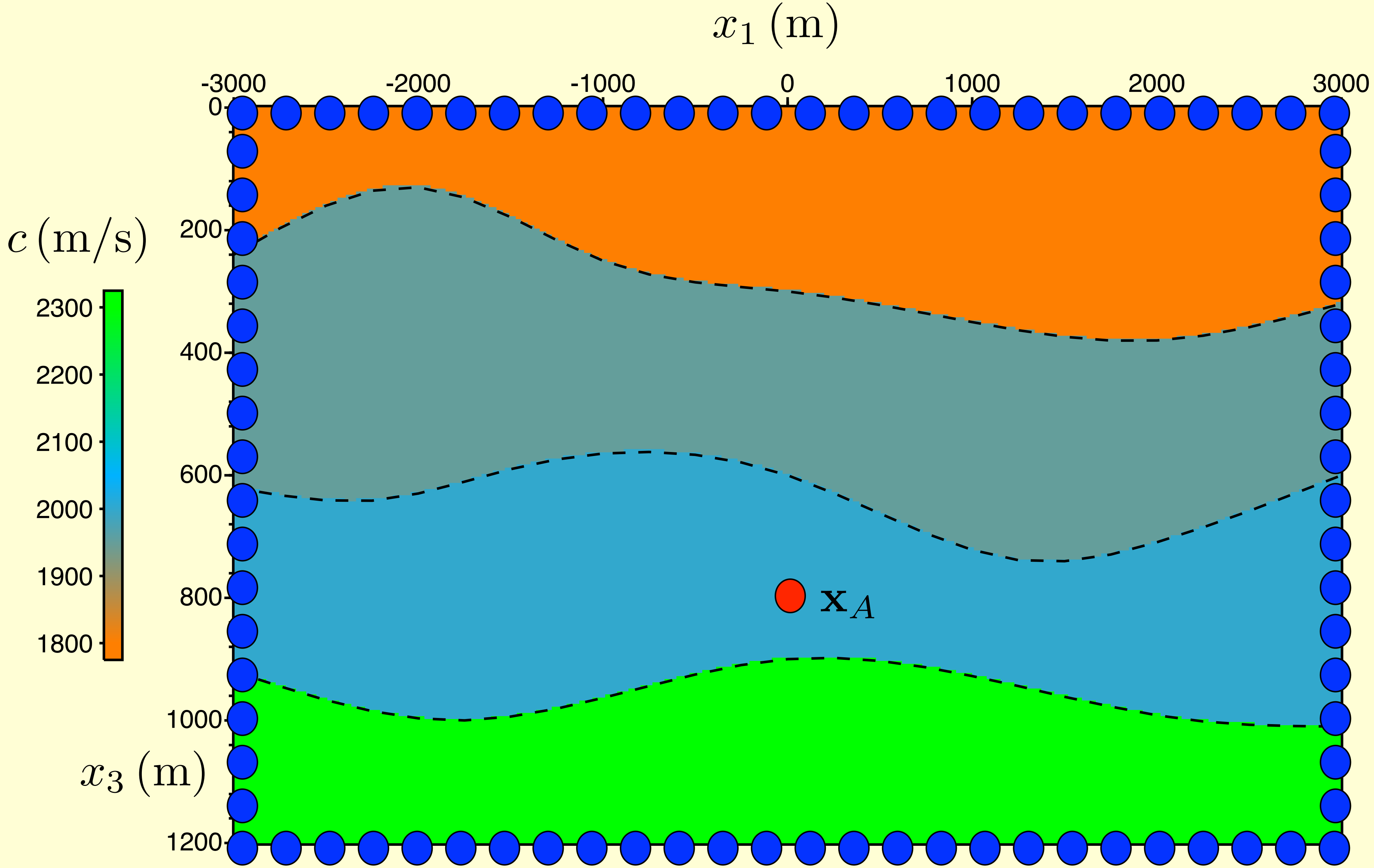

Omni-directional time-reversal experiment

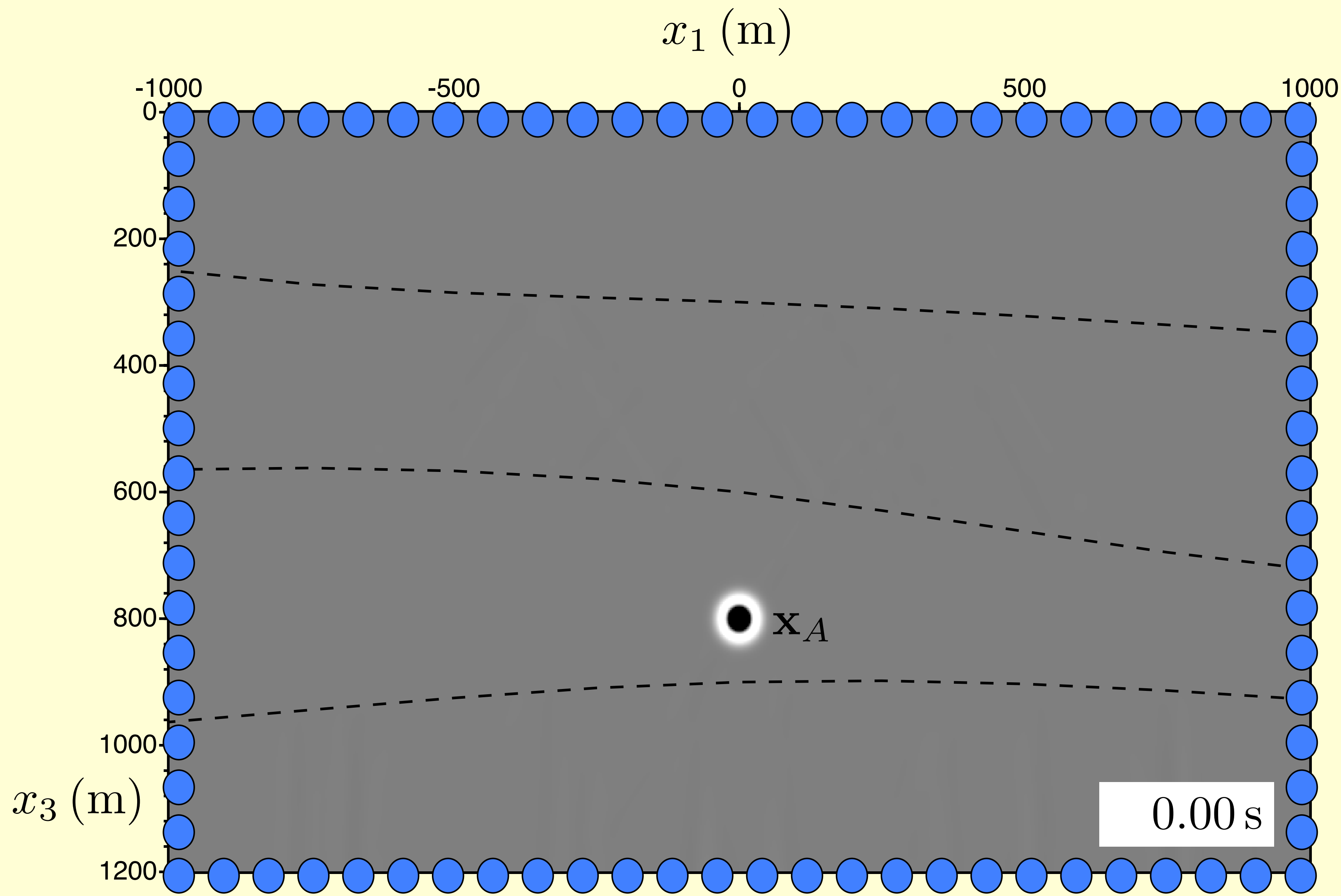

Omni-directional time-reversal experiment

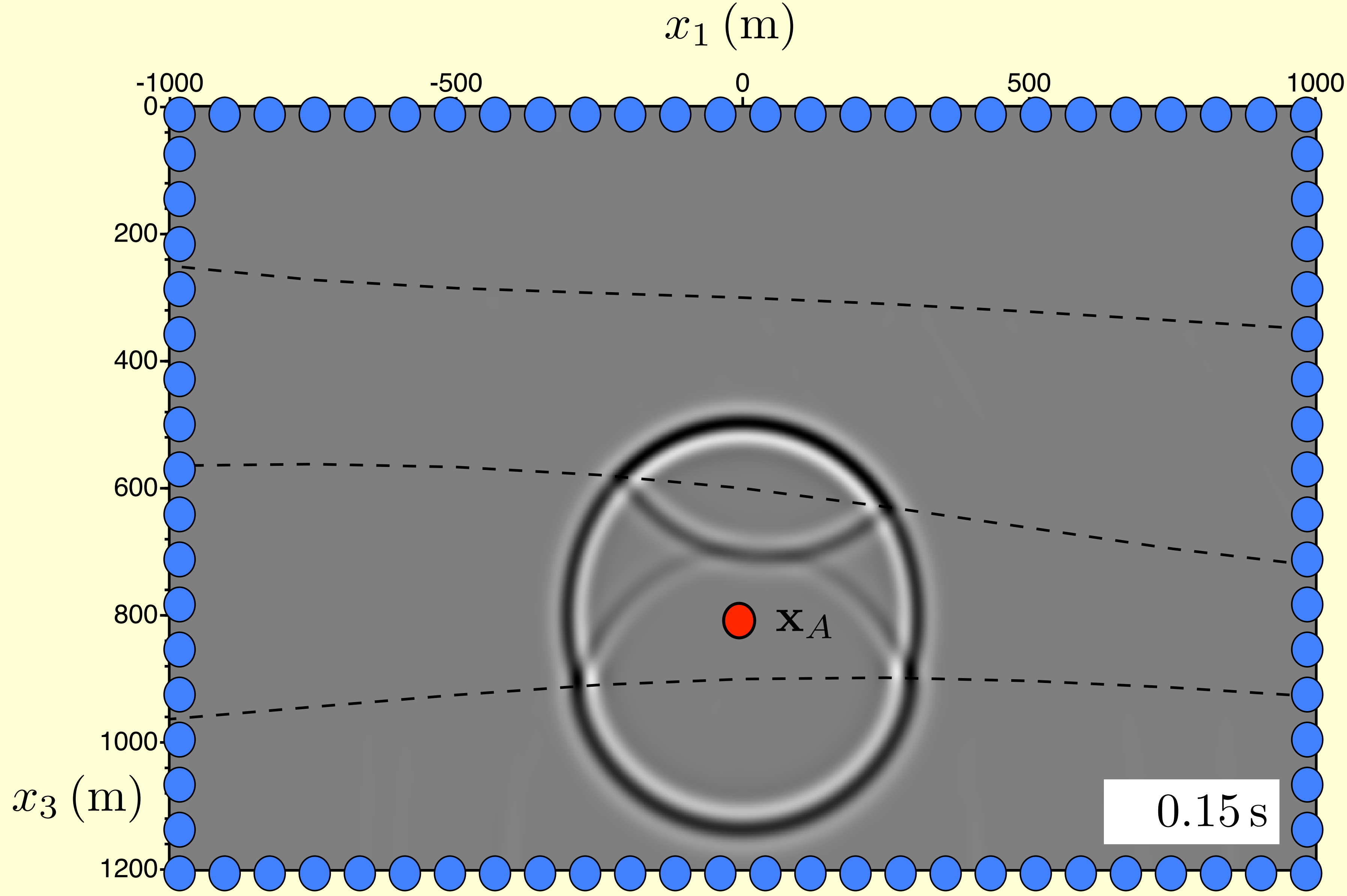

Omni-directional time-reversal experiment

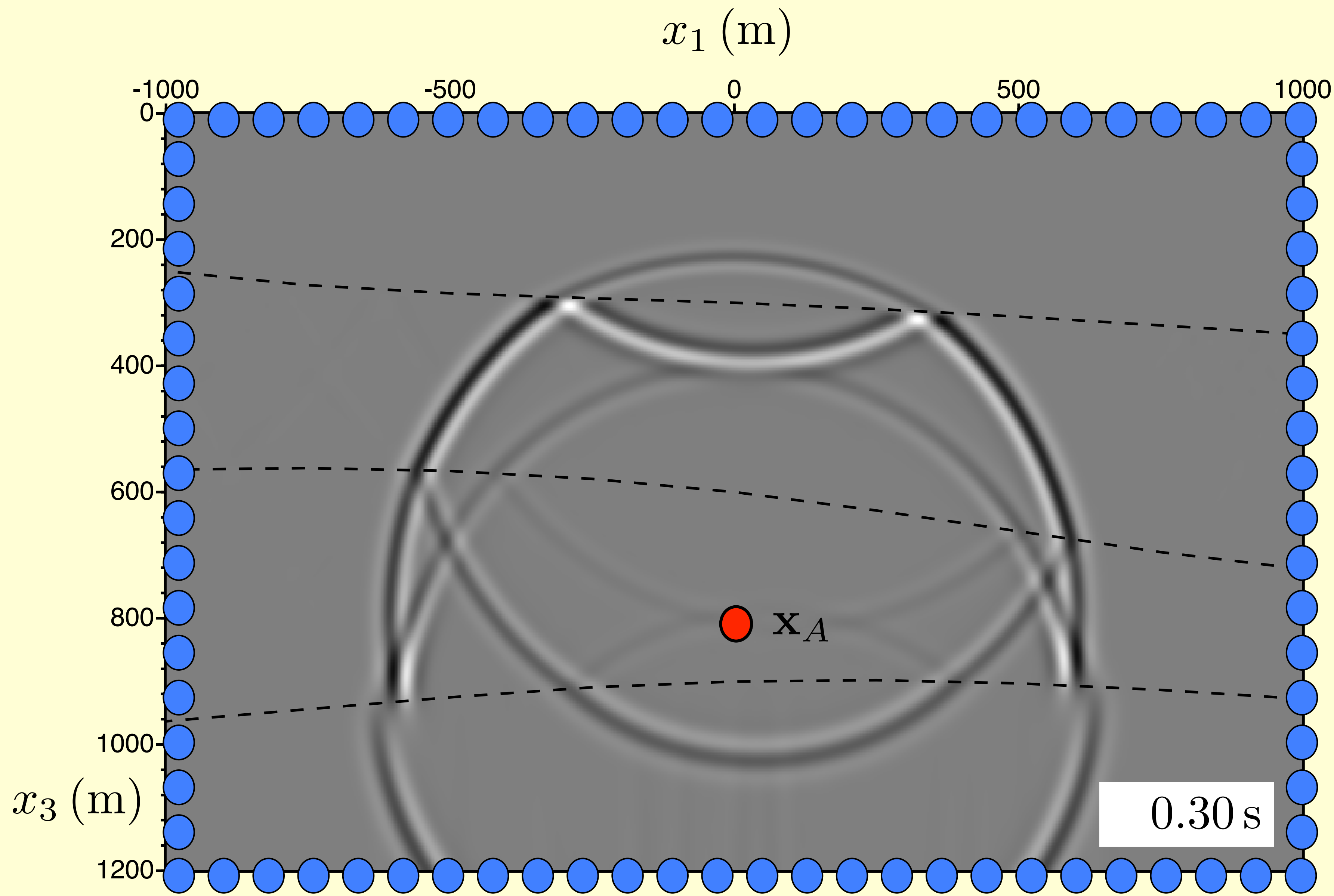

Omni-directional time-reversal experiment

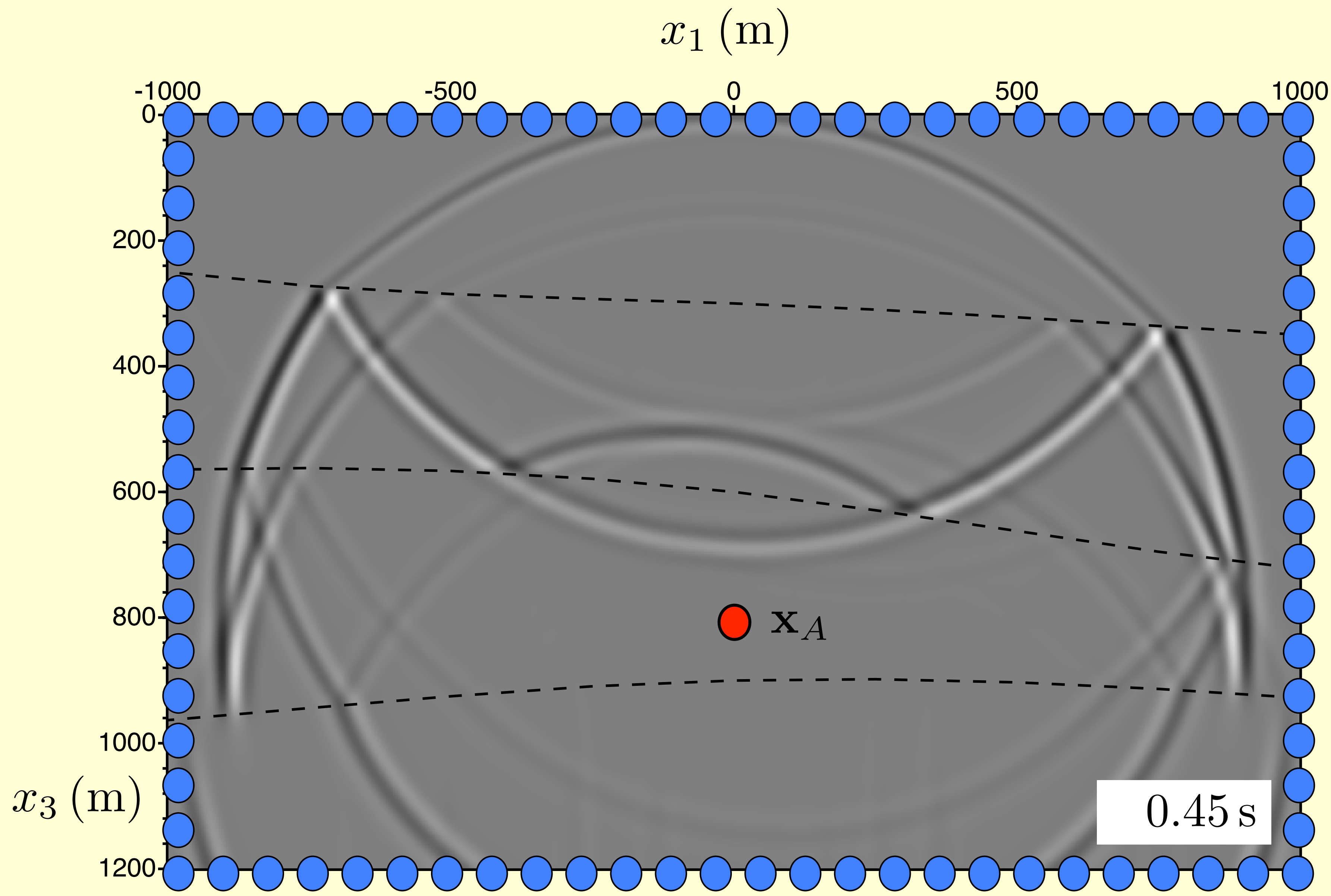

Omni-directional time-reversal experiment

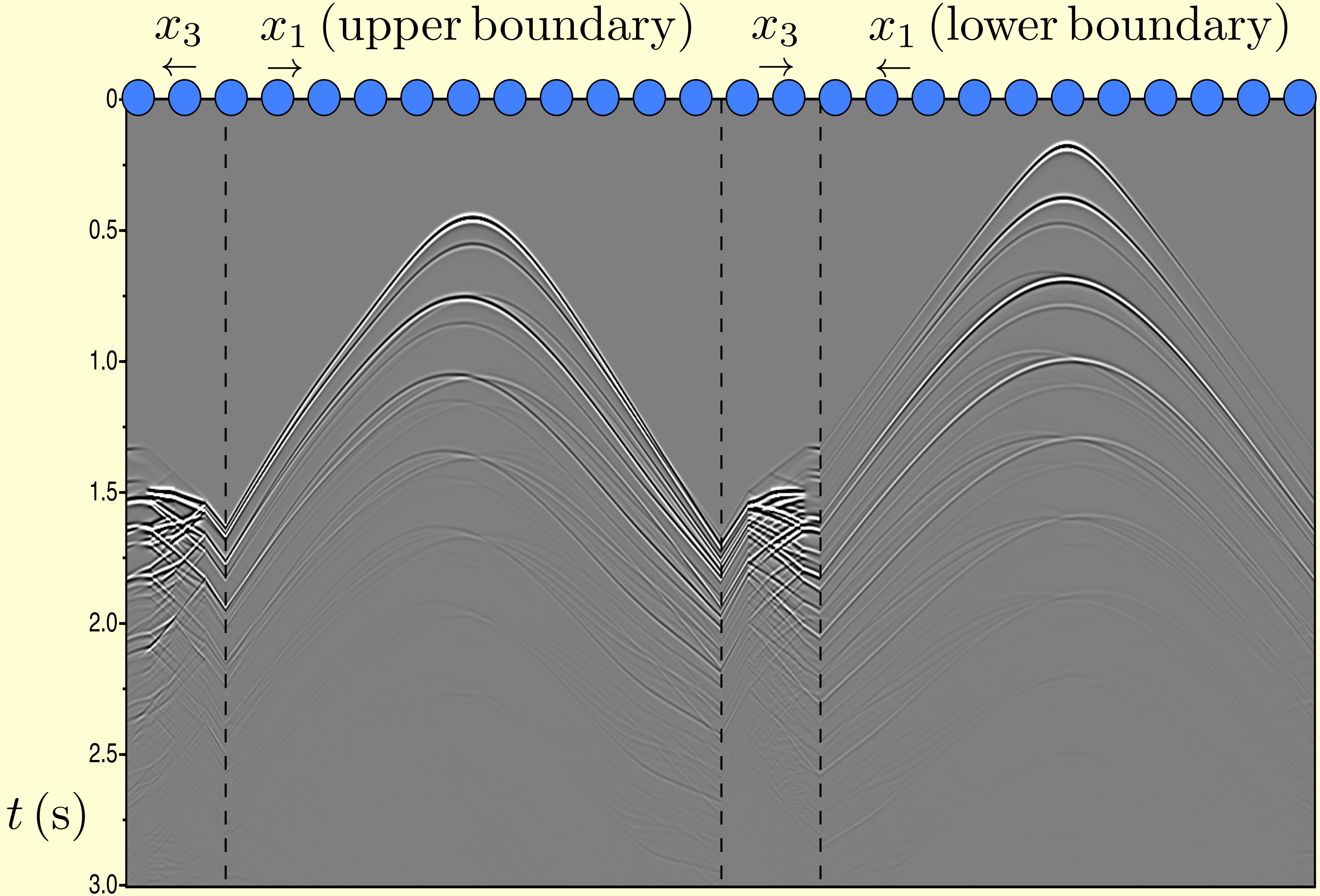

Omni-directional time-reversal experiment

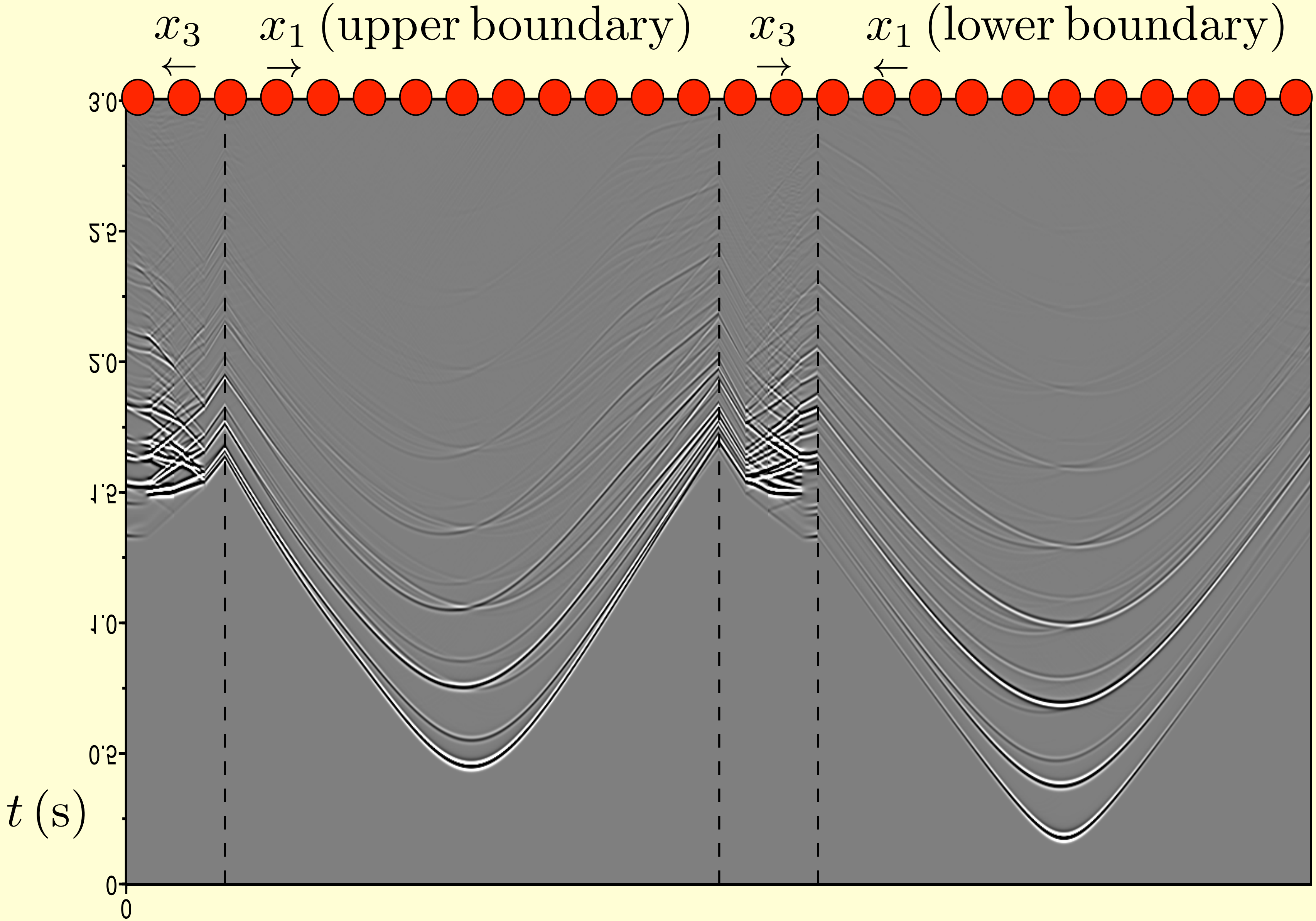

Omni-directional time-reversal experiment

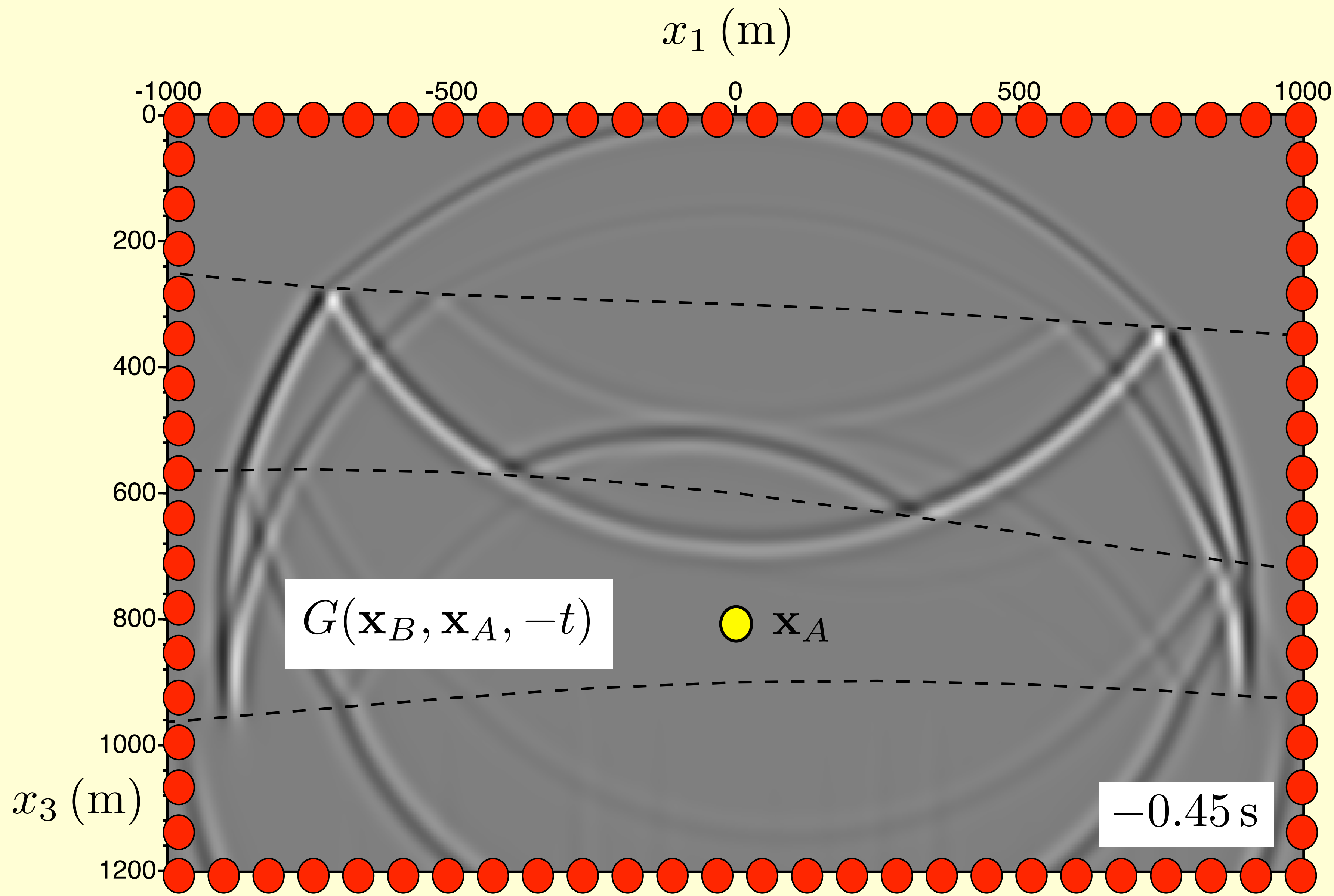

Omni-directional time-reversal experiment

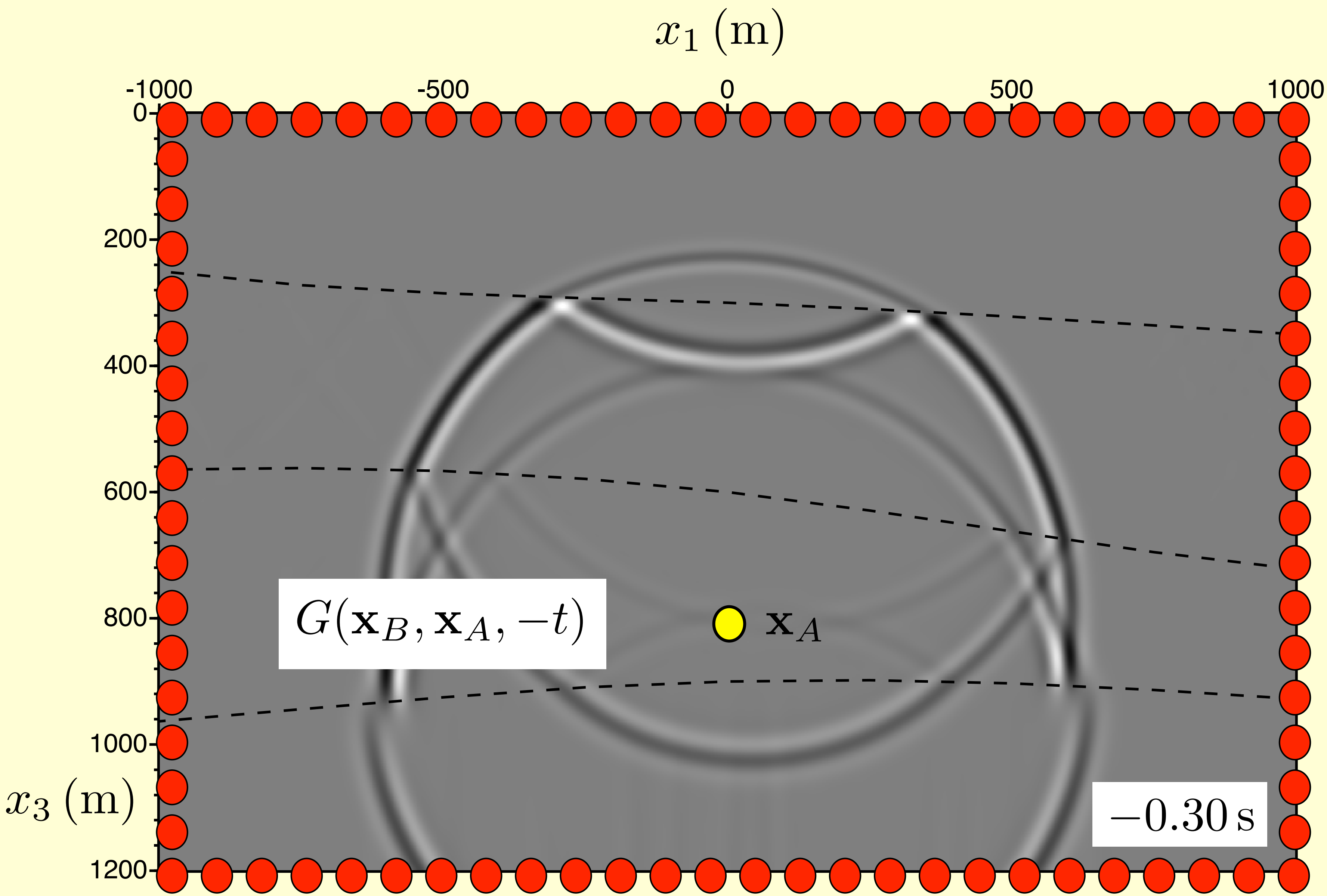

Omni-directional time-reversal experiment

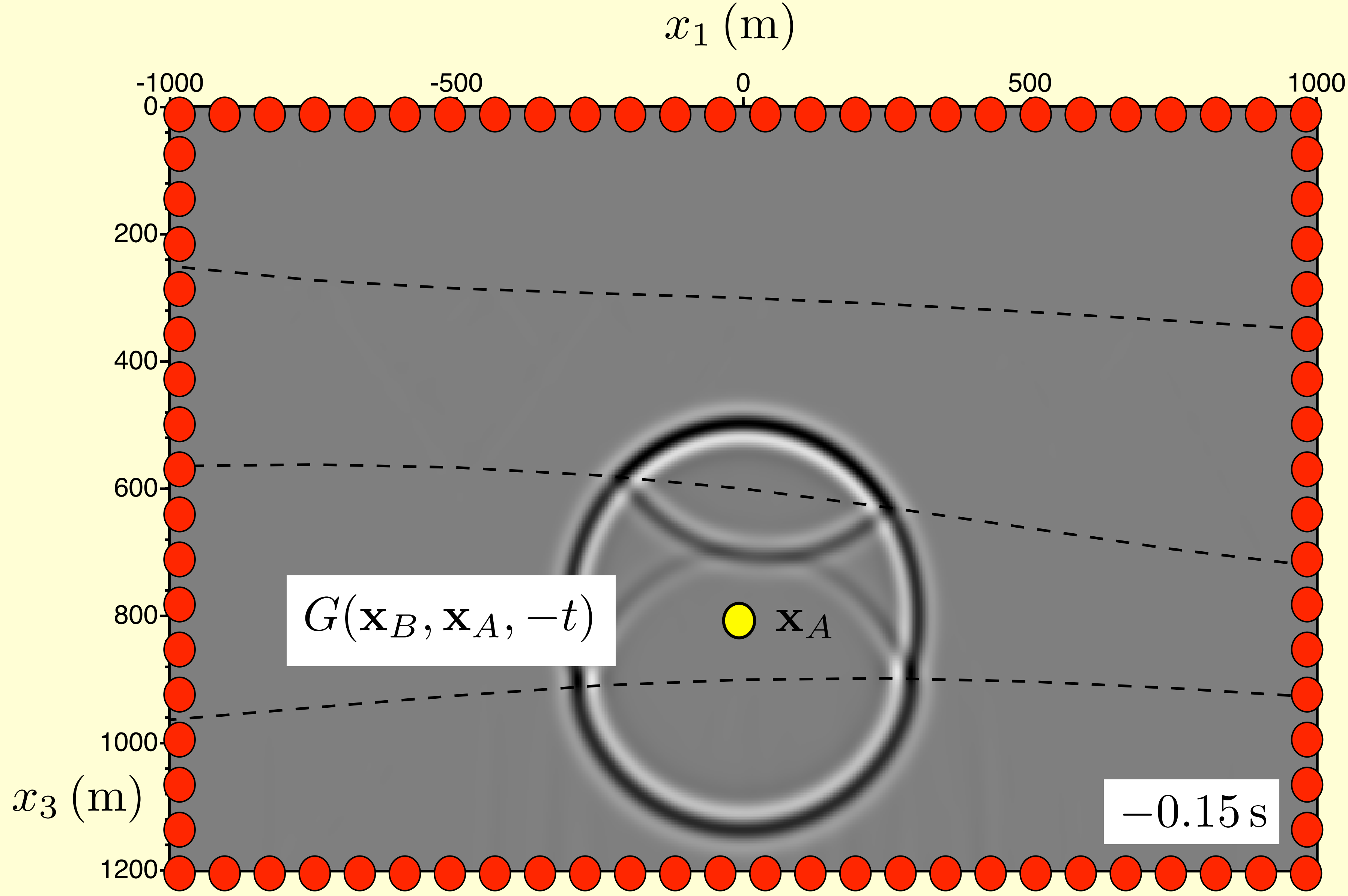

Omni-directional time-reversal experiment

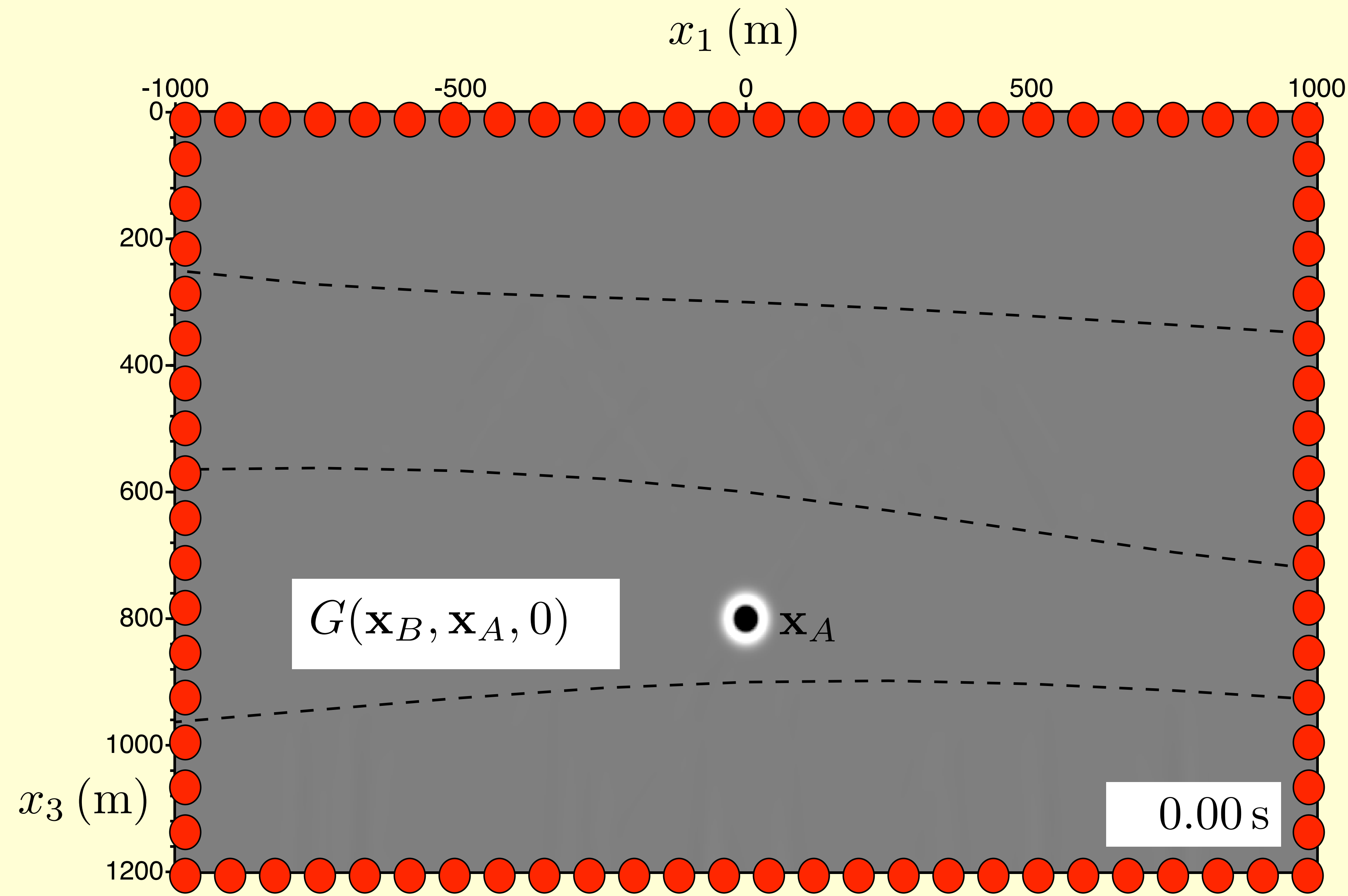

Omni-directional time-reversal experiment

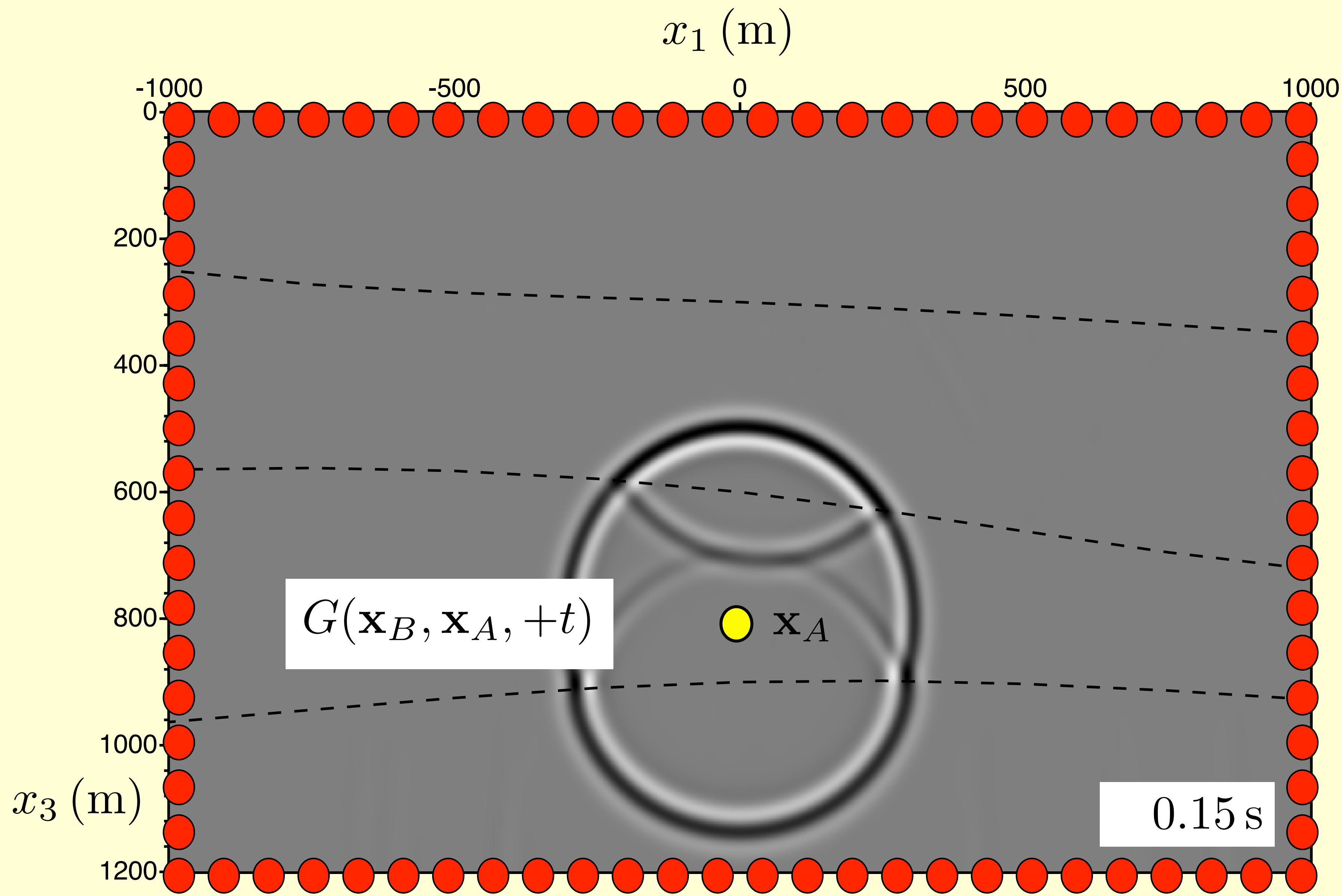

Omni-directional time-reversal experiment

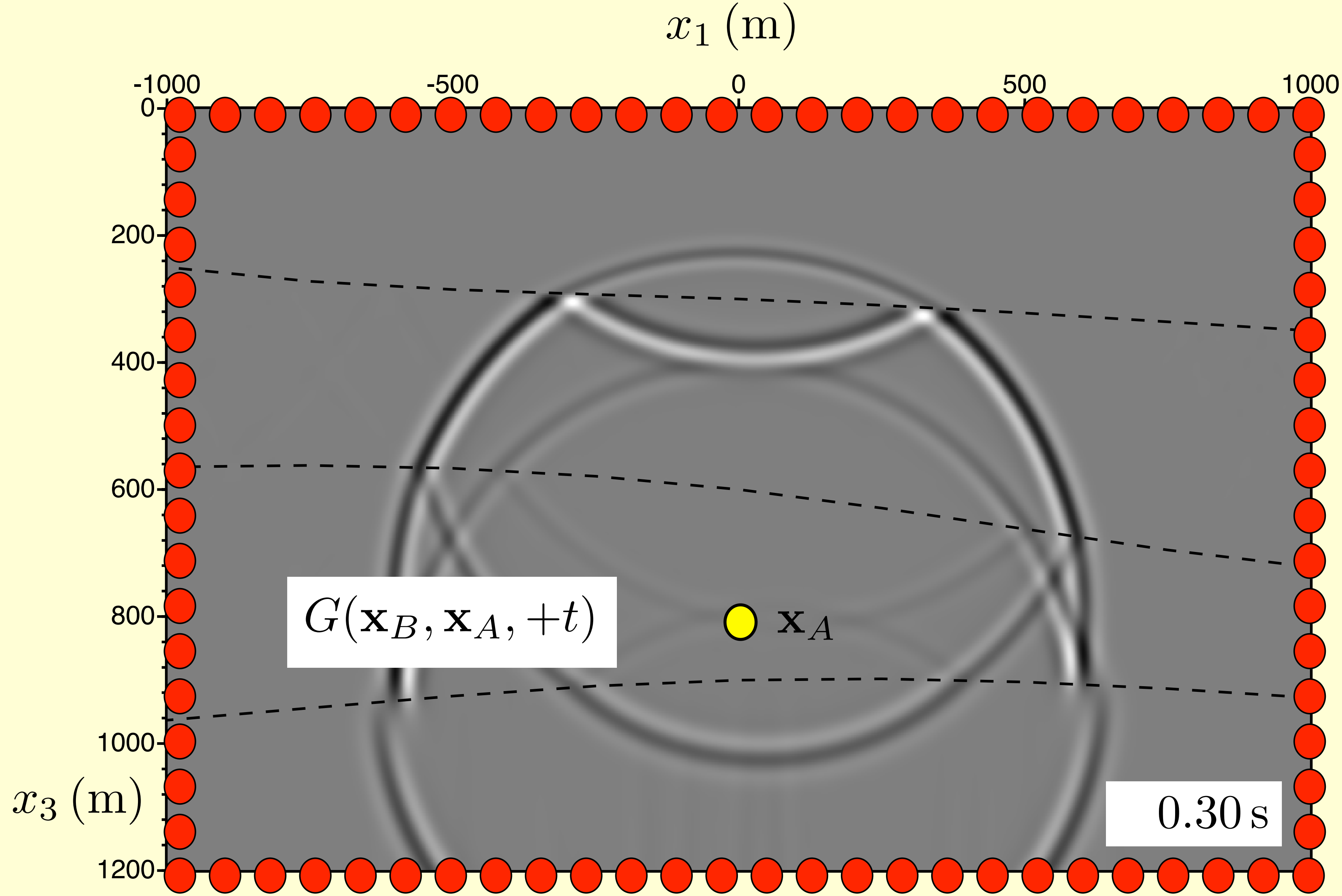

Omni-directional time-reversal experiment

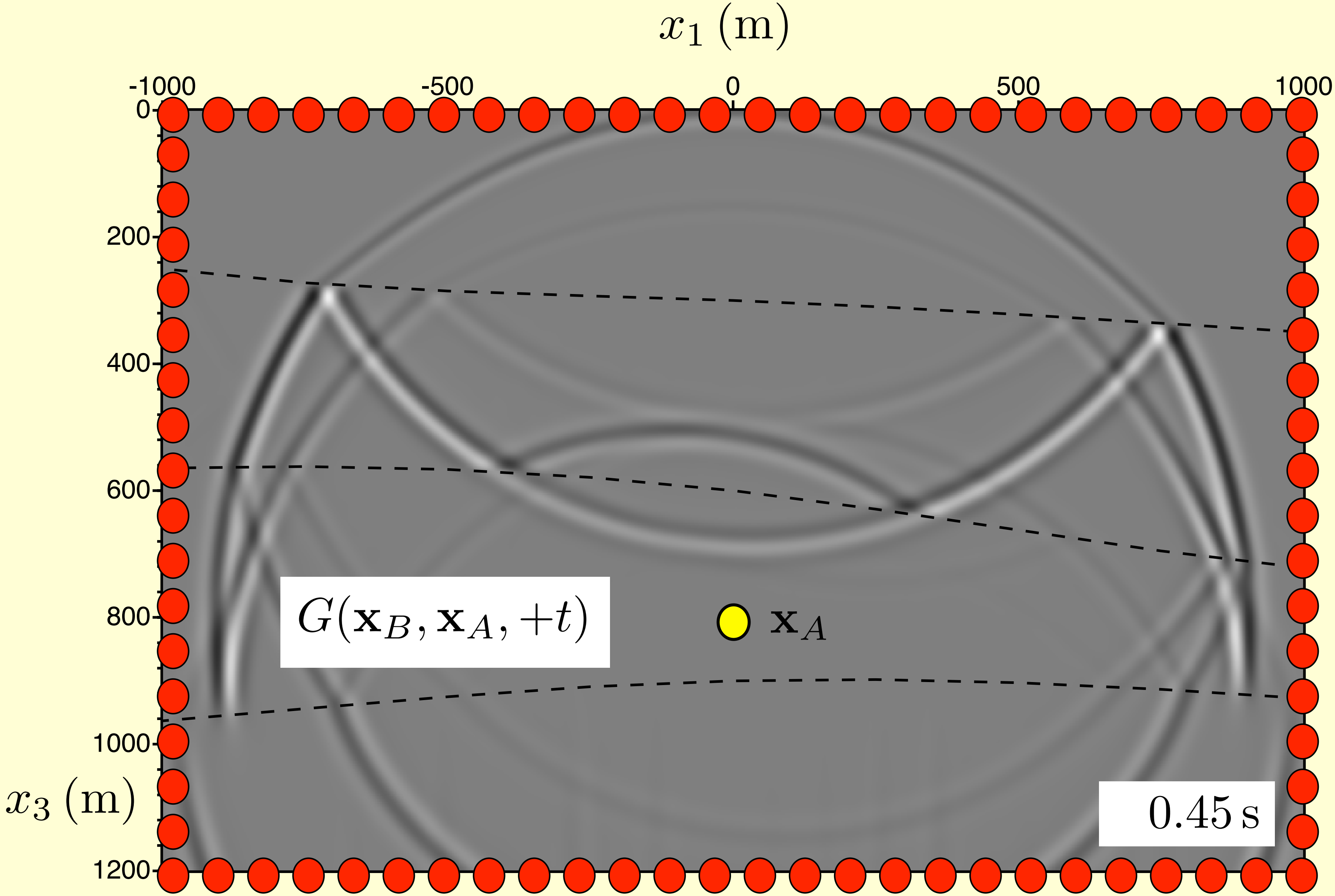

Omni-directional time-reversal experiment

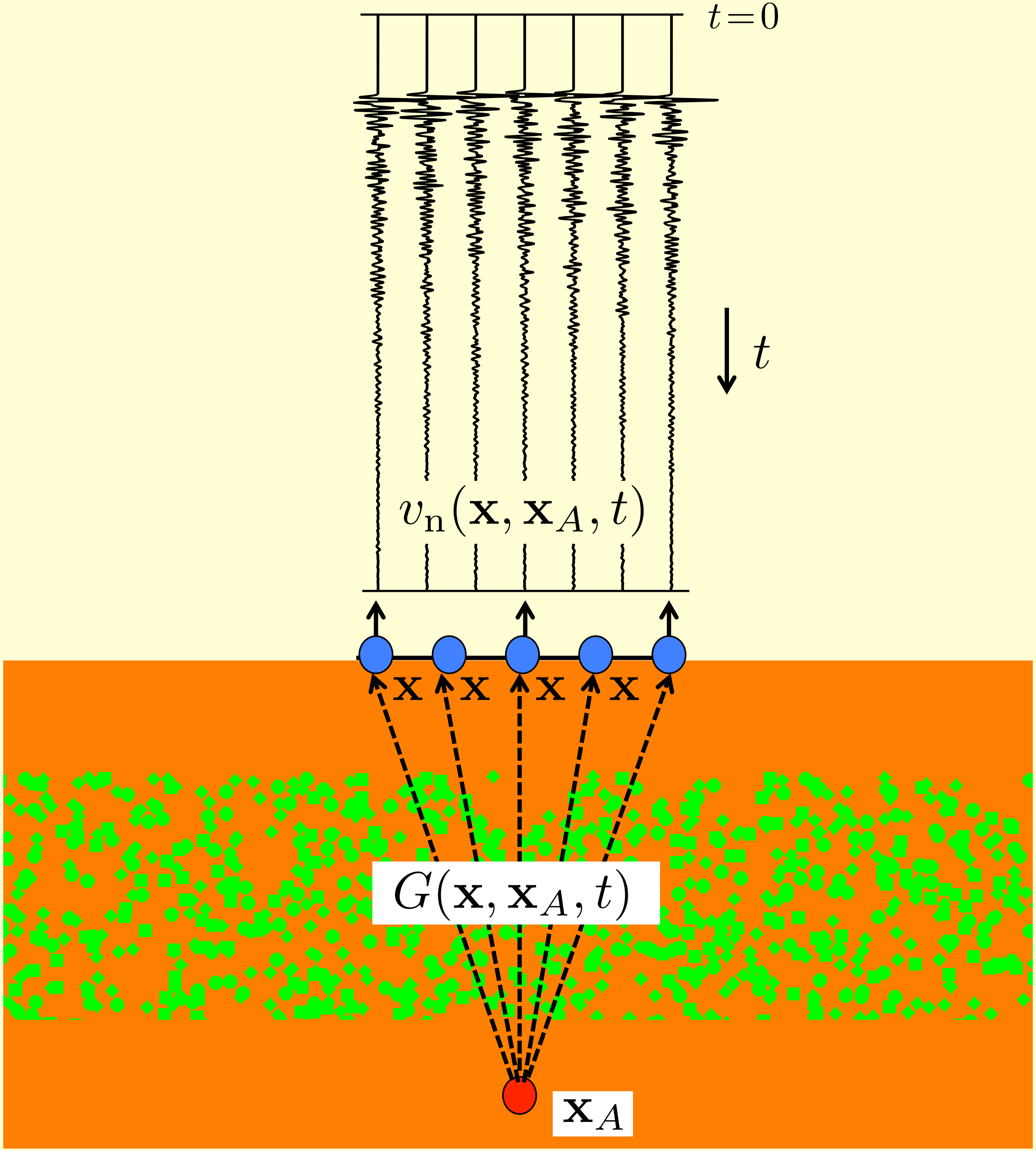

$t=0$
t
$v_\mathrm{n}(\mathbf{x},\mathbf{x}_A,t)$
$\mathbf{x}$ $\mathbf{x}$ $\mathbf{x}$ $\mathbf{x}$
$G(\mathbf{x},\mathbf{x}_A,t)$
$\mathbf{x}_A$

Fink et al.

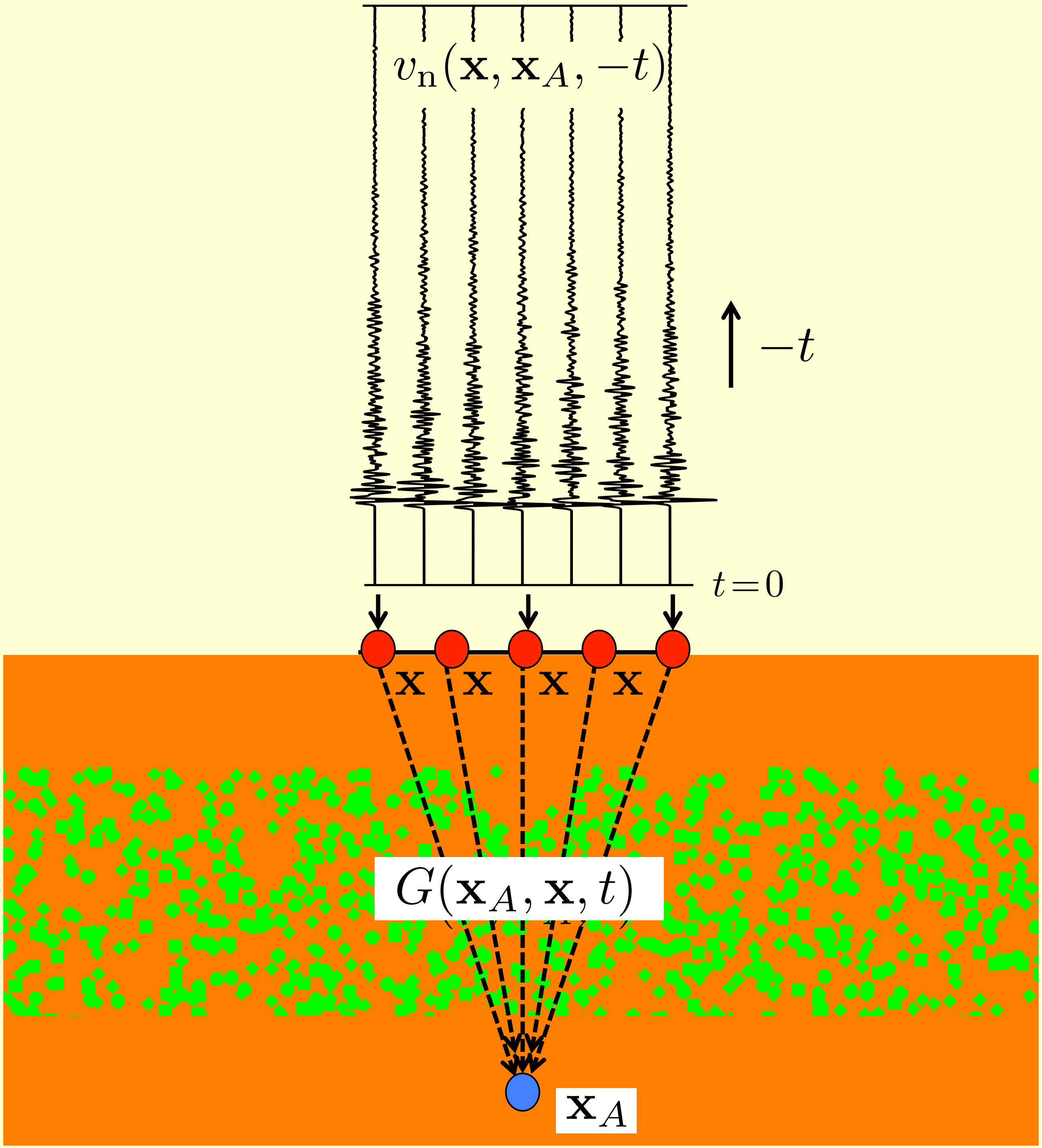
$v_{\mathrm{n}}(\mathbf{x}, \mathbf{x}_A, -t)$
$-t$
$t=0$
$\mathbf{x}$ $\mathbf{x}$ $\mathbf{x}$ $\mathbf{x}$
$G(\mathbf{x}_A, \mathbf{x}, t)$
$\mathbf{x}_A$

Fink et al.

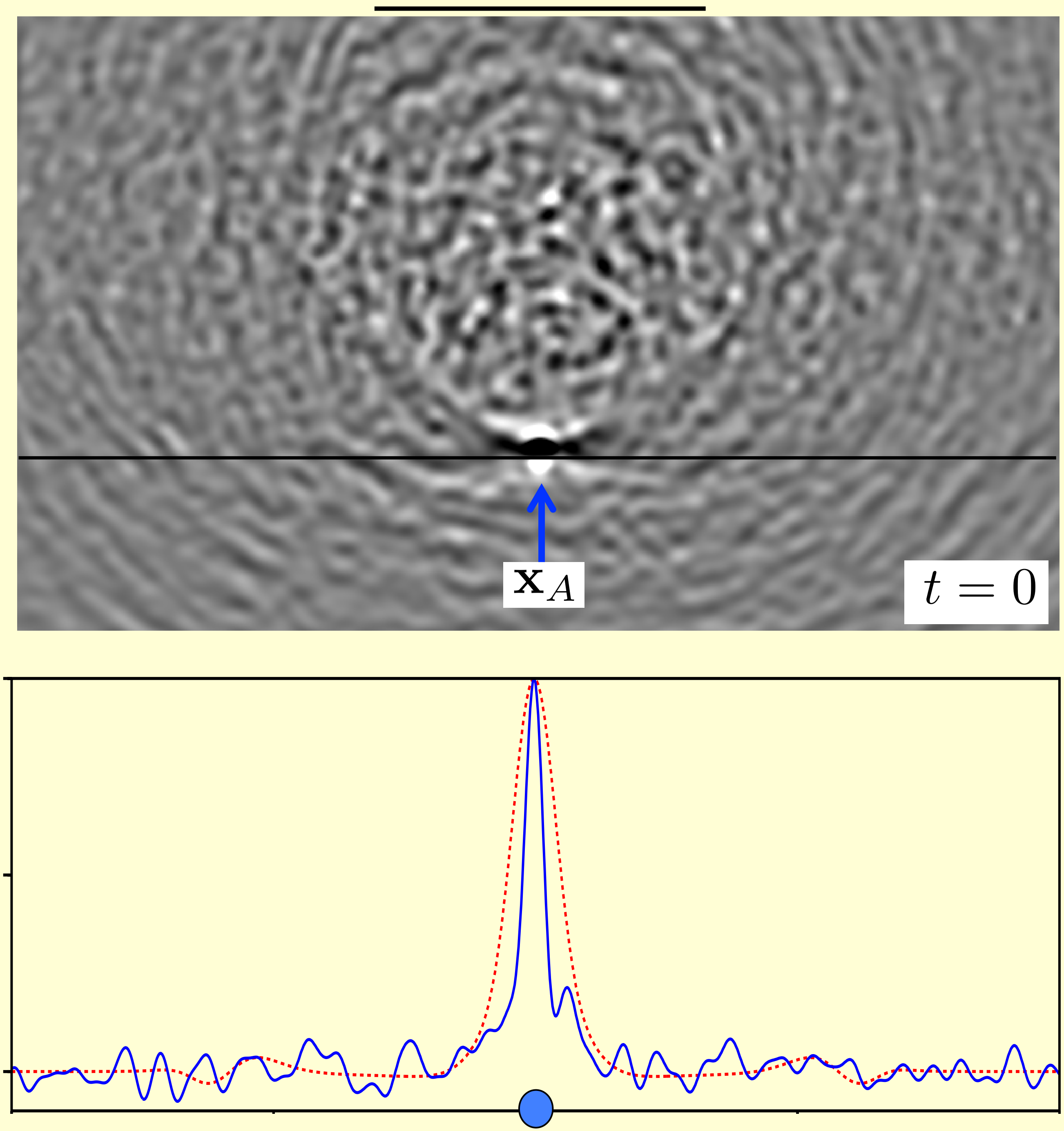

Fink et al.

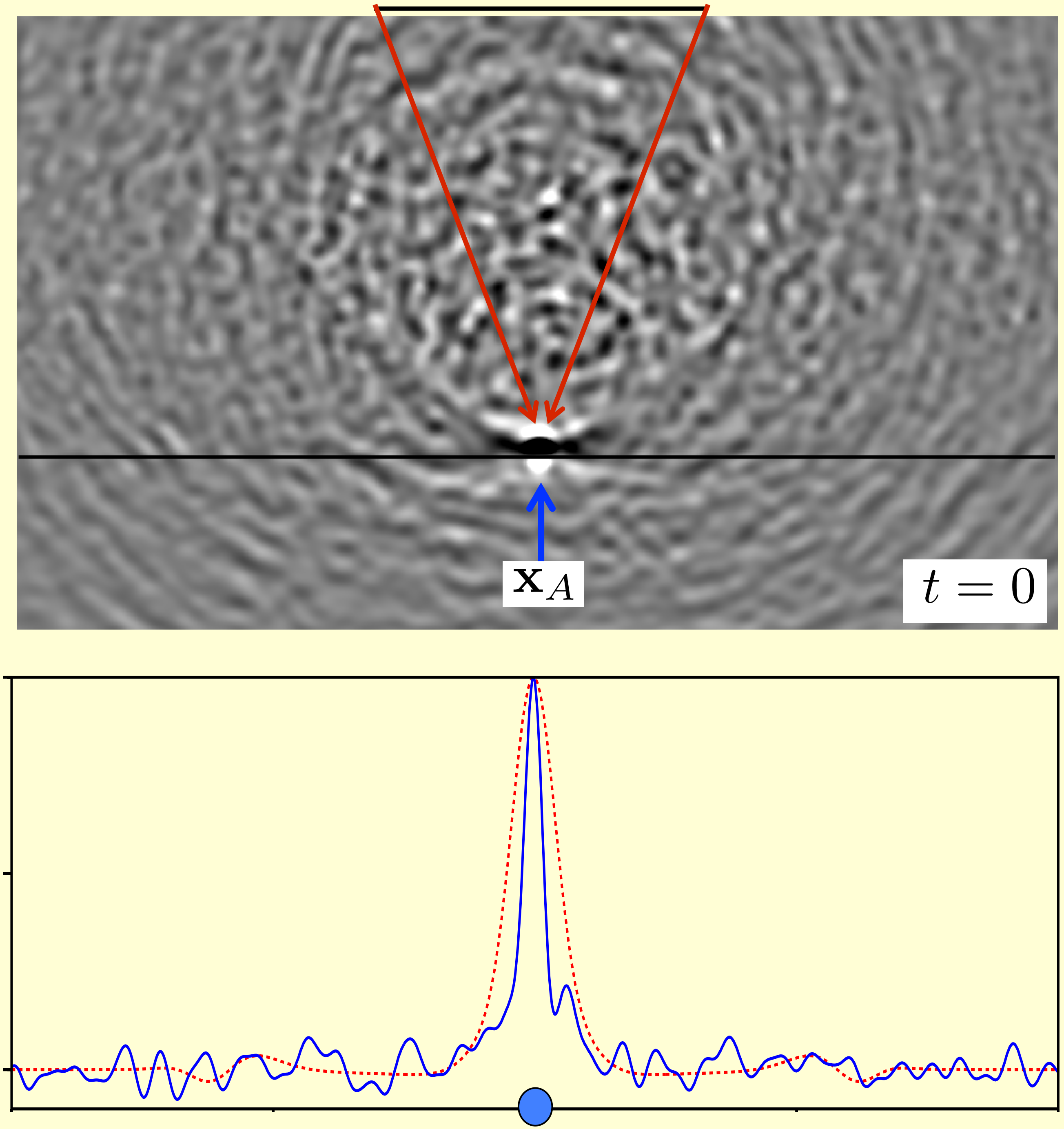

Fink et al.

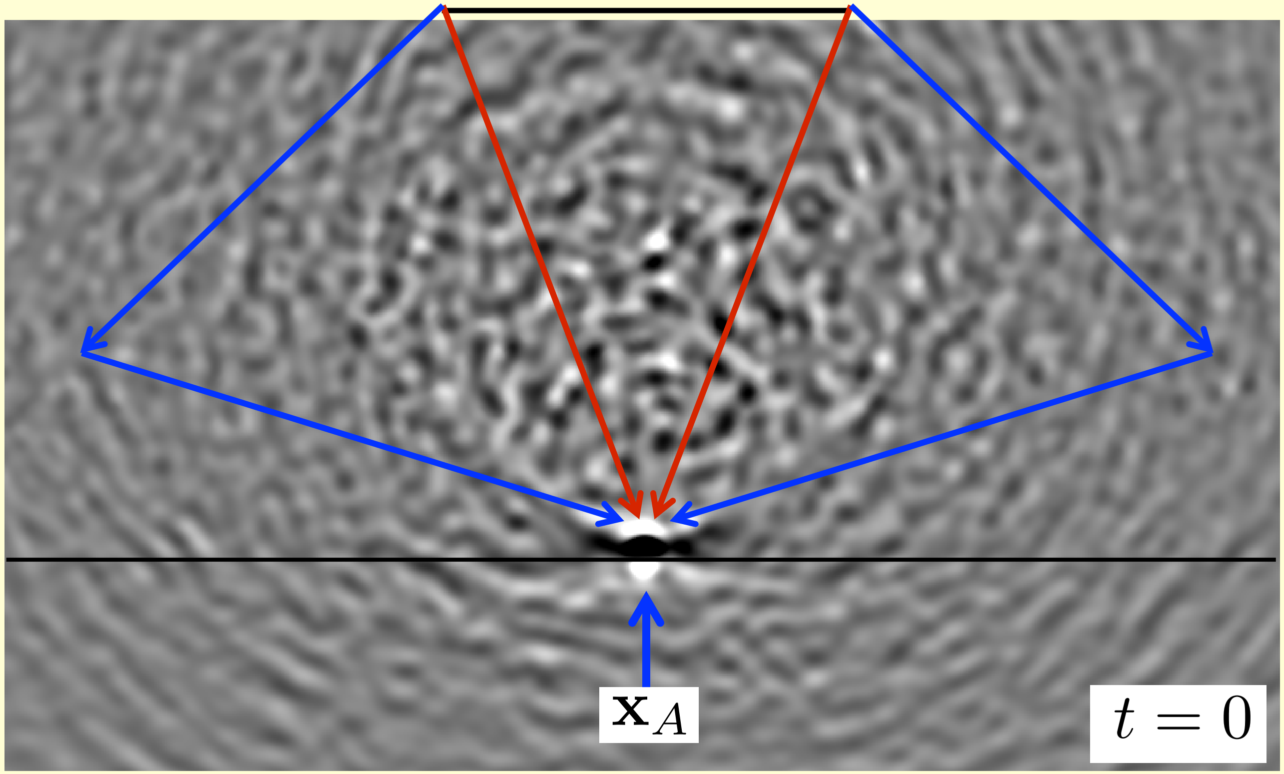

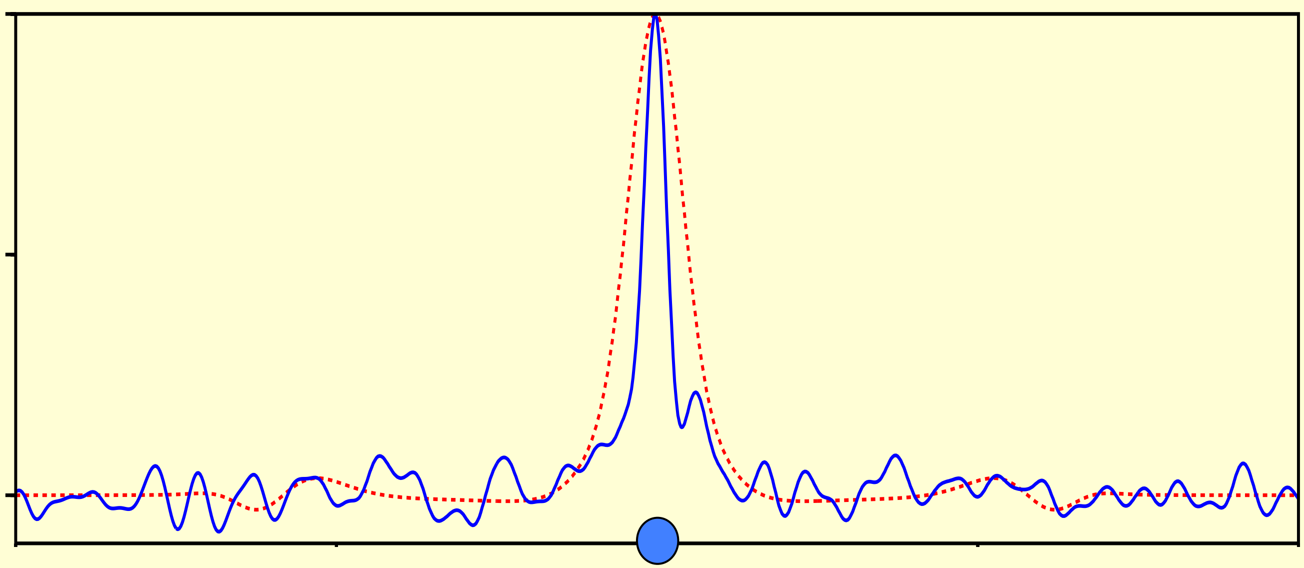

Fink et al.

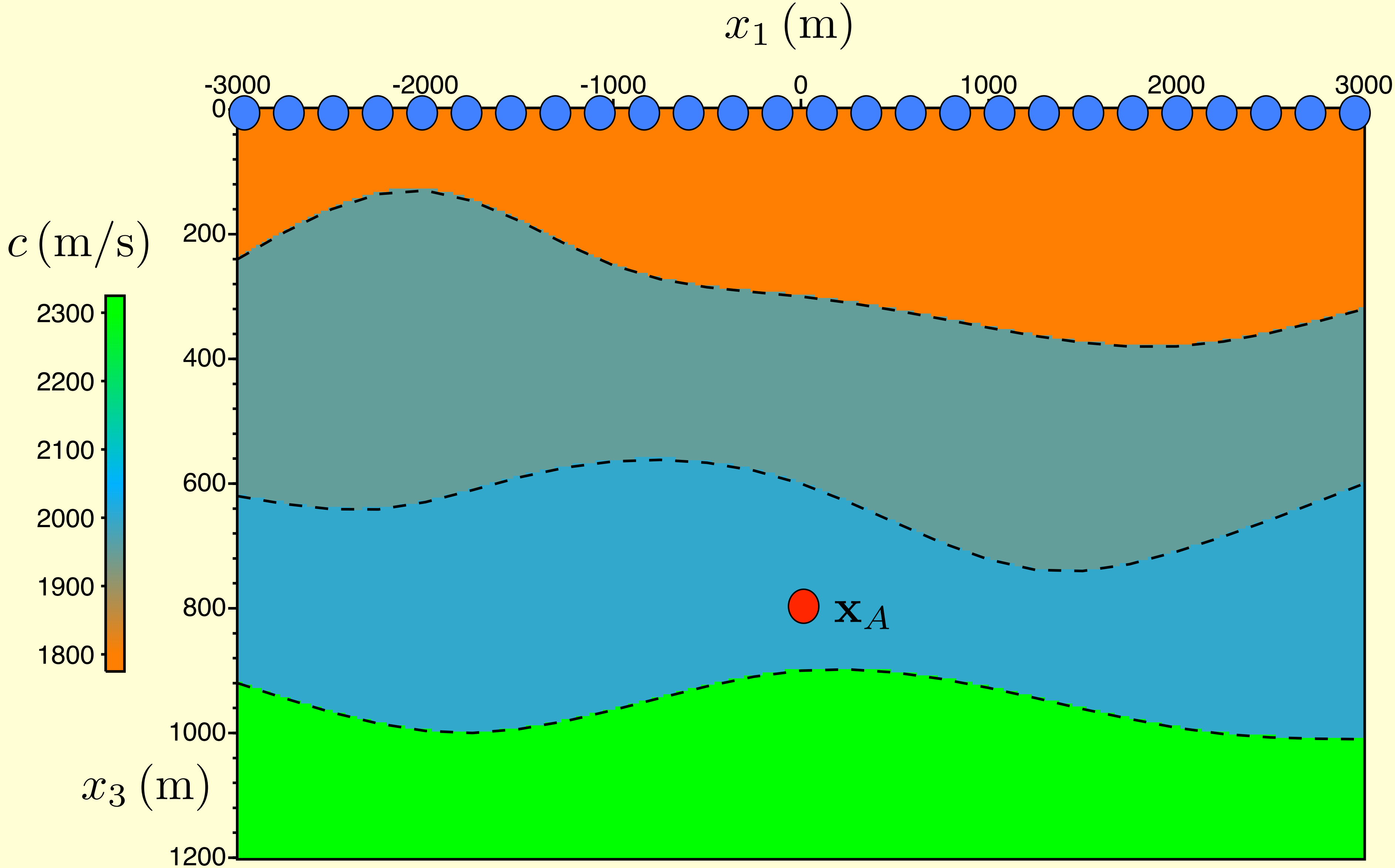

Single-sided time-reversal experiment

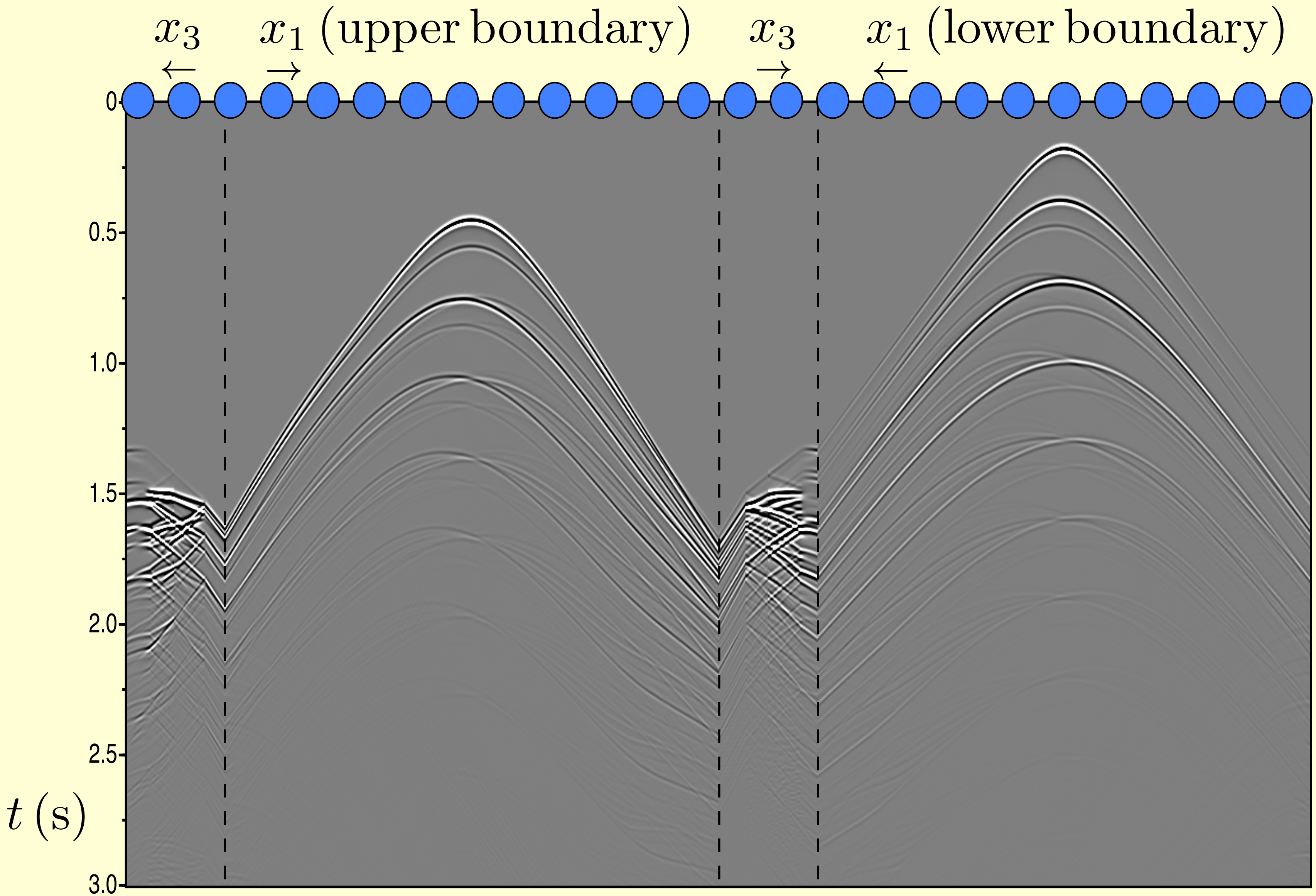

Single-sided time-reversal experiment

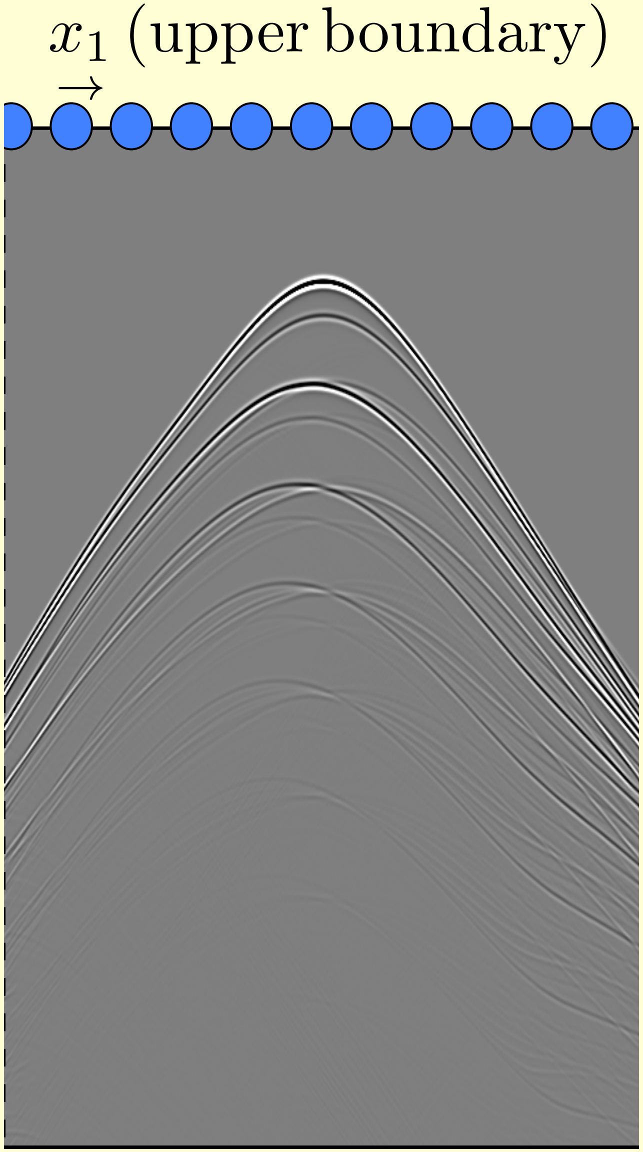

Single-sided time-reversal experiment

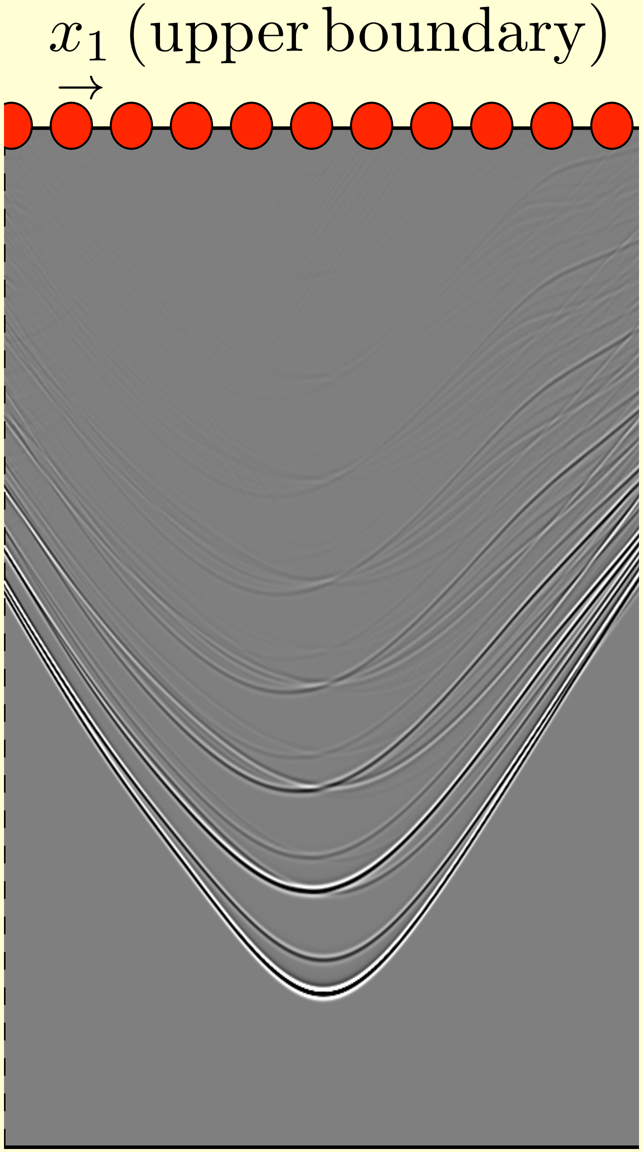

Single-sided time-reversal experiment

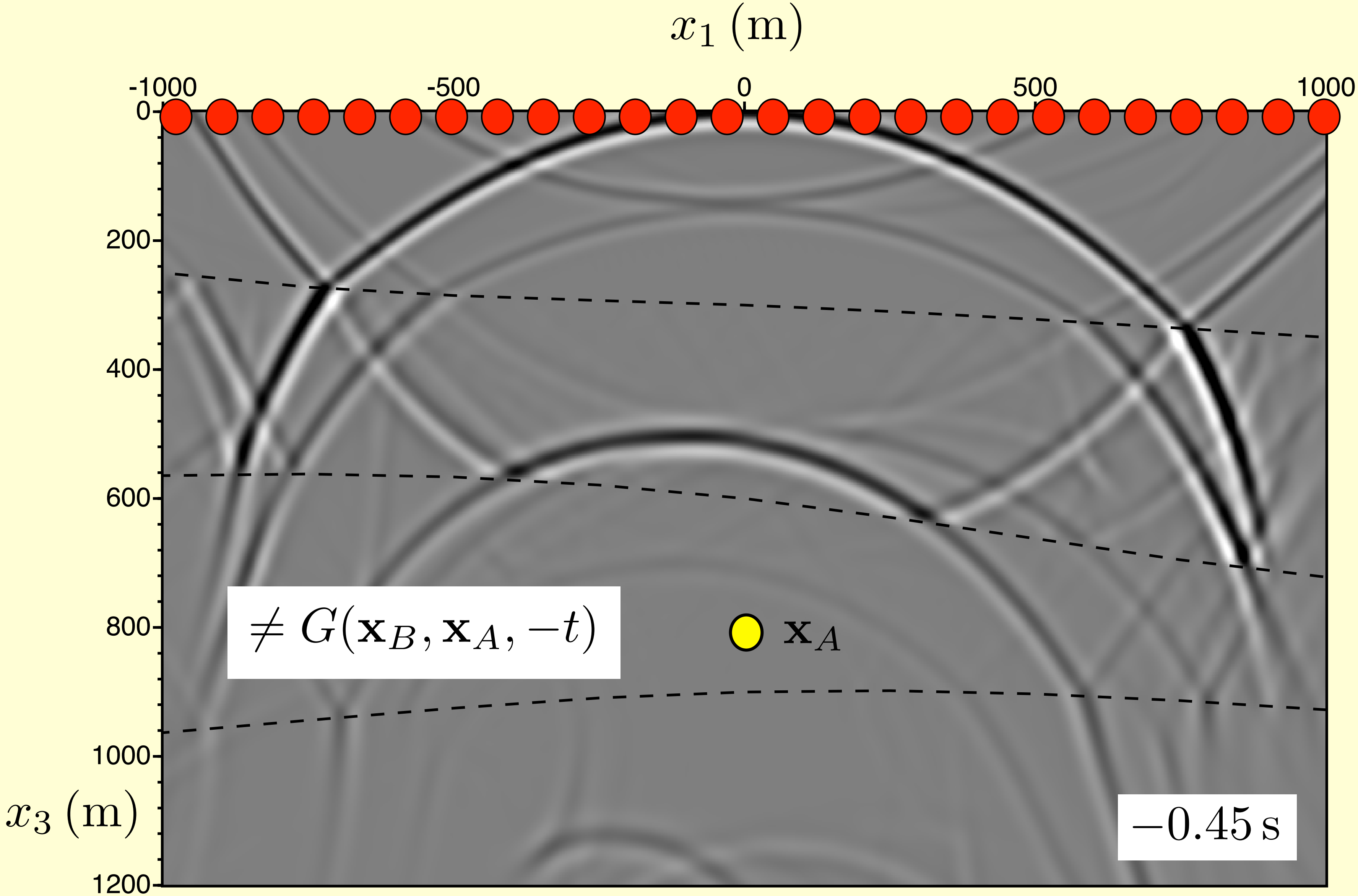

Single-sided time-reversal experiment

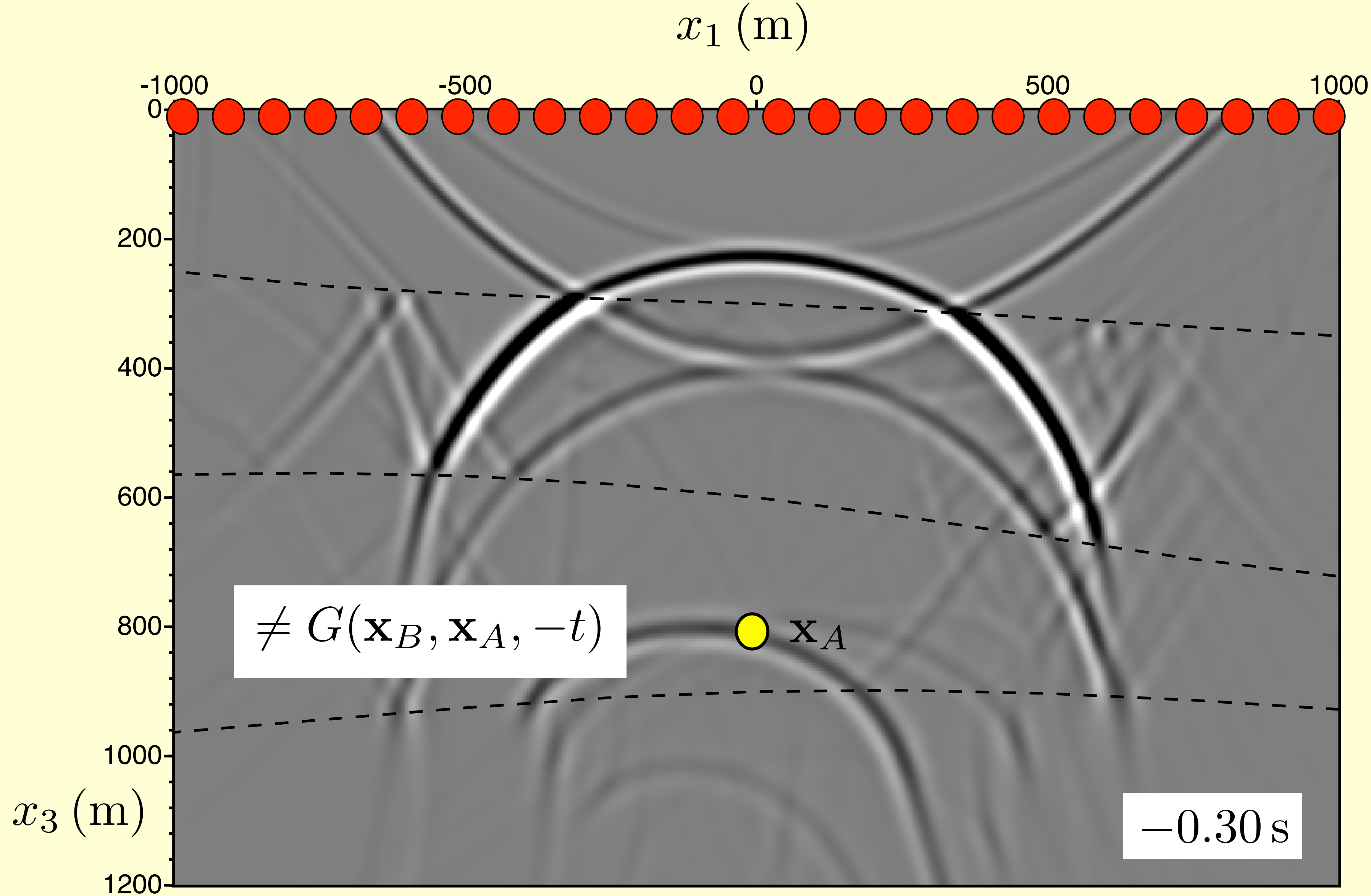

Single-sided time-reversal experiment

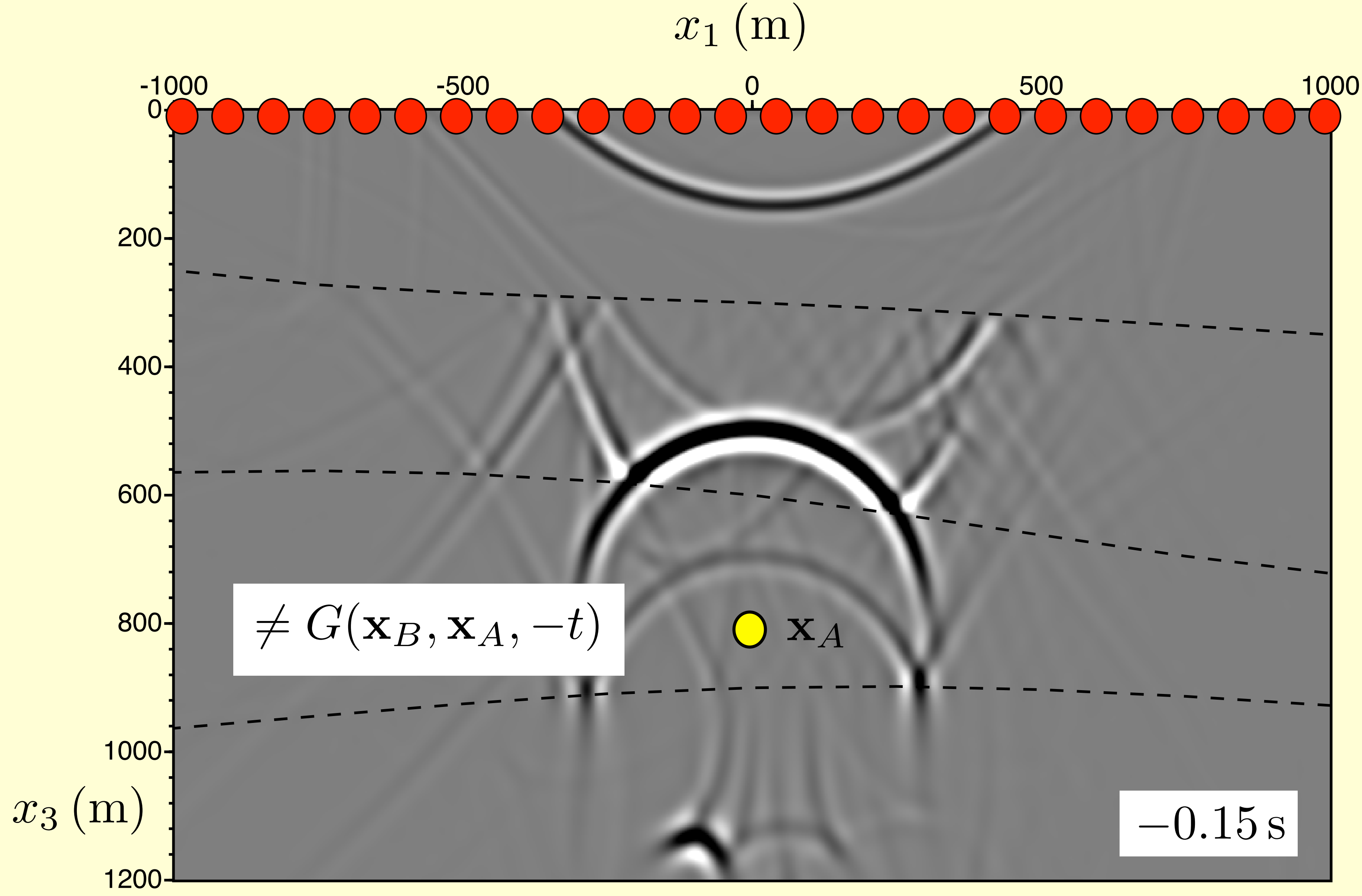

Single-sided time-reversal experiment

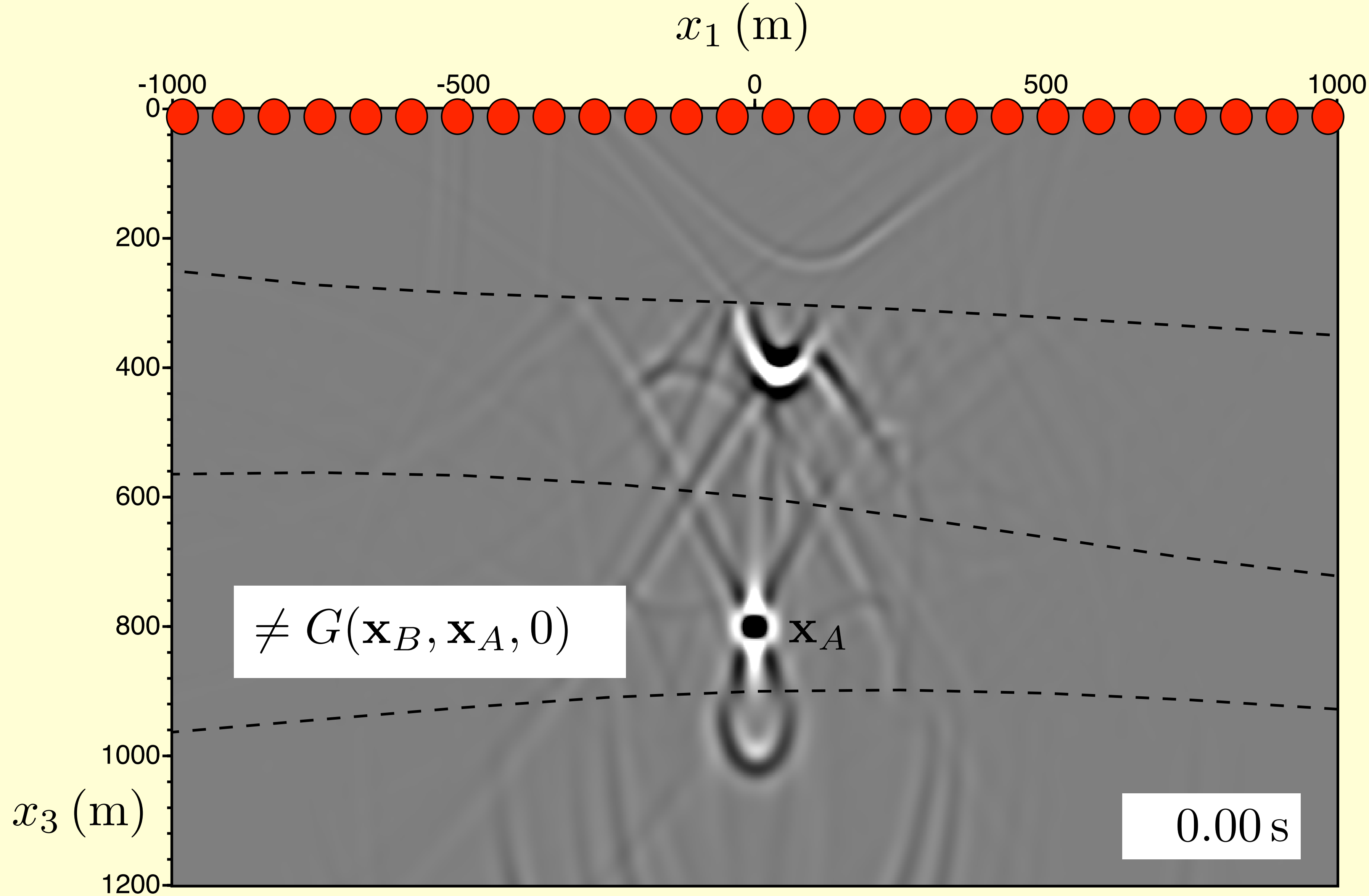

Single-sided time-reversal experiment

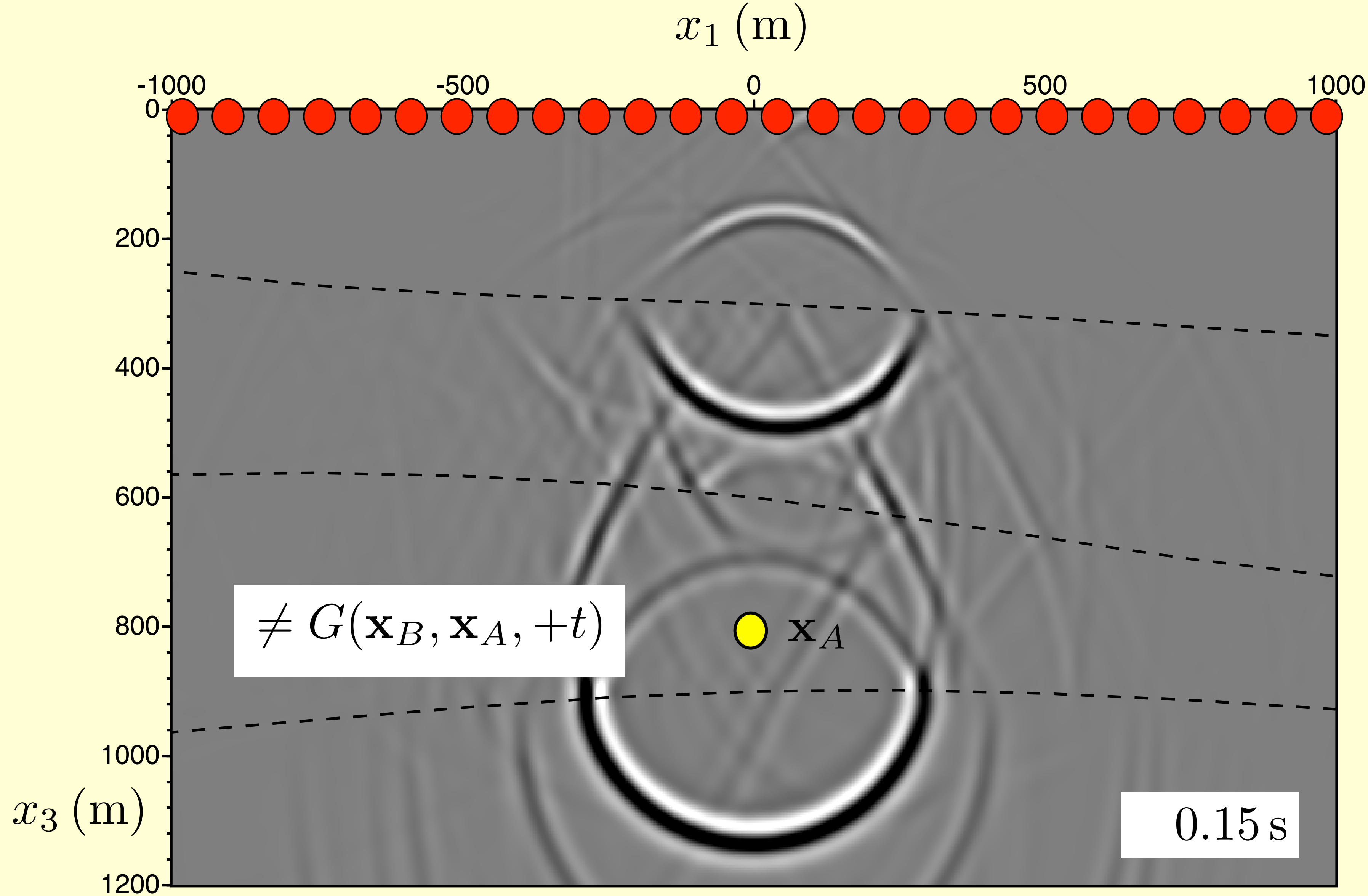

Single-sided time-reversal experiment

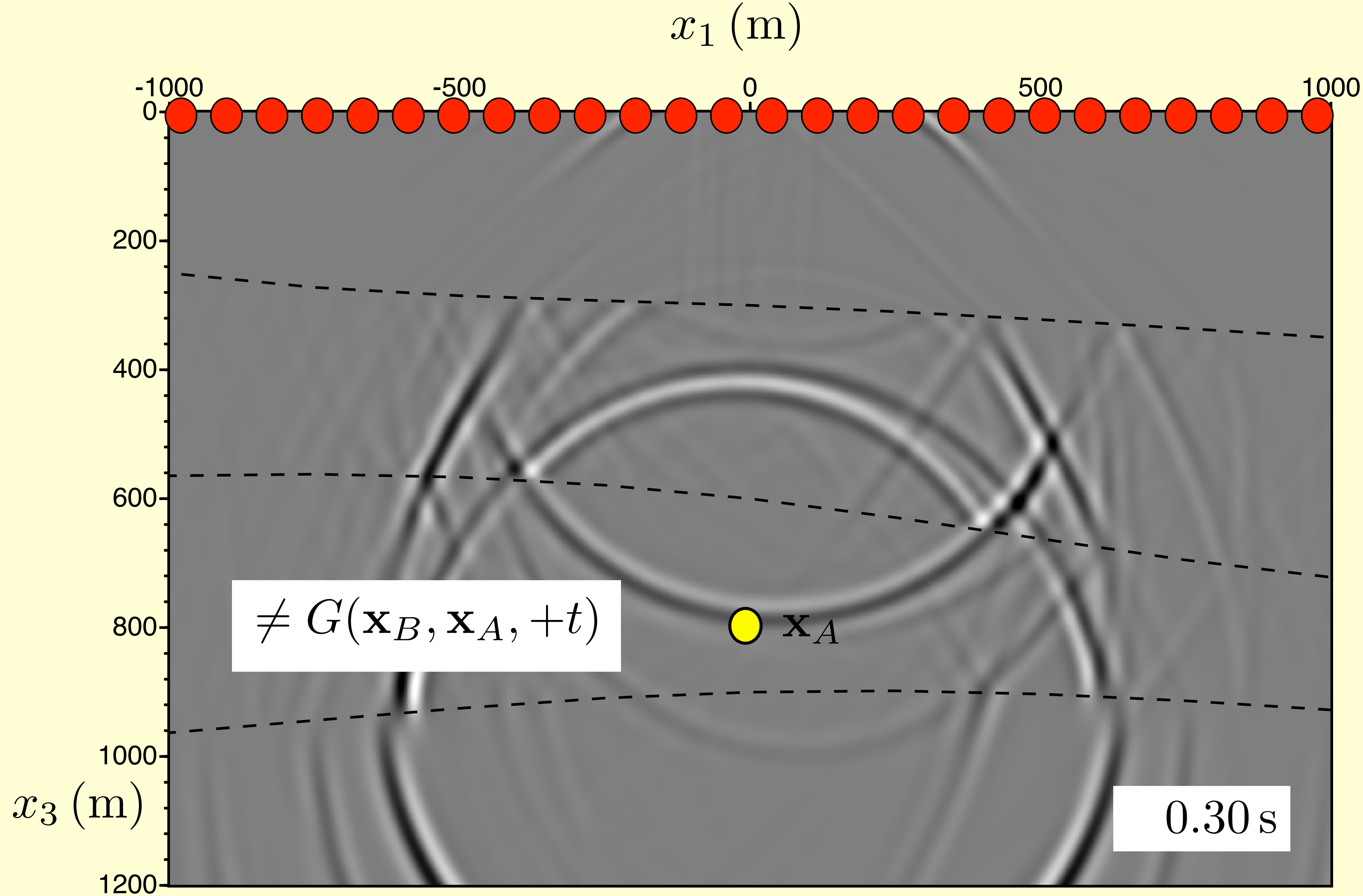

Single-sided time-reversal experiment

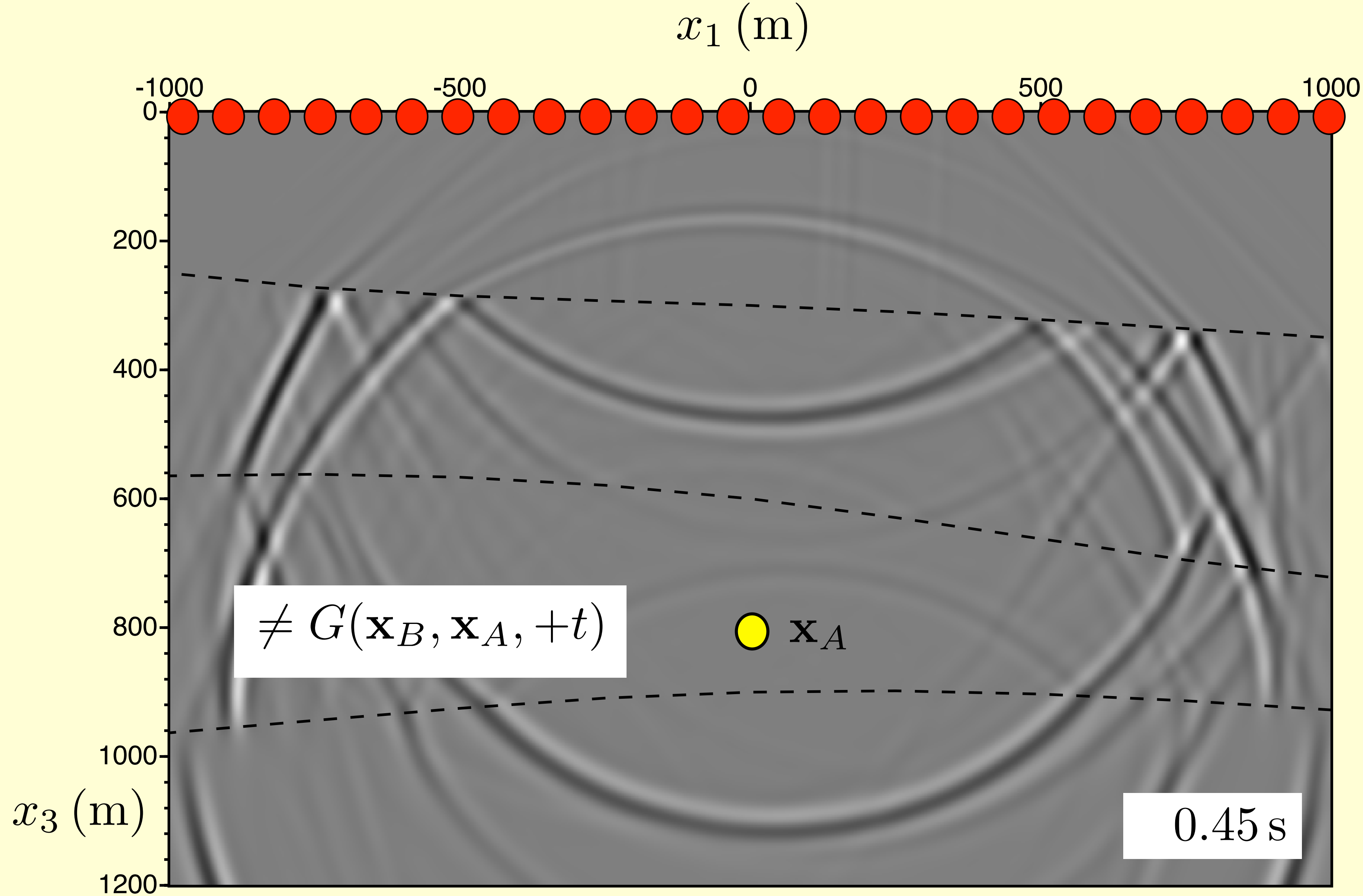

Single-sided time-reversal experiment

Possible solutions:

Iterative time-reversal

(Prada, Wu and Fink, 1991, JASA; Montaldo et al., IEEE, 2005)

Characteristics:

- Physical re-emission (e.g. ultrasonic applications)
- Focuses on strong scatterer, or
- Uses measured transmission response

Iterative Marchenko method

(Broggini and Snieder, 2012, EJP; Wapenaar et al., PRL, 2013)

Characteristics:

- Numerical re-emission (e.g. seismic applications)
- Derives focusing function from reflection response
- Uses estimate of direct arrival of transmission response

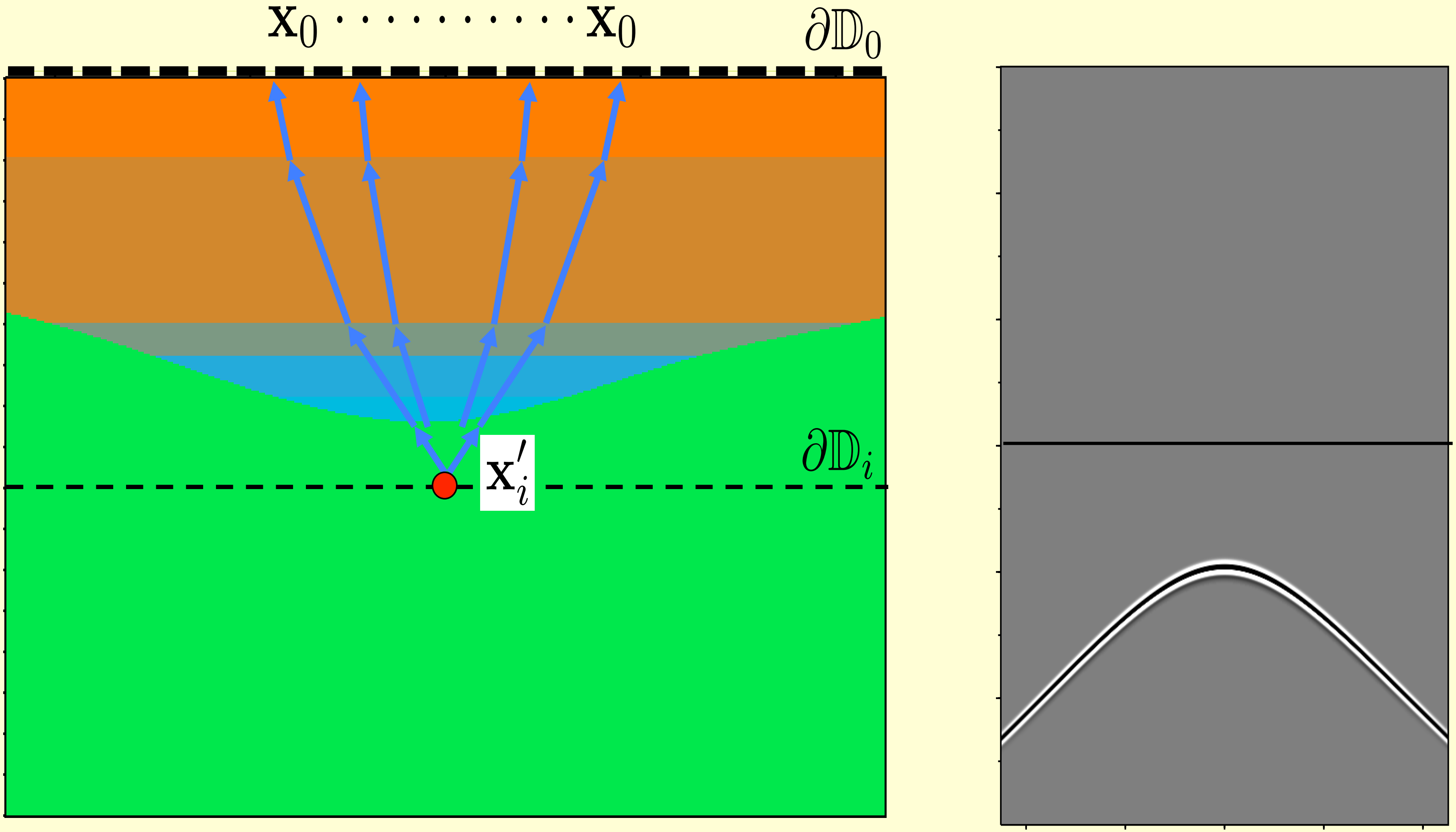

Introduction of the focusing function

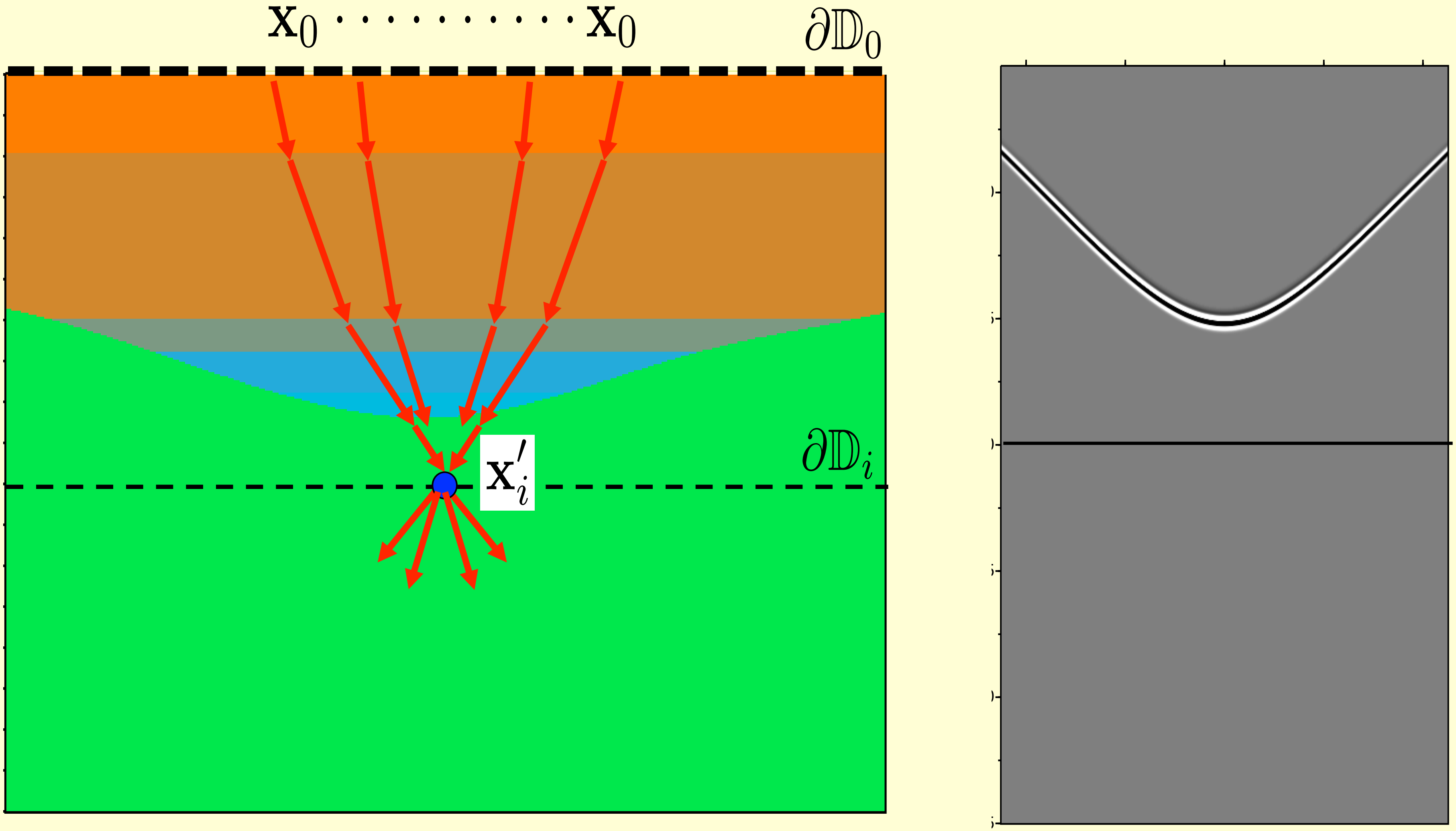

Introduction of the focusing function

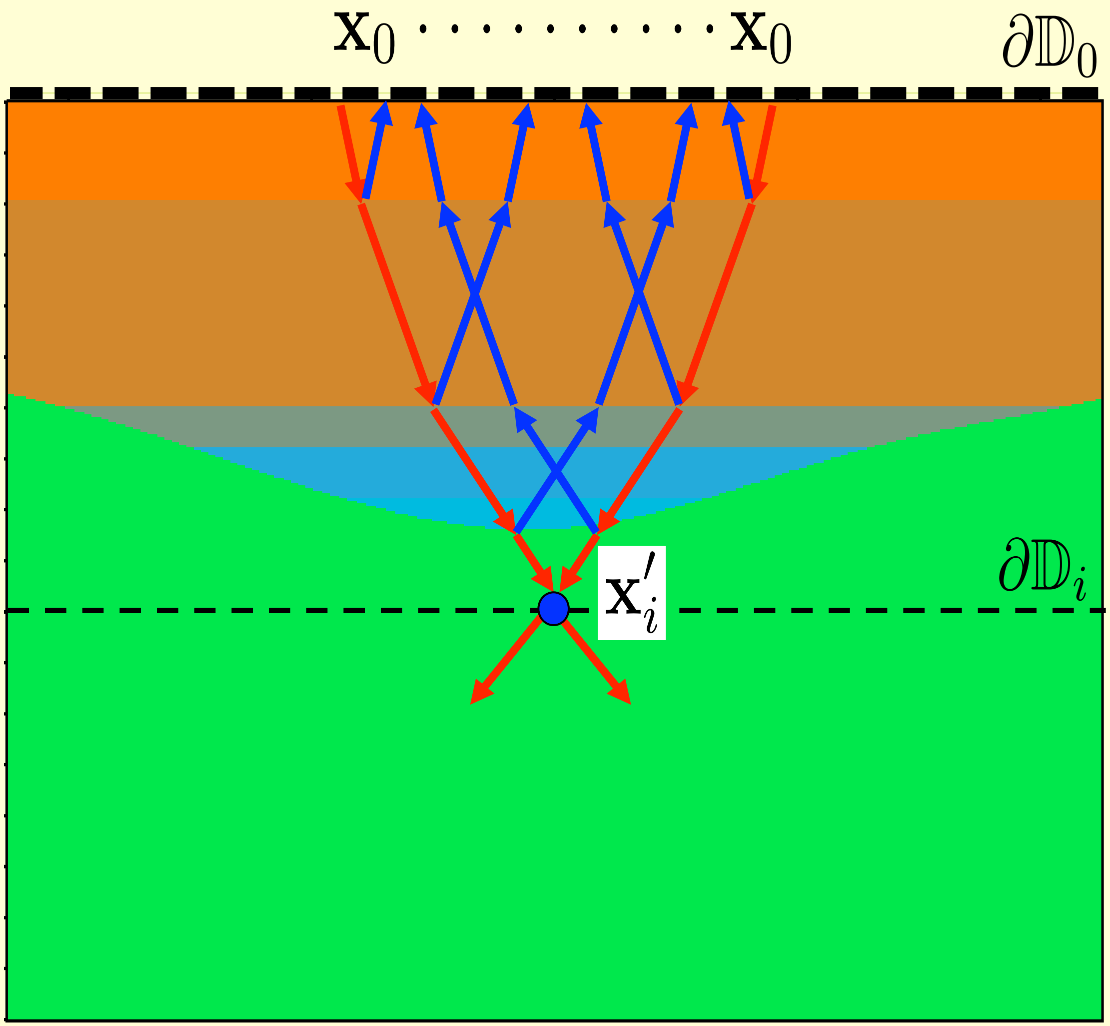

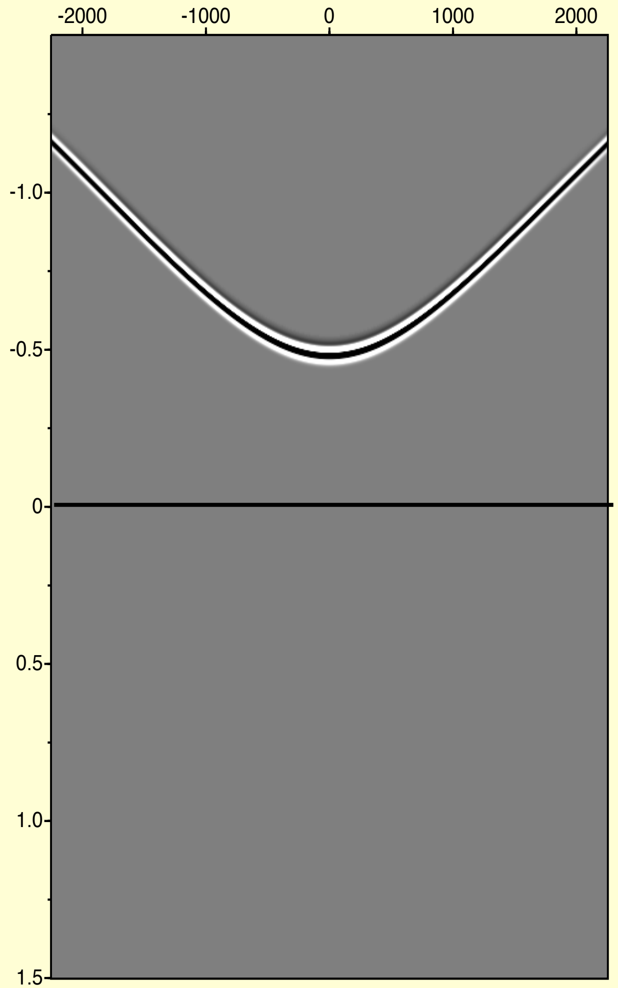

Introduction of the focusing function

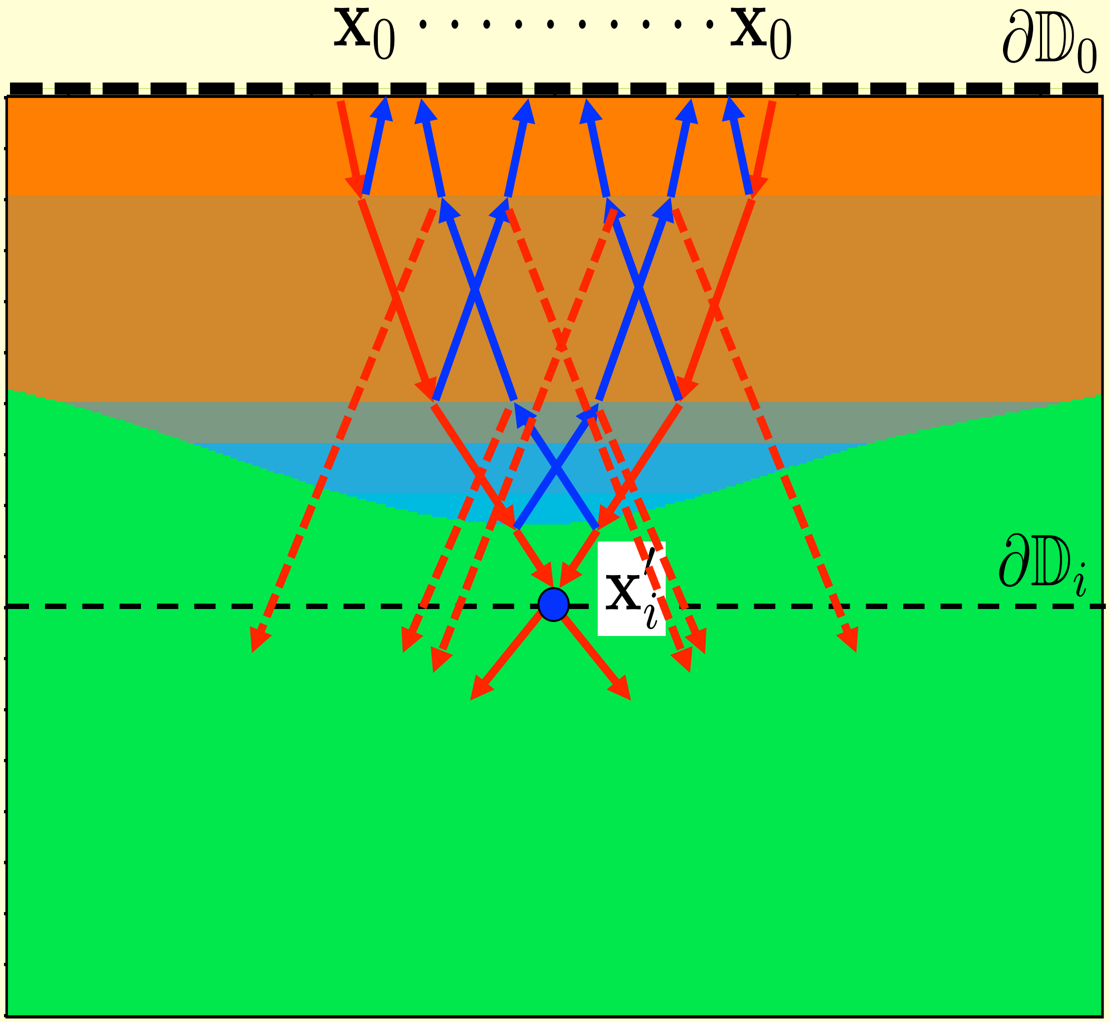

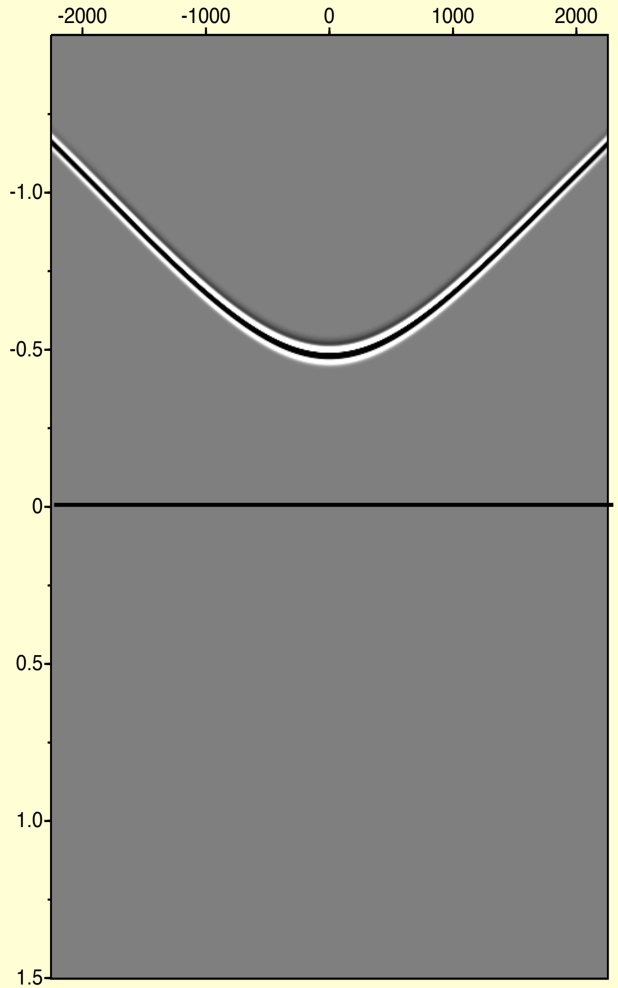

Introduction of the focusing function

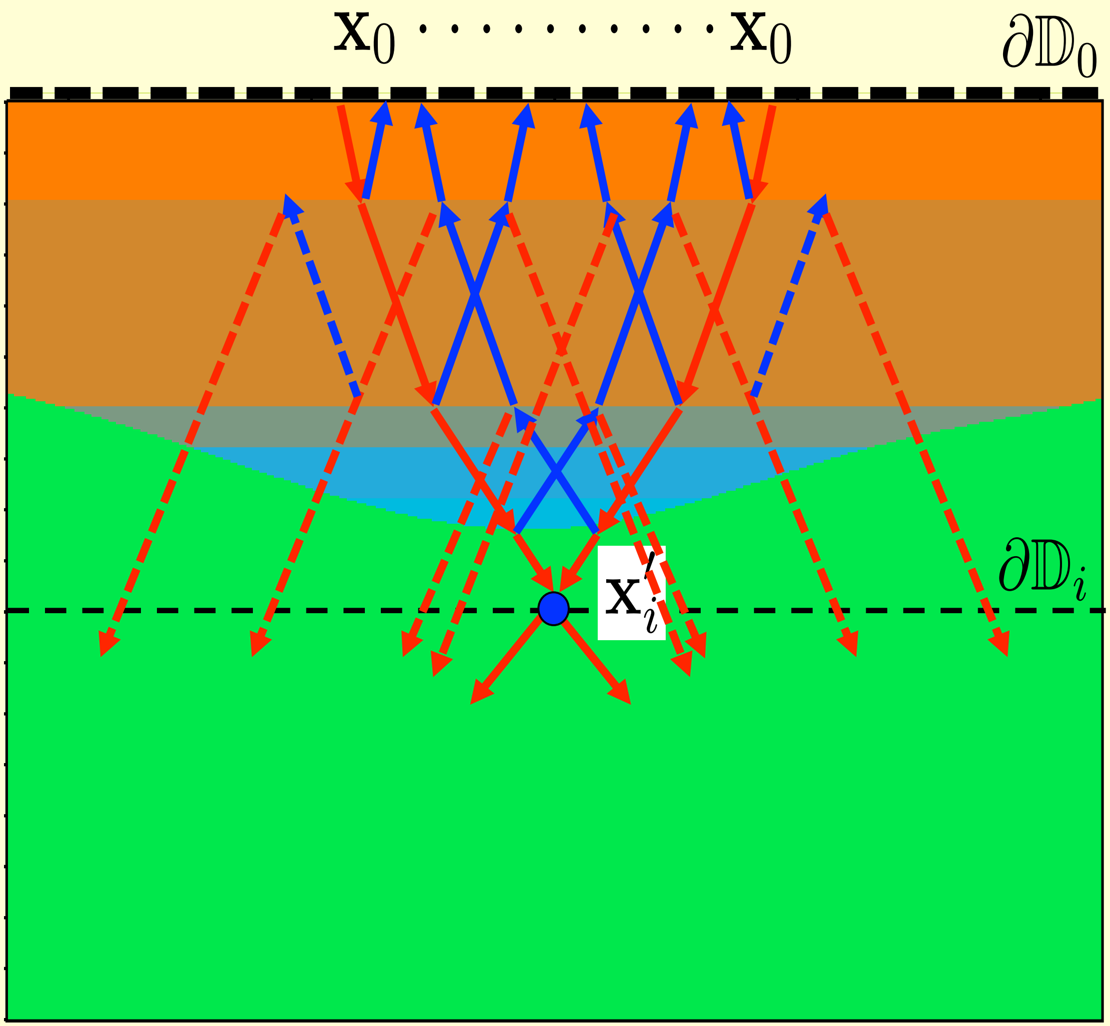

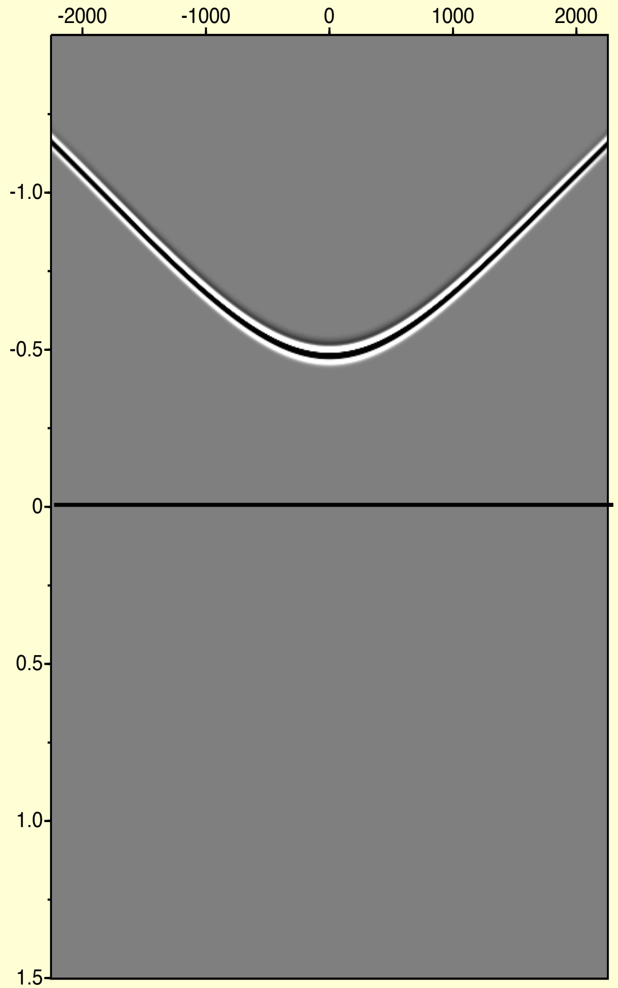

Introduction of the focusing function

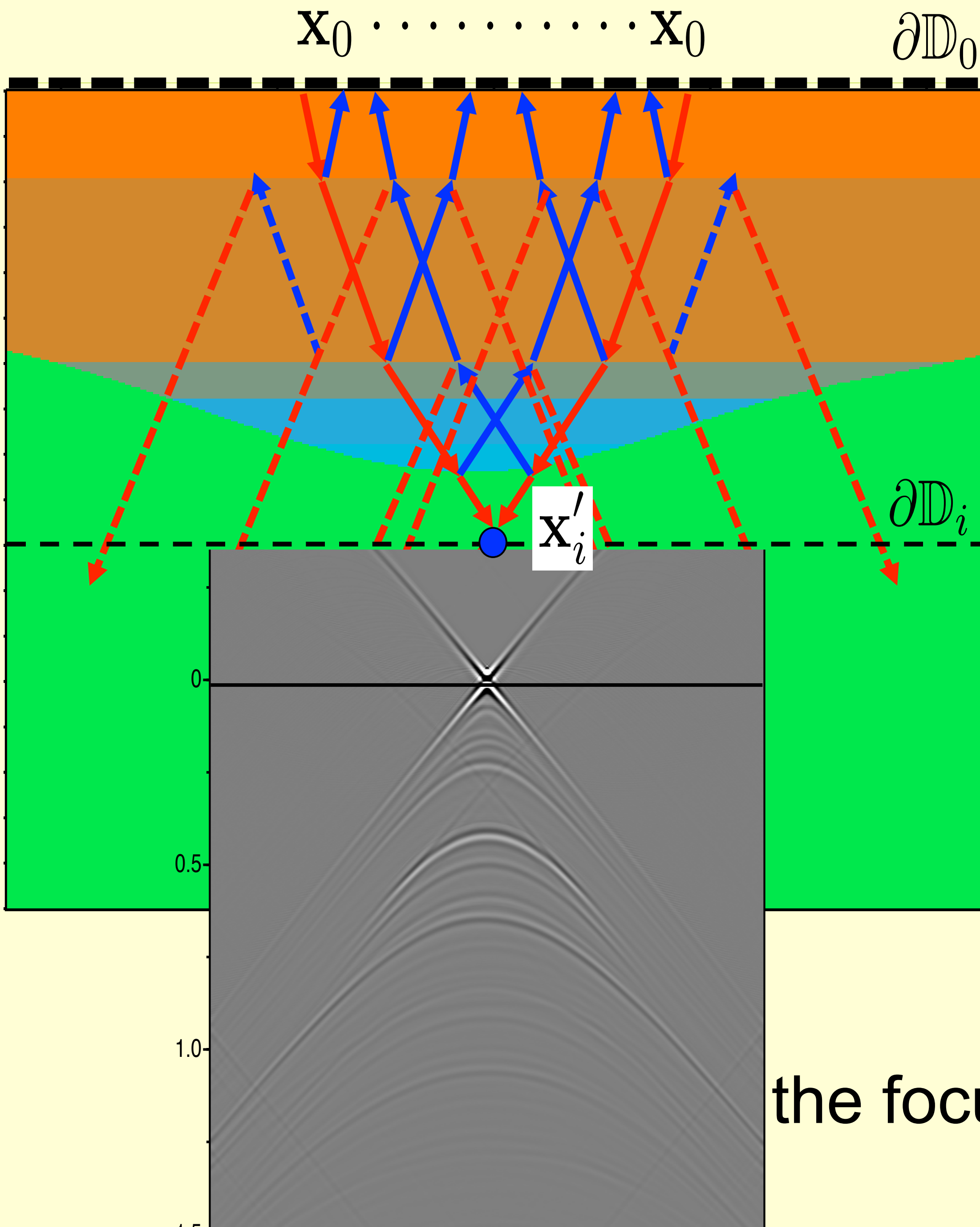

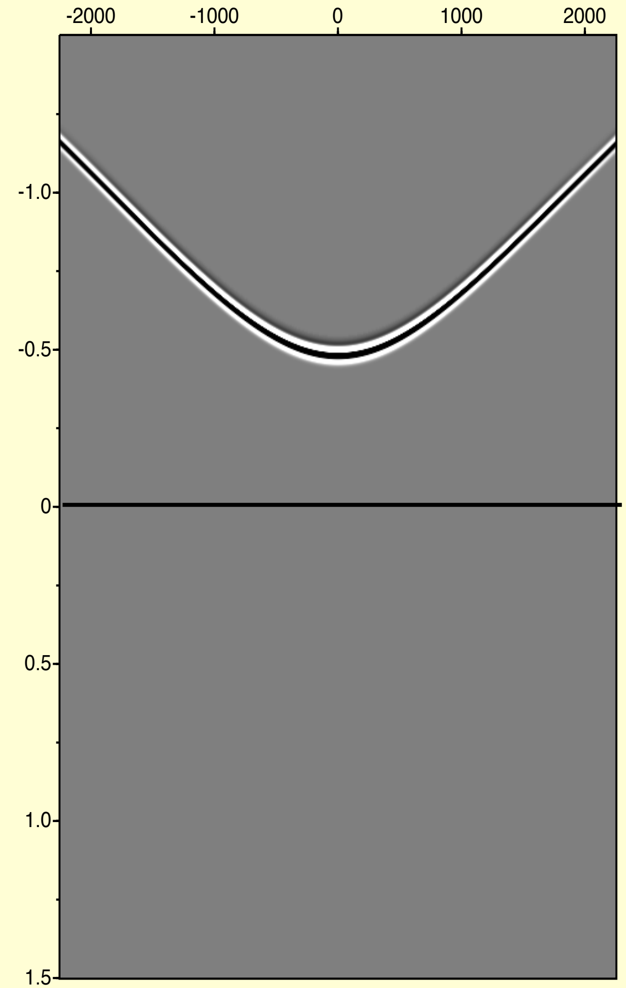

the focusing function

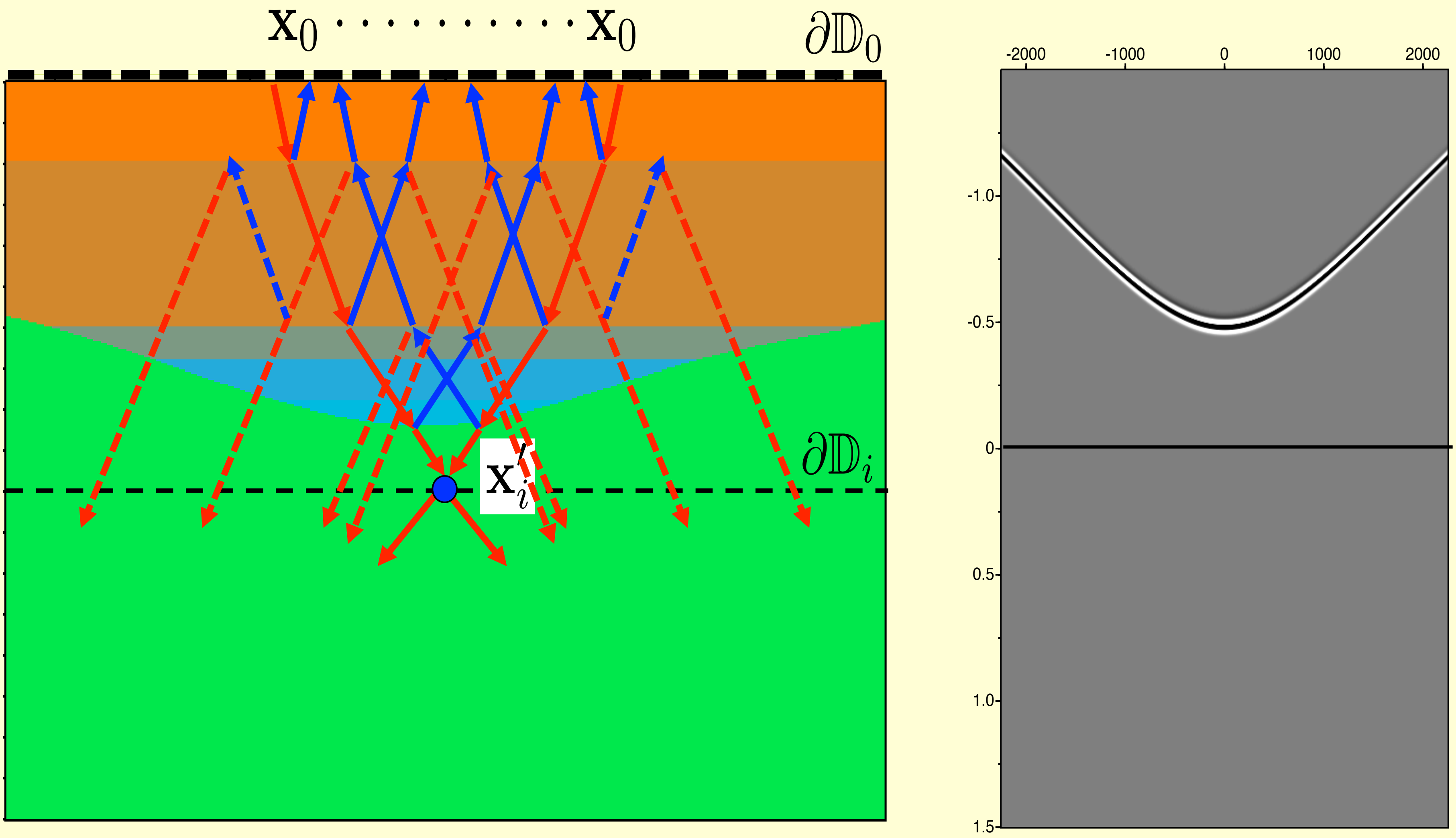

Introduction of the focusing function

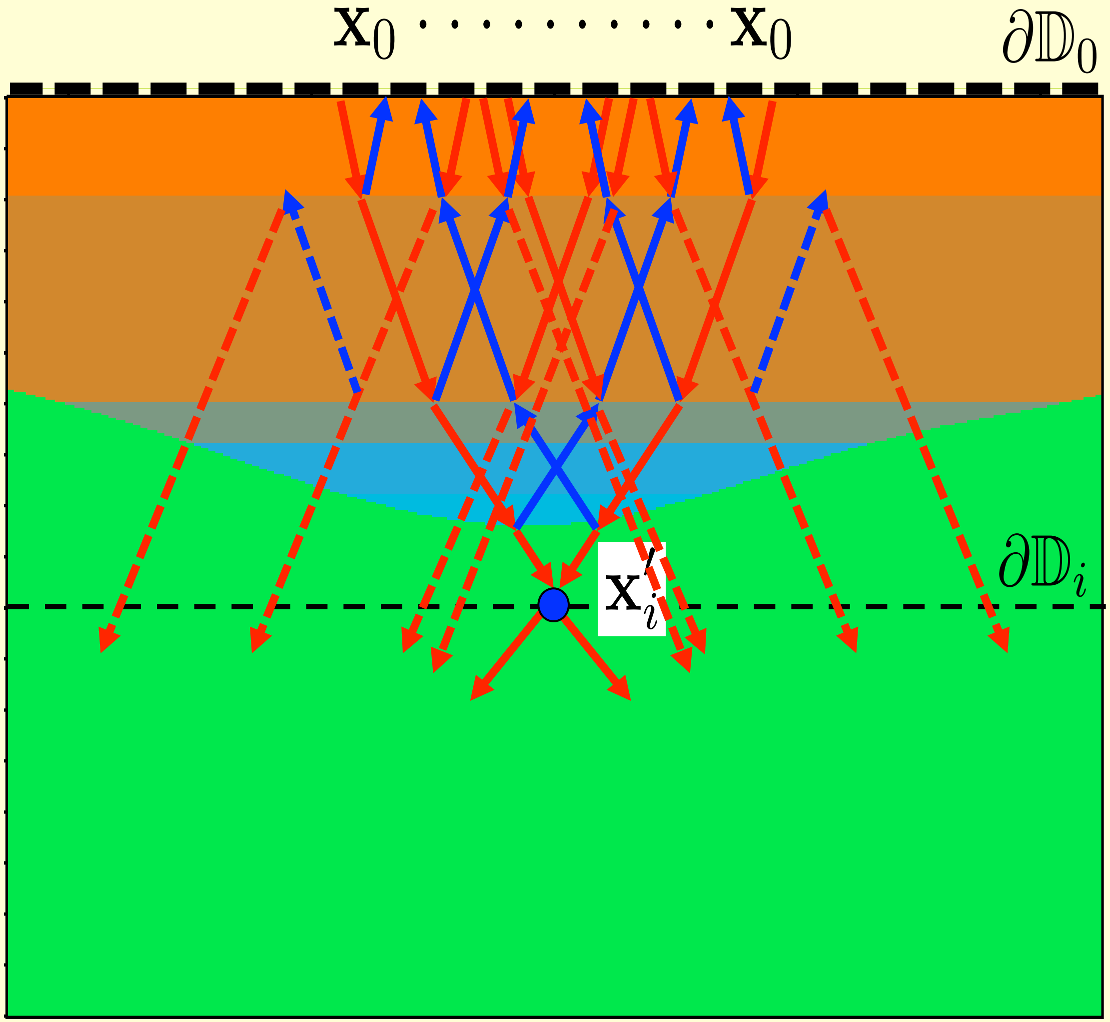

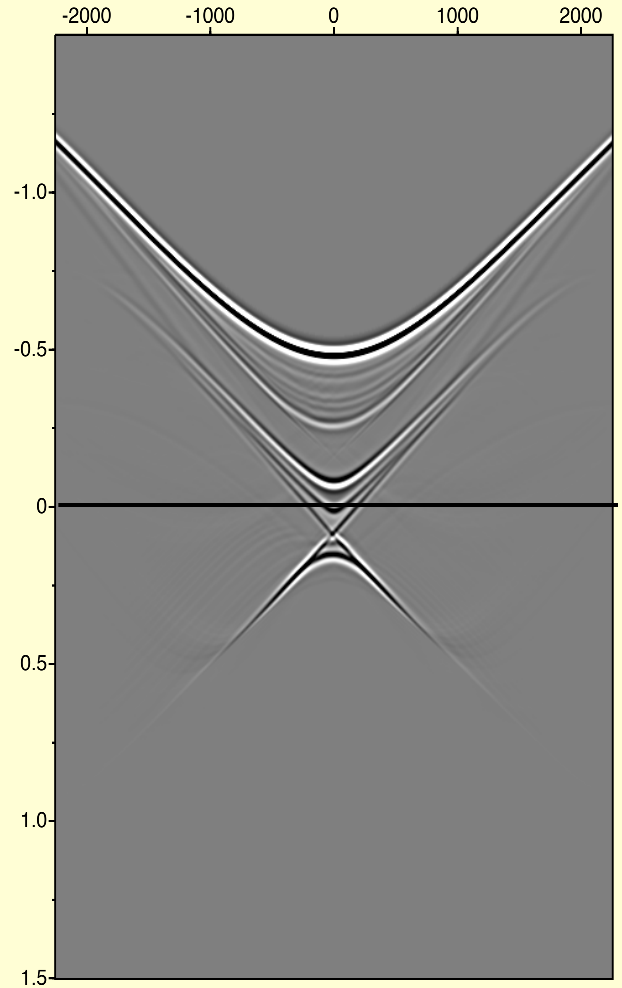

Introduction of the focusing function

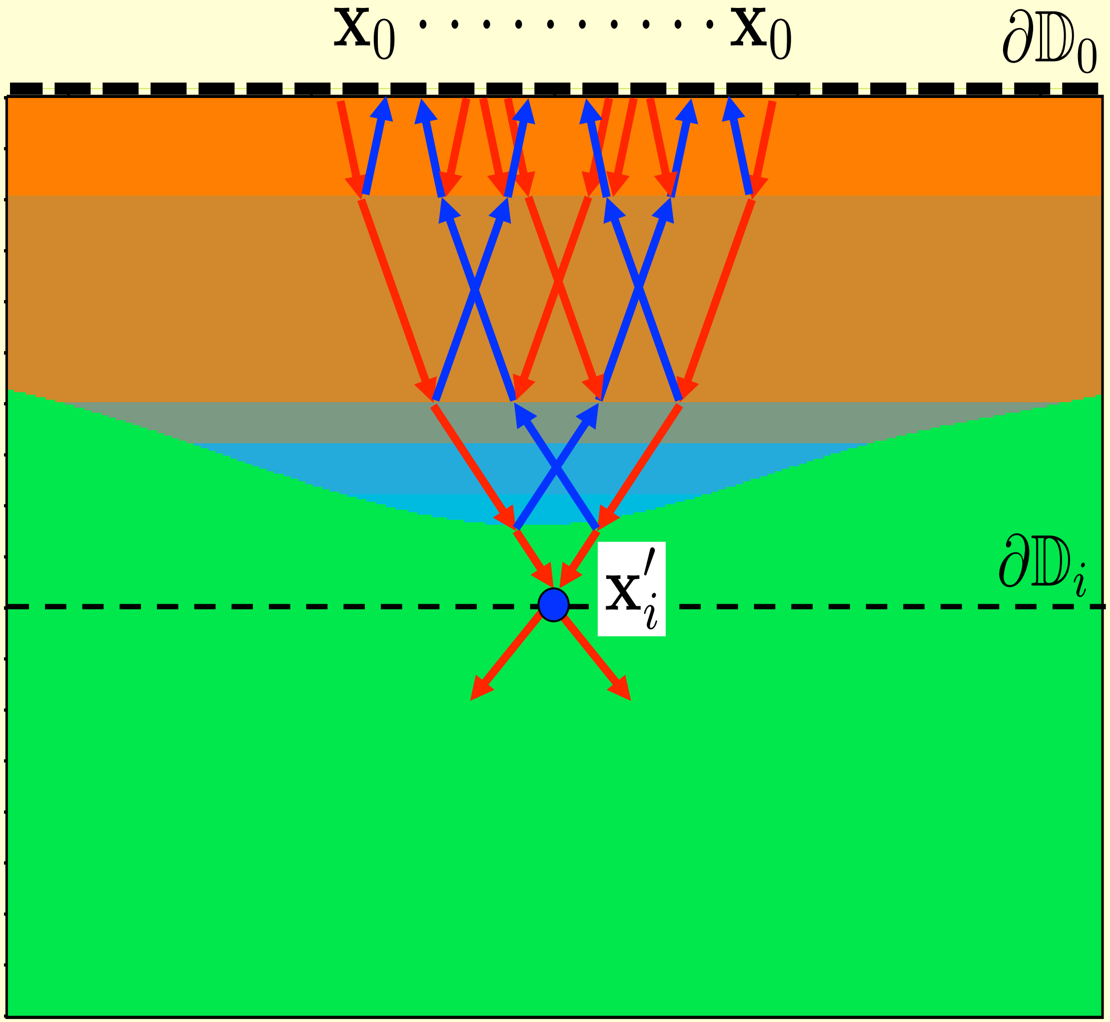

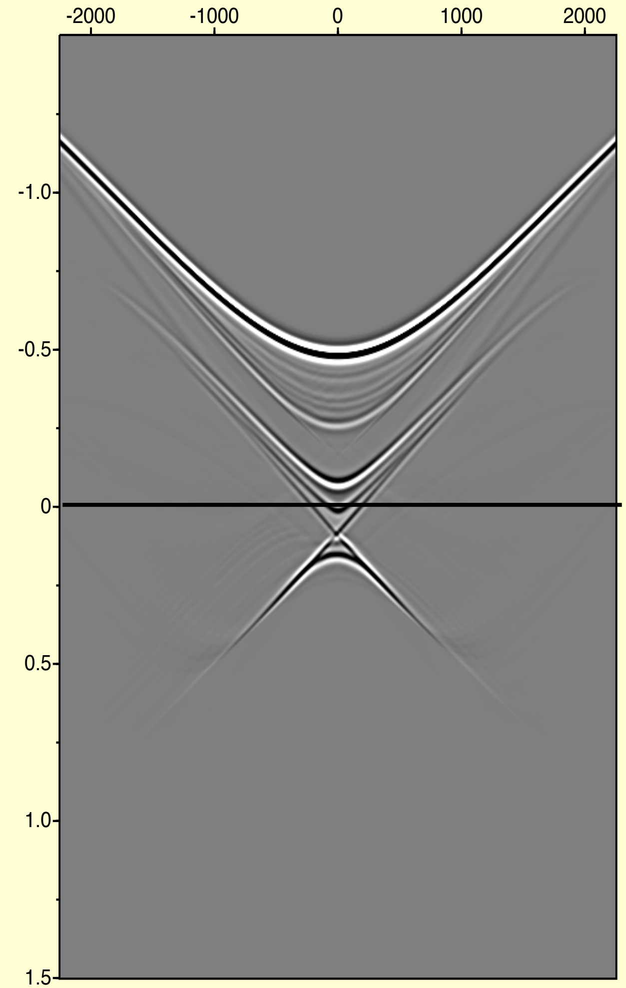

Introduction of the focusing function

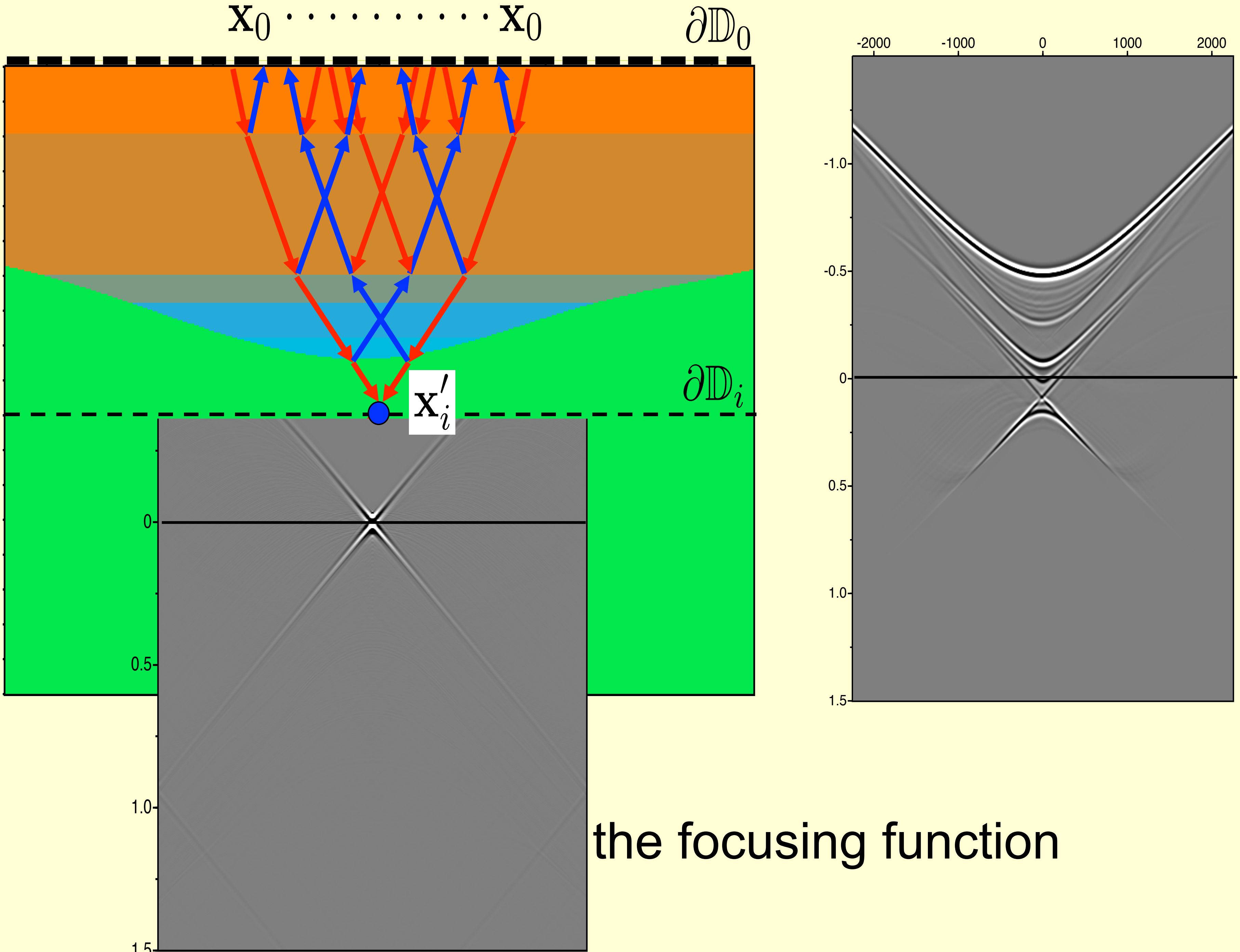

the focusing function

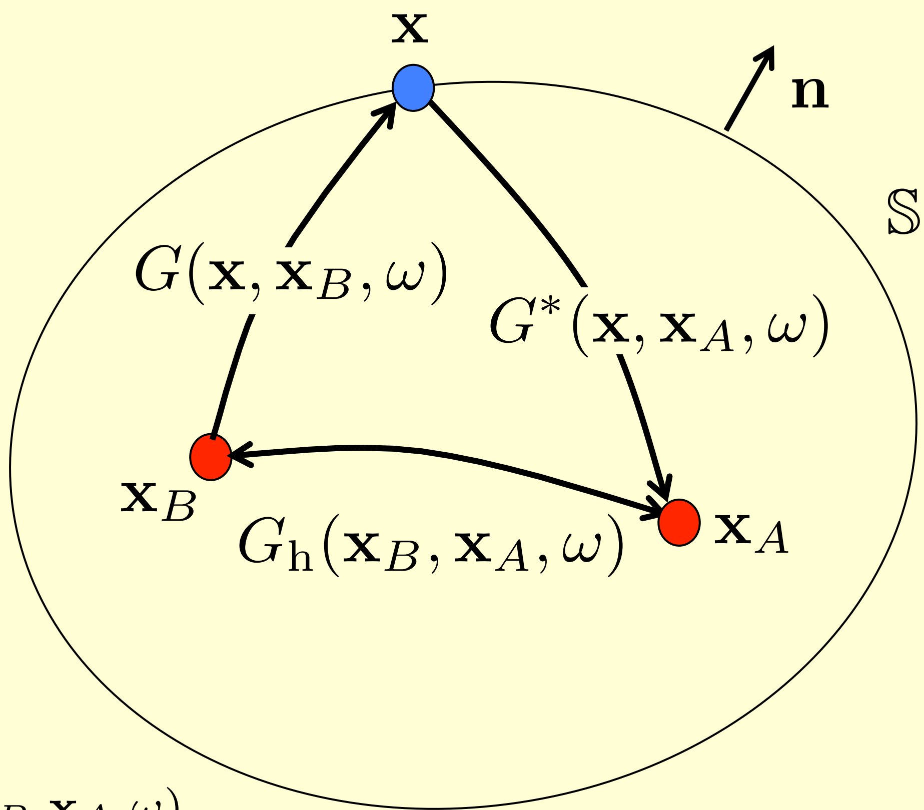

$$\overbrace{G(\mathbf{x}_B,\mathbf{x}_A,\omega)+G^*(\mathbf{x}_B,\mathbf{x}_A,\omega)}^{G_{\rm h}(\mathbf{x}_B,\mathbf{x}_A,\omega)} =$$

$$\frac{1}{i\omega\rho}\oint_{\mathbb{S}}\Big(G^*(\mathbf{x},\mathbf{x}_A,\omega)\partial_k G(\mathbf{x},\mathbf{x}_B,\omega)$$

$$-\partial_k G^*(\mathbf{x},\mathbf{x}_A,\omega)G(\mathbf{x},\mathbf{x}_B,\omega)\Big)n_k{\rm d}^2\mathbf{x}$$

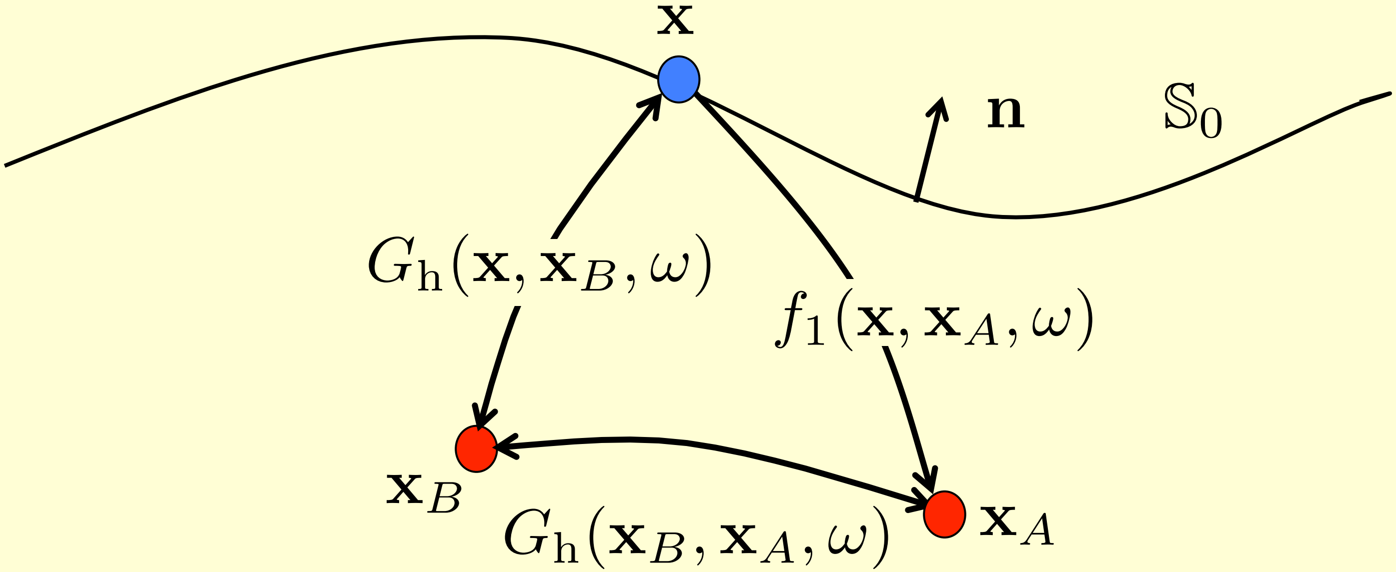

$$\overbrace{G(\mathbf{x}_B,\mathbf{x}_A,\omega)+G^*(\mathbf{x}_B,\mathbf{x}_A,\omega)}^{G_\mathrm{h}(\mathbf{x}_B,\mathbf{x}_A,\omega)} =$$

$$\frac{2}{\omega\rho}\int_{\mathbb{S}_0}\Big(\Im\{f_1(\mathbf{x},\mathbf{x}_A,\omega)\}\partial_k G_\mathrm{h}(\mathbf{x},\mathbf{x}_B,\omega)$$

$$-\Im\{\partial_k f_1(\mathbf{x},\mathbf{x}_A,\omega)\}G_\mathrm{h}(\mathbf{x},\mathbf{x}_B,\omega)\Big)n_k\mathrm{d}^2\mathbf{x}$$

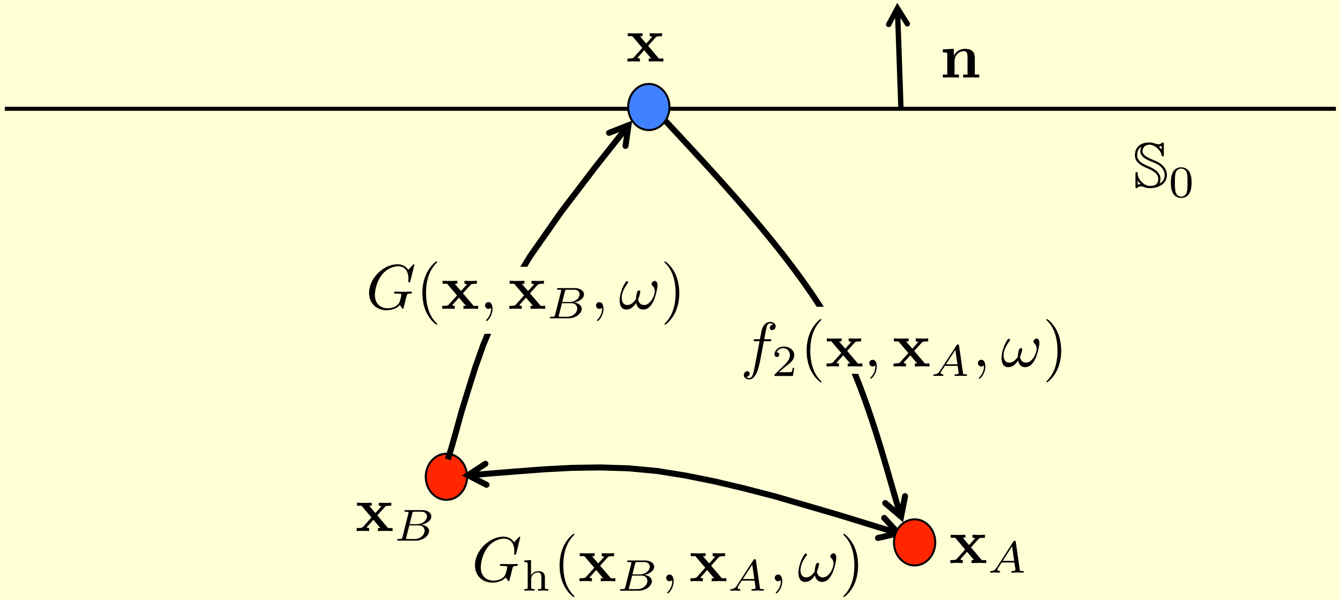

$$\overbrace{G(\mathbf{x}_B, \mathbf{x}_A, \omega) + G^*(\mathbf{x}_B, \mathbf{x}_A, \omega)}^{G_\mathrm{h}(\mathbf{x}_B, \mathbf{x}_A, \omega)} =$$

$$\Re\Big(\frac{4}{i\omega\rho}\int_{\mathbb{S}_0} G(\mathbf{x}, \mathbf{x}_B, \omega)\partial_3 f_2(\mathbf{x}, \mathbf{x}_A, \omega)\mathrm{d}^2\mathbf{x}\Big)$$

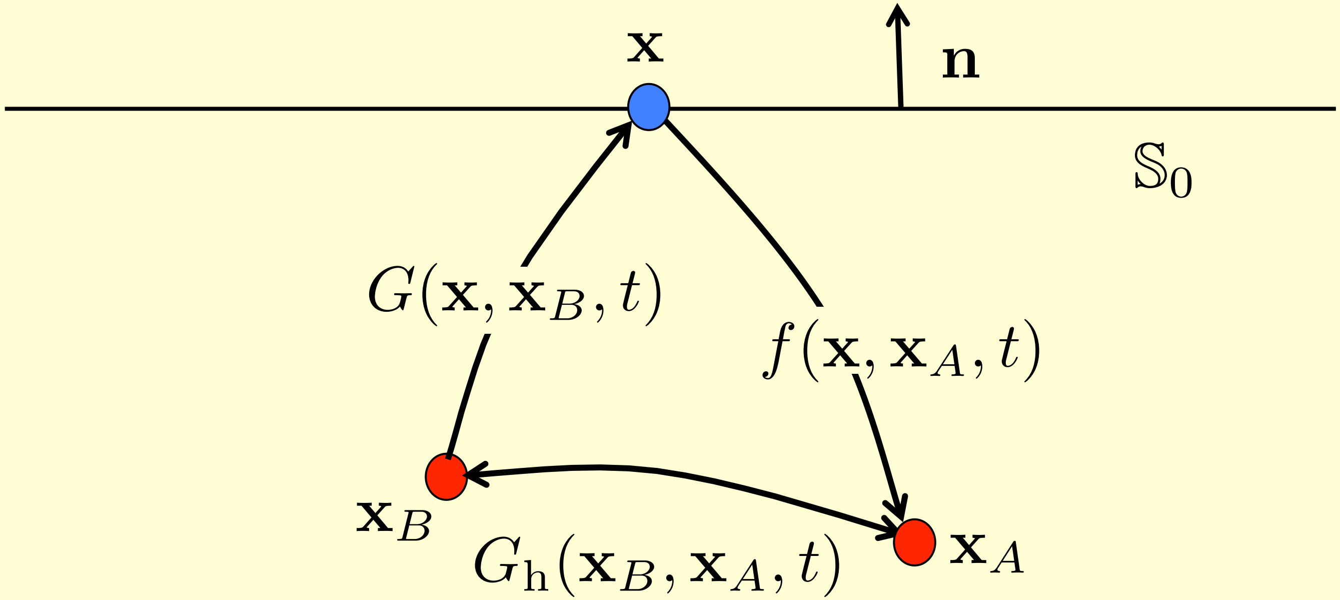

$$\overbrace{G(\mathbf{x}_B,\mathbf{x}_A,t)+G(\mathbf{x}_B,\mathbf{x}_A,-t)}^{G_\mathrm{h}(\mathbf{x}_B,\mathbf{x}_A,t)} =$$

$$2\int_{\mathbb{S}_0} G(\mathbf{x}_B,\mathbf{x},t) * f(\mathbf{x},\mathbf{x}_A,t)\mathrm{d}\mathbf{x}$$

$$+2\int_{\mathbb{S}_0} G(\mathbf{x}_B,\mathbf{x},-t) * f(\mathbf{x},\mathbf{x}_A,-t)\mathrm{d}\mathbf{x}$$

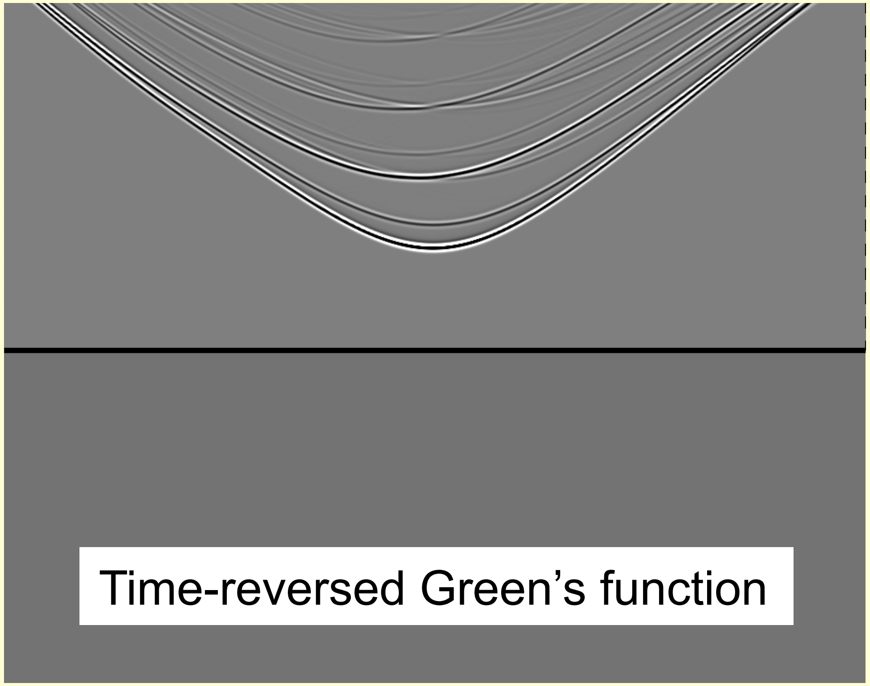

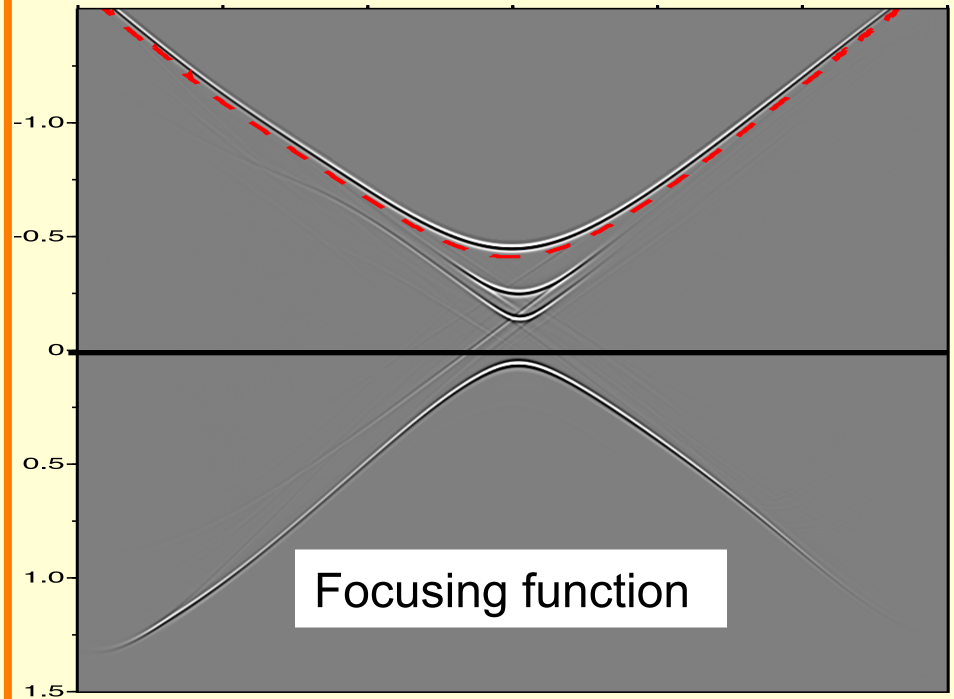

$$\overbrace{G(\mathbf{x}_B,\mathbf{x}_A,t)+G(\mathbf{x}_B,\mathbf{x}_A,-t)}^{G_{\rm h}(\mathbf{x}_B,\mathbf{x}_A,t)}=$$

$$\oint_{\mathbb{S}} G(\mathbf{x},\mathbf{x}_B,t)*\partial_i G(\mathbf{x},\mathbf{x}_A,-t)n_i{\rm d}\mathbf{x}$$

$$\overbrace{G(\mathbf{x}_B,\mathbf{x}_A,t)+G(\mathbf{x}_B,\mathbf{x}_A,-t)}^{G_{\rm h}(\mathbf{x}_B,\mathbf{x}_A,t)}=$$

$$2\int_{\mathbb{S}_0} G(\mathbf{x}_B,\mathbf{x},t)*f(\mathbf{x},\mathbf{x}_A,t){\rm d}\mathbf{x}$$

$$+2\int_{\mathbb{S}_0} G(\mathbf{x}_B,\mathbf{x},-t)*f(\mathbf{x},\mathbf{x}_A,-t){\rm d}\mathbf{x}$$

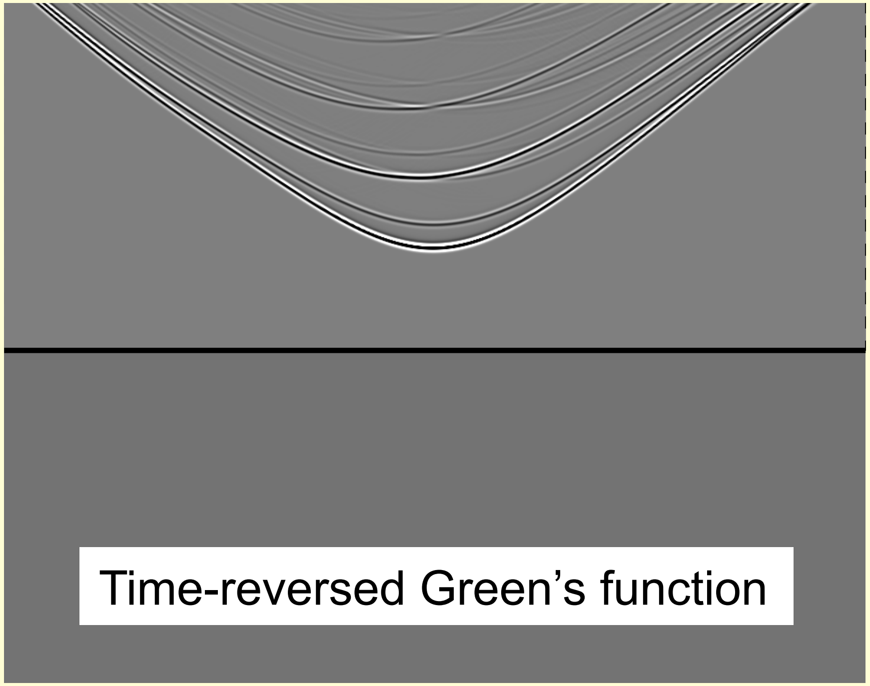

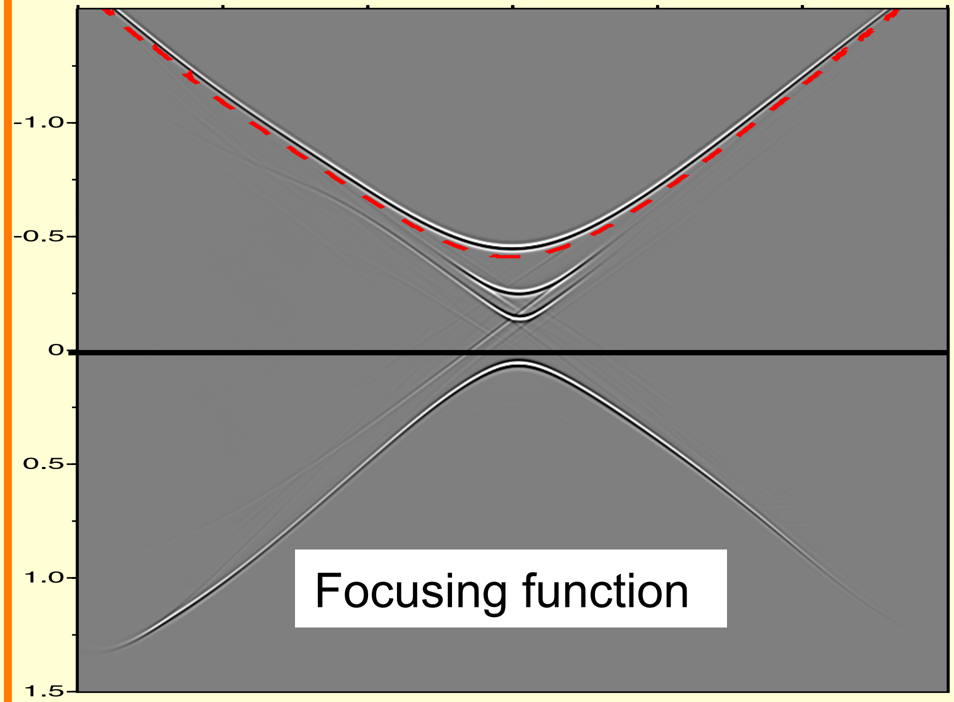

$$\overbrace{G(\mathbf{x}_B,\mathbf{x}_A,t)+G(\mathbf{x}_B,\mathbf{x}_A,-t)}^{G_{\rm h}(\mathbf{x}_B,\mathbf{x}_A,t)}=$$

$$\oint_{\mathbb{S}} G(\mathbf{x},\mathbf{x}_B,t)*\partial_i G(\mathbf{x},\mathbf{x}_A,-t)n_i{\rm d}\mathbf{x}$$

$$\overbrace{G(\mathbf{x}_B,\mathbf{x}_A,t)+G(\mathbf{x}_B,\mathbf{x}_A,-t)}^{G_{\rm h}(\mathbf{x}_B,\mathbf{x}_A,t)}=$$

$$2\int_{\mathbb{S}_0} G(\mathbf{x}_B,\mathbf{x},t)*f(\mathbf{x},\mathbf{x}_A,t){\rm d}\mathbf{x}$$

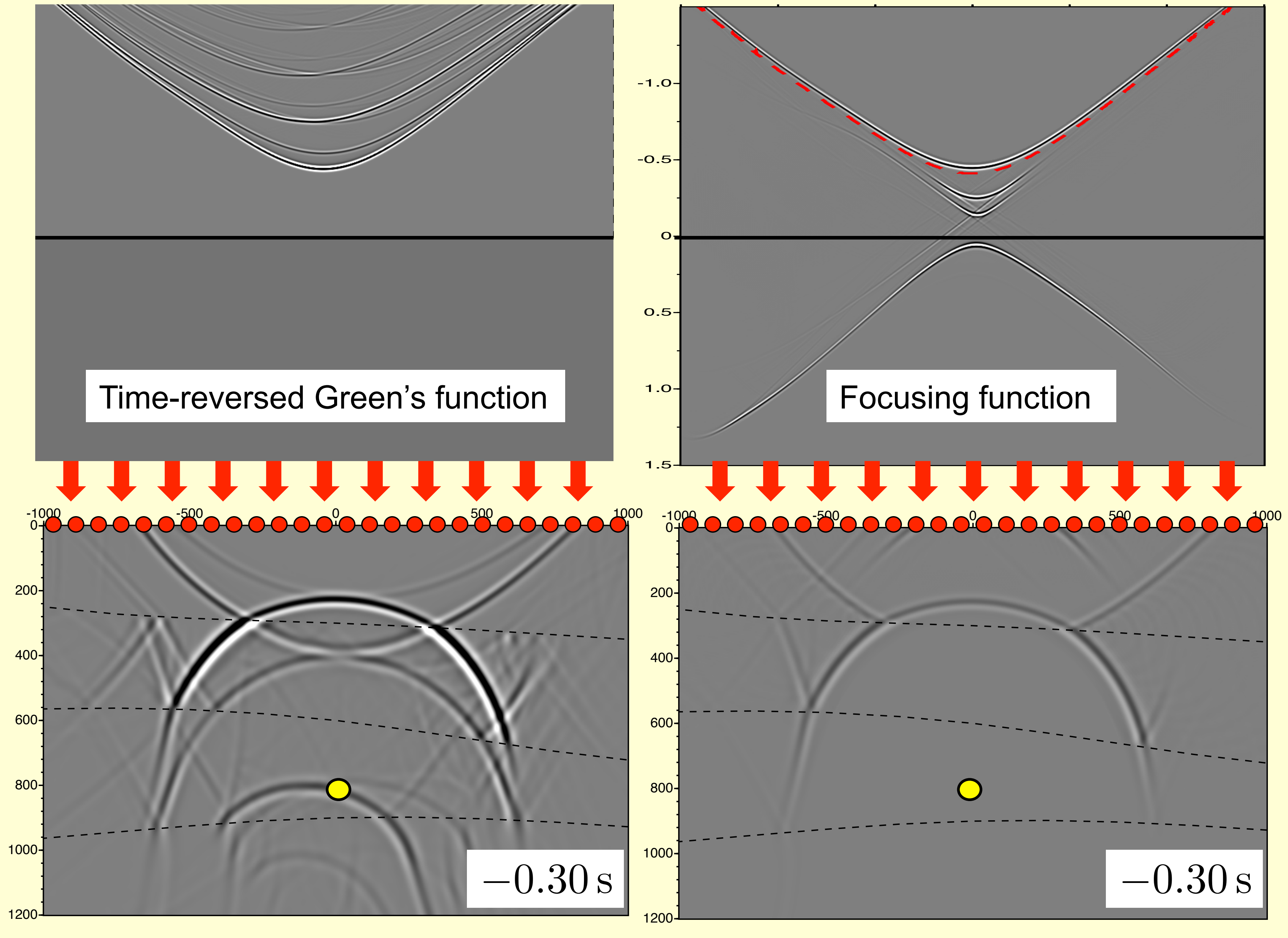

Time-reversed Green's function
Focusing function
-1.0
-0.5
0
0.5
1.0
1.5
-1000
-500
0
500
1000
200
400
600
800
1000
1200
−0.30 s
−0.30 s

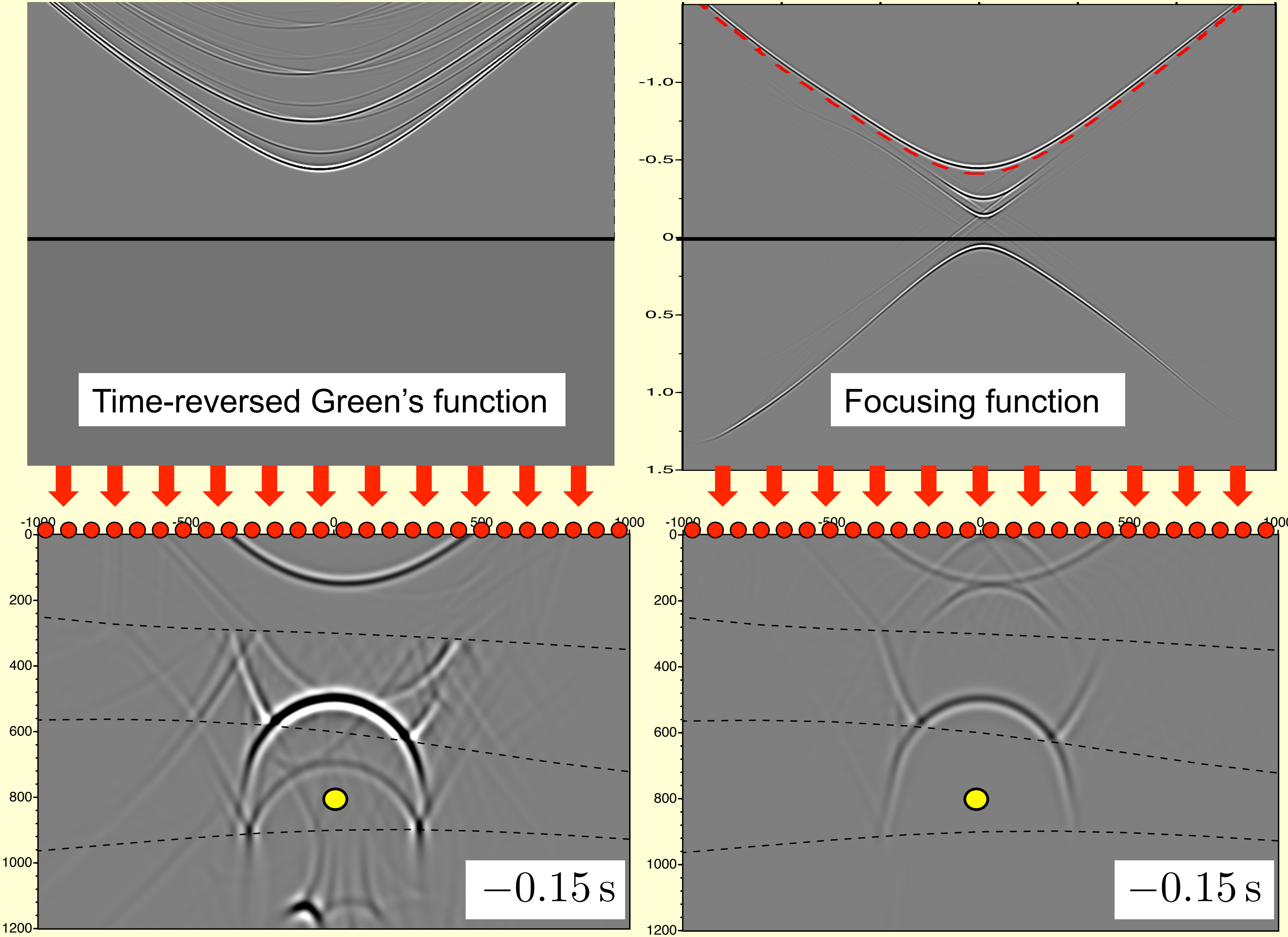

Time-reversed Green's function
Focusing function
-1.0
-0.5
0
0.5
1.0
1.5
-1000
-500
0
500
1000
0
200
400
600
800
1000
1200
−0.15 s
−0.15 s

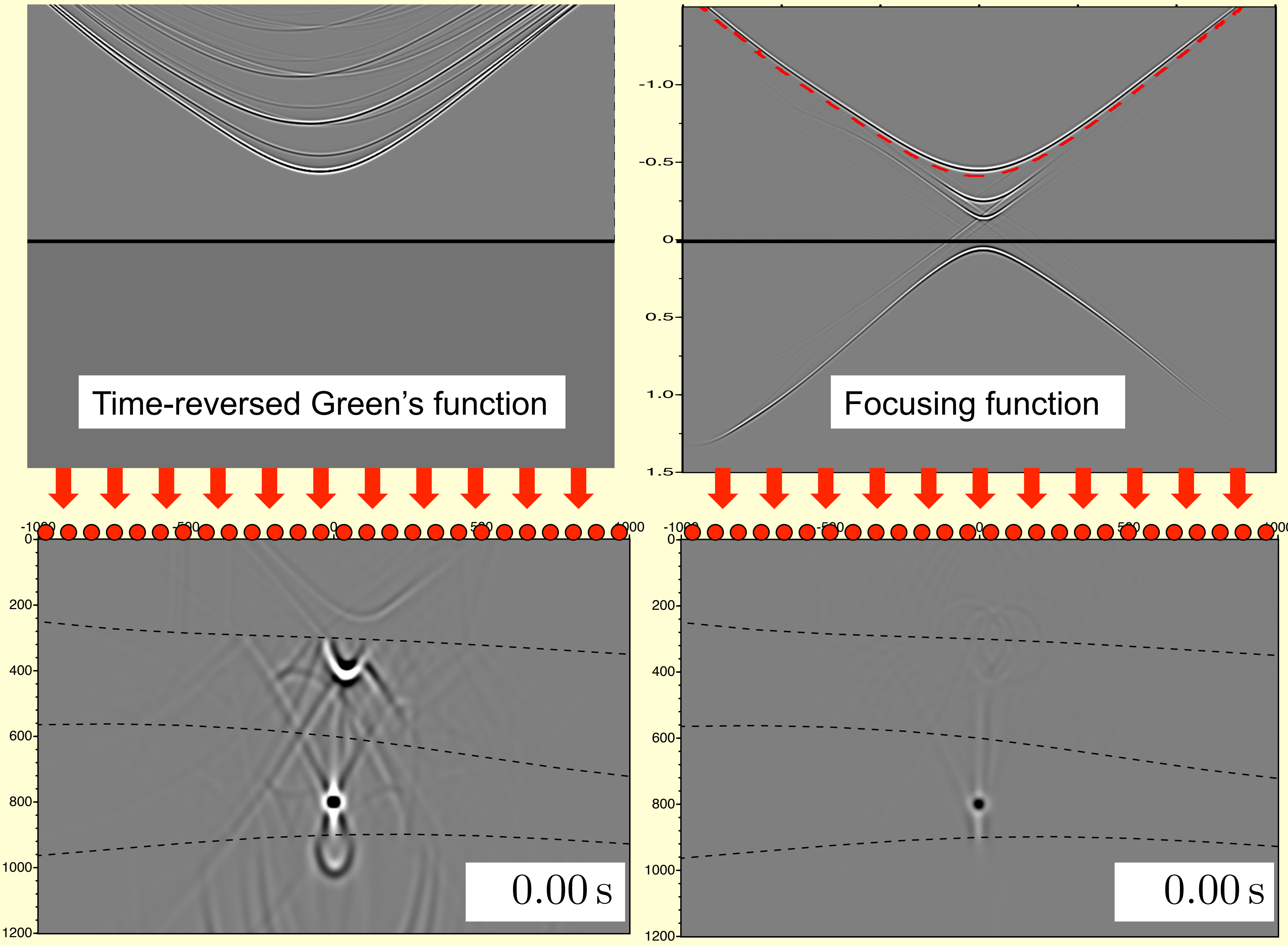

Time-reversed Green's function
Focusing function
0.00 s
0.00 s

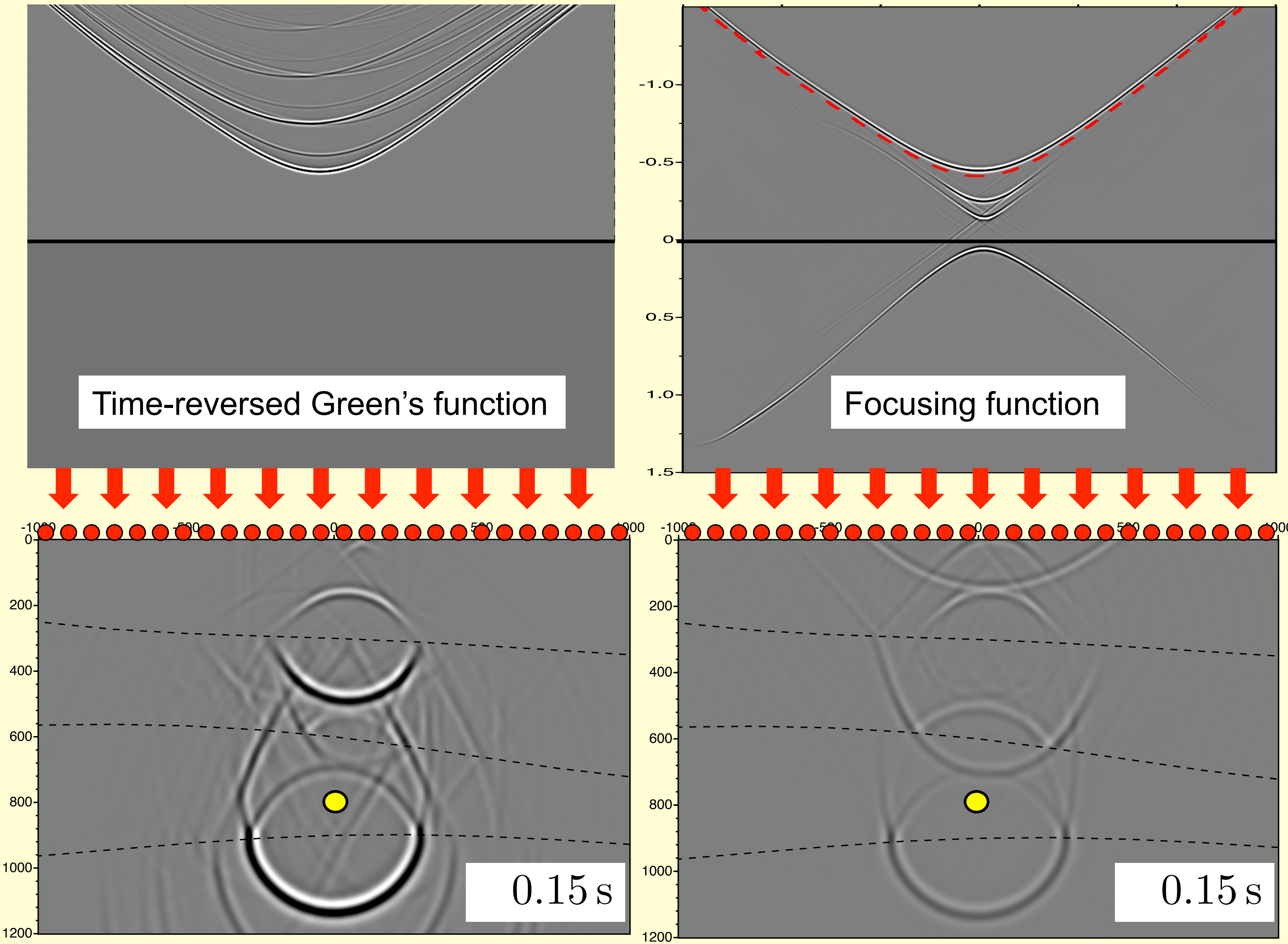
Time-reversed Green's function
Focusing function
-1.0
-0.5
0
0.5
1.0
1.5
-1000
-500
0
500
1000
0
200
400
600
800
1000
1200
0.15 s
0.15 s

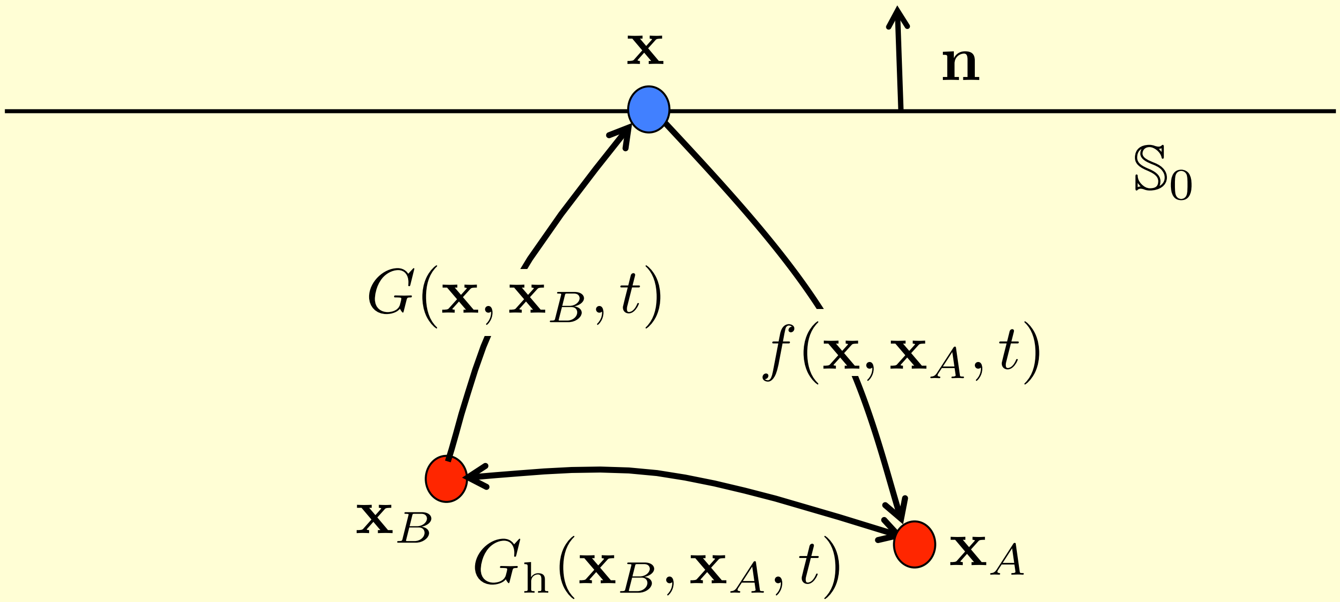

$$\overbrace{G(\mathbf{x}_B,\mathbf{x}_A,t)+G(\mathbf{x}_B,\mathbf{x}_A,-t)}^{G_{\rm h}(\mathbf{x}_B,\mathbf{x}_A,t)} =$$

$$2\int_{\mathbb{S}_0} G(\mathbf{x}_B,\mathbf{x},t)*f(\mathbf{x},\mathbf{x}_A,t)\mathrm{d}\mathbf{x}$$
$$+2\int_{\mathbb{S}_0} G(\mathbf{x}_B,\mathbf{x},-t)*f(\mathbf{x},\mathbf{x}_A,-t)\mathrm{d}\mathbf{x}$$

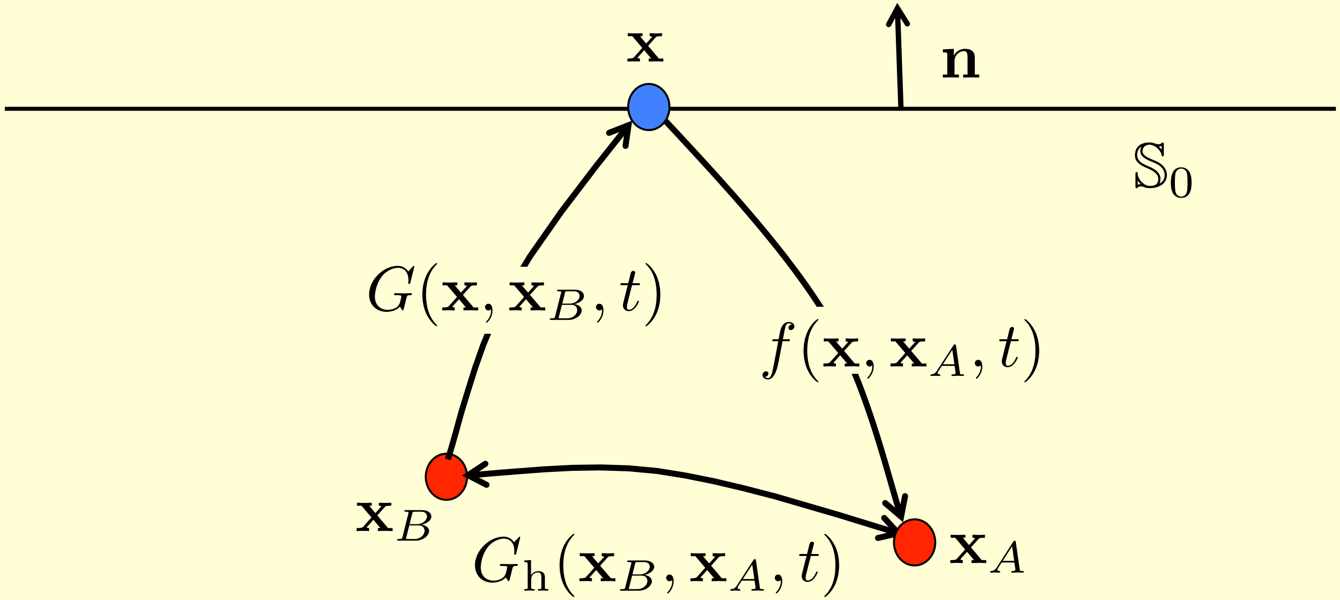

$$G(\mathbf{x}_B,\mathbf{x}_A,t) + \text{asymm. artefacts} =$$

$$2\int_{\mathbb{S}_0} G(\mathbf{x}_B,\mathbf{x},t) * f(\mathbf{x},\mathbf{x}_A,t)\mathrm{d}\mathbf{x}$$

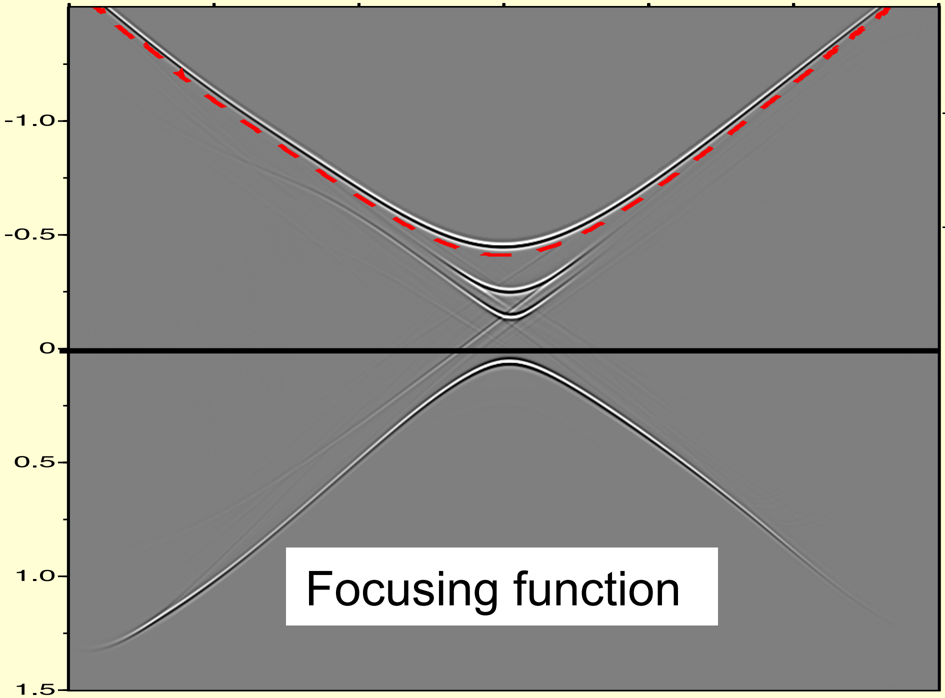

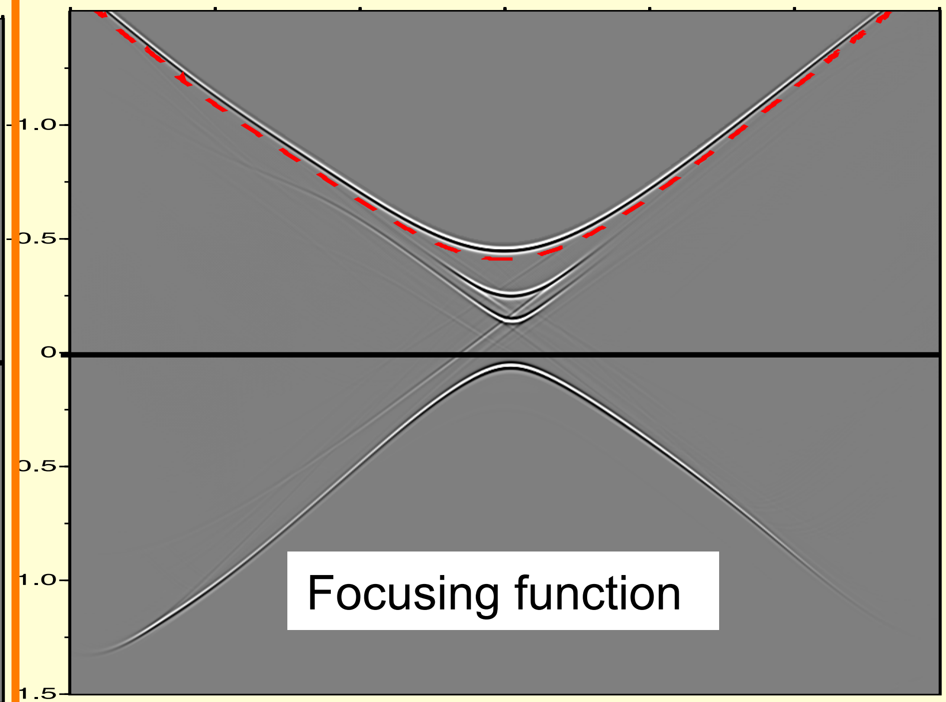

$$G(\mathbf{x}_B, \mathbf{x}_A, t) + \text{asymm. artefacts} = 2\int_{\mathbb{S}_0} G(\mathbf{x}_B, \mathbf{x}, t) * f(\mathbf{x}, \mathbf{x}_A, t)\mathrm{d}\mathbf{x}$$

$$G(\mathbf{x}_B, \mathbf{x}_A, -t) - \text{asymm. artefacts} = 2\int_{\mathbb{S}_0} G(\mathbf{x}_B, \mathbf{x}, -t) * f(\mathbf{x}, \mathbf{x}_A, -t)\mathrm{d}\mathbf{x}$$

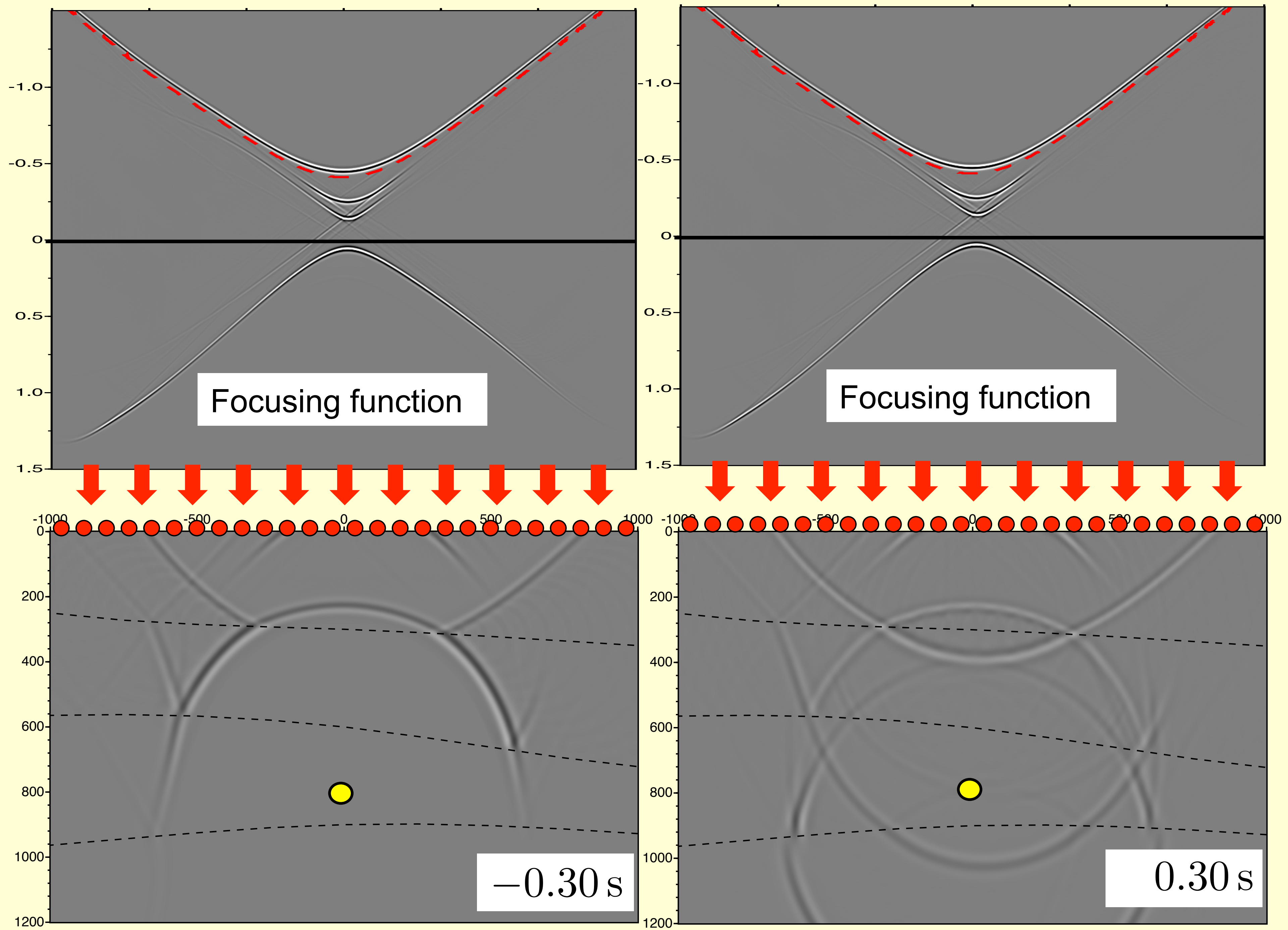

Focusing function
Focusing function
-1.0
-0.5
0
0.5
1.0
1.5
-1000
-500
0
500
1000
200
400
600
800
1000
1200
−0.30 s
0.30 s

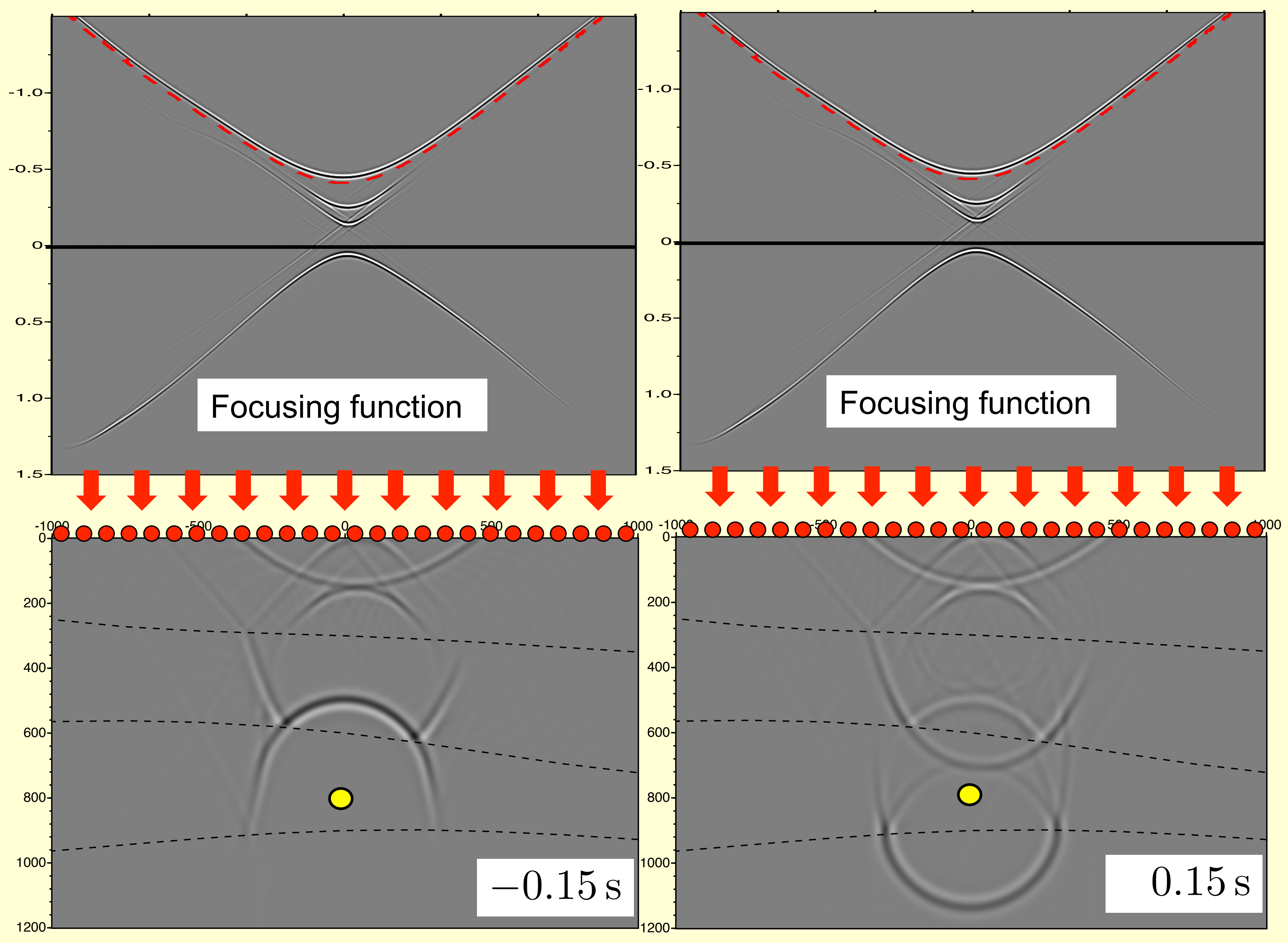

Focusing function
Focusing function
−0.15 s
0.15 s

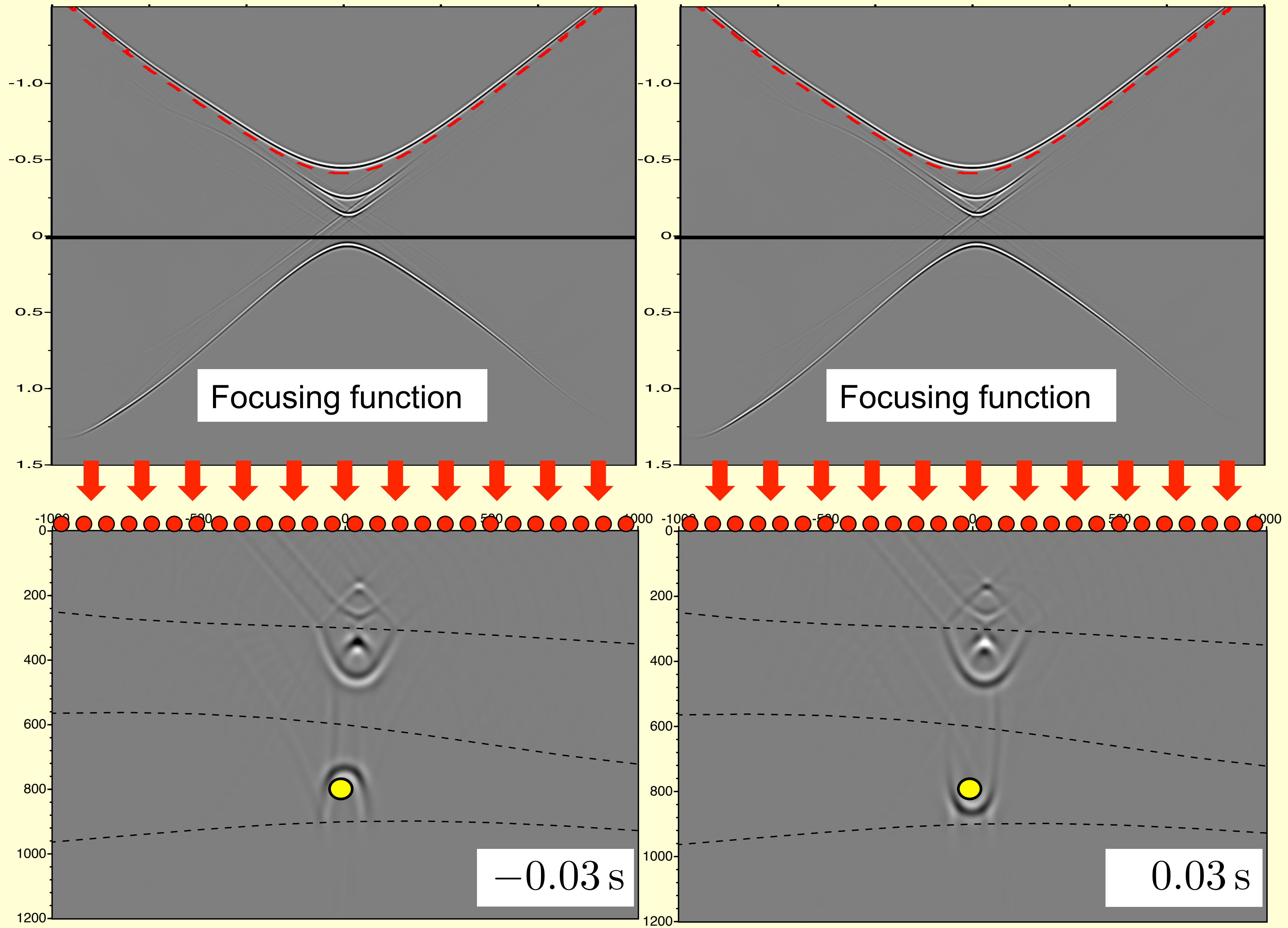

Focusing function
Focusing function
−0.03 s
0.03 s

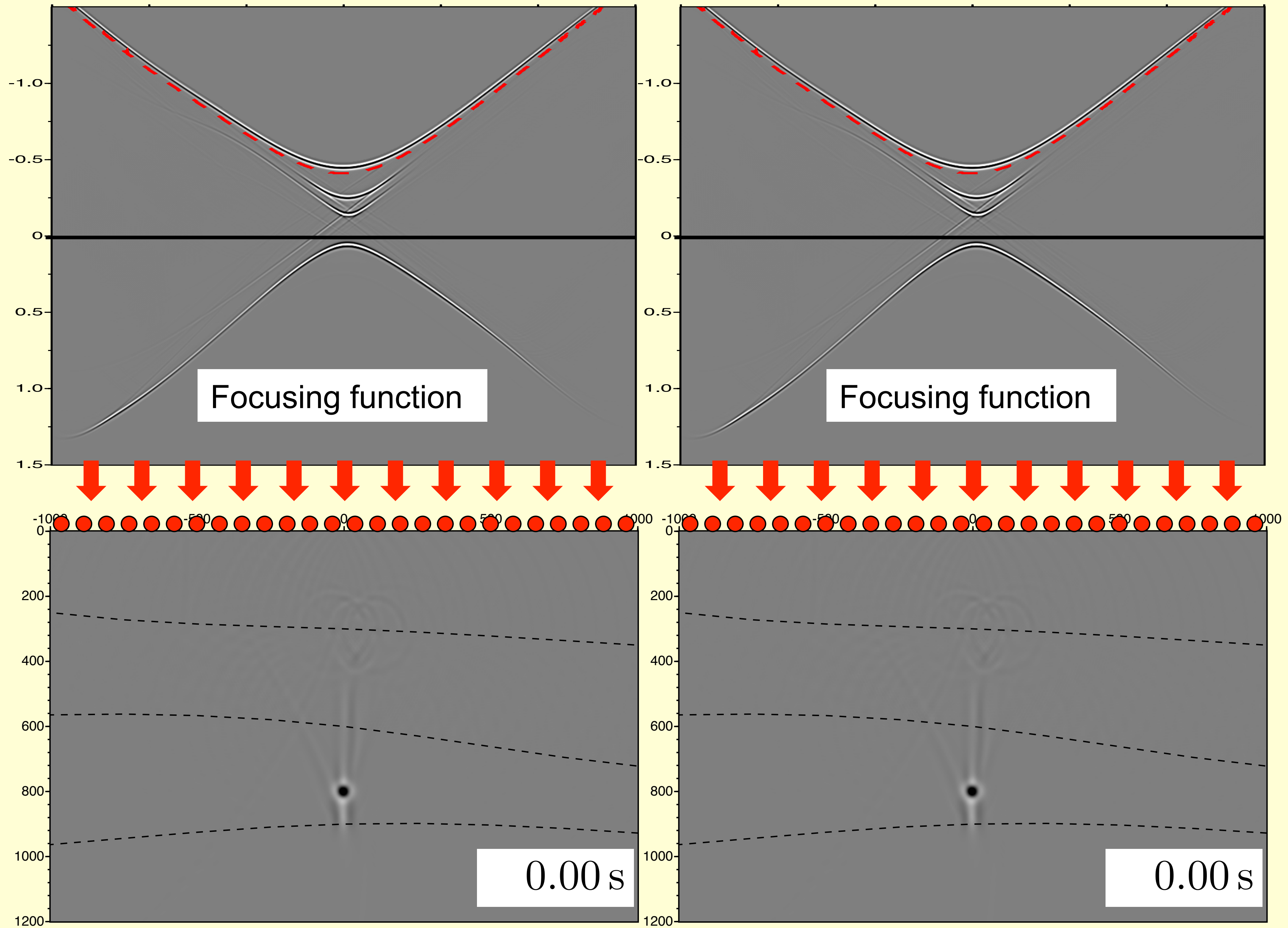

Focusing function
Focusing function
0.00 s
0.00 s

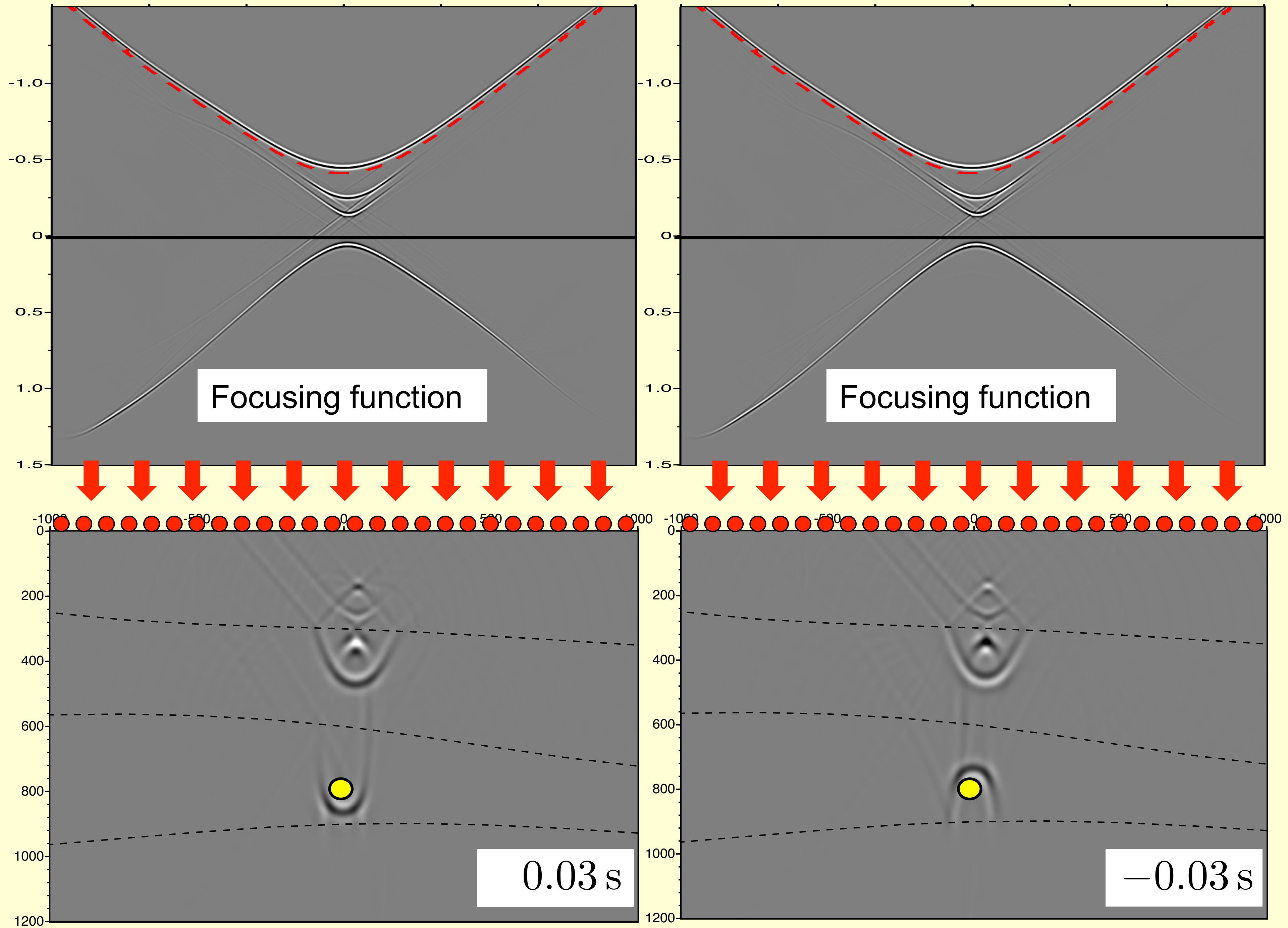
Focusing function
Focusing function
0.03 s
−0.03 s

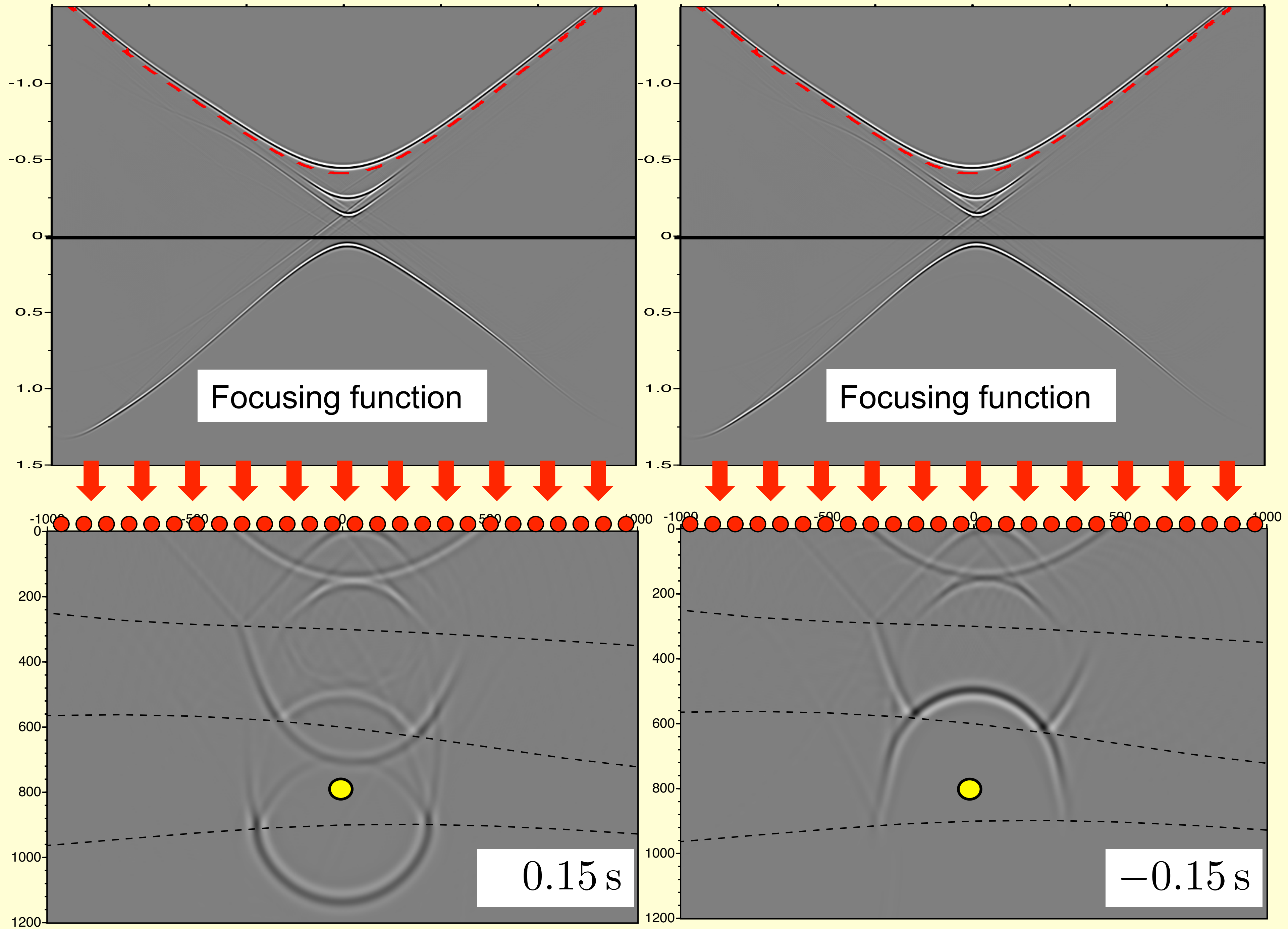
Focusing function
Focusing function
0.15 s
−0.15 s
-1.0
-0.5
0
0.5
1.0
1.5
-1000
-500
0
500
1000
200
400
600
800
1000
1200

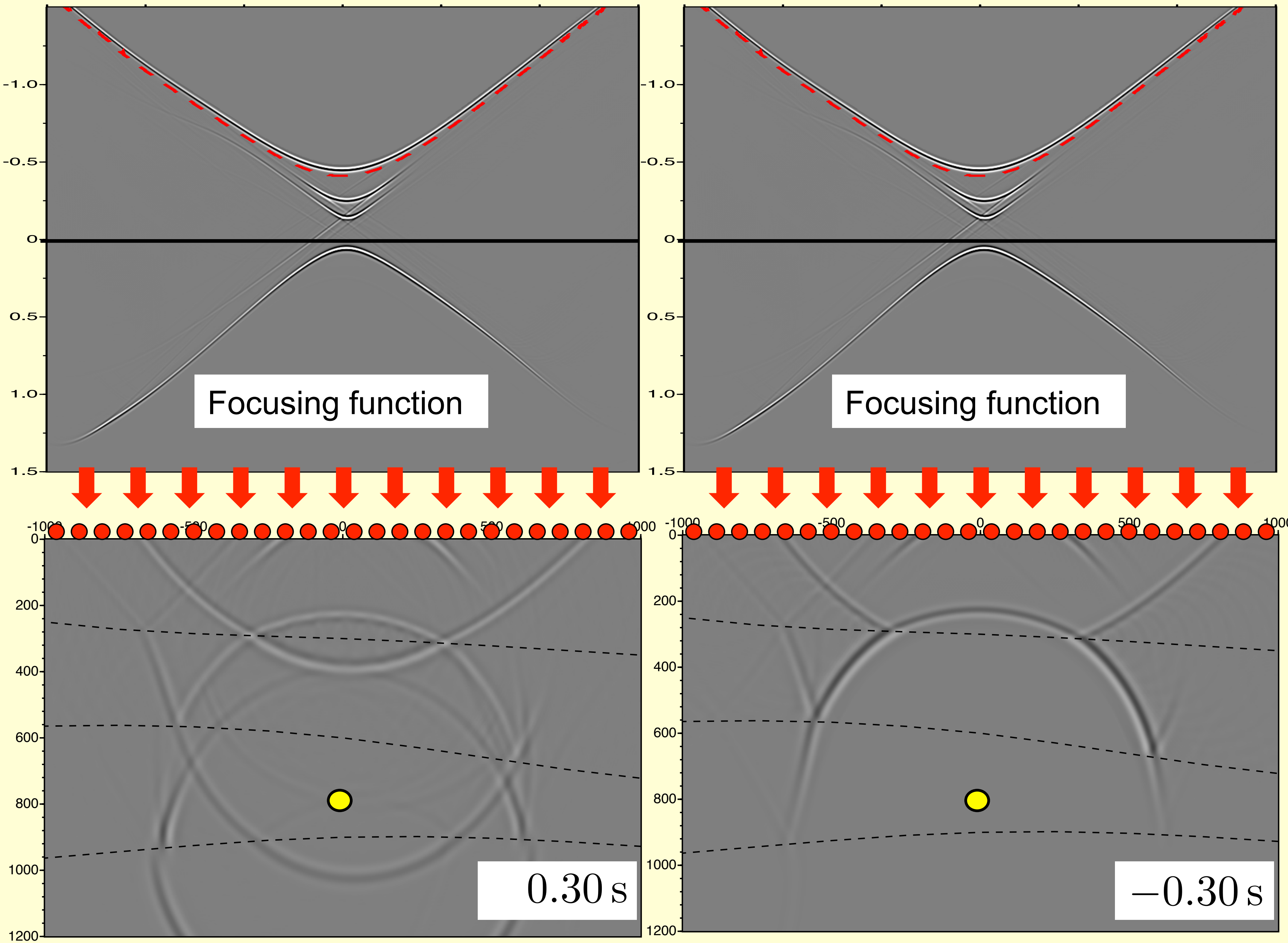
Focusing function
Focusing function
0.30 s
−0.30 s

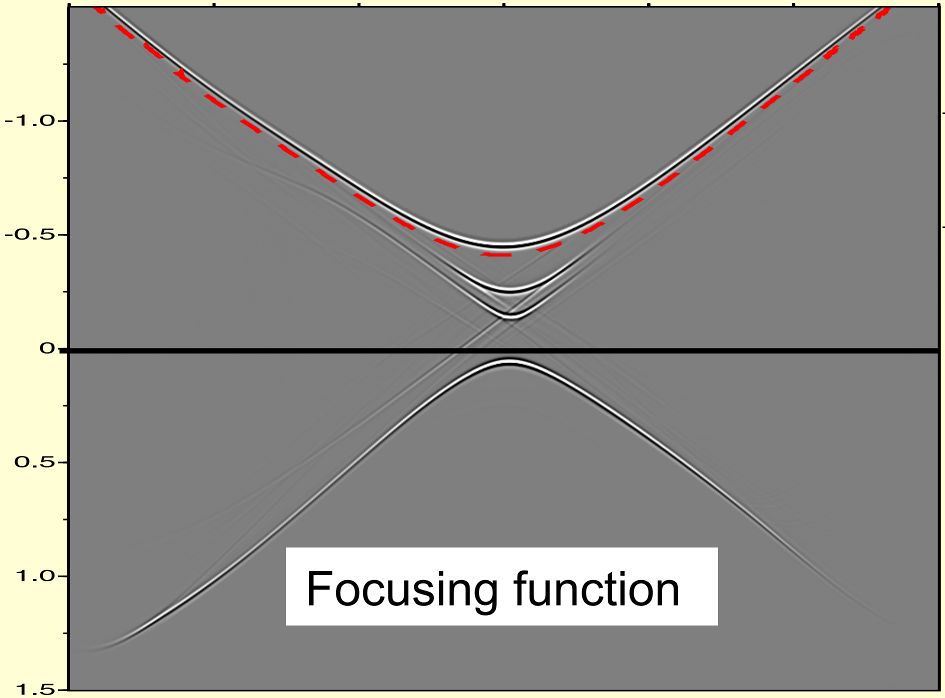

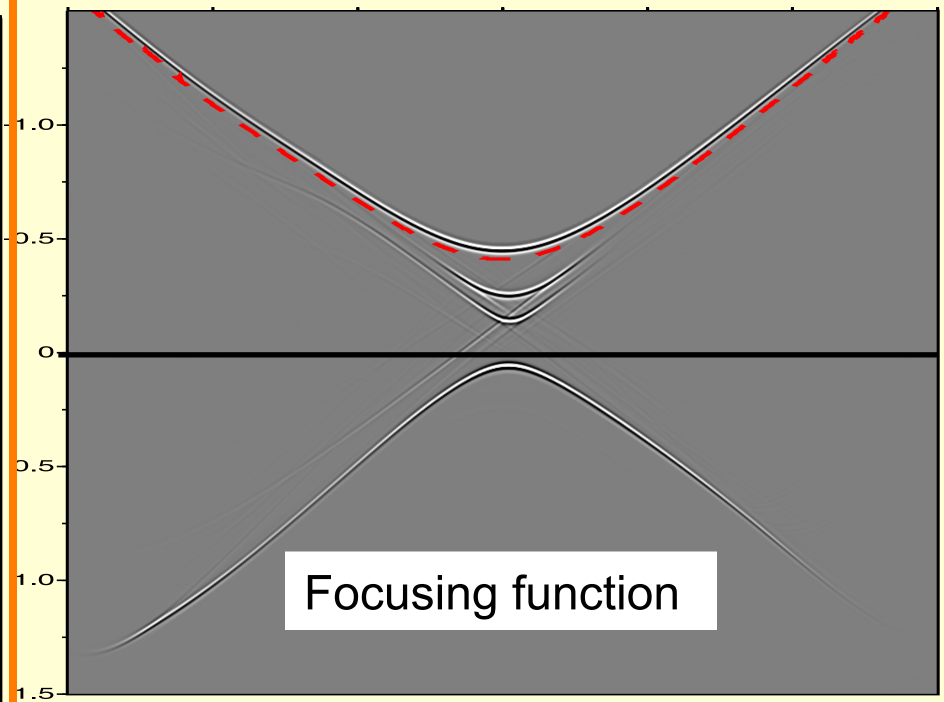

$$G(\mathbf{x}_B, \mathbf{x}_A, t) + \text{asymm. artefacts} = 2\int_{\mathbb{S}_0} G(\mathbf{x}_B, \mathbf{x}, t) * f(\mathbf{x}, \mathbf{x}_A, t)\mathrm{d}\mathbf{x}$$

$$G(\mathbf{x}_B, \mathbf{x}_A, -t) - \text{asymm. artefacts} = 2\int_{\mathbb{S}_0} G(\mathbf{x}_B, \mathbf{x}, -t) * f(\mathbf{x}, \mathbf{x}_A, -t)\mathrm{d}\mathbf{x}$$

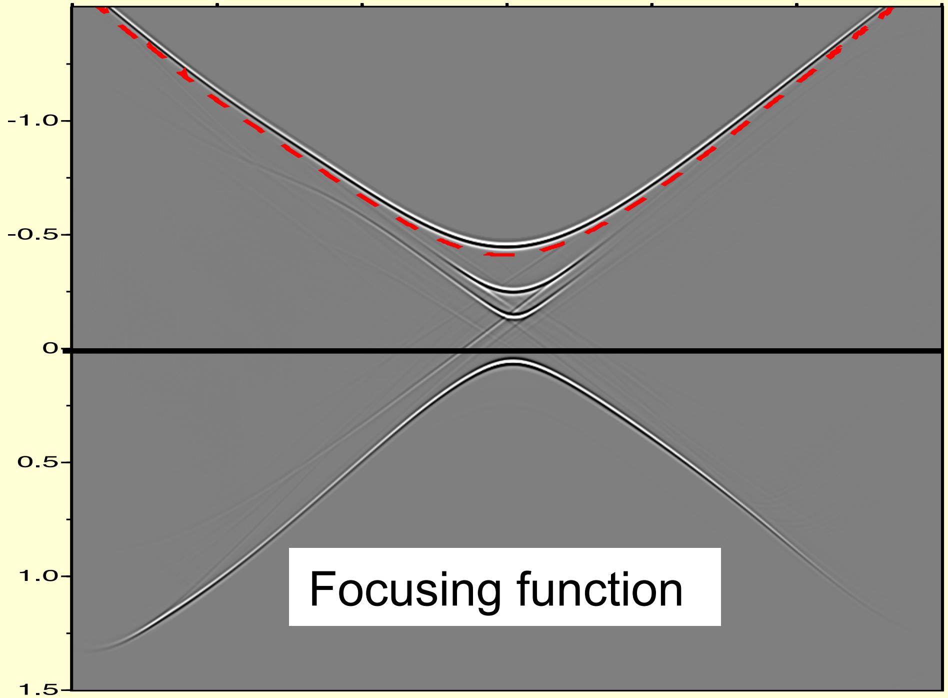

$$\overbrace{G(\mathbf{x}_B,\mathbf{x}_A,t)+G(\mathbf{x}_B,\mathbf{x}_A,-t)}^{G_{\rm h}(\mathbf{x}_B,\mathbf{x}_A,t)} =$$

$$2\int_{\mathbb{S}_0} G(\mathbf{x}_B,\mathbf{x},t)*f(\mathbf{x},\mathbf{x}_A,t){\rm d}\mathbf{x}$$

$$+2\int_{\mathbb{S}_0} G(\mathbf{x}_B,\mathbf{x},-t)*f(\mathbf{x},\mathbf{x}_A,-t){\rm d}\mathbf{x}$$

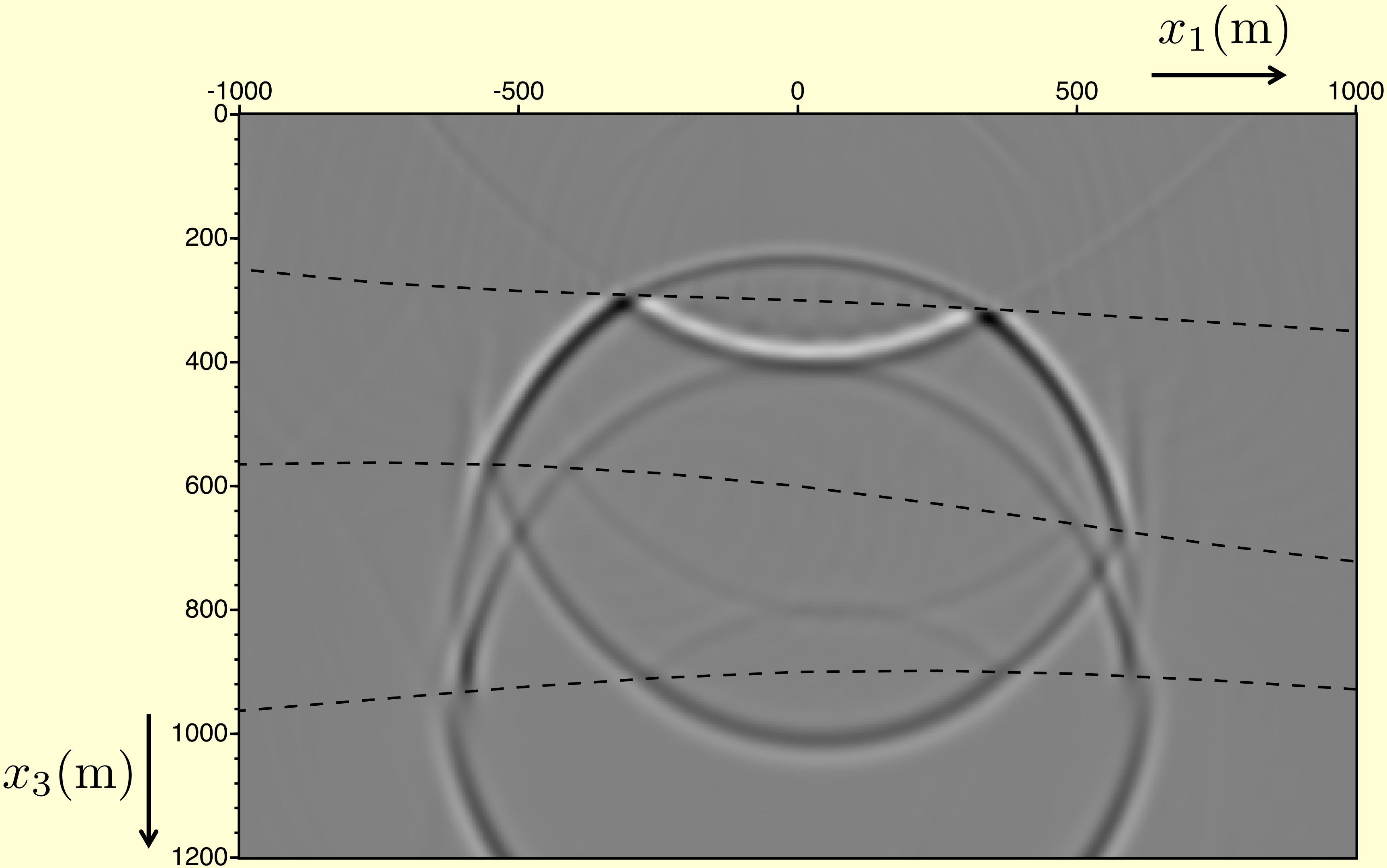

$t = -0.30\mathrm{s}$

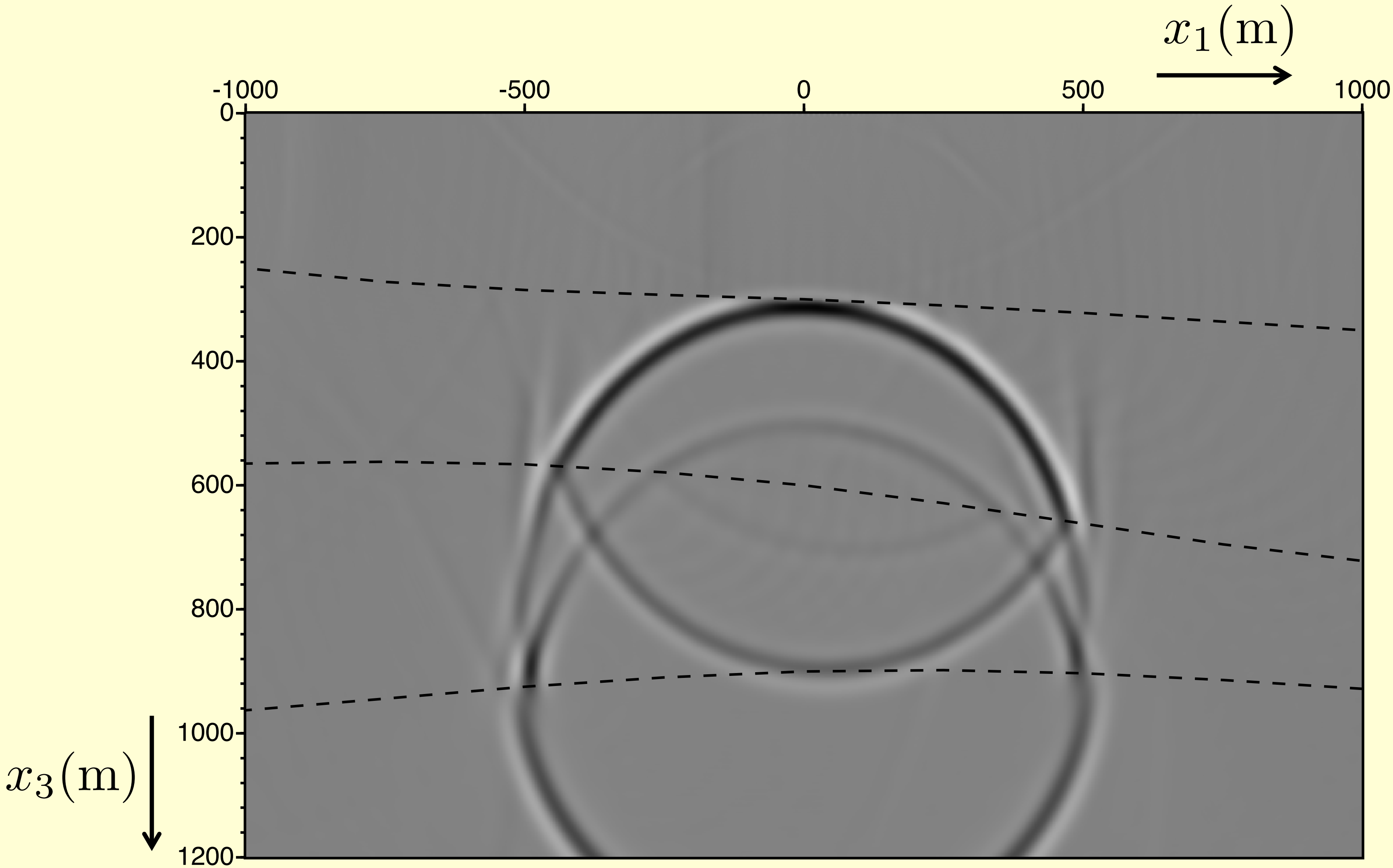

$t = -0.25\mathrm{s}$

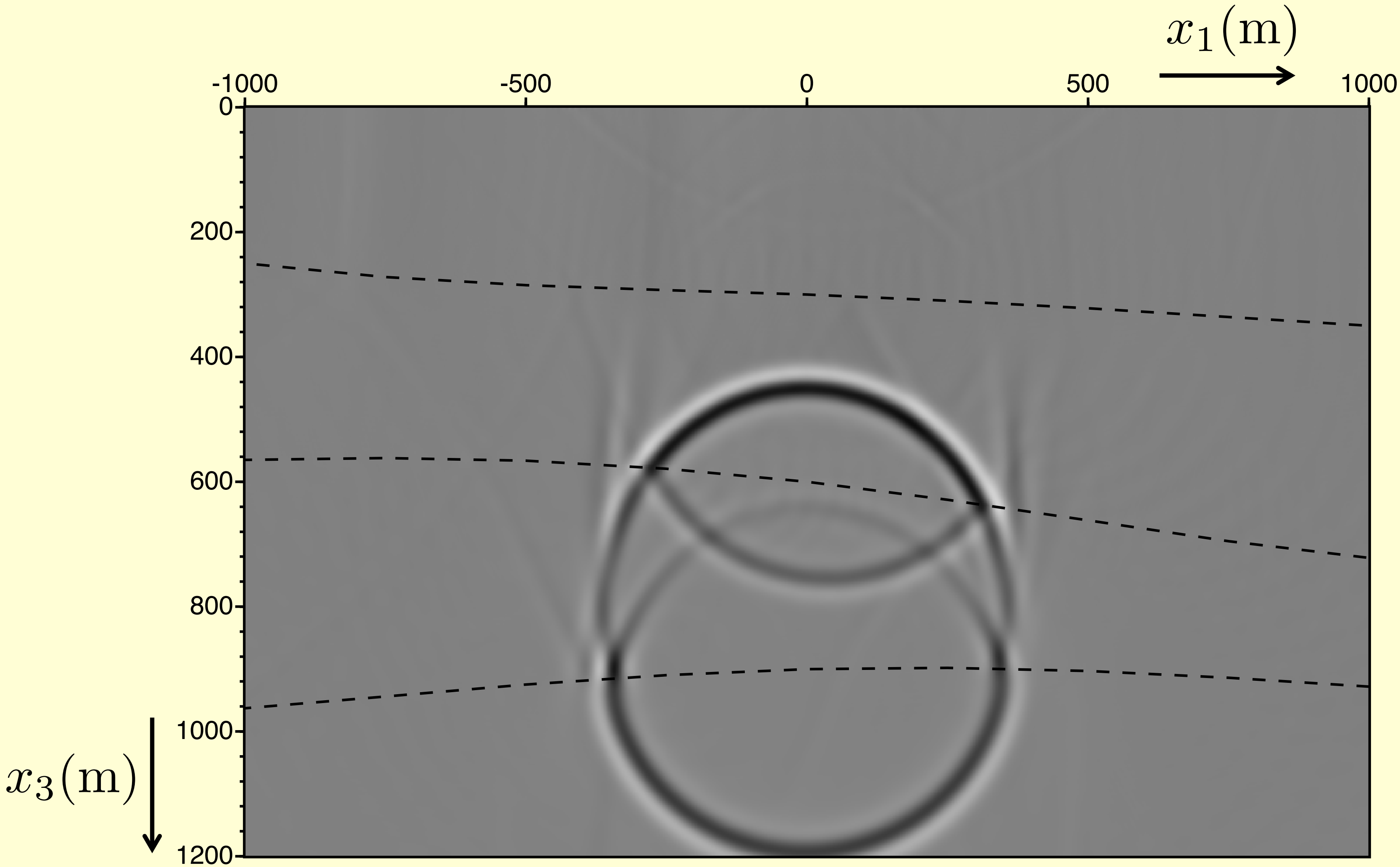

$t = -0.18\mathrm{s}$

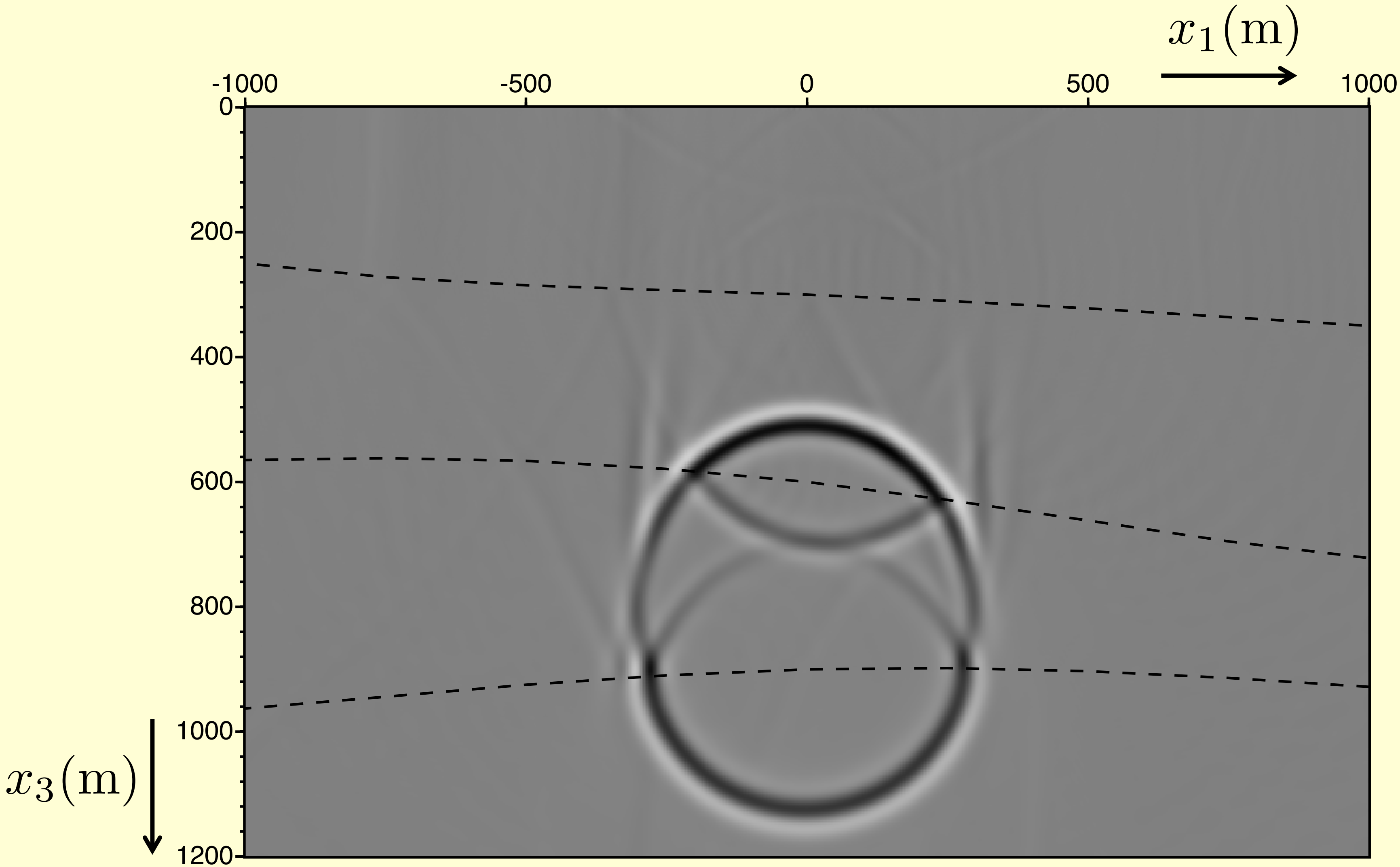

$t = -0.15\mathrm{s}$

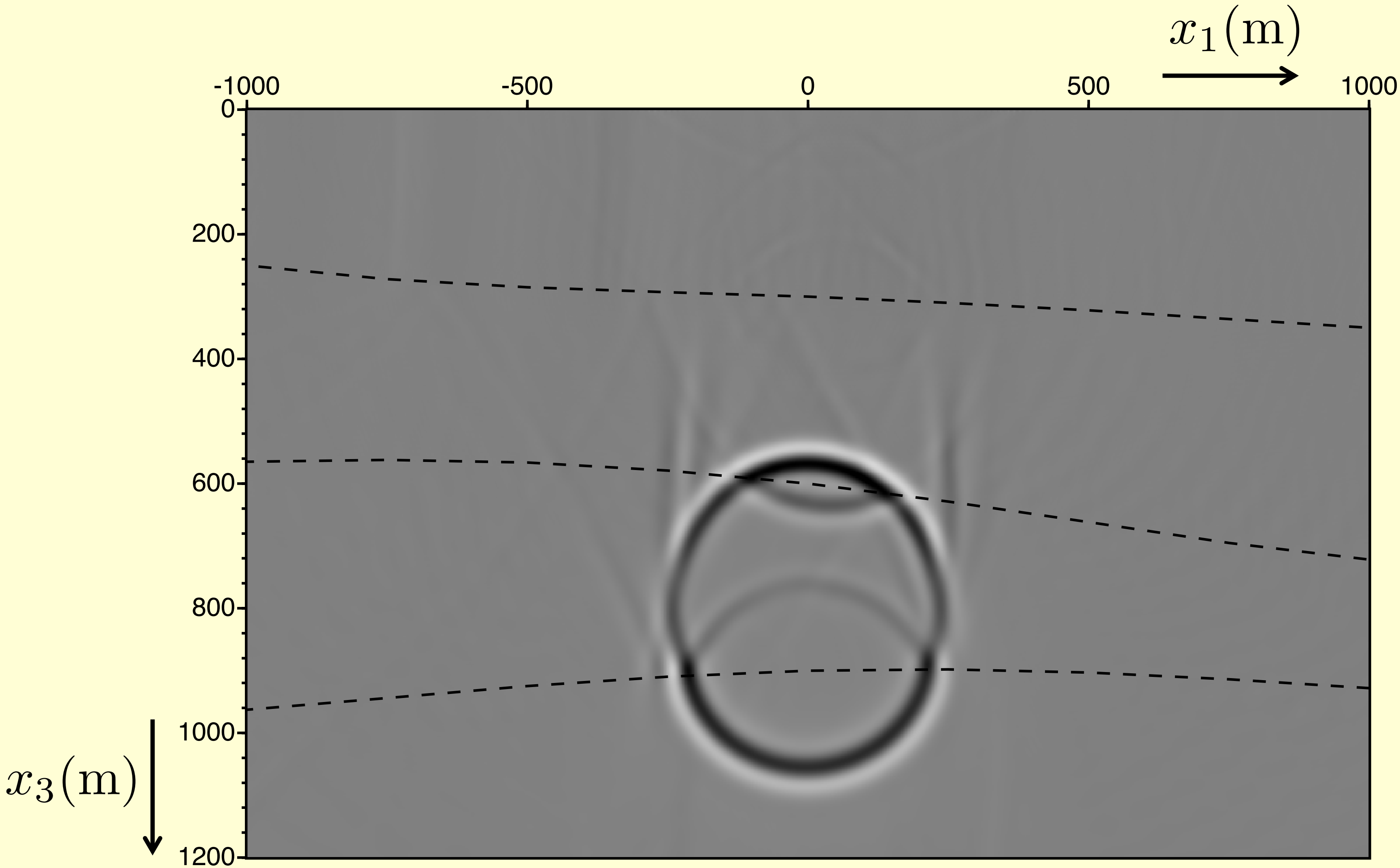

$t = -0.12\mathrm{s}$

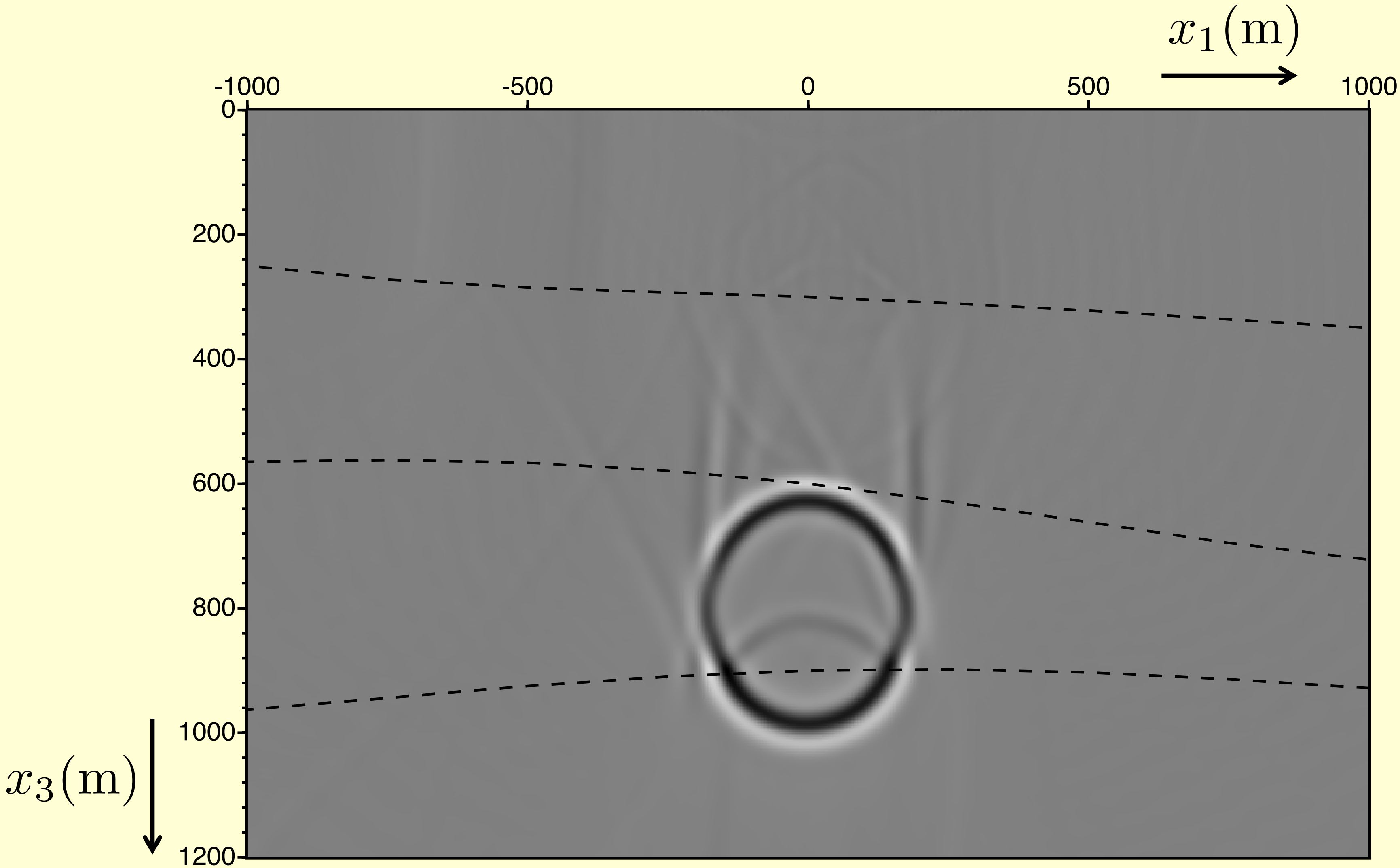

$t = -0.09$s

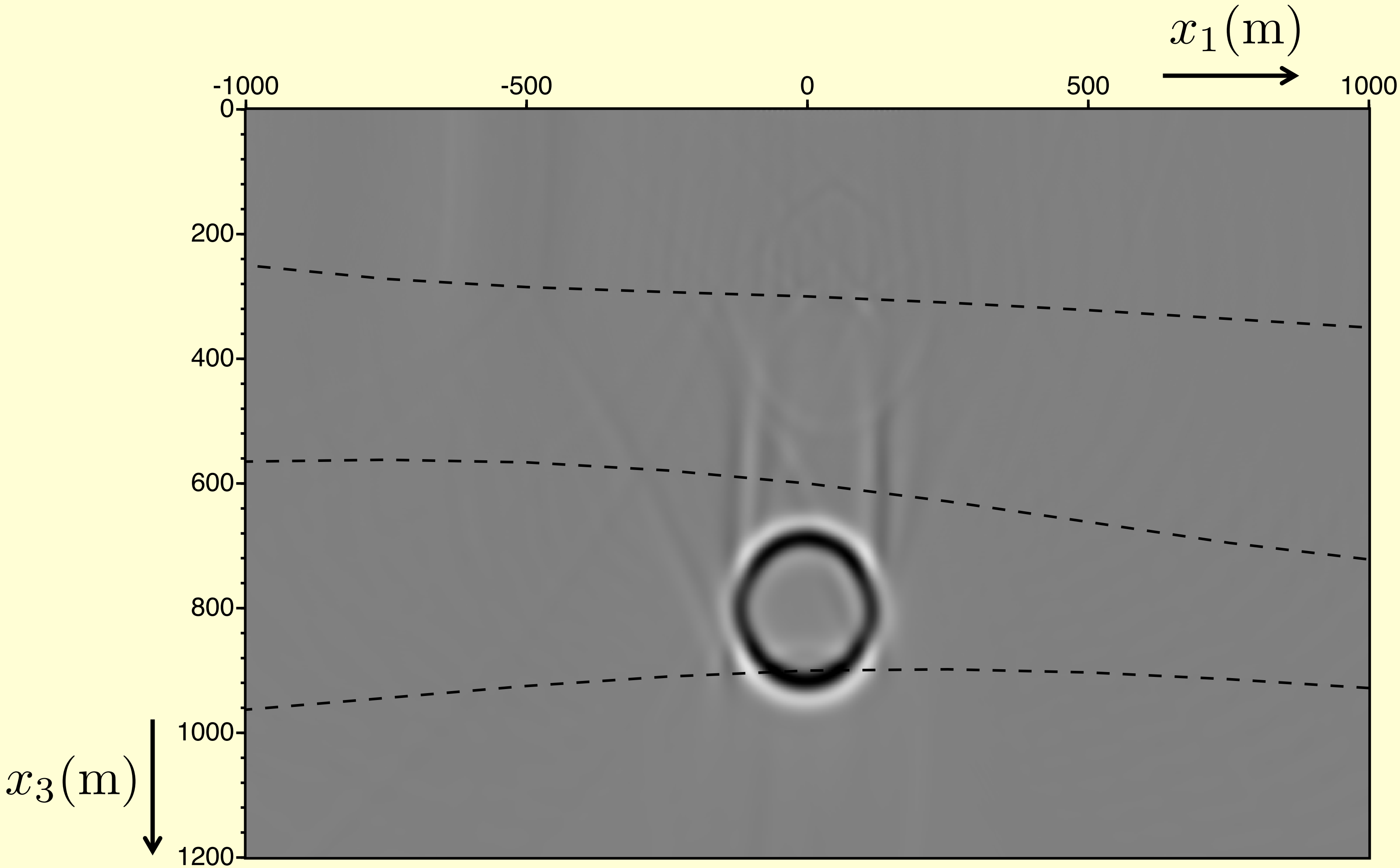

$t = -0.06$s

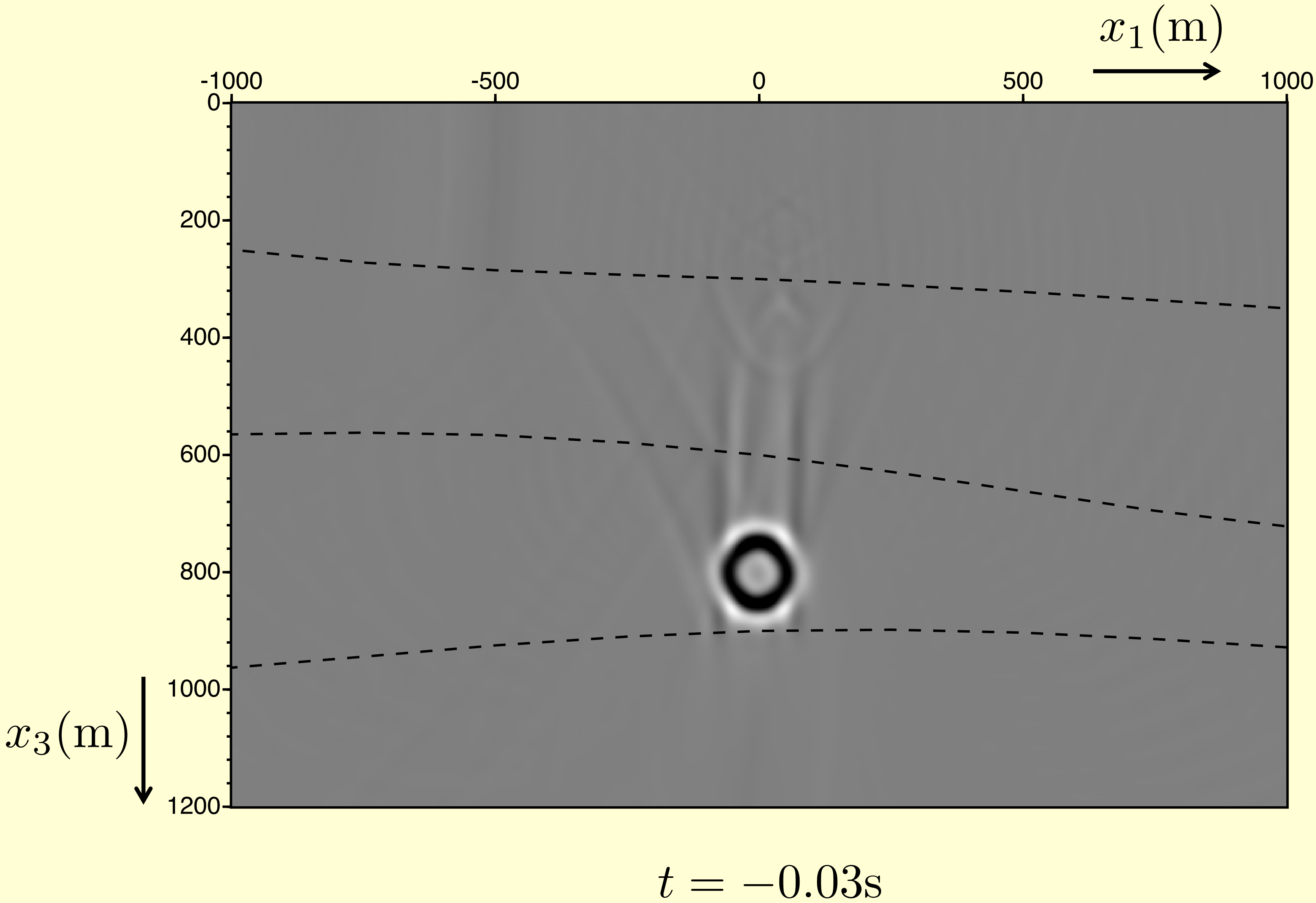

$x_1(\mathrm{m})$
-1000
-500
0
500
1000
0
200
400
600
800
1000
1200
$x_3(\mathrm{m})$
$t = -0.03\mathrm{s}$

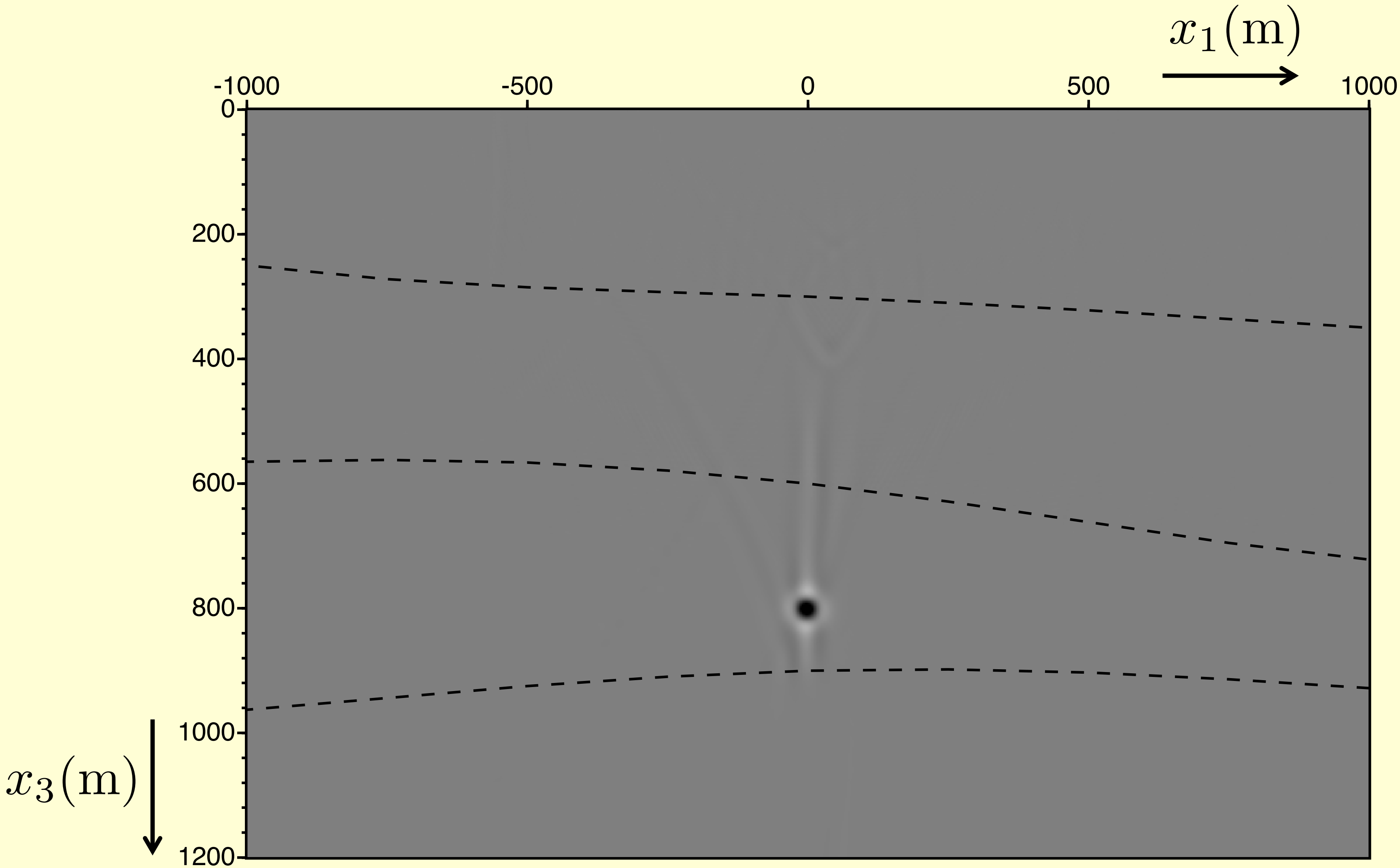

$t = 0.0\text{s}$

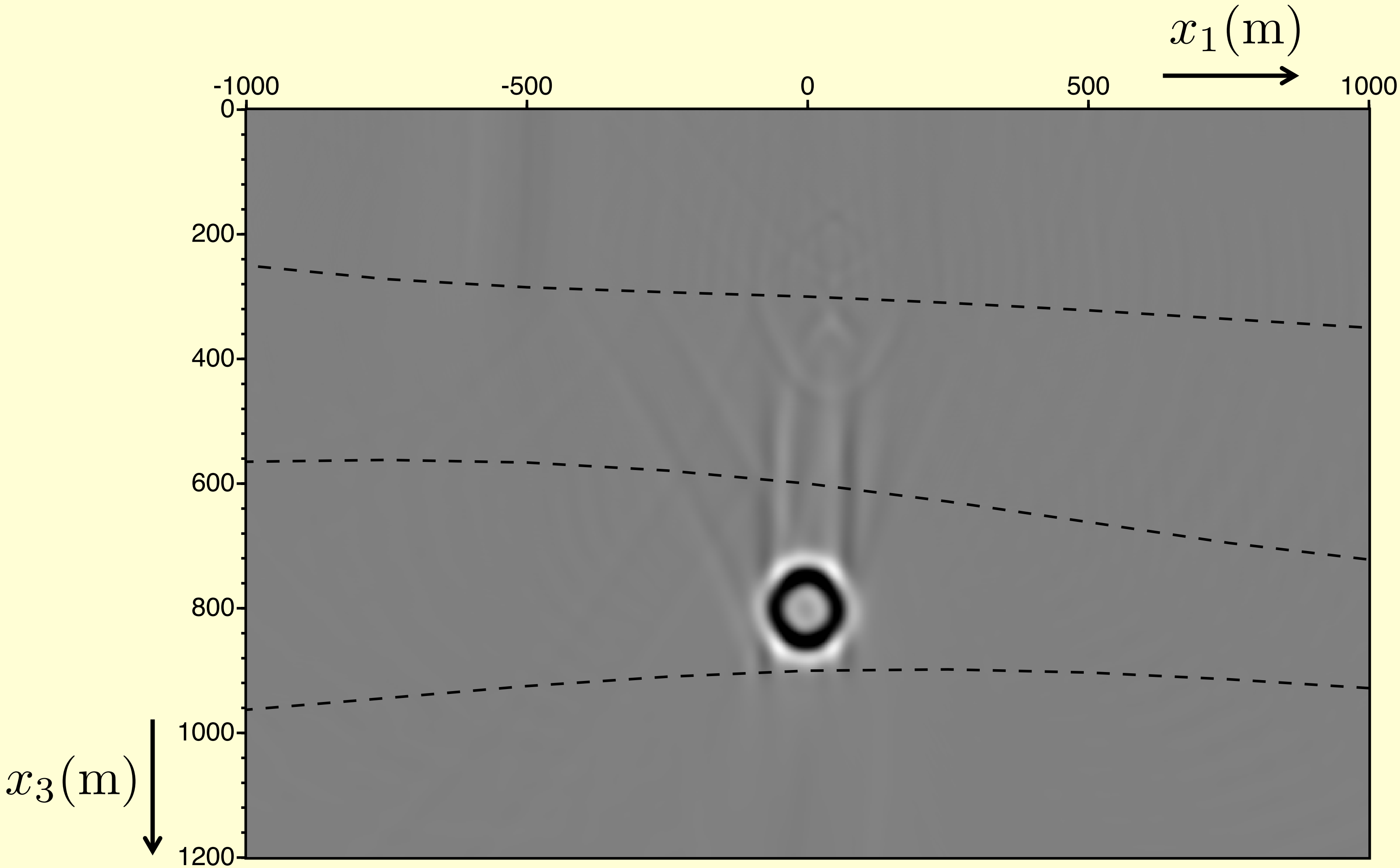

$t = 0.03\mathrm{s}$

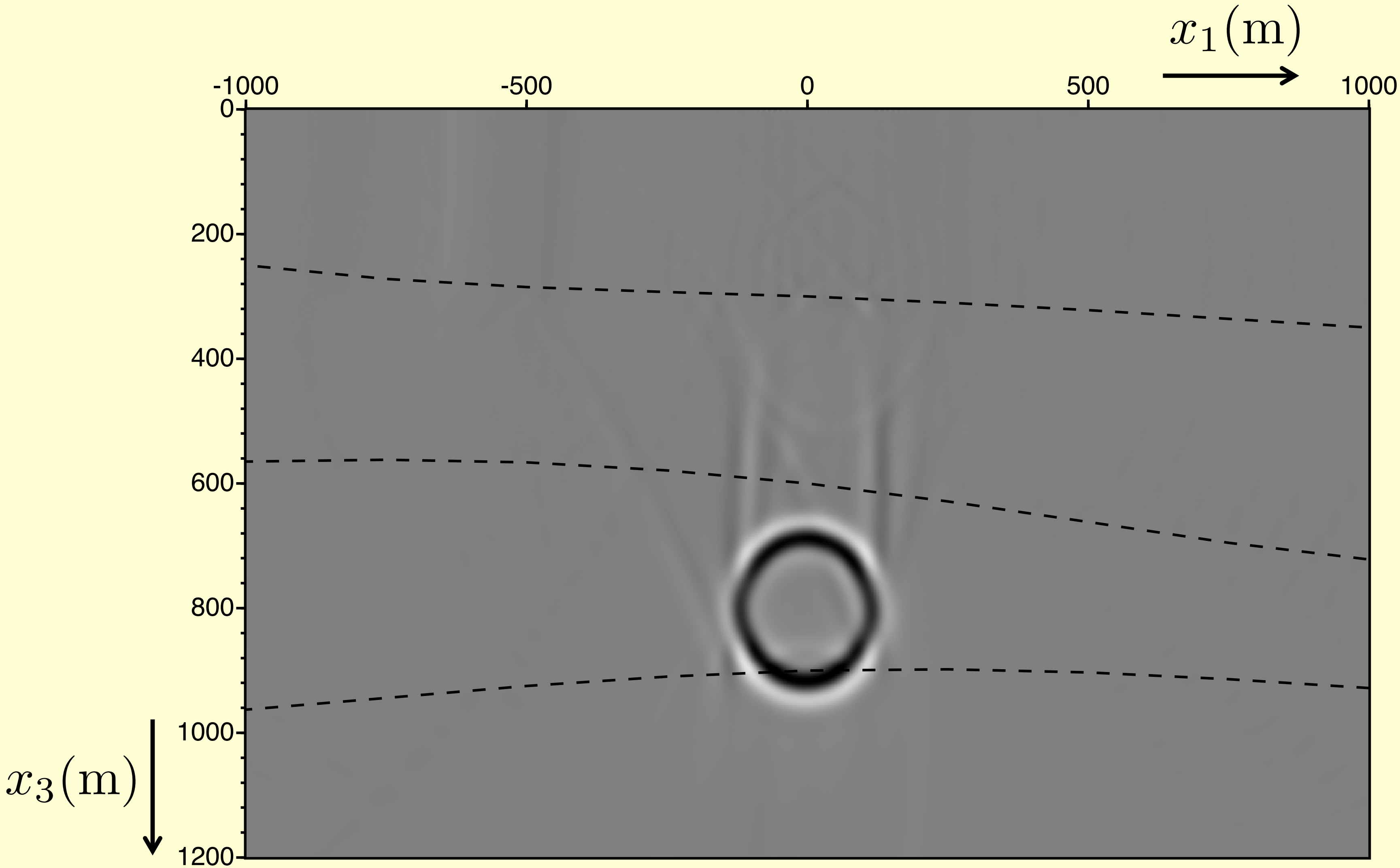

$t = 0.06$s

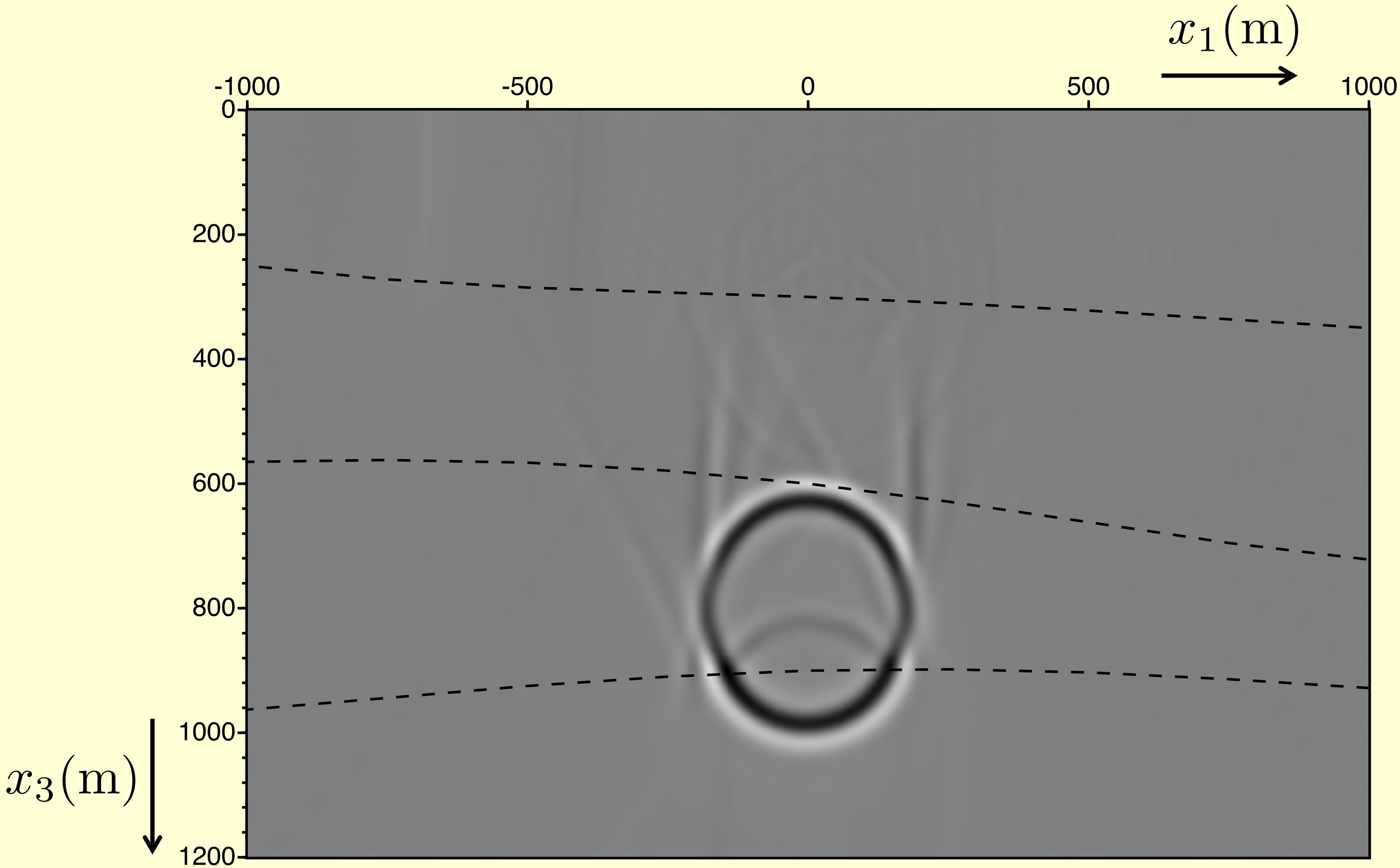

$t = 0.09\mathrm{s}$

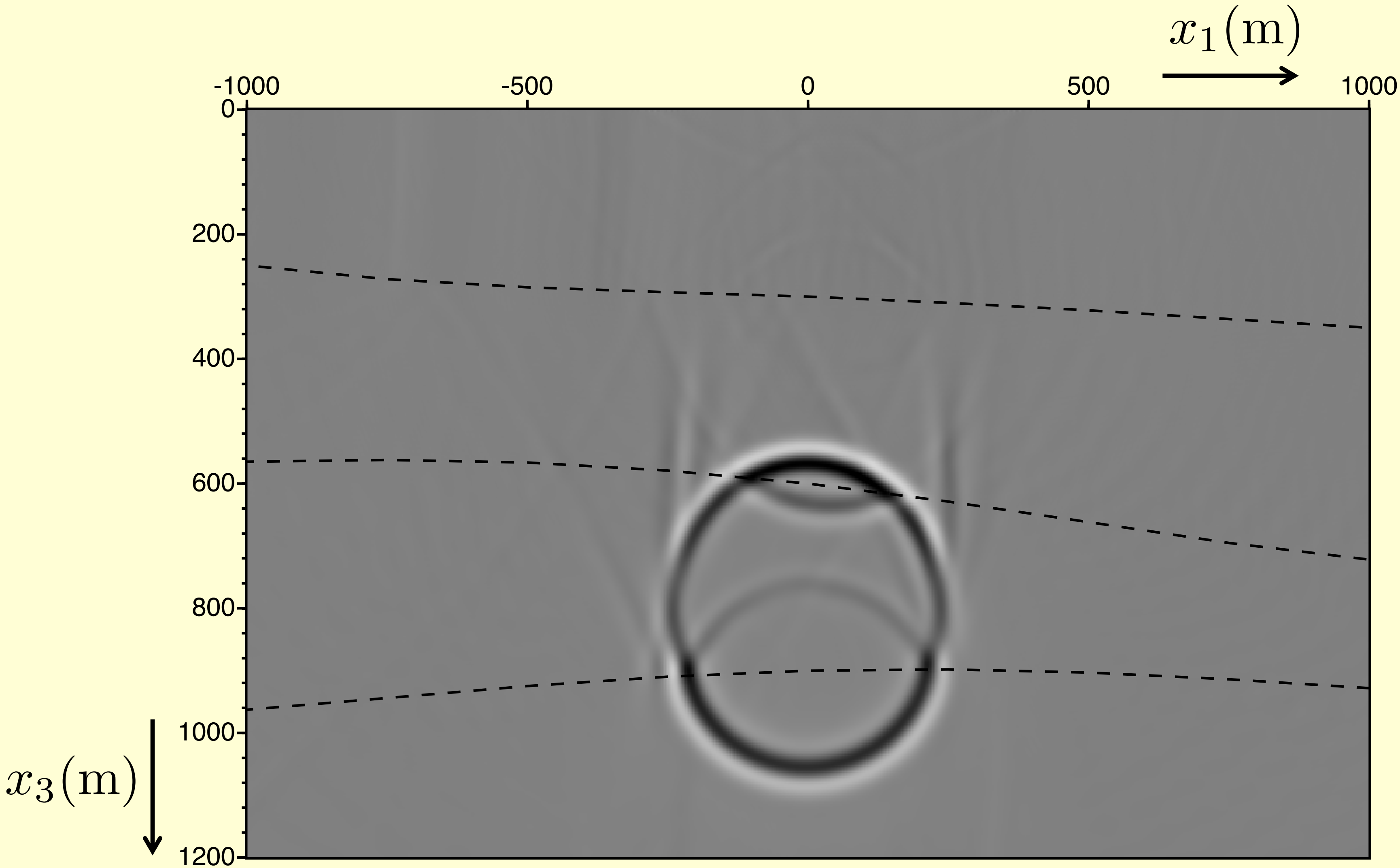

$t = 0.12\mathrm{s}$

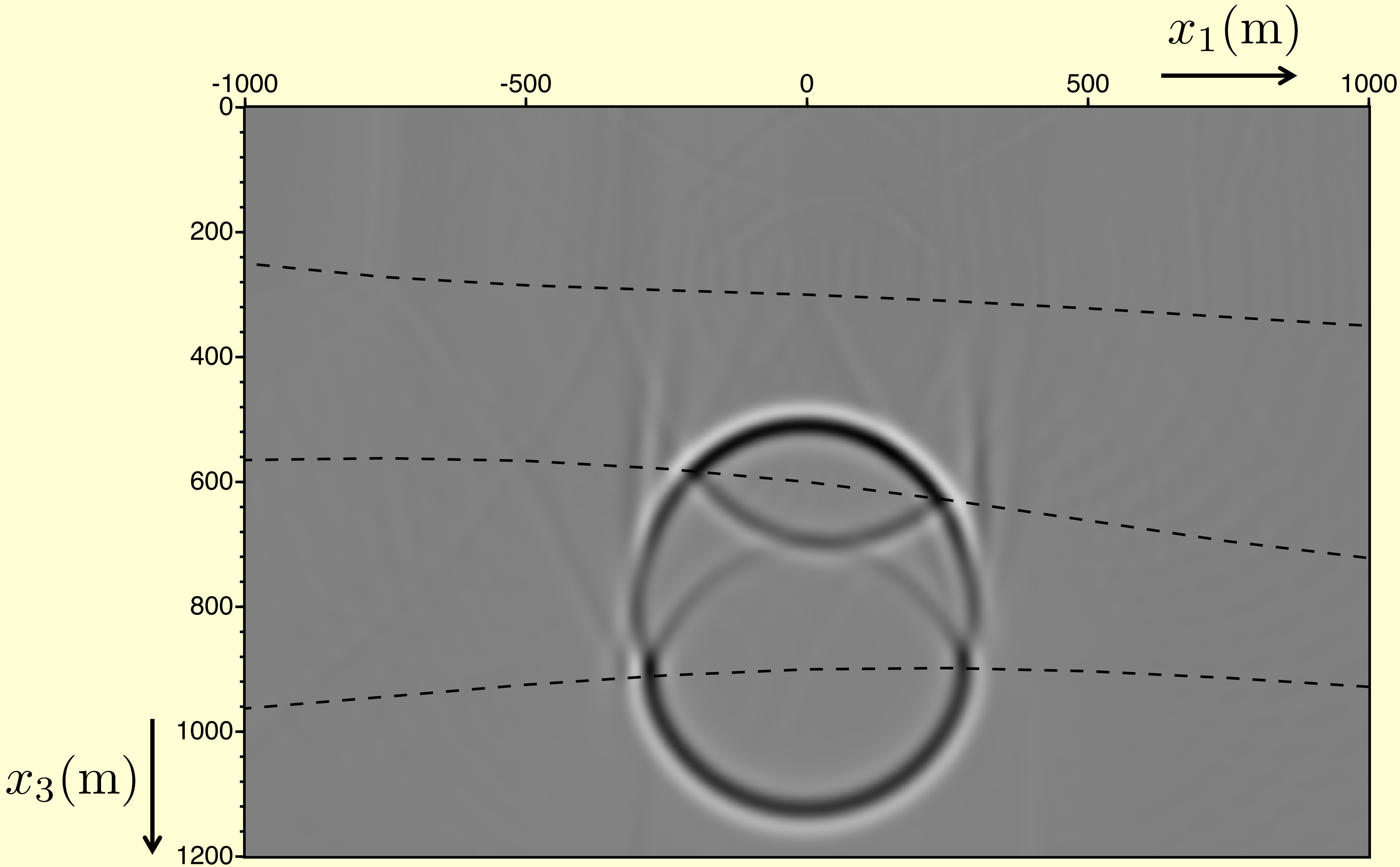

$t = 0.15\mathrm{s}$

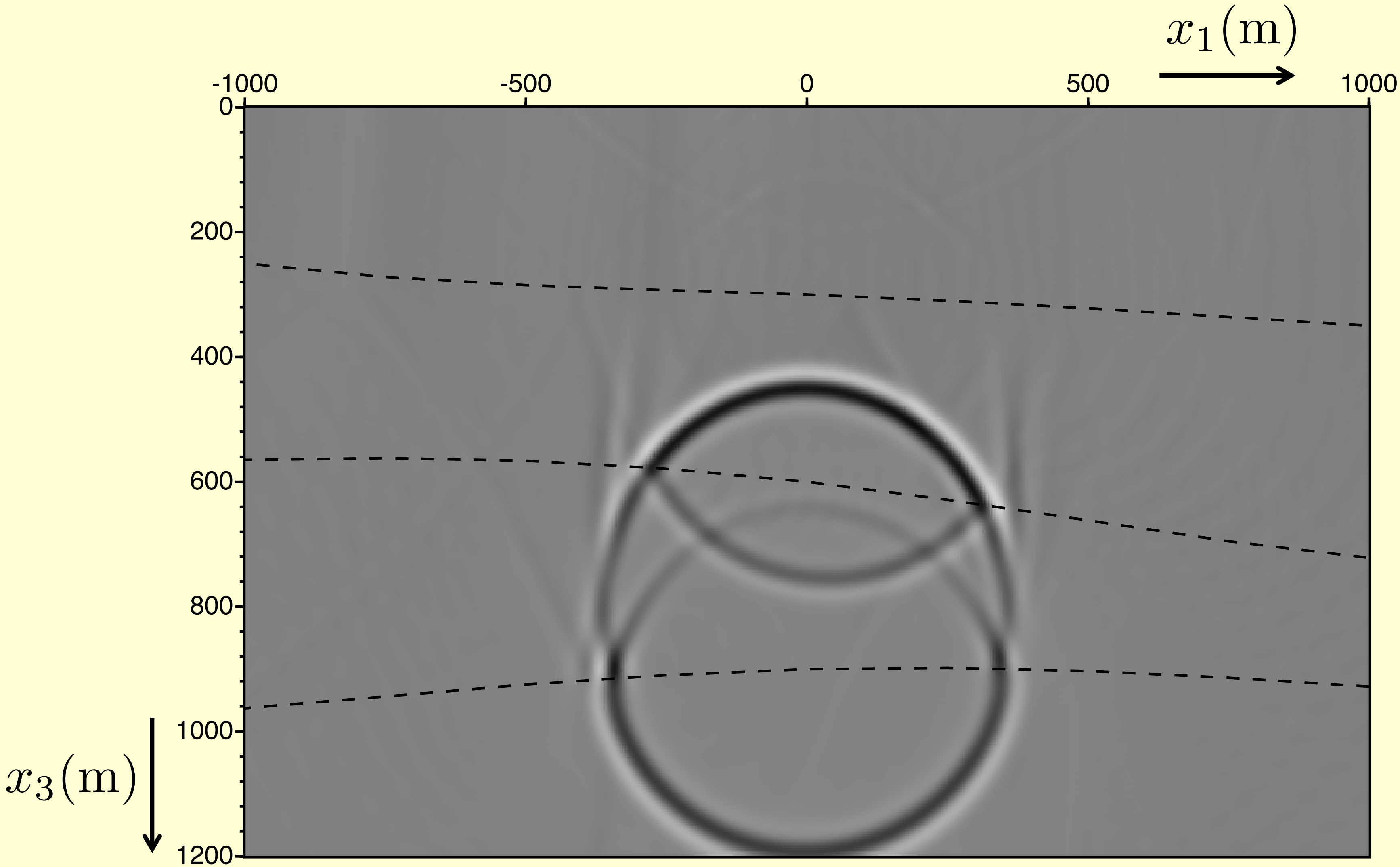

$t = 0.18\mathrm{s}$

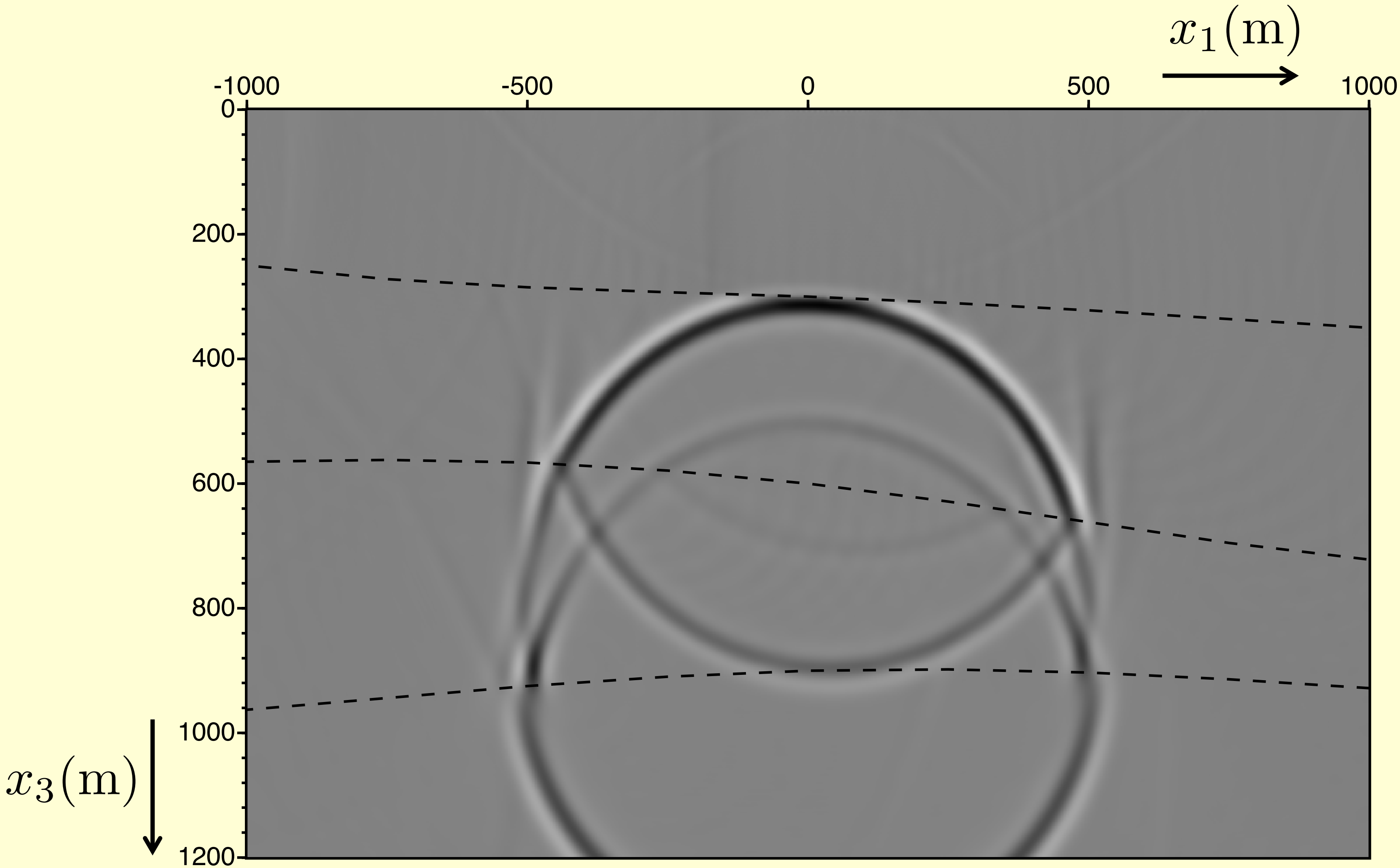

$t = 0.25\mathrm{s}$

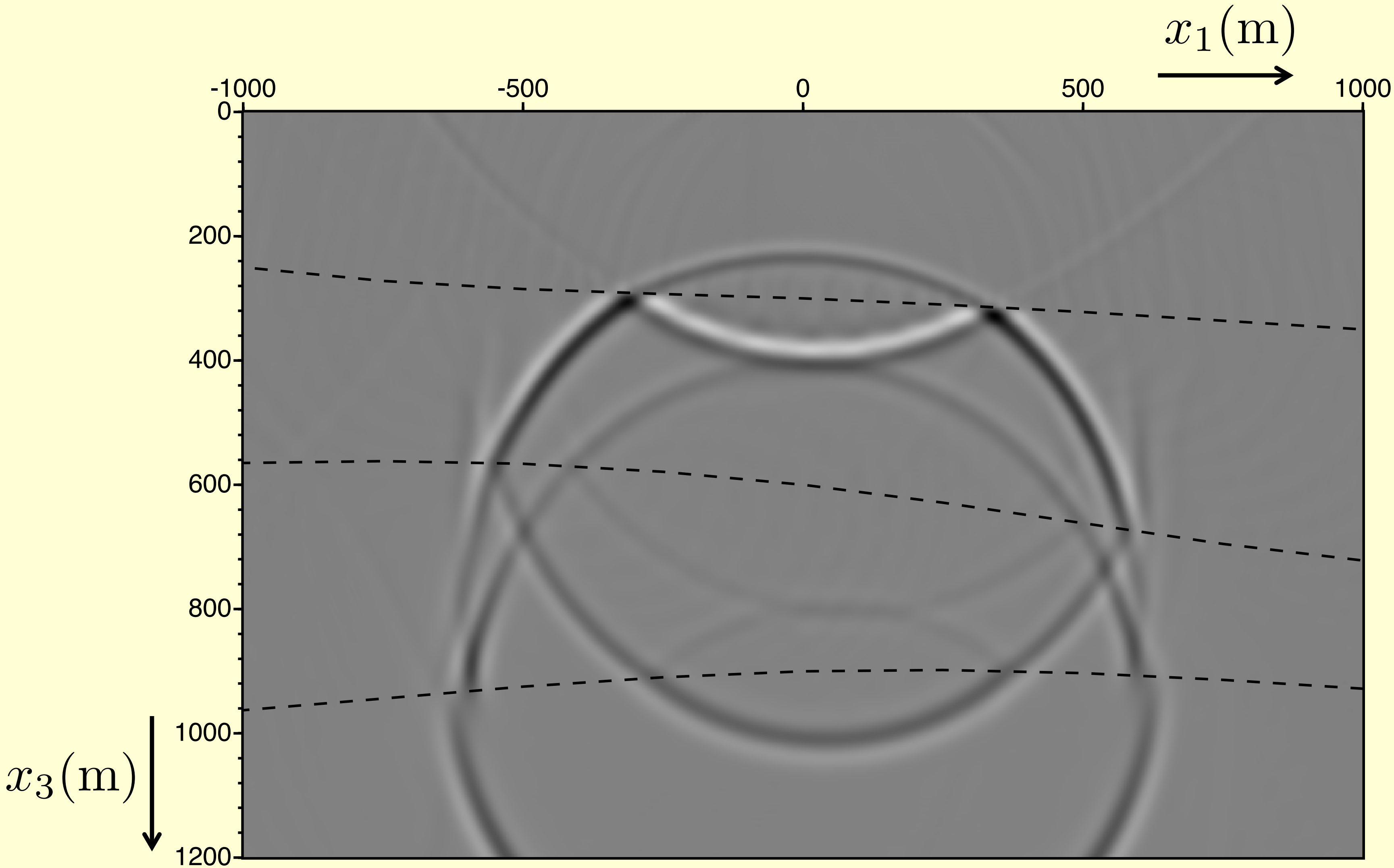

$t = 0.30$s

Seismic interferometry

or

Green’s function retrieval from ambient noise

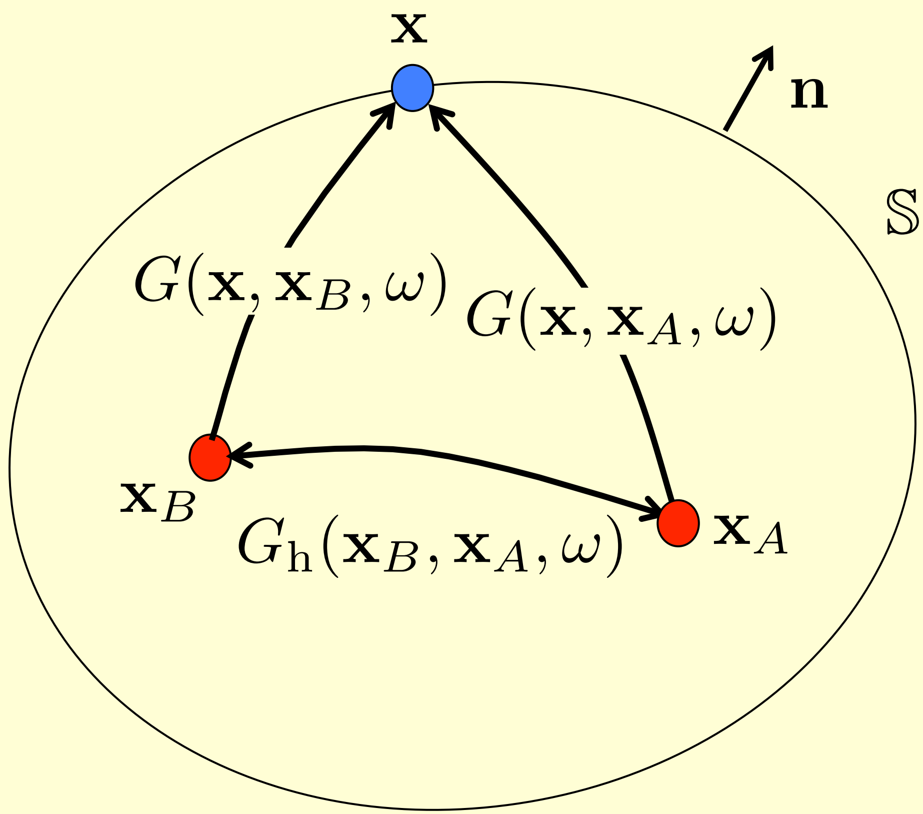

$$G(\mathbf{x}_B, \mathbf{x}_A, \omega) + G^*(\mathbf{x}_B, \mathbf{x}_A, \omega) =$$

$$\frac{1}{i\omega\rho} \oint_{\mathbb{S}} \Big(G^*(\mathbf{x}, \mathbf{x}_A, \omega) \partial_k G(\mathbf{x}, \mathbf{x}_B, \omega)$$

$$- \partial_k G^*(\mathbf{x}, \mathbf{x}_A, \omega) G(\mathbf{x}, \mathbf{x}_B, \omega) \Big) n_k \mathrm{d}^2\mathbf{x}$$

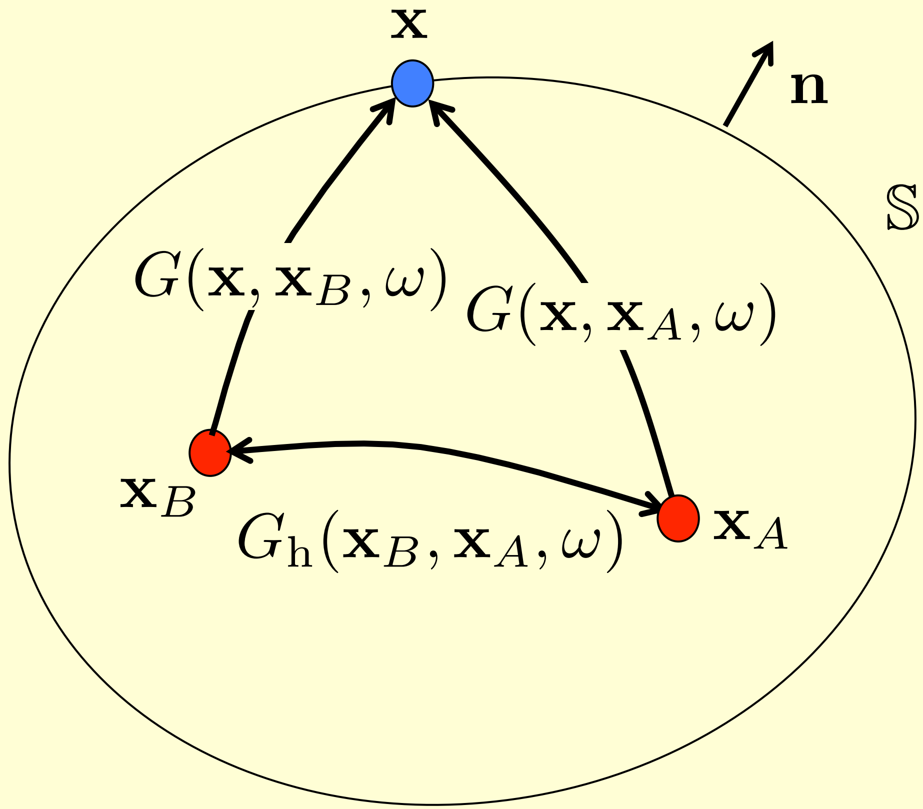

$$G(\mathbf{x}_B, \mathbf{x}_A, \omega) + G^*(\mathbf{x}_B, \mathbf{x}_A, \omega) =$$

$$-\frac{2}{i\omega\rho} \oint_{\mathbb{S}} G(\mathbf{x}, \mathbf{x}_B, \omega) \partial_k G^*(\mathbf{x}, \mathbf{x}_A, \omega) n_k \mathrm{d}^2\mathbf{x}$$

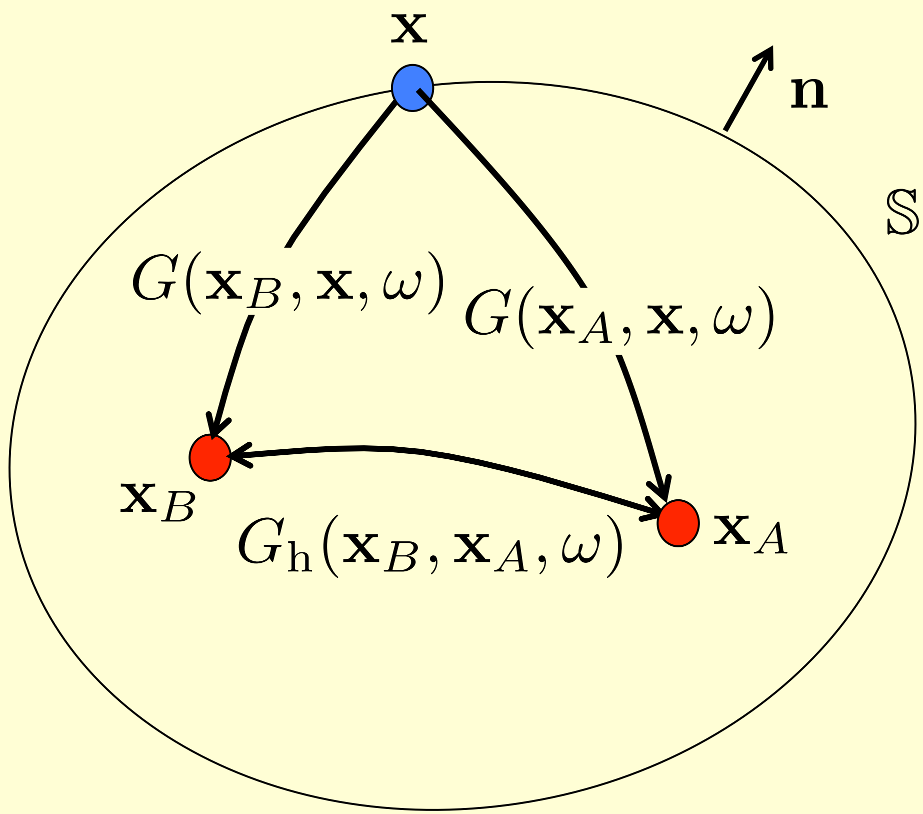

$$G(\mathbf{x}_B, \mathbf{x}_A, \omega) + G^*(\mathbf{x}_B, \mathbf{x}_A, \omega) \approx$$

$$\frac{2}{\rho_0 c_0} \oint_{\mathbb{S}} G(\mathbf{x}_B, \mathbf{x}, \omega) G^*(\mathbf{x}_A, \mathbf{x}, \omega) \mathrm{d}\mathbf{x}$$

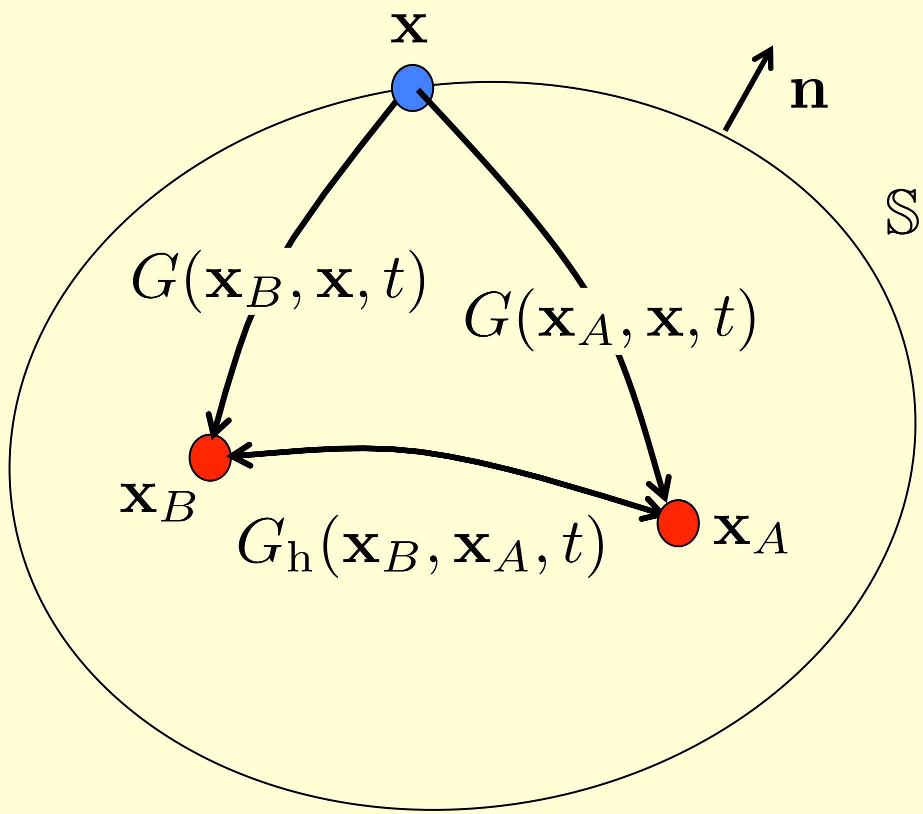

$$G(\mathbf{x}_B, \mathbf{x}_A, t) + G(\mathbf{x}_B, \mathbf{x}_A, -t) \approx$$

$$\frac{2}{\rho_0 c_0} \oint_{\mathbb{S}} G(\mathbf{x}_B, \mathbf{x}, t) * G(\mathbf{x}_A, \mathbf{x}, -t) \mathrm{d}\mathbf{x}$$

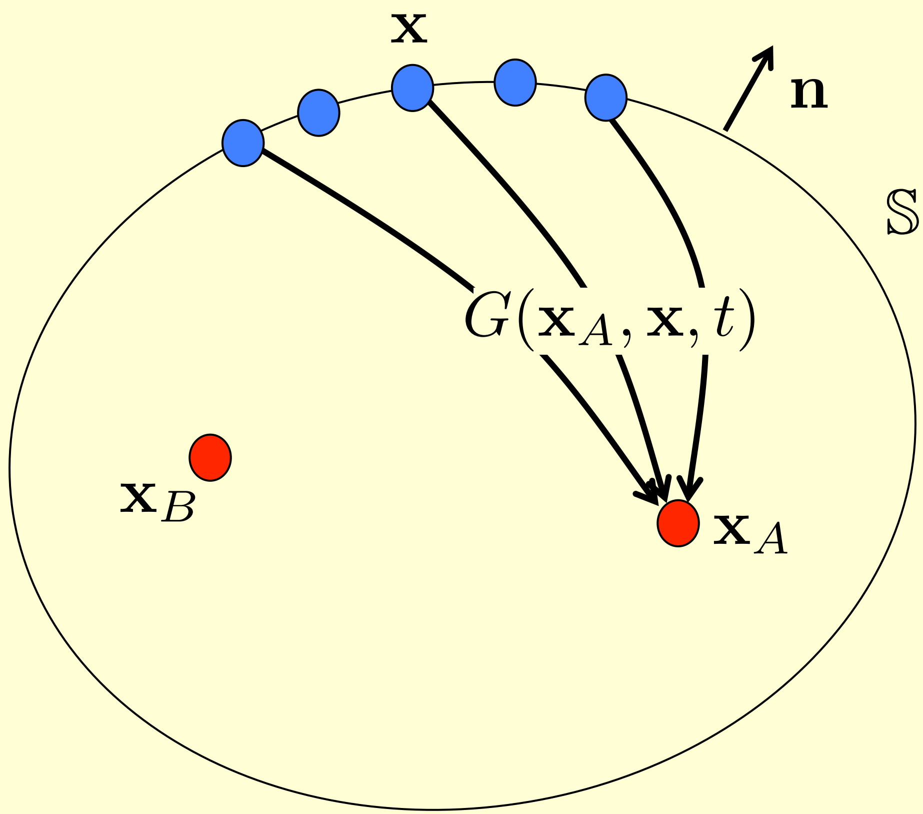

$$p(\mathbf{x}_A, t) = \oint_{\mathbb{S}} G(\mathbf{x}_A, \mathbf{x}, t) * N(\mathbf{x}, t) \mathrm{d}\mathbf{x}$$

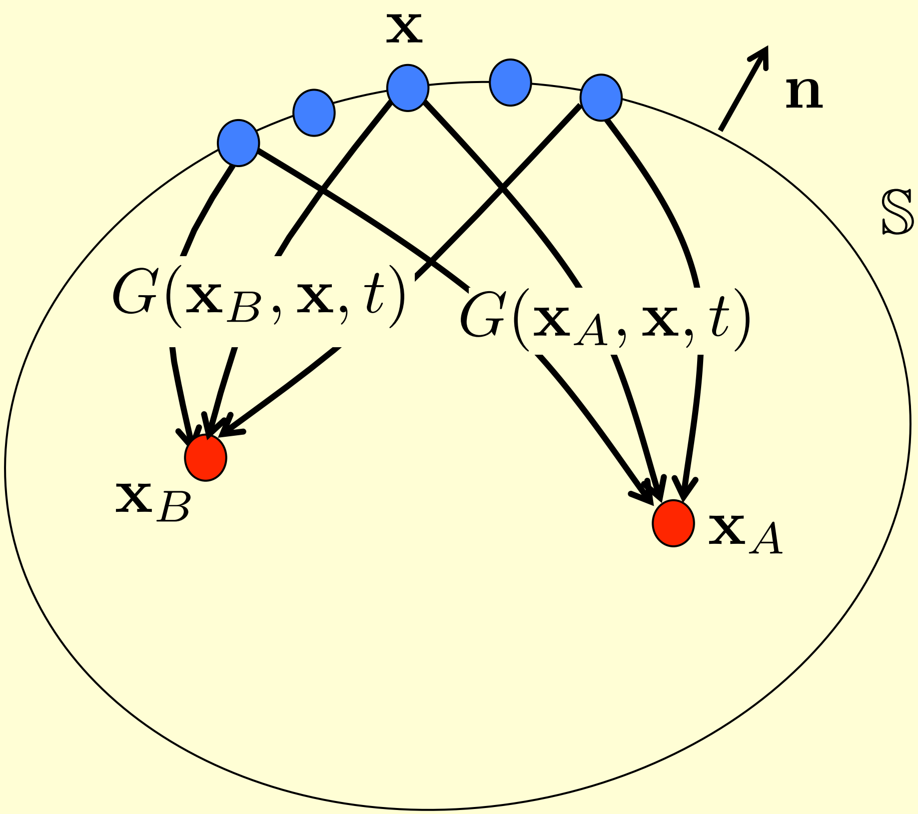

$$p(\mathbf{x}_A, t) = \oint_{\mathbb{S}} G(\mathbf{x}_A, \mathbf{x}, t) * N(\mathbf{x}, t) \mathrm{d}\mathbf{x}$$

$$p(\mathbf{x}_B, t) = \oint_{\mathbb{S}} G(\mathbf{x}_B, \mathbf{x}', t) * N(\mathbf{x}', t) \mathrm{d}\mathbf{x}'$$

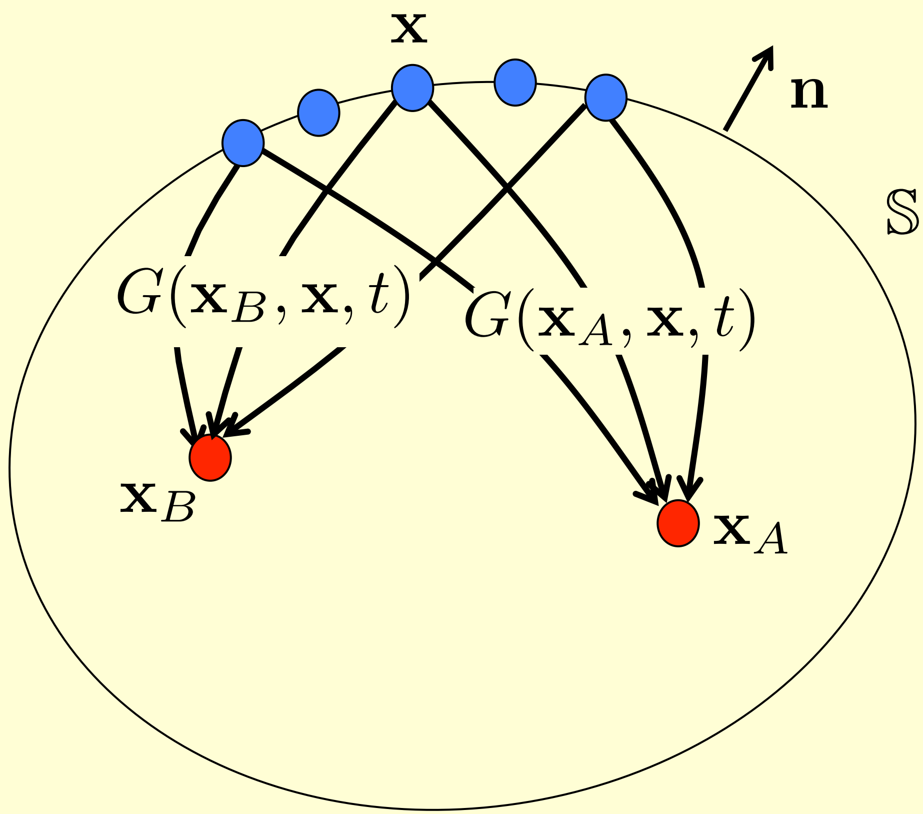

$$p(\mathbf{x}_A, t) = \oint_{\mathbb{S}} G(\mathbf{x}_A, \mathbf{x}, t) * N(\mathbf{x}, t) \mathrm{d}\mathbf{x}$$

$$p(\mathbf{x}_B, t) = \oint_{\mathbb{S}} G(\mathbf{x}_B, \mathbf{x}', t) * N(\mathbf{x}', t) \mathrm{d}\mathbf{x}'$$

$$\langle N(\mathbf{x}', t) * N(\mathbf{x}, -t) \rangle = \delta(\mathbf{x} - \mathbf{x}') C_N(t)$$

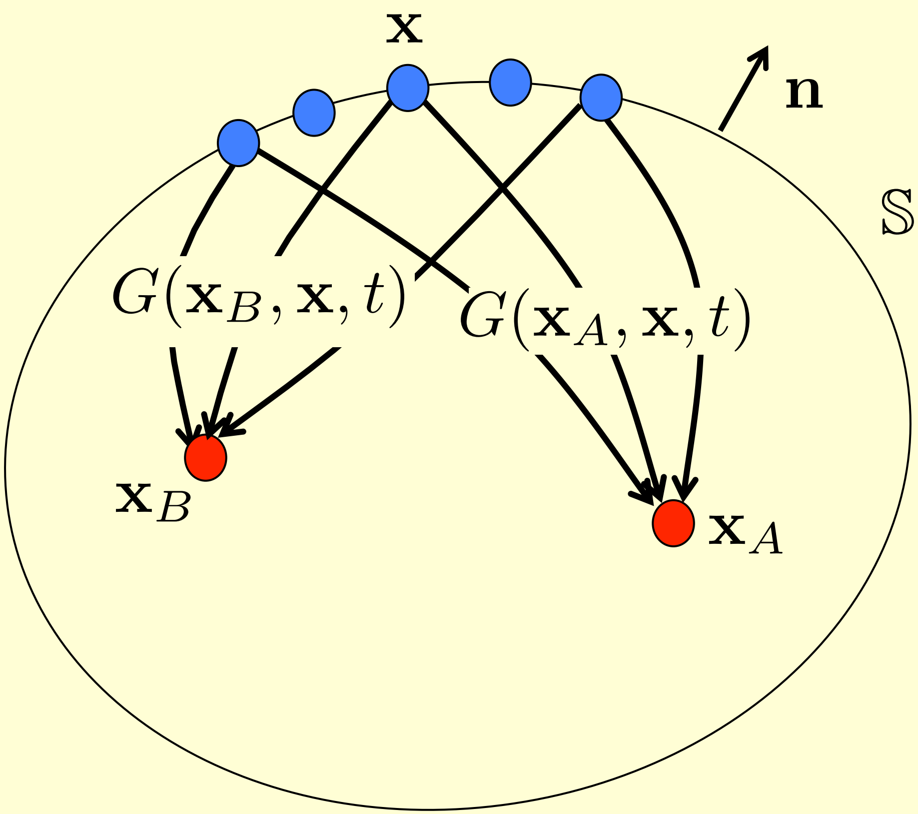

$$p(\mathbf{x}_A, t) = \oint_{\mathbb{S}} G(\mathbf{x}_A, \mathbf{x}, t) * N(\mathbf{x}, t) \mathrm{d}\mathbf{x}$$

$$p(\mathbf{x}_B, t) = \oint_{\mathbb{S}} G(\mathbf{x}_B, \mathbf{x}', t) * N(\mathbf{x}', t) \mathrm{d}\mathbf{x}'$$

$$\langle p(\mathbf{x}_B, t) * p(\mathbf{x}_A, -t) \rangle = \oint_{\mathbb{S}} G(\mathbf{x}_B, \mathbf{x}, t) * G(\mathbf{x}_A, \mathbf{x}, -t) * C_N(t) \mathrm{d}\mathbf{x}$$

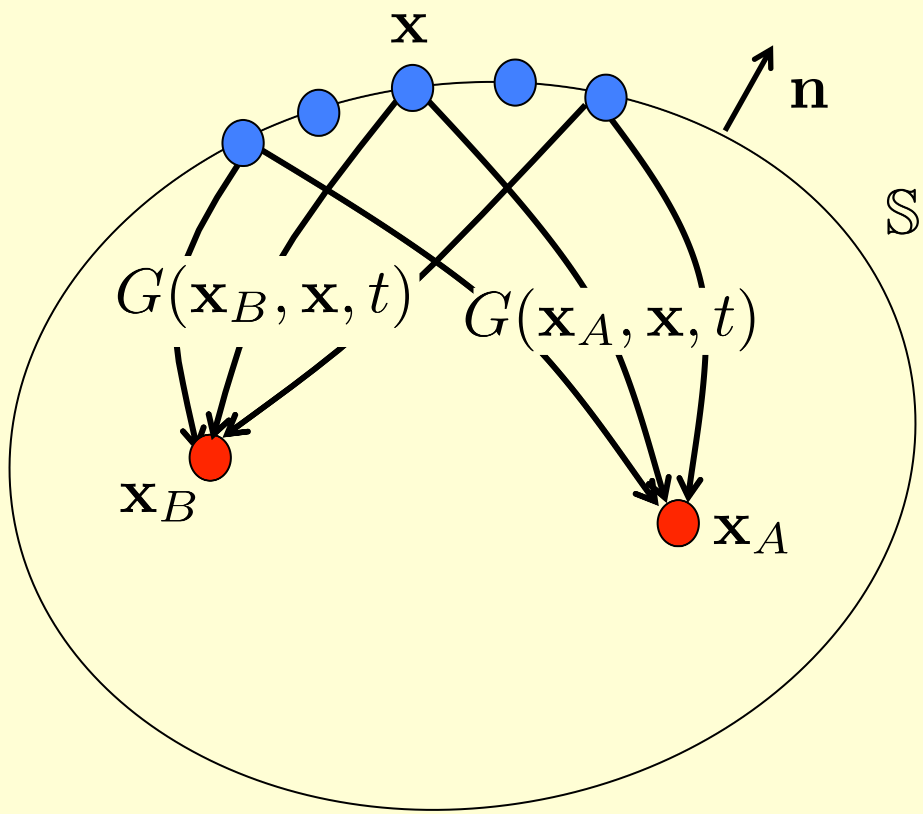

$$G(\mathbf{x}_B, \mathbf{x}_A, t) + G(\mathbf{x}_B, \mathbf{x}_A, -t) \approx$$

$$\frac{2}{\rho_0 c_0} \oint_{\mathbb{S}} G(\mathbf{x}_B, \mathbf{x}, t) * G(\mathbf{x}_A, \mathbf{x}, -t) \mathrm{d}\mathbf{x}$$

$$\langle p(\mathbf{x}_B, t) * p(\mathbf{x}_A, -t) \rangle = \oint_{\mathbb{S}} G(\mathbf{x}_B, \mathbf{x}, t) * G(\mathbf{x}_A, \mathbf{x}, -t) * C_N(t) \mathrm{d}\mathbf{x}$$

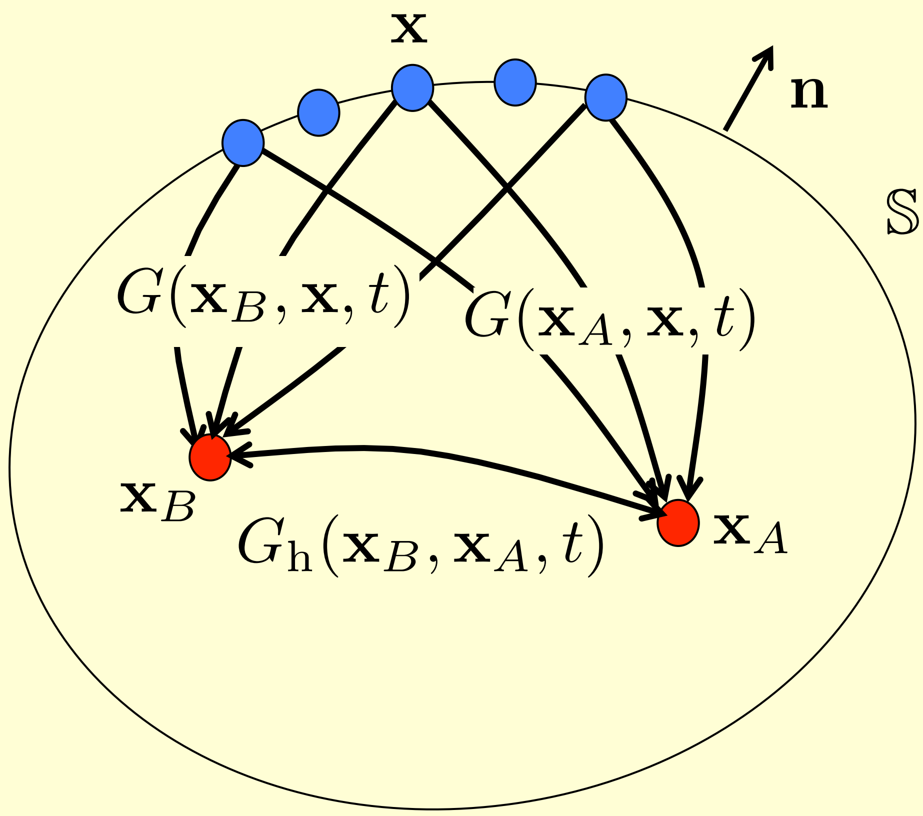

$$\langle p(\mathbf{x}_B, t) * p(\mathbf{x}_A, -t)\rangle \propto \{G(\mathbf{x}_B, \mathbf{x}_A, t) + G(\mathbf{x}_B, \mathbf{x}_A, -t)\} * C_N(t)$$

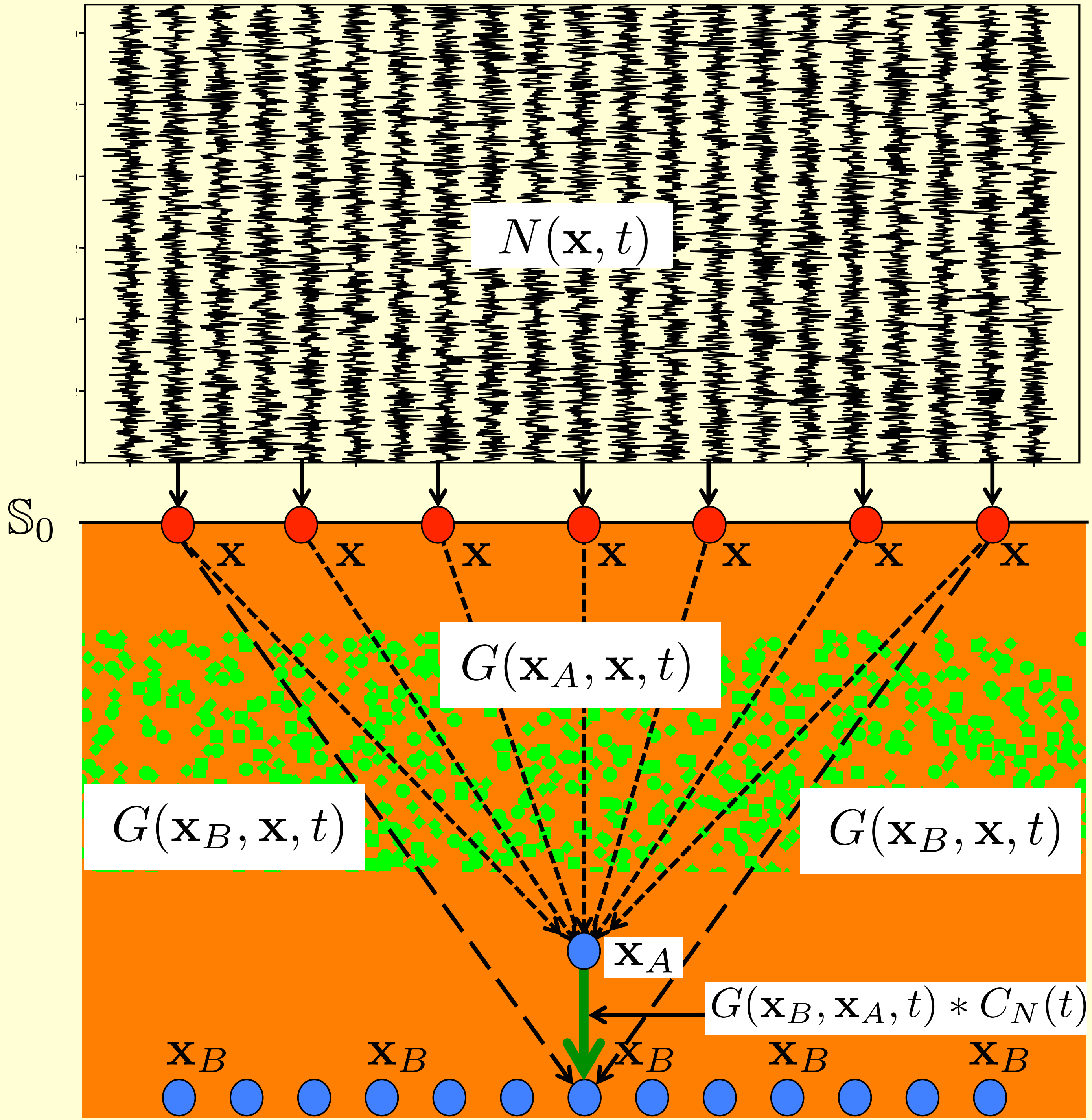

$N(\mathbf{x}, t)$
$\mathbb{S}_0$
$\mathbf{x}$
$\mathbf{x}$
$\mathbf{x}$
$\mathbf{x}$
$\mathbf{x}$
$\mathbf{x}$
$\mathbf{x}$
$G(\mathbf{x}_A, \mathbf{x}, t)$
$G(\mathbf{x}_B, \mathbf{x}, t)$
$G(\mathbf{x}_B, \mathbf{x}, t)$
$\mathbf{x}_A$
$G(\mathbf{x}_B, \mathbf{x}_A, t) * C_N(t)$
$\mathbf{x}_B$
$\mathbf{x}_B$
$\mathbf{x}_B$
$\mathbf{x}_B$
$\mathbf{x}_B$

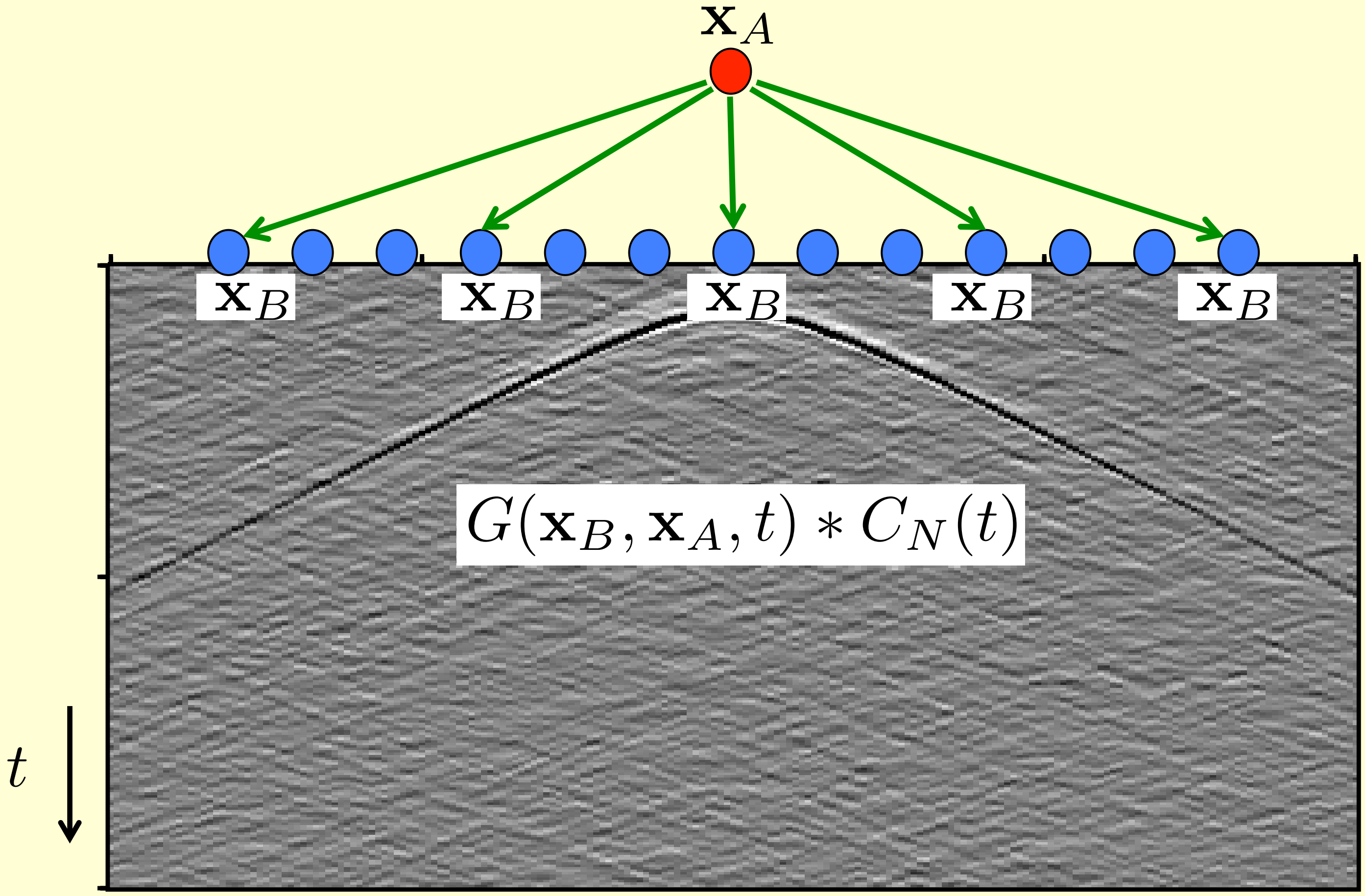
$\mathbf{x}_A$
$\mathbf{x}_B$
$\mathbf{x}_B$
$\mathbf{x}_B$
$\mathbf{x}_B$
$\mathbf{x}_B$
$G(\mathbf{x}_B, \mathbf{x}_A, t) * C_N(t)$
t

Eikonal tomography: surface wave tomography by phase front tracking across a regional broad-band seismic array

Fan-Chi Lin,[1] Michael H. Ritzwoller[1] and Roel Snieder[2]

Geophys. J. Int. (2009) **177,** 1091–1110

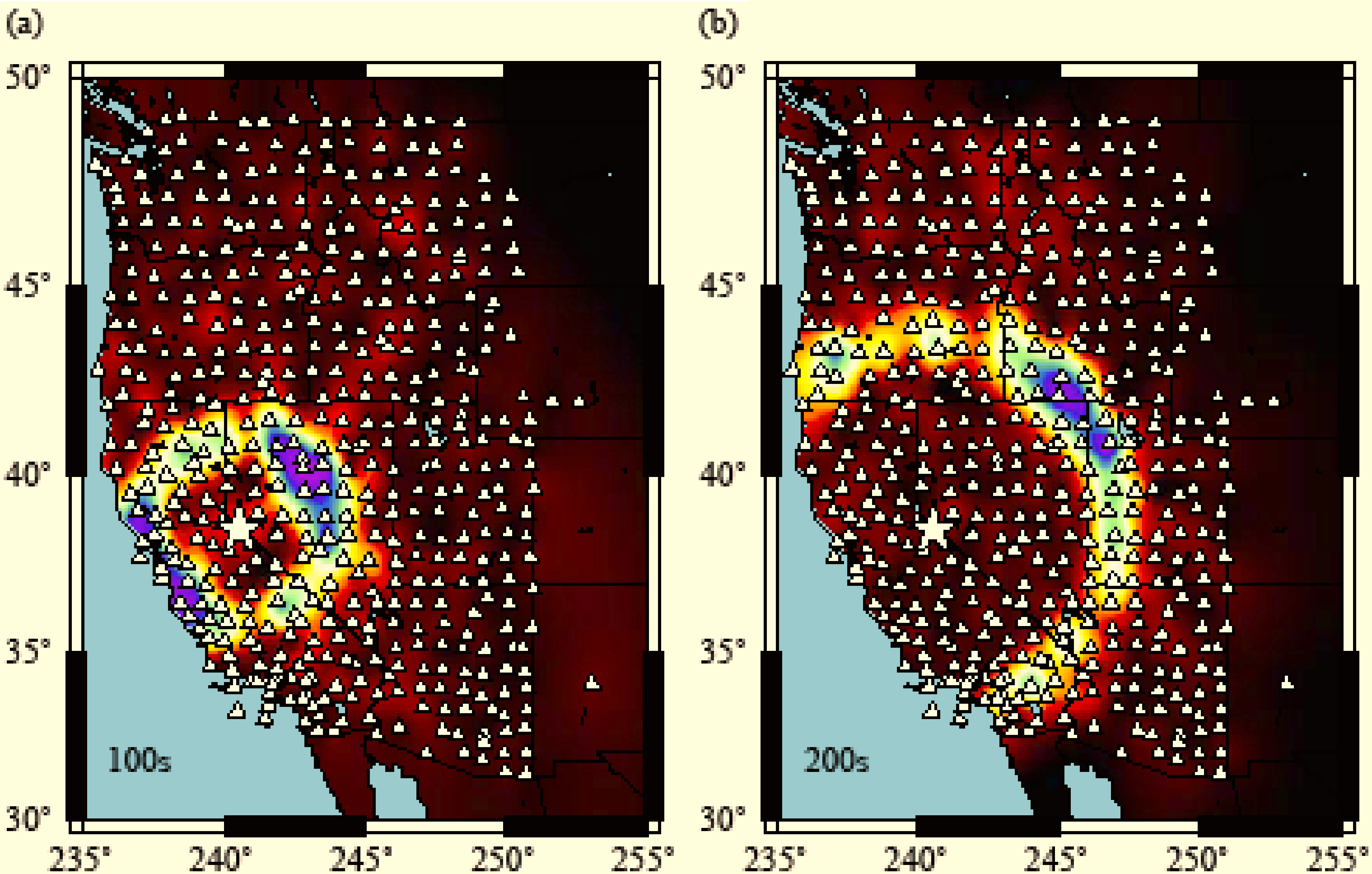

GEOPHYSICS, VOL. 74, NO. 5 (SEPTEMBER-OCTOBER 2009); P. A63–A67, 5 FIGS.
10.1190/1.3193529

Reflection images from ambient seismic noise

Deyan Draganov[1], Xander Campman[2], Jan Thorbecke[1], Arie Verdel[2], and Kees Wapenaar[1]

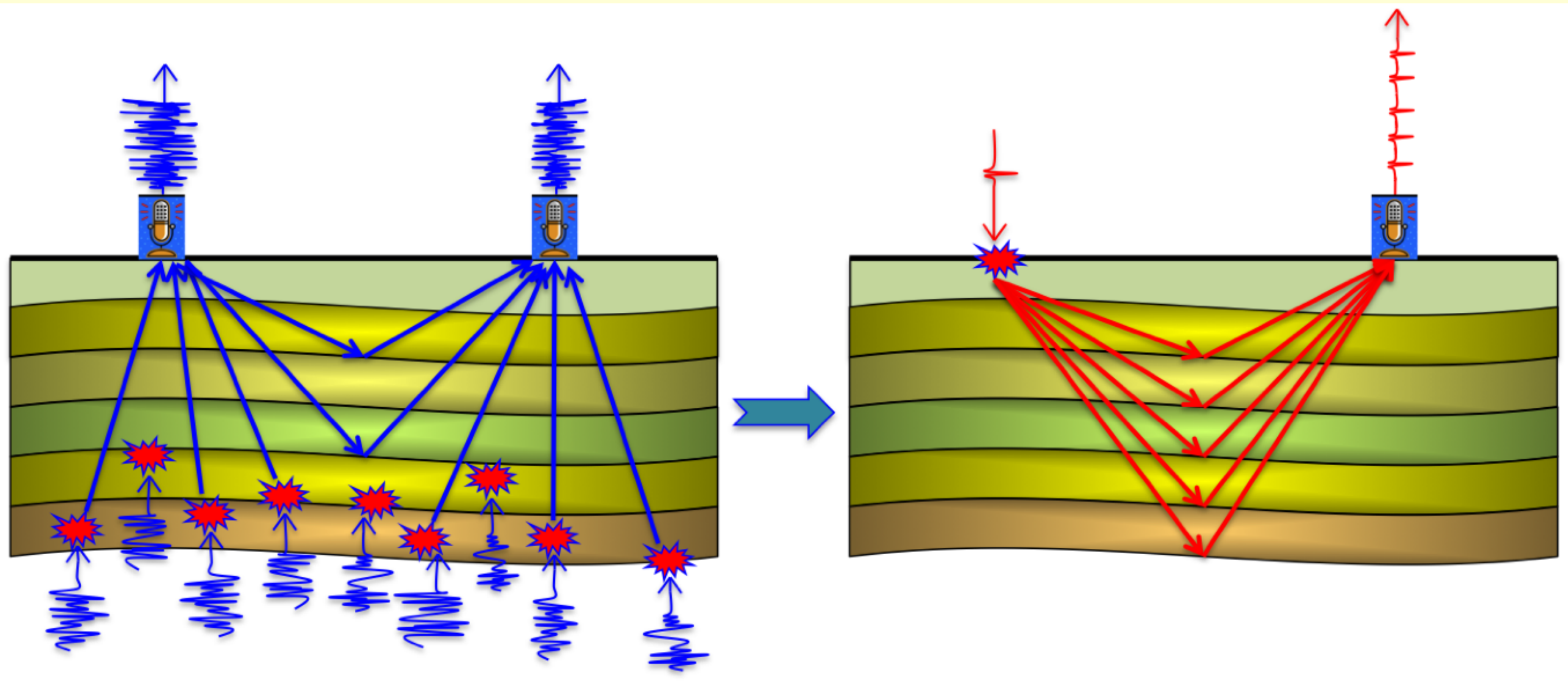

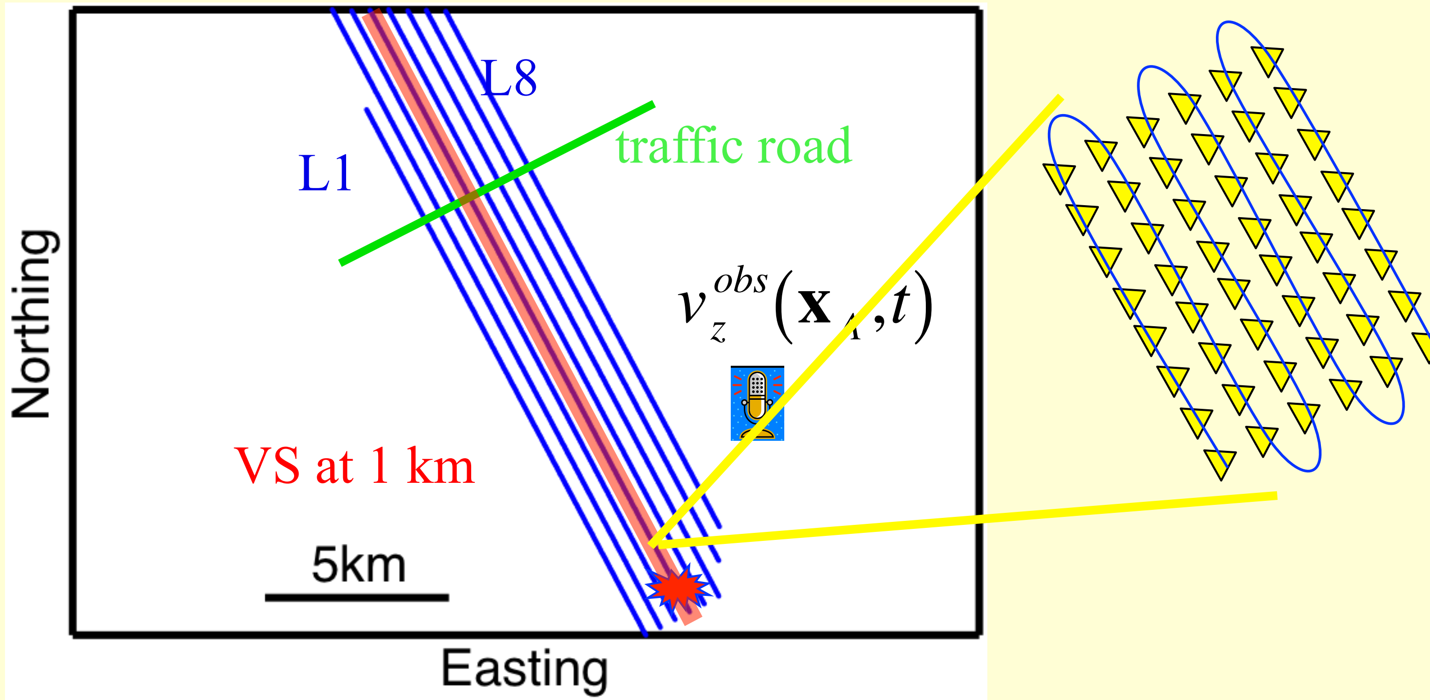

- 8 lines with 500 m spacing
- About 400 receiver positions per line
- Receiver positions at every 50 m
- Each receiver position = geophone group

- About 11 hours of recording time
- About 900 noise panels of 47 s

- Active-source data recorded along the same lines

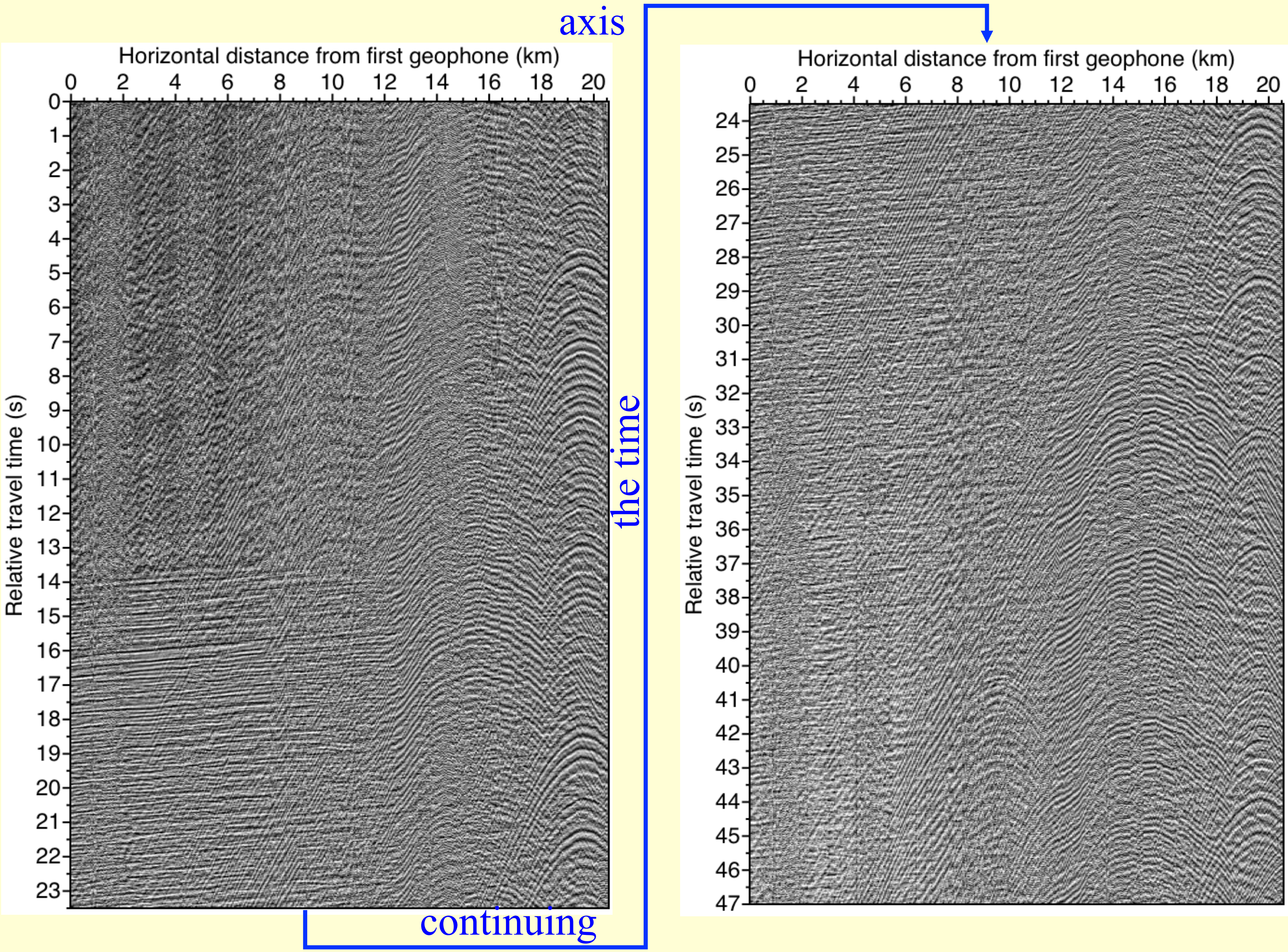
Horizontal distance from first geophone (km)
Relative travel time (s)
continuing the time axis
Horizontal distance from first geophone (km)
Relative travel time (s)

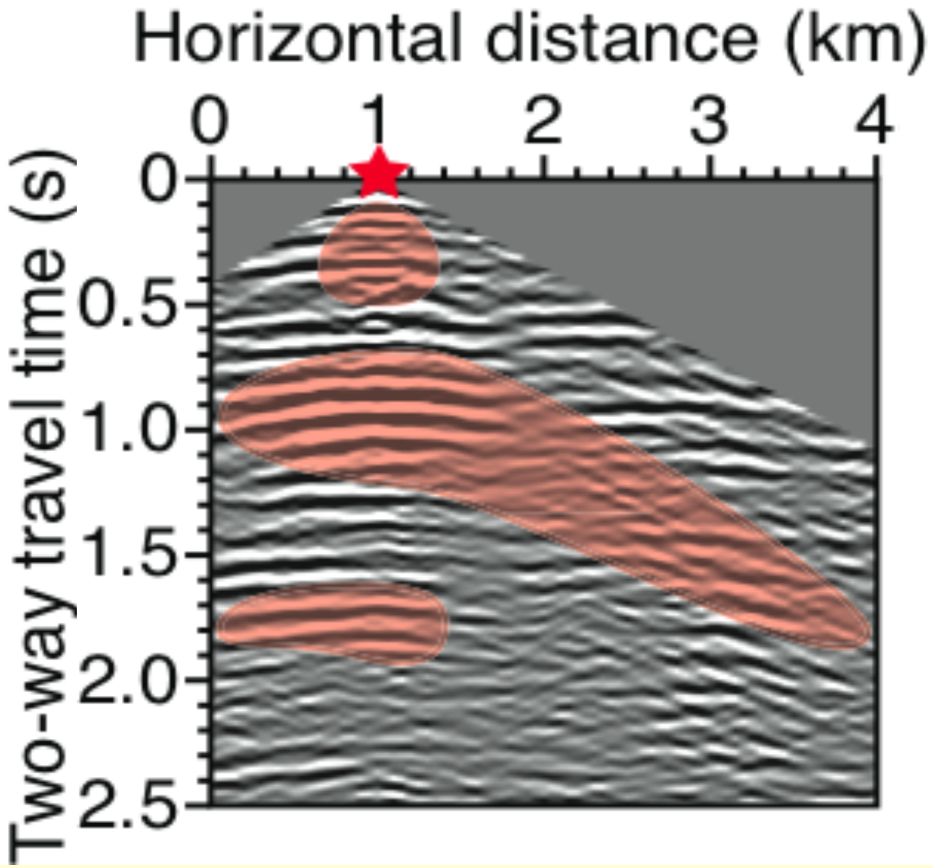

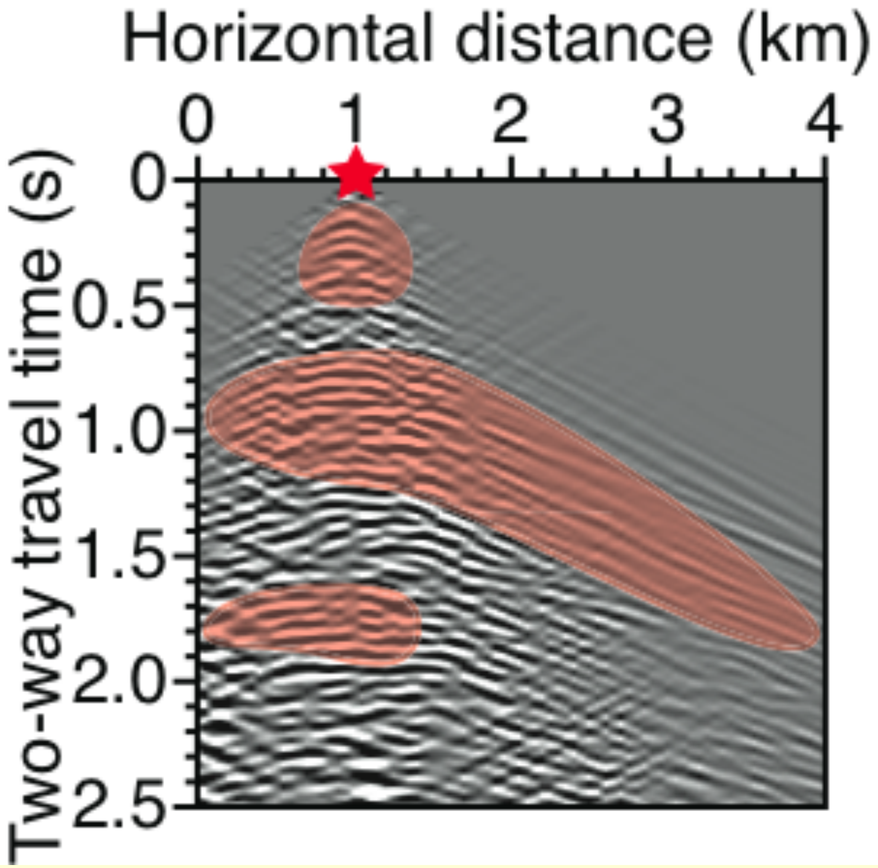

Retrieved reflection response

Measured reflection response

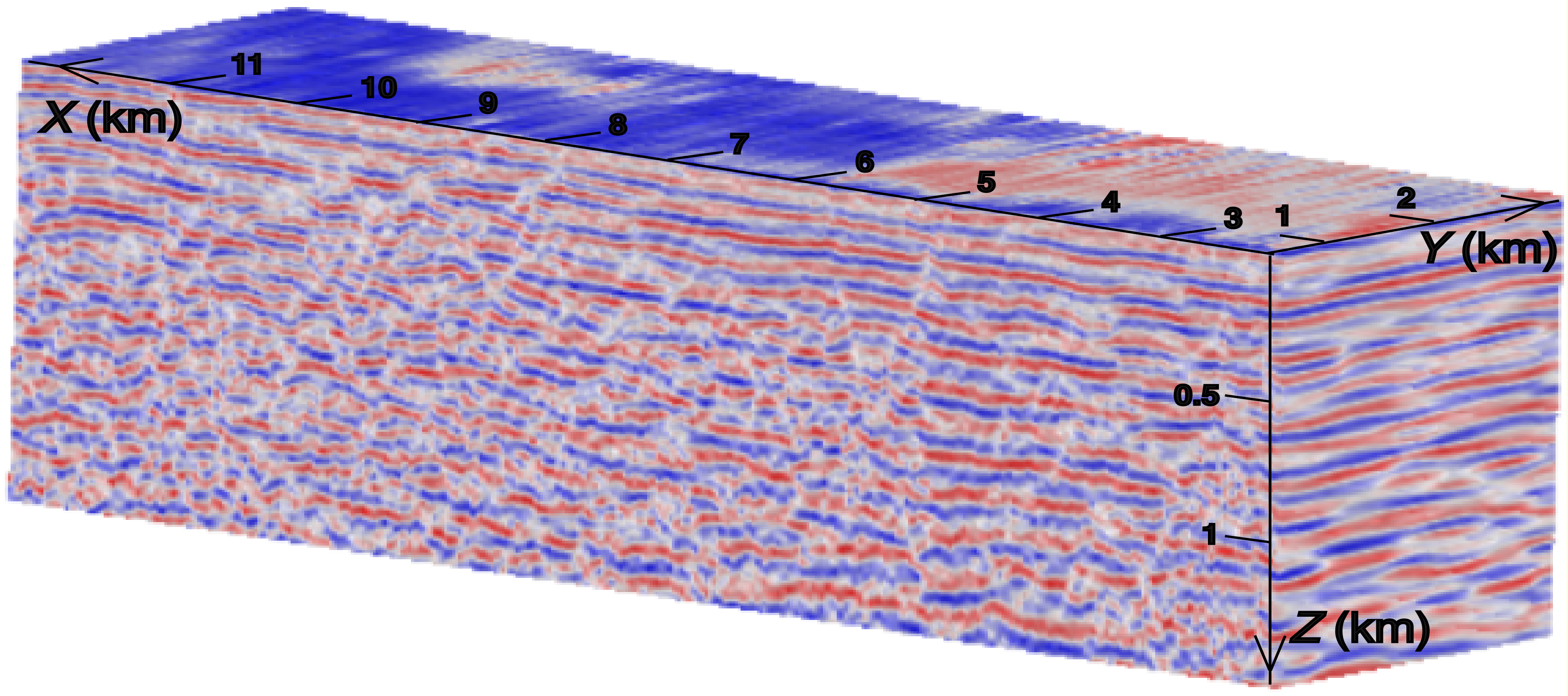

Pseudo-3D image: geology below the Libyan desert
(Deyan Draganov, in cooperation with Shell)

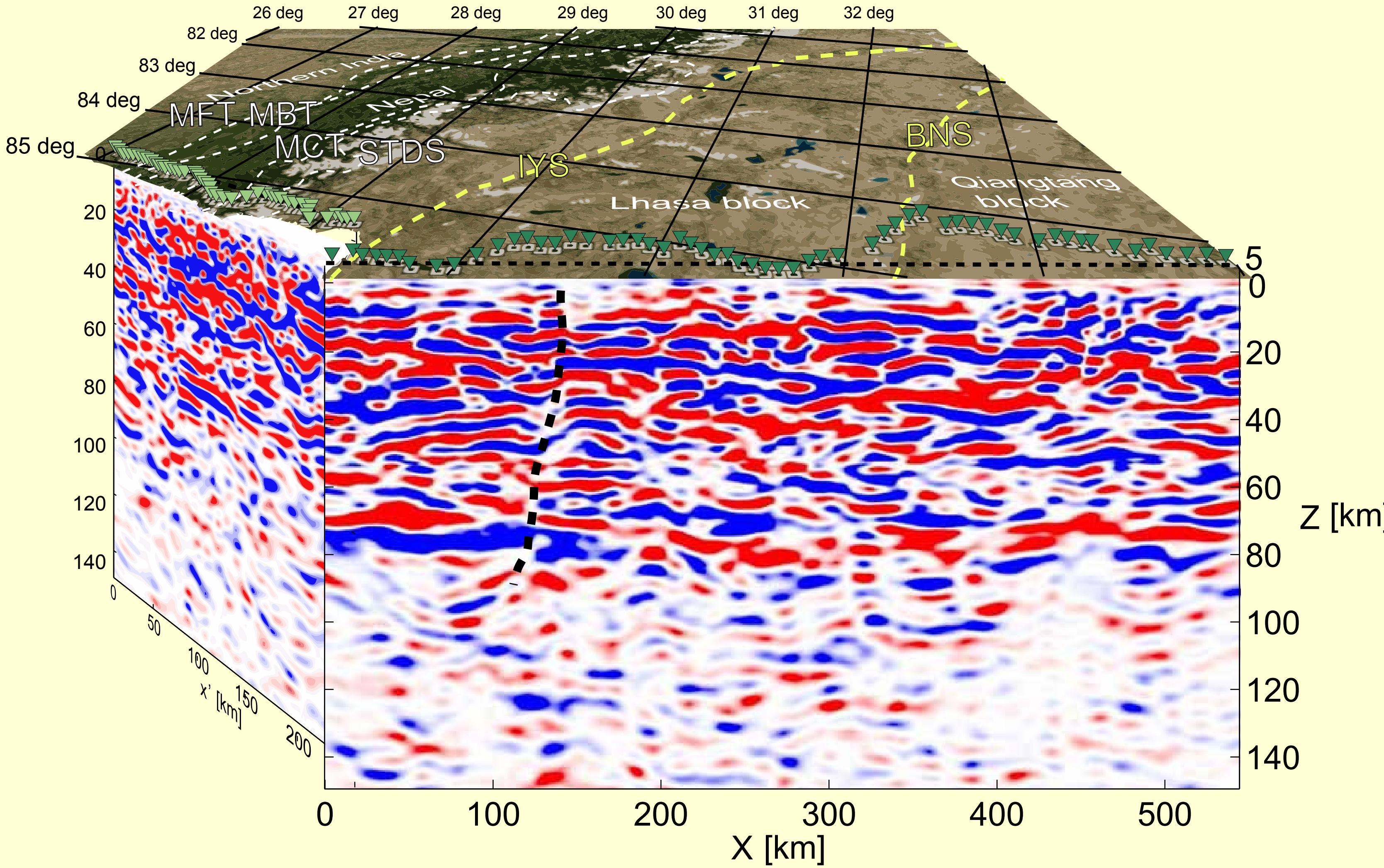

Tectonic blocks below the Tibetan Plateau, obtained from teleseismic data
(Elmer Ruigrok)

Seismic imaging of reflection data by double focusing

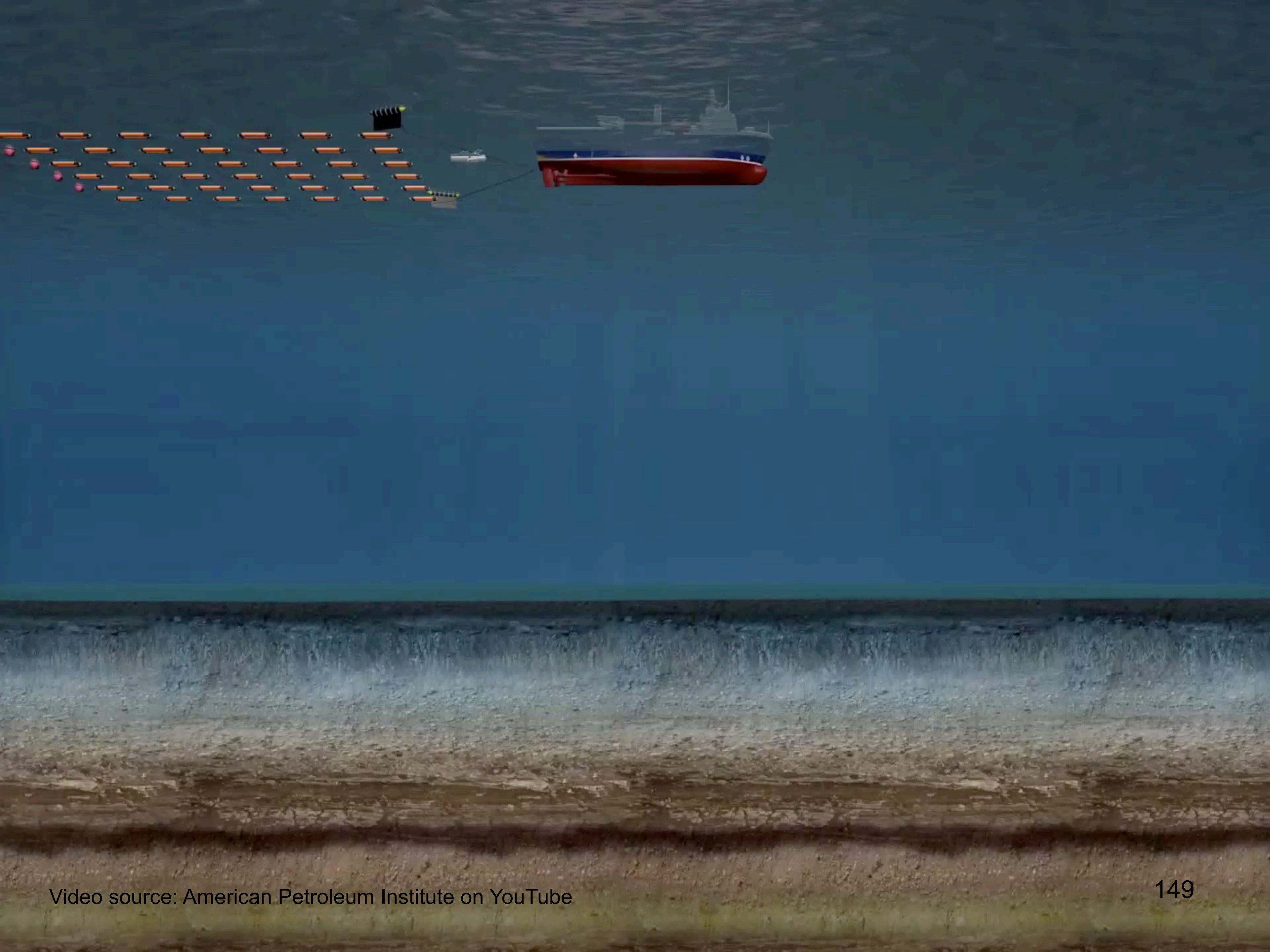

Video source: American Petroleum Institute on YouTube

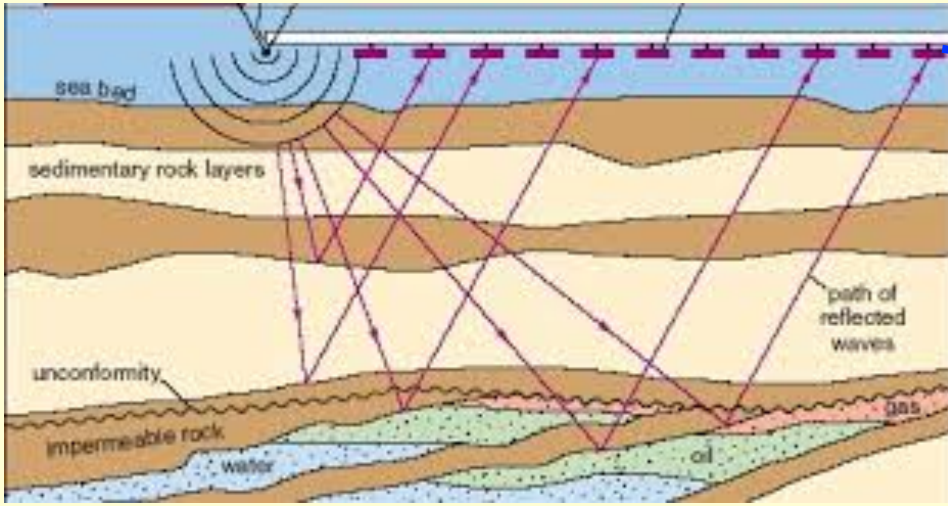

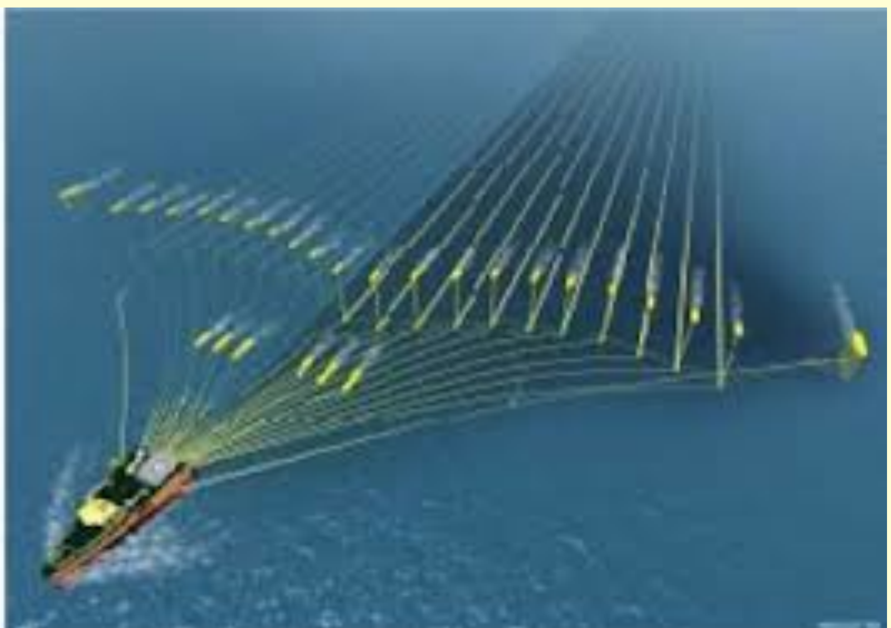

$$\begin{bmatrix} x \\ x \\ x \\ x \\ x \\ x \\ x \end{bmatrix}$$

Data matrix
(reflection matrix)
for each frequency

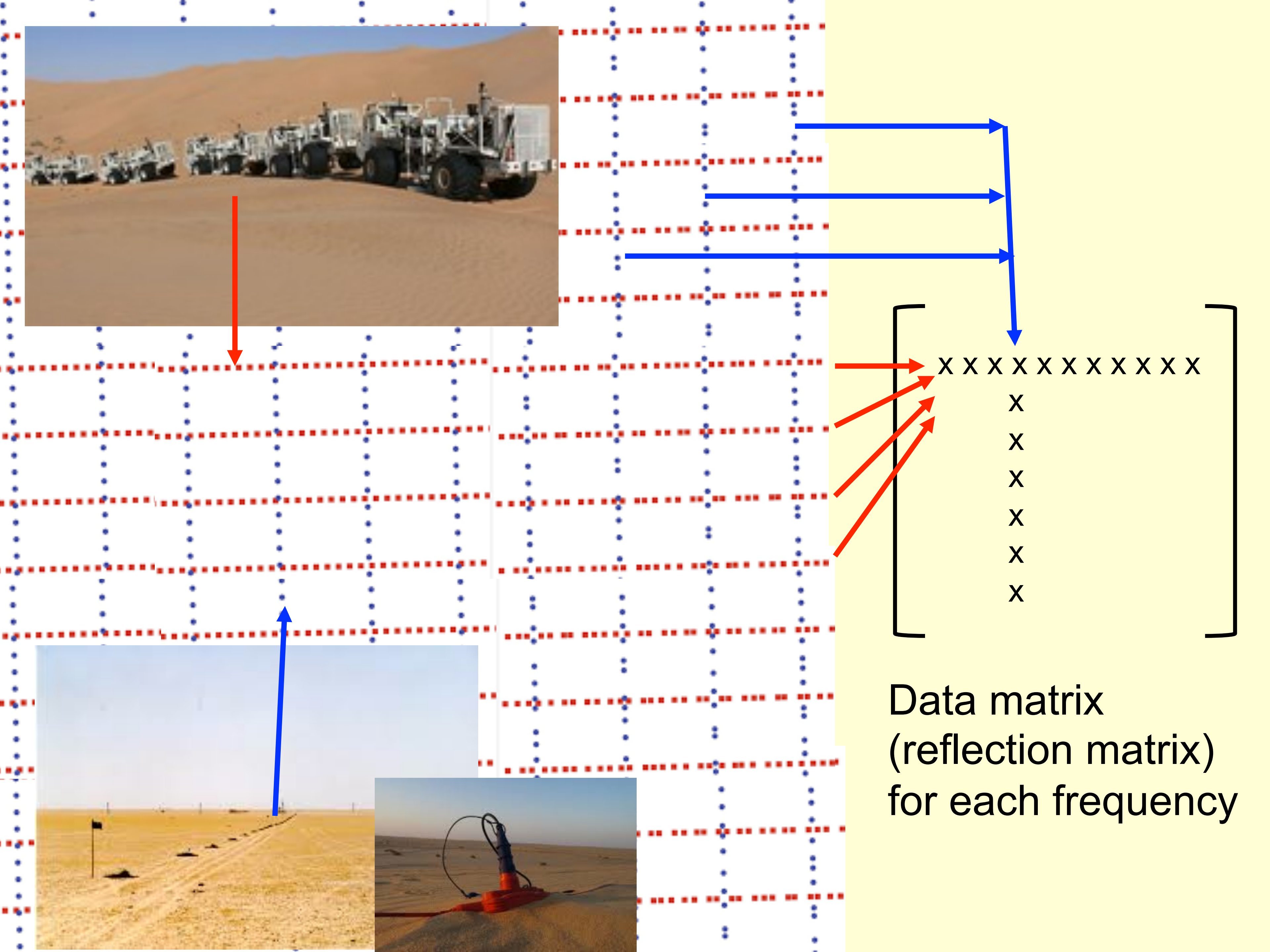
x x x x x x x x x x x
x
x
x
x
x
x
Data matrix
(reflection matrix)
for each frequency

A unified approach to acoustical reflection imaging. II: The inverse problem

A. J. Berkhout and C. P. A. Wapenaar
Delft University of Technology, Laboratory of Seismics and Acoustics, P.O. Box 5046, 2600 GA Delft, The Netherlands

(Received 20 December 1990; accepted for publication 19 October 1992)

Using the forward matrix model, as derived in part I [A. J. Berkhout, J. Acoust. Soc. Am. **93**, 2005–2016 (1993)], it is shown that the first and main part of numerical acoustic imaging consists of a wave field extrapolation process by double matrix inversion. Physically, the wave field extrapolation process means that the downward propagation effects and the upward propagation effects are eliminated from the measurements. Next, the reflection information is extracted from the wave field extrapolation result. Optionally, the reflection information is translated to discipline-oriented material parameters by some data fitting process. Double focusing, i.e., focusing in emission and focusing in detection, is closely related to the above numerical imaging process. Finally, it is shown that imaging of zero-offset or puls-echo data can be formulated by single matrix inversion, involving phase shifts only.

PACS numbers: 43.60.Gk, 43.60.Pt

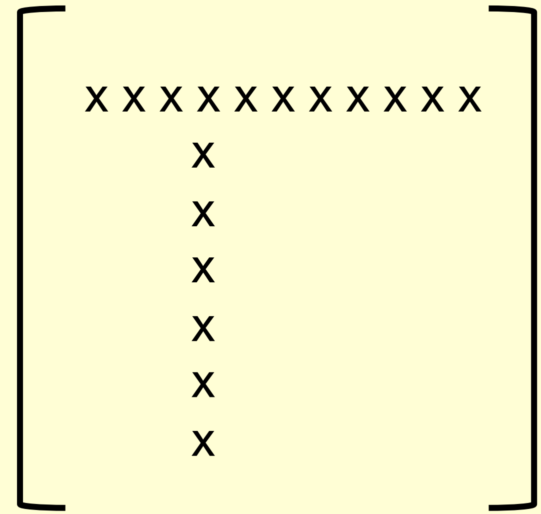

Ber(c)khout and Wapenaar, 1993, JASA

$$\mathbf{X}(z_m,z_m) = \mathbf{F}^-(z_m,z_0)\mathbf{X}(z_0,z_0)\mathbf{F}^+(z_0,z_m) \quad (4a)$$

with

$$\mathbf{F}^-(z_m,z_0) = [\mathbf{W}^-(z_0,z_m)]^{-1} \approx [\overline{\mathbf{W}}^+(z_m,z_0)]^* \quad (4b)$$

$$\mathbf{F}^+(z_0,z_m) = [\mathbf{W}^+(z_m,z_0)]^{-1} \approx [\overline{\mathbf{W}}^-(z_0,z_m)]^*, \quad (4c)$$

where $\overline{\mathbf{W}}$ is based on the macro model and where * denotes complex conjugation.

In the seismic exploration inversion process (4a) is generally referred to as "redatuming." From (4a) it follows that

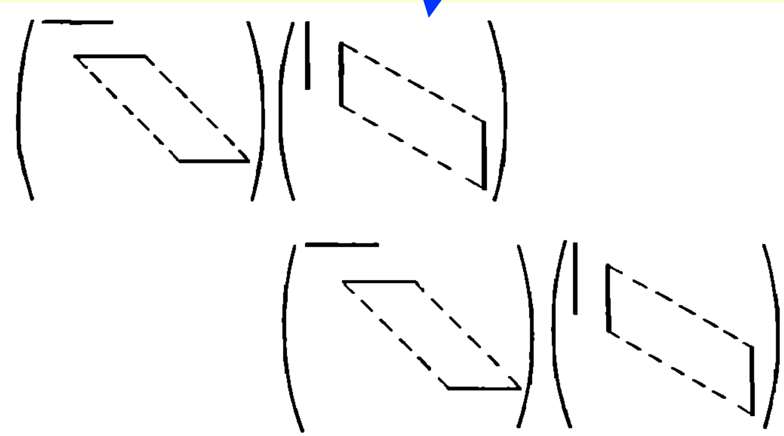

"Redatuming"

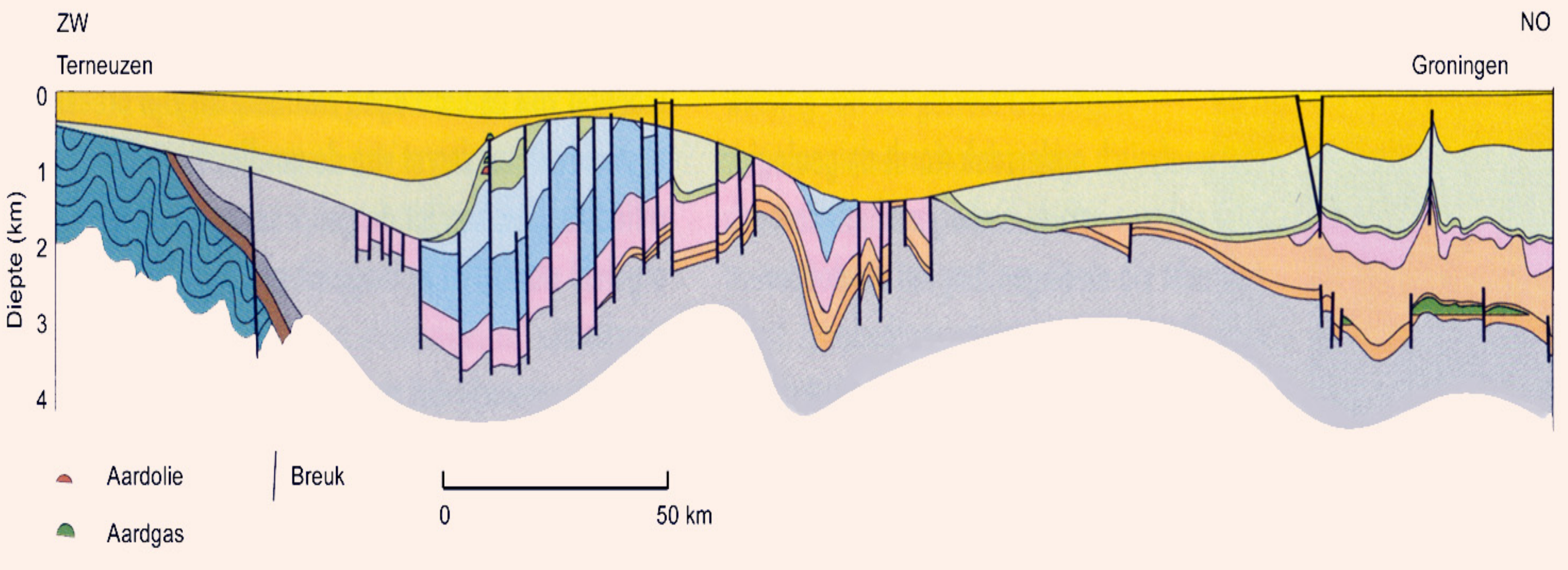

ZW
NO
Terneuzen
Groningen
0
1
2
3
4
Diepte (km)
Aardolie
Aardgas
Breuk
0
50 km

The challenge: internal multiple reflections

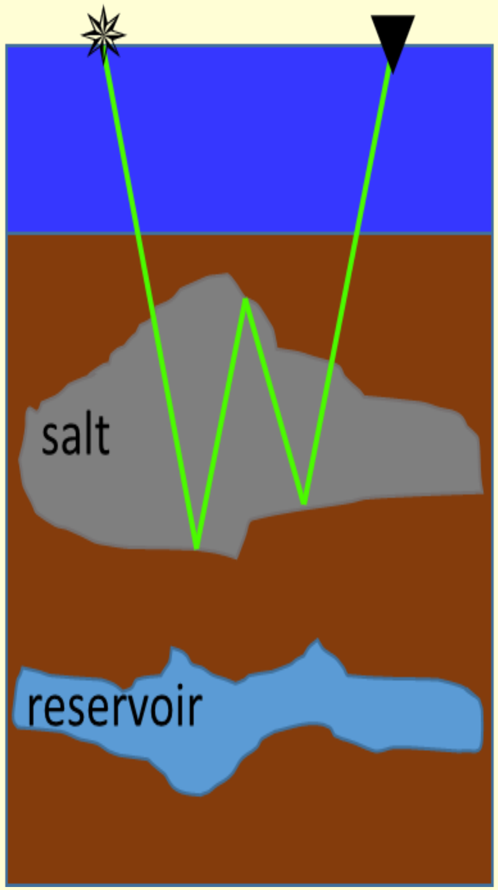

The challenge: internal multiple reflections

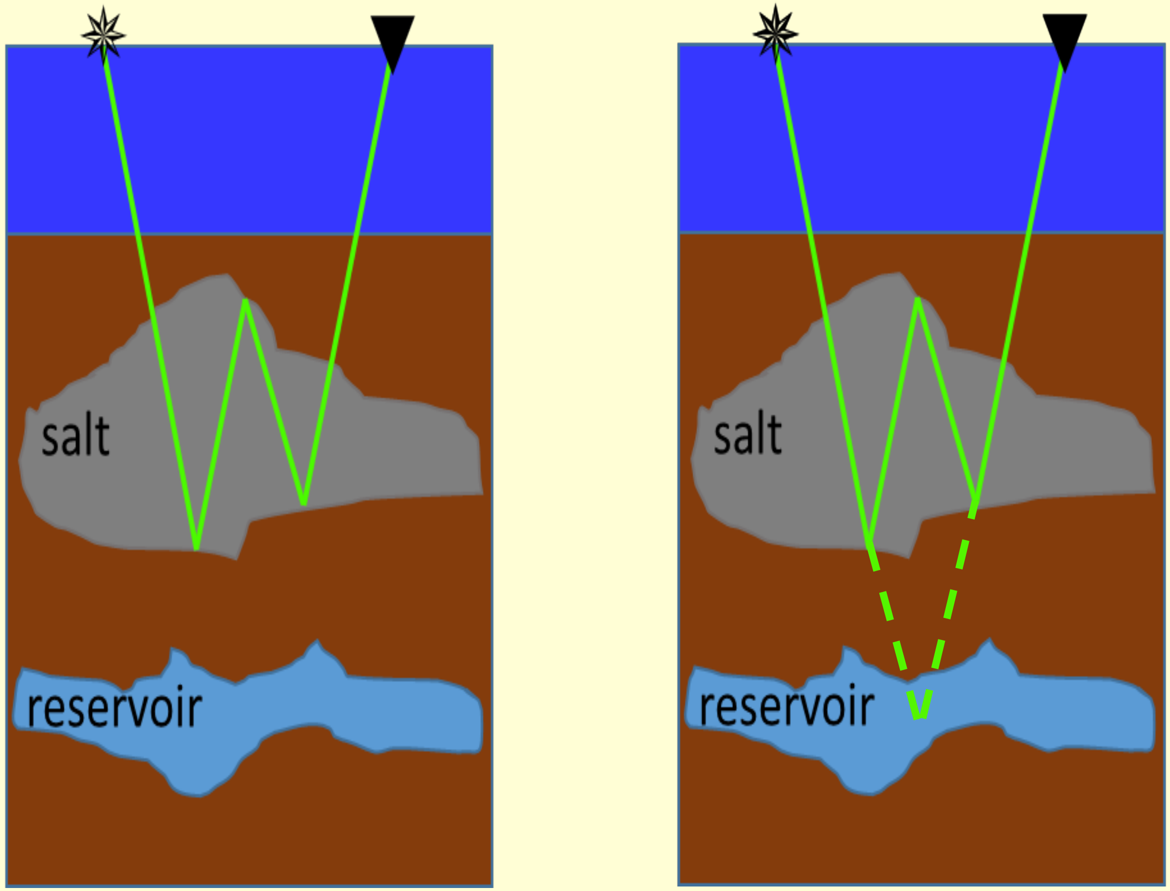

Multi-source ( ), multi-receiver ( ) reflection data

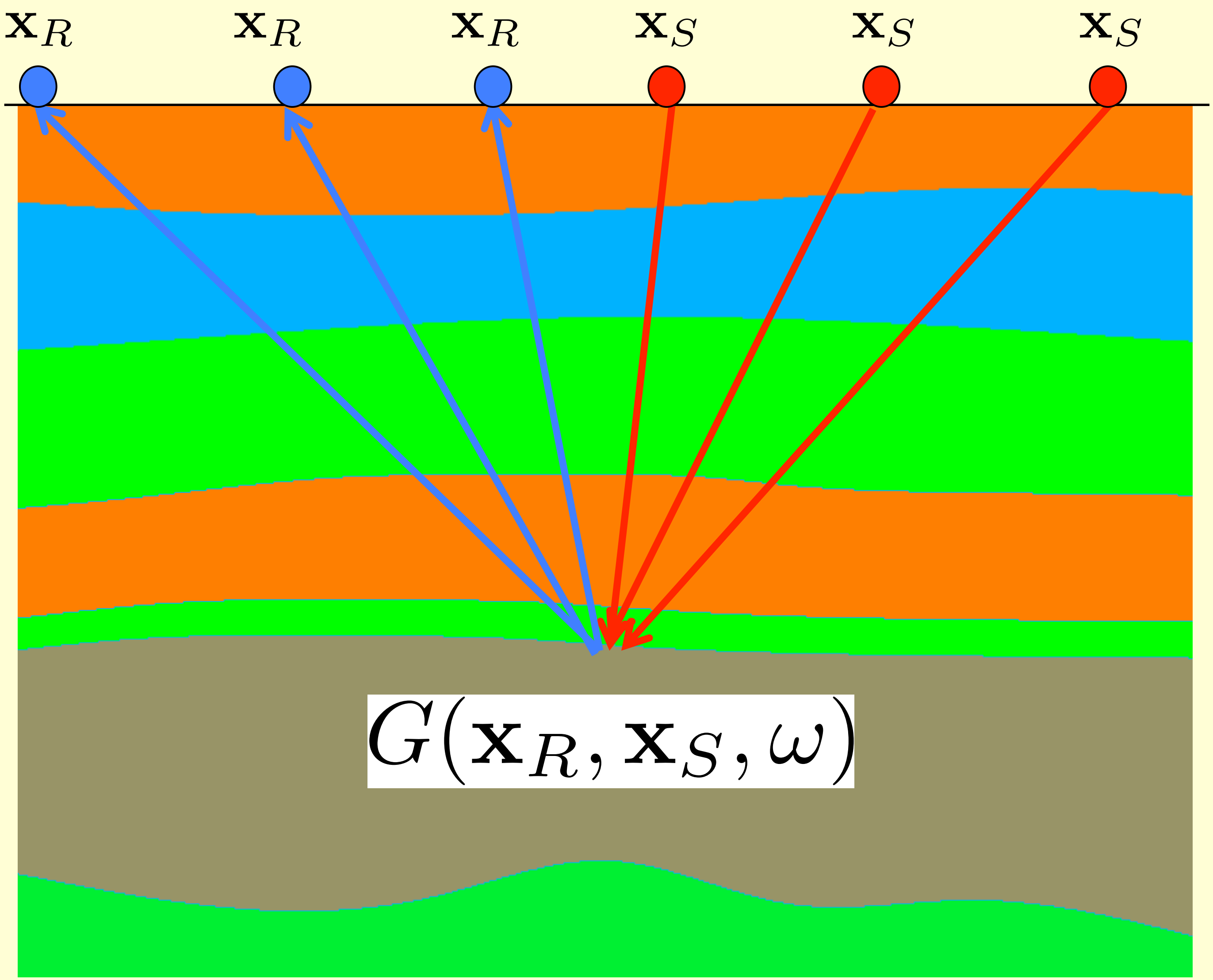

Focusing onto a virtual source

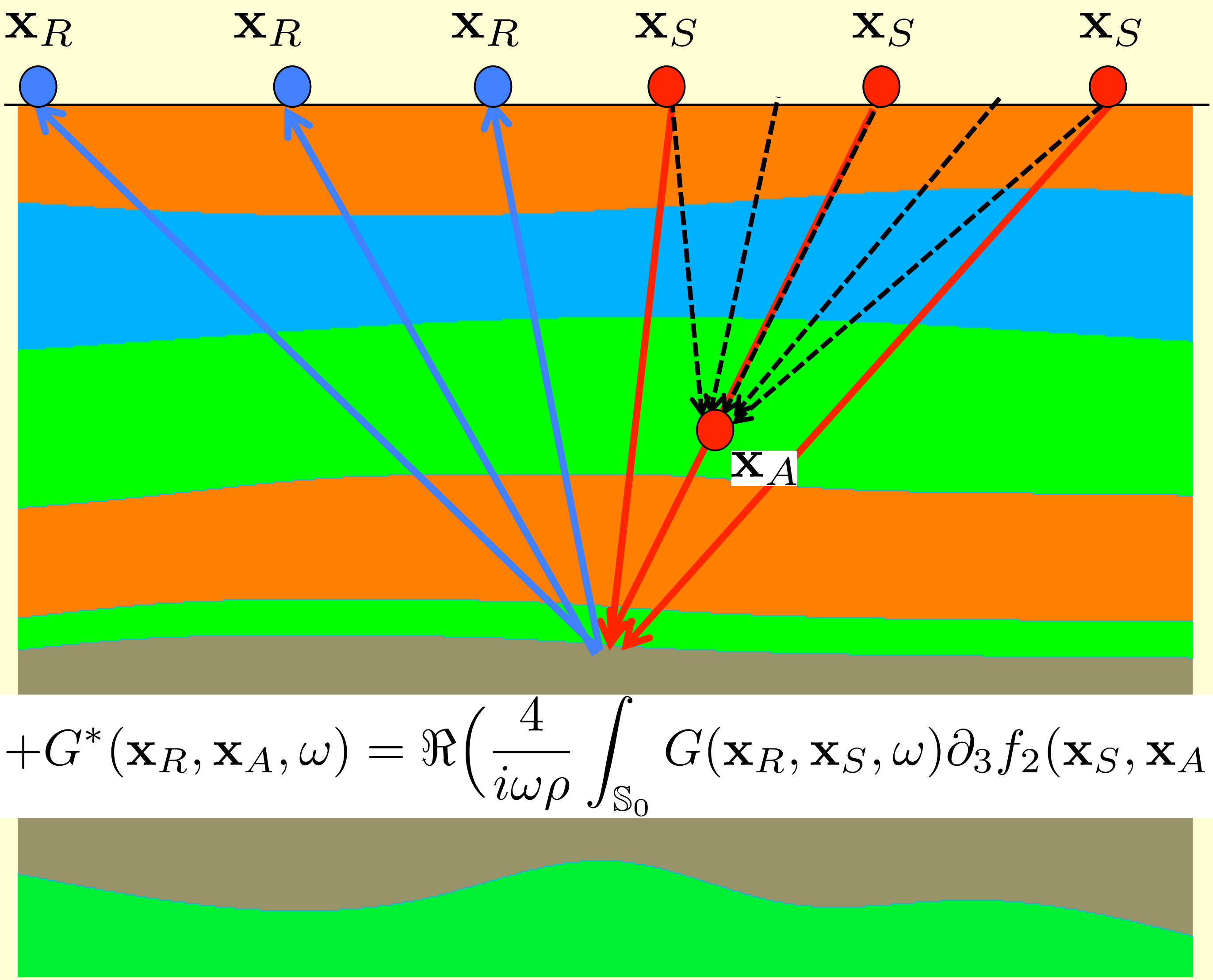

$$G(\mathbf{x}_R,\mathbf{x}_A,\omega)+G^*(\mathbf{x}_R,\mathbf{x}_A,\omega)=\Re\left(\frac{4}{i\omega\rho}\int_{\mathbb{S}_0}G(\mathbf{x}_R,\mathbf{x}_S,\omega)\partial_3 f_2(\mathbf{x}_S,\mathbf{x}_A,\omega)\mathrm{d}^2\mathbf{x}_S\right)$$

Focusing onto a virtual source

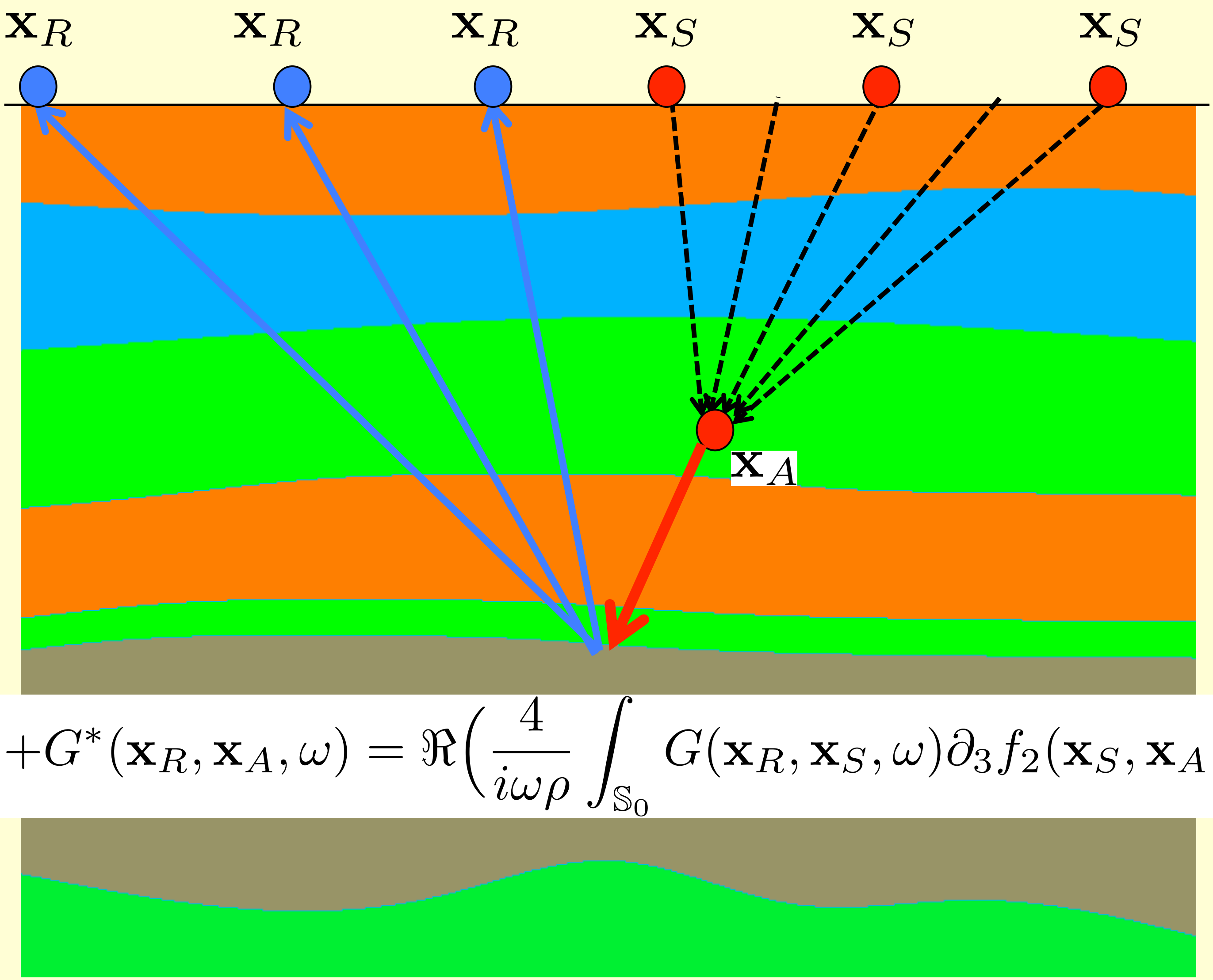

$$G(\mathbf{x}_R,\mathbf{x}_A,\omega)+G^*(\mathbf{x}_R,\mathbf{x}_A,\omega)=\Re\left(\frac{4}{i\omega\rho}\int_{\mathbb{S}_0}G(\mathbf{x}_R,\mathbf{x}_S,\omega)\partial_3 f_2(\mathbf{x}_S,\mathbf{x}_A,\omega)\mathrm{d}^2\mathbf{x}_S\right)$$

Focusing onto a virtual receiver

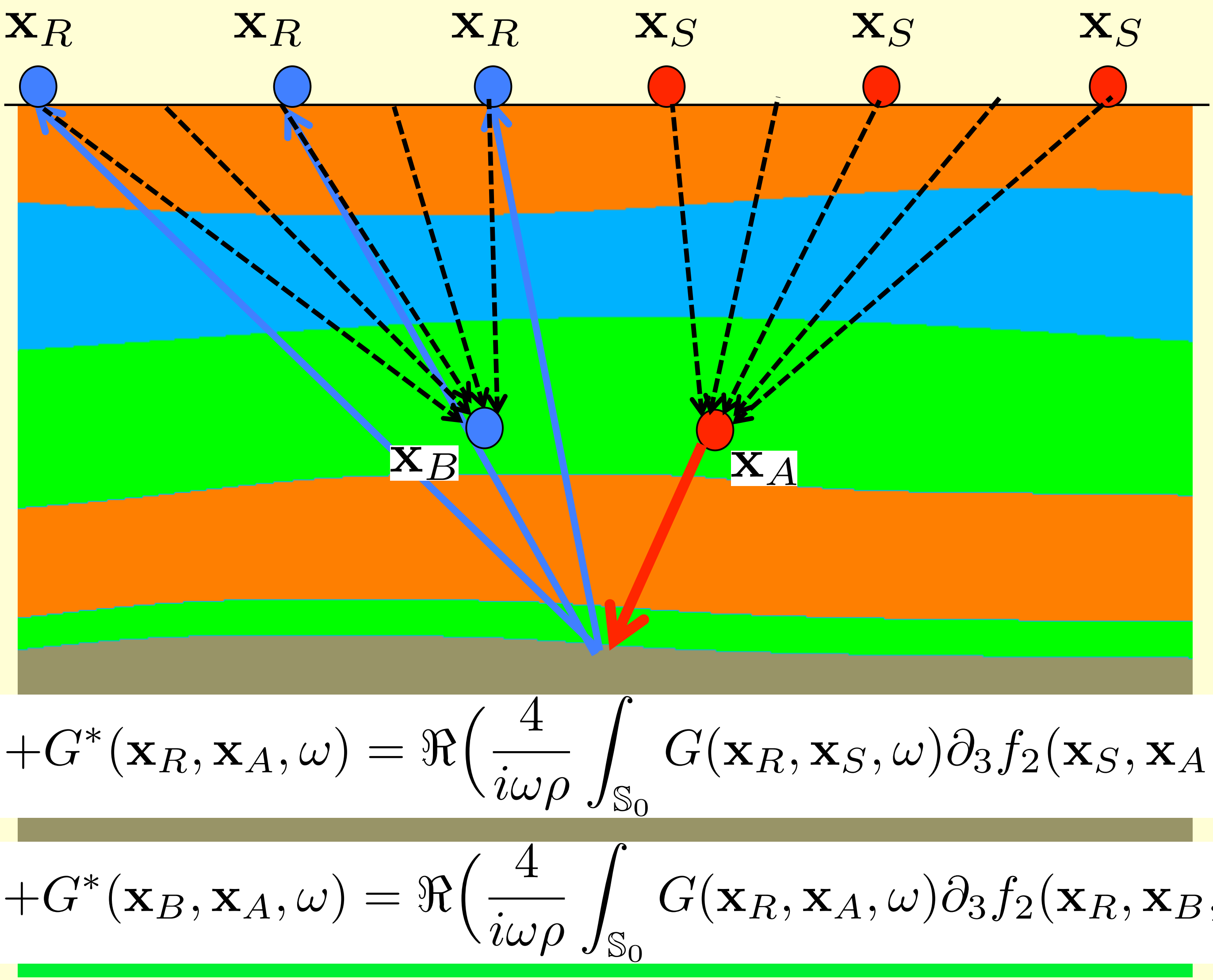

$$G(\mathbf{x}_R,\mathbf{x}_A,\omega)+G^*(\mathbf{x}_R,\mathbf{x}_A,\omega)=\Re\Big(\frac{4}{i\omega\rho}\int_{\mathbb{S}_0}G(\mathbf{x}_R,\mathbf{x}_S,\omega)\partial_3 f_2(\mathbf{x}_S,\mathbf{x}_A,\omega)\mathrm{d}^2\mathbf{x}_S\Big)$$

$$G(\mathbf{x}_B,\mathbf{x}_A,\omega)+G^*(\mathbf{x}_B,\mathbf{x}_A,\omega)=\Re\Big(\frac{4}{i\omega\rho}\int_{\mathbb{S}_0}G(\mathbf{x}_R,\mathbf{x}_A,\omega)\partial_3 f_2(\mathbf{x}_R,\mathbf{x}_B,\omega)\mathrm{d}^2\mathbf{x}_R\Big)$$

Focusing onto a virtual receiver

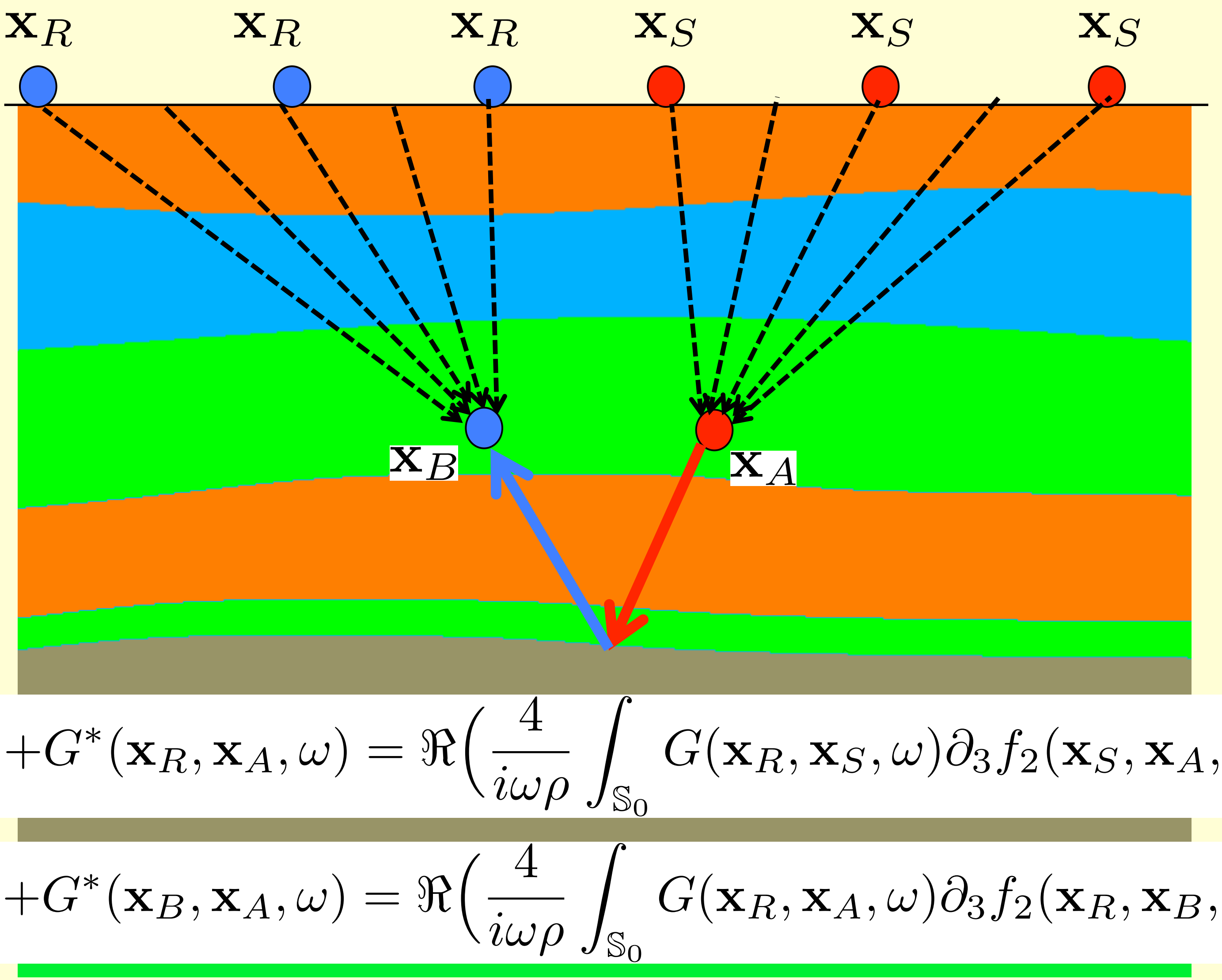

$$G(\mathbf{x}_R,\mathbf{x}_A,\omega)+G^*(\mathbf{x}_R,\mathbf{x}_A,\omega)=\Re\Big(\frac{4}{i\omega\rho}\int_{\mathbb{S}_0}G(\mathbf{x}_R,\mathbf{x}_S,\omega)\partial_3 f_2(\mathbf{x}_S,\mathbf{x}_A,\omega)\mathrm{d}^2\mathbf{x}_S\Big)$$

$$G(\mathbf{x}_B,\mathbf{x}_A,\omega)+G^*(\mathbf{x}_B,\mathbf{x}_A,\omega)=\Re\Big(\frac{4}{i\omega\rho}\int_{\mathbb{S}_0}G(\mathbf{x}_R,\mathbf{x}_A,\omega)\partial_3 f_2(\mathbf{x}_R,\mathbf{x}_B,\omega)\mathrm{d}^2\mathbf{x}_R\Big)$$

Virtual source, virtual receiver data

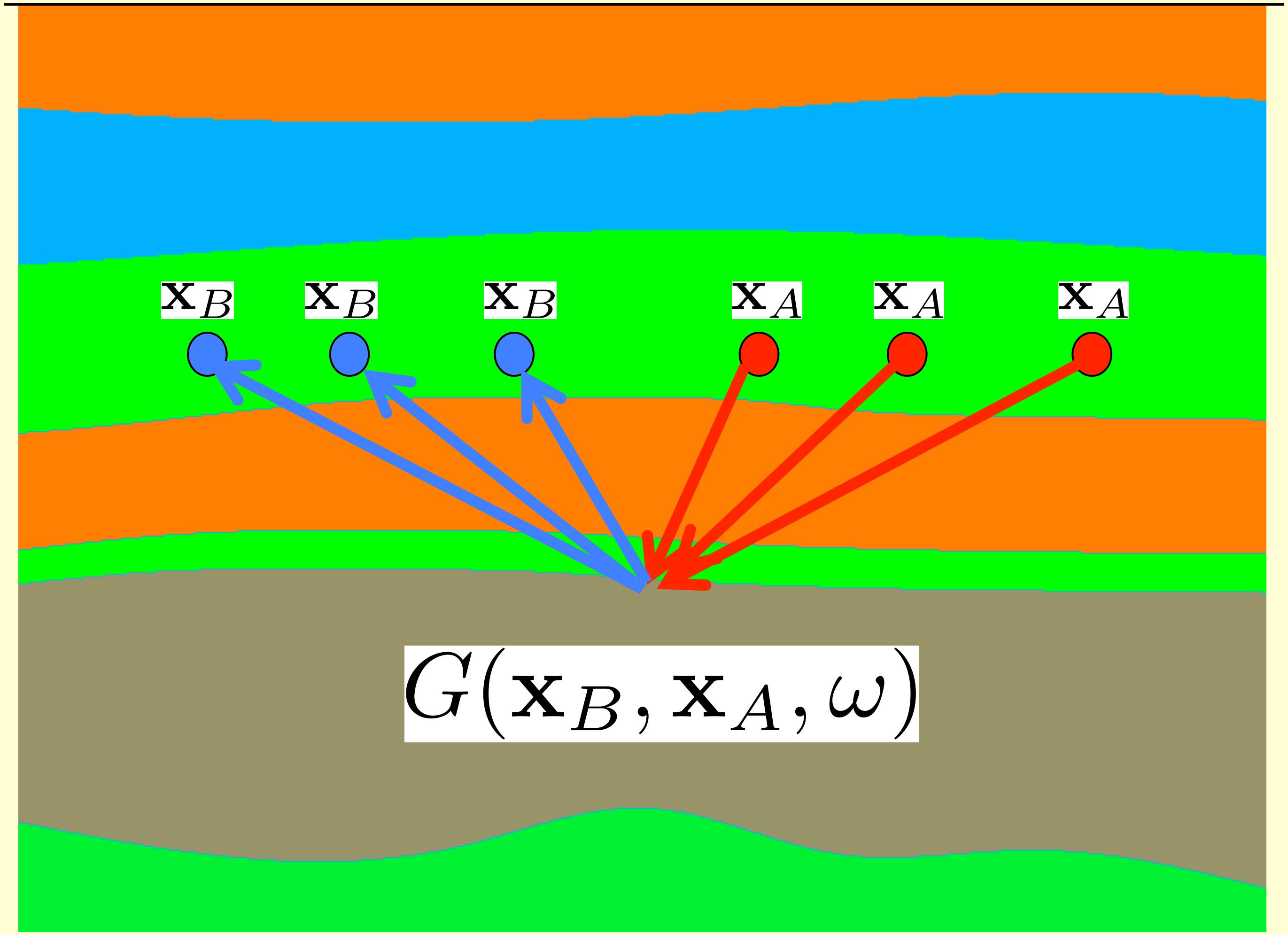

Virtual source, virtual receiver data used for reflection imaging

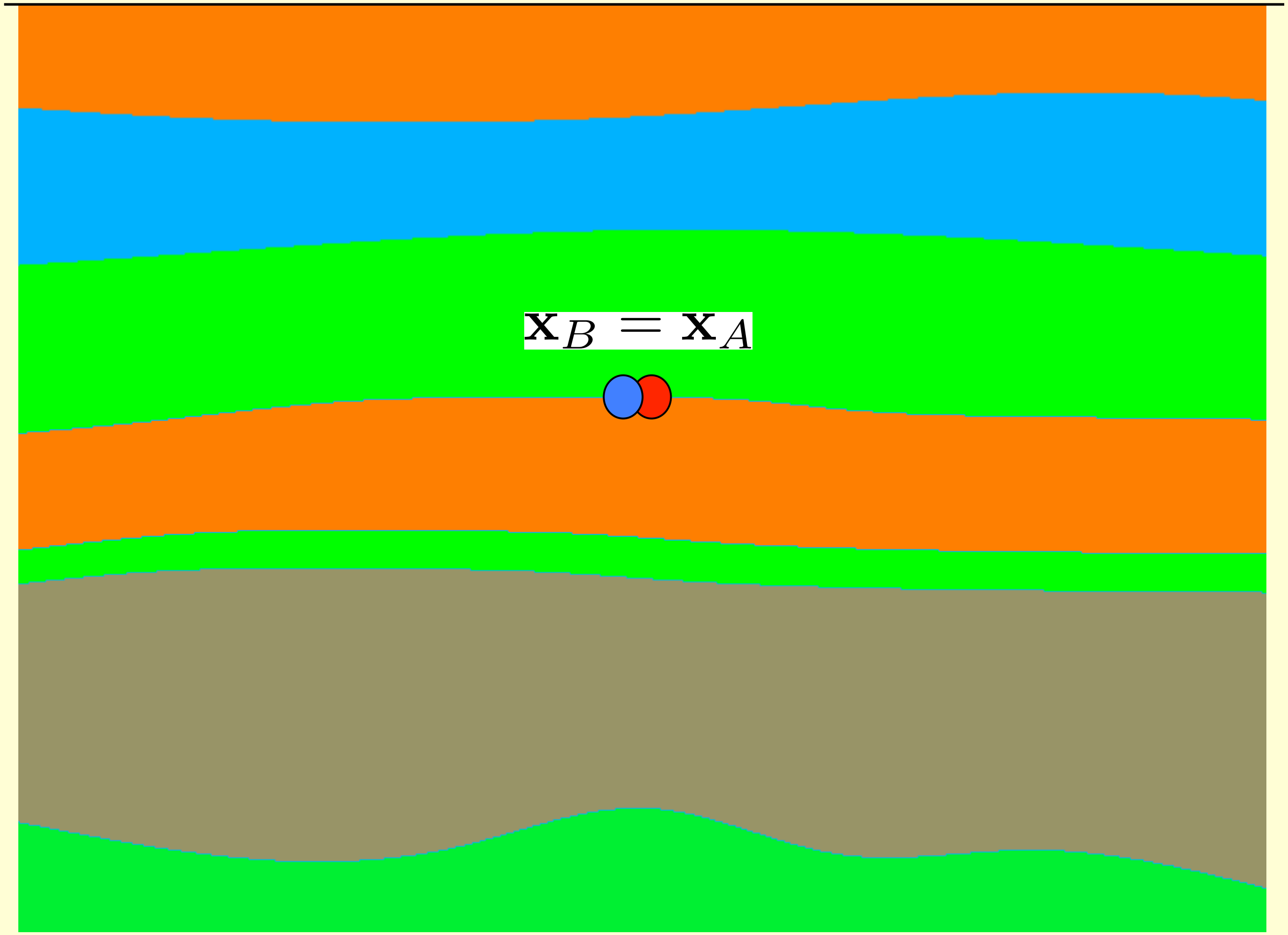

Virtual source, virtual receiver data used for reflection imaging (standard)

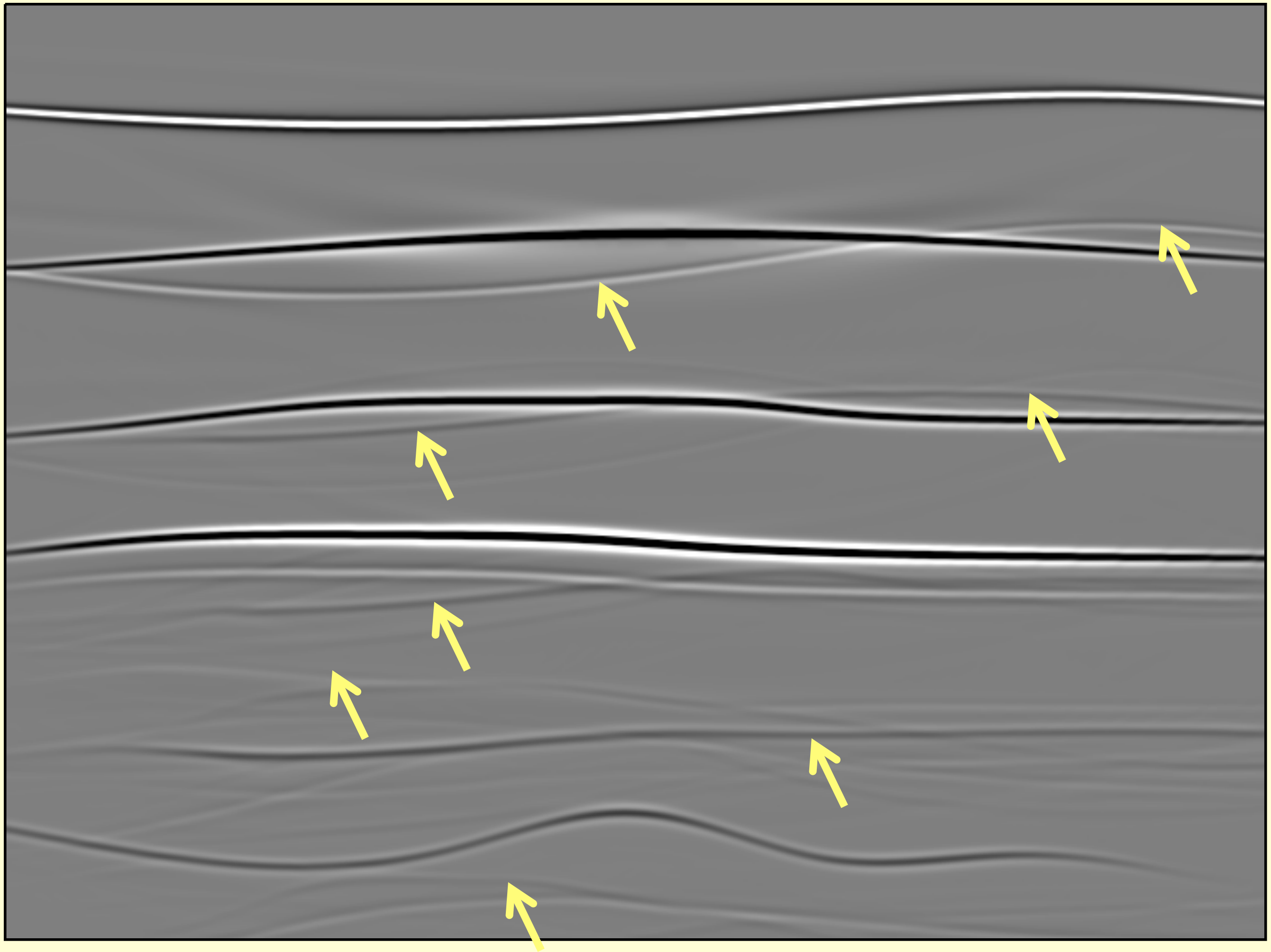

Virtual source, virtual receiver data
used for reflection imaging (Marchenko)

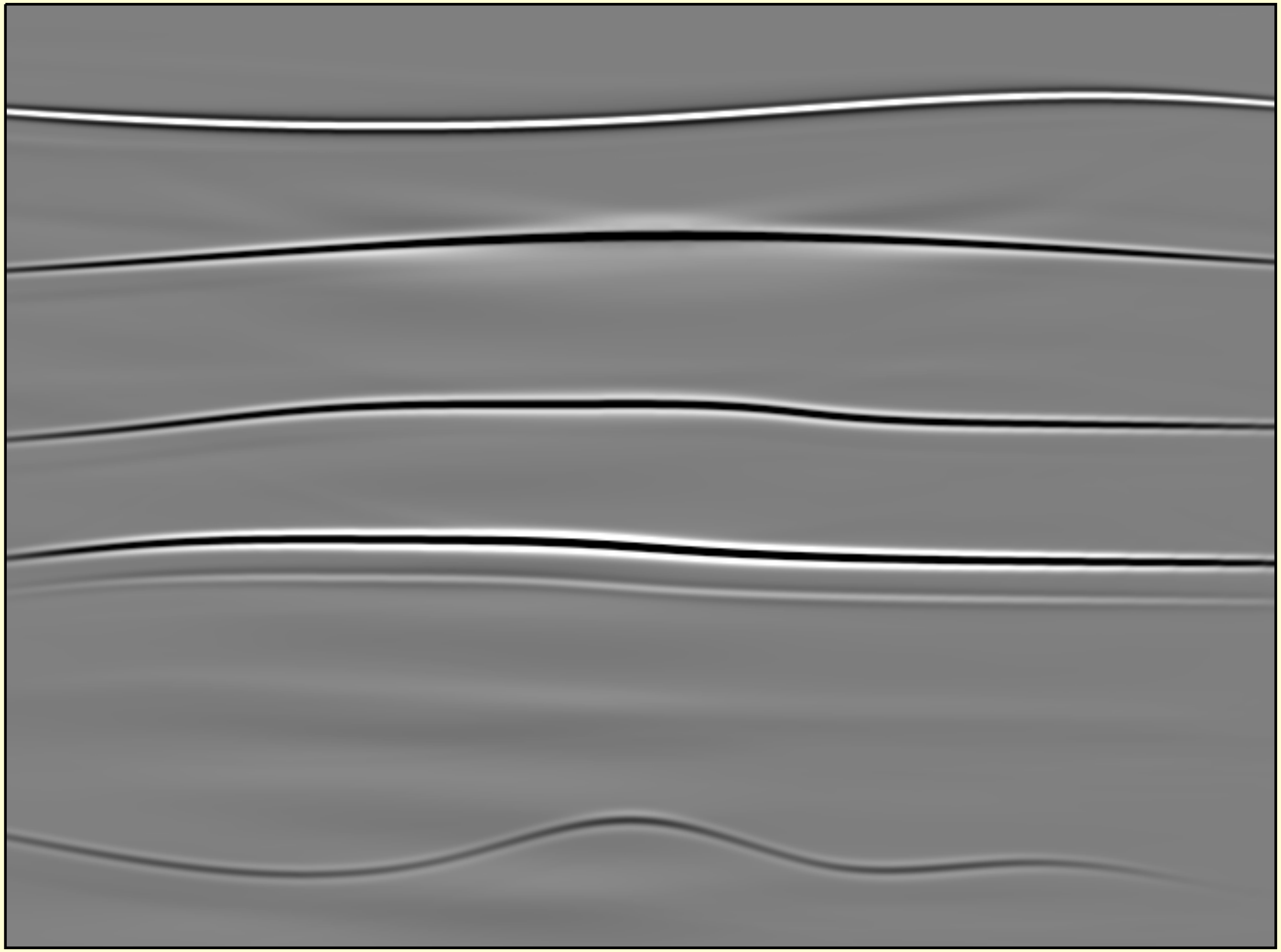

2D field data: standard imaging

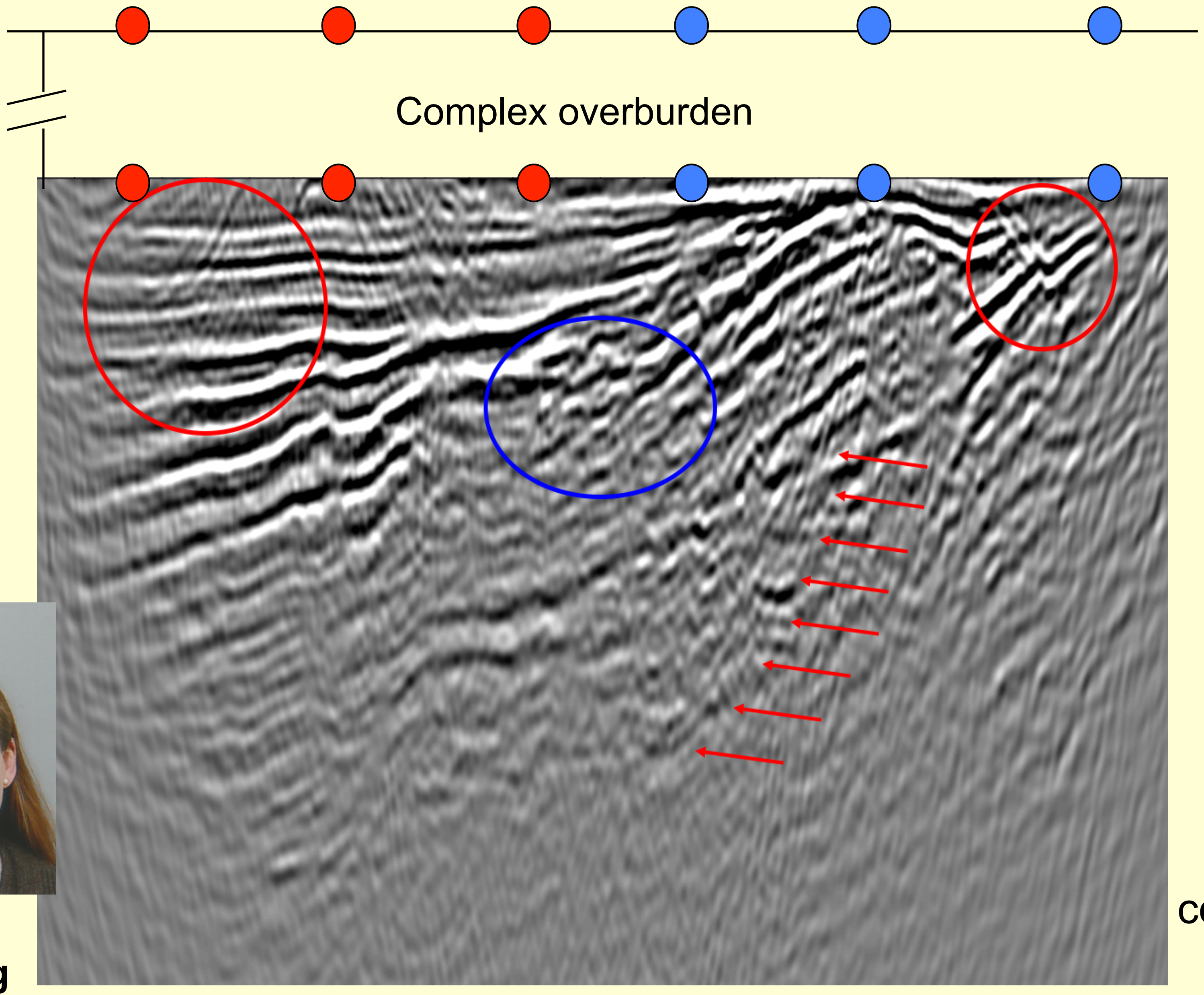

Myrna Staring

Data courtesy: CGG

2D field data: Marchenko-based double focusing

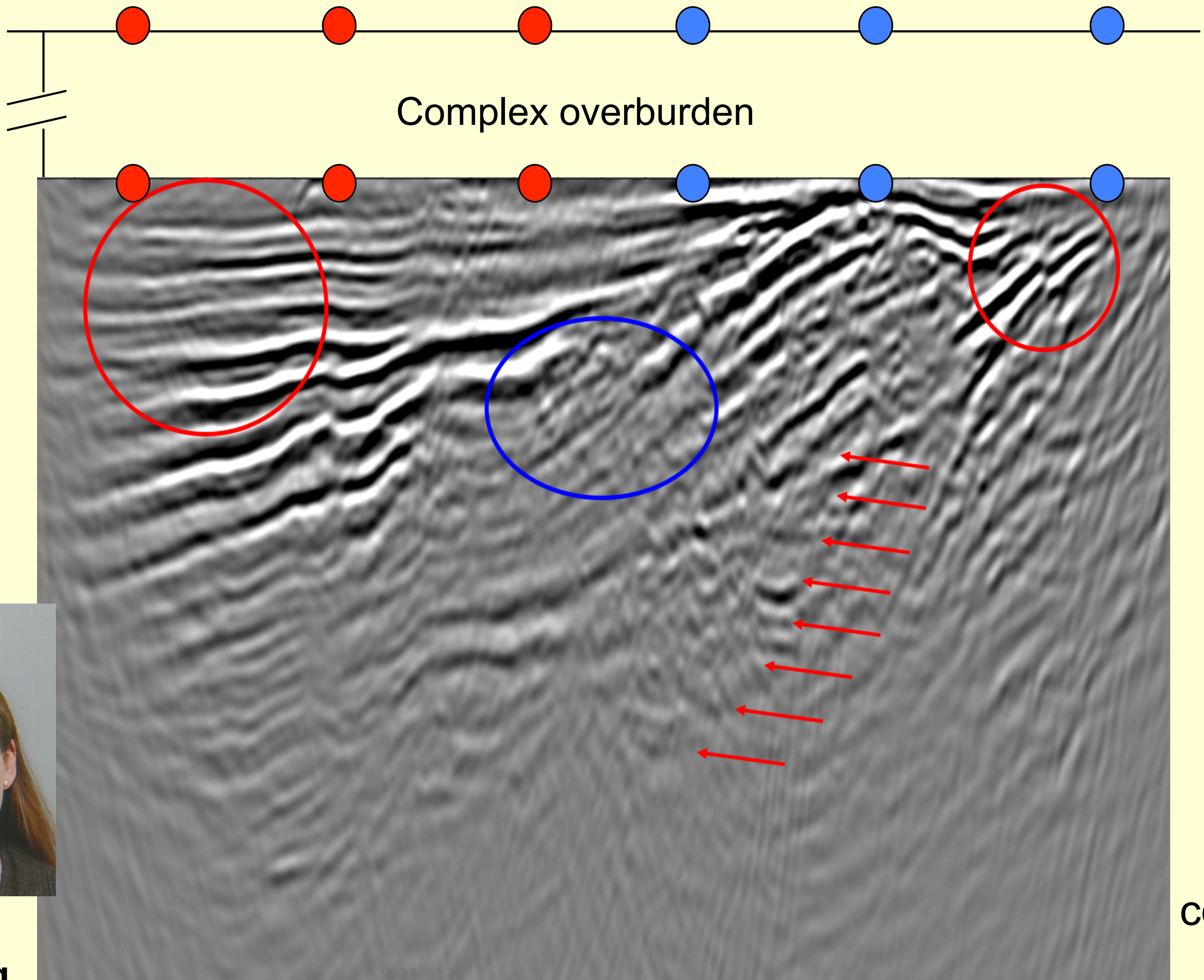

Myrna Staring

Data courtesy: CGG

3D field data: standard imaging

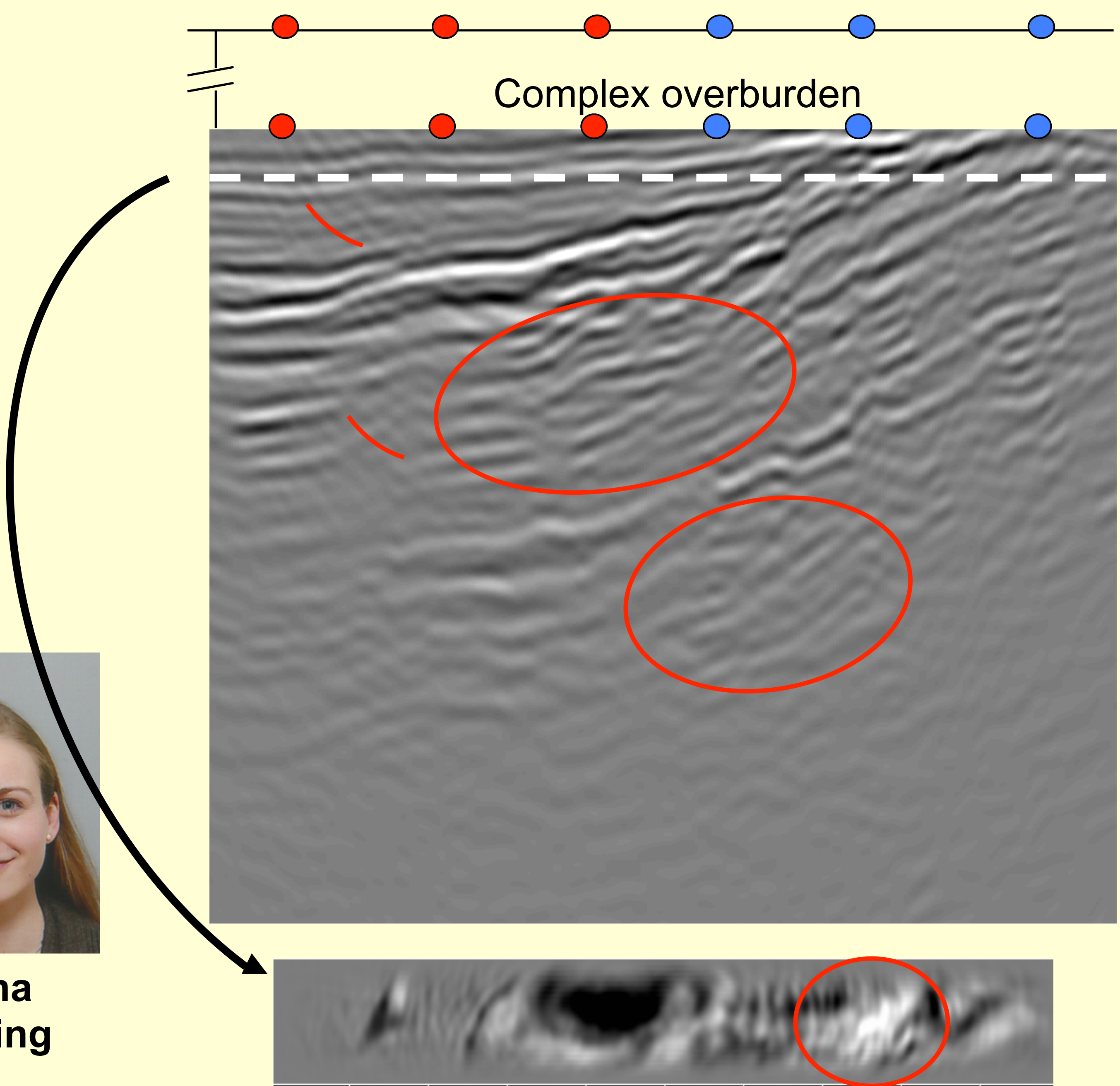

Myrna Staring

Data courtesy: CGG

3D field data: Marchenko-based double focusing

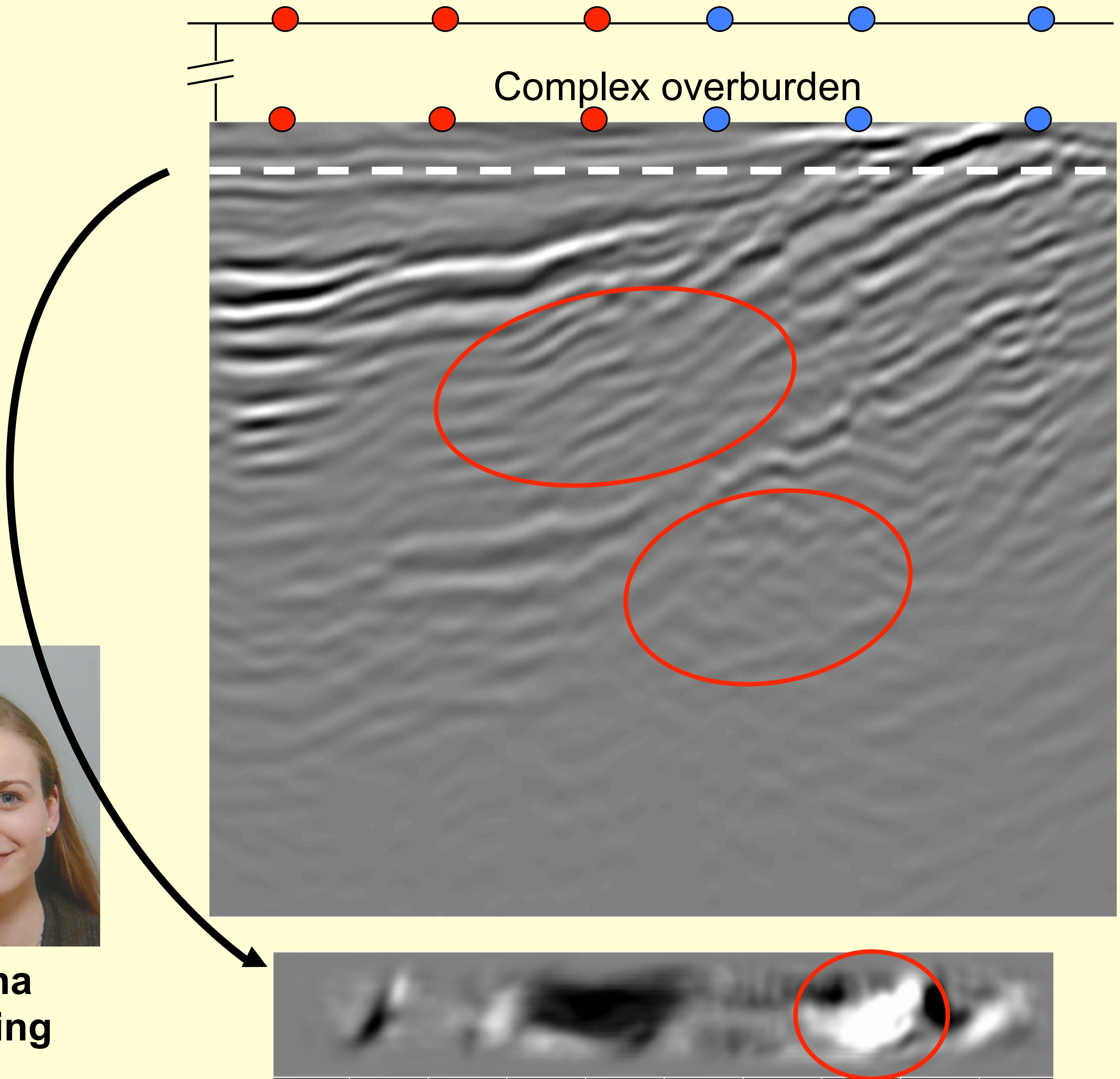

Myrna Staring

Data courtesy: CGG

Forecasting and monitoring of induced seismicity

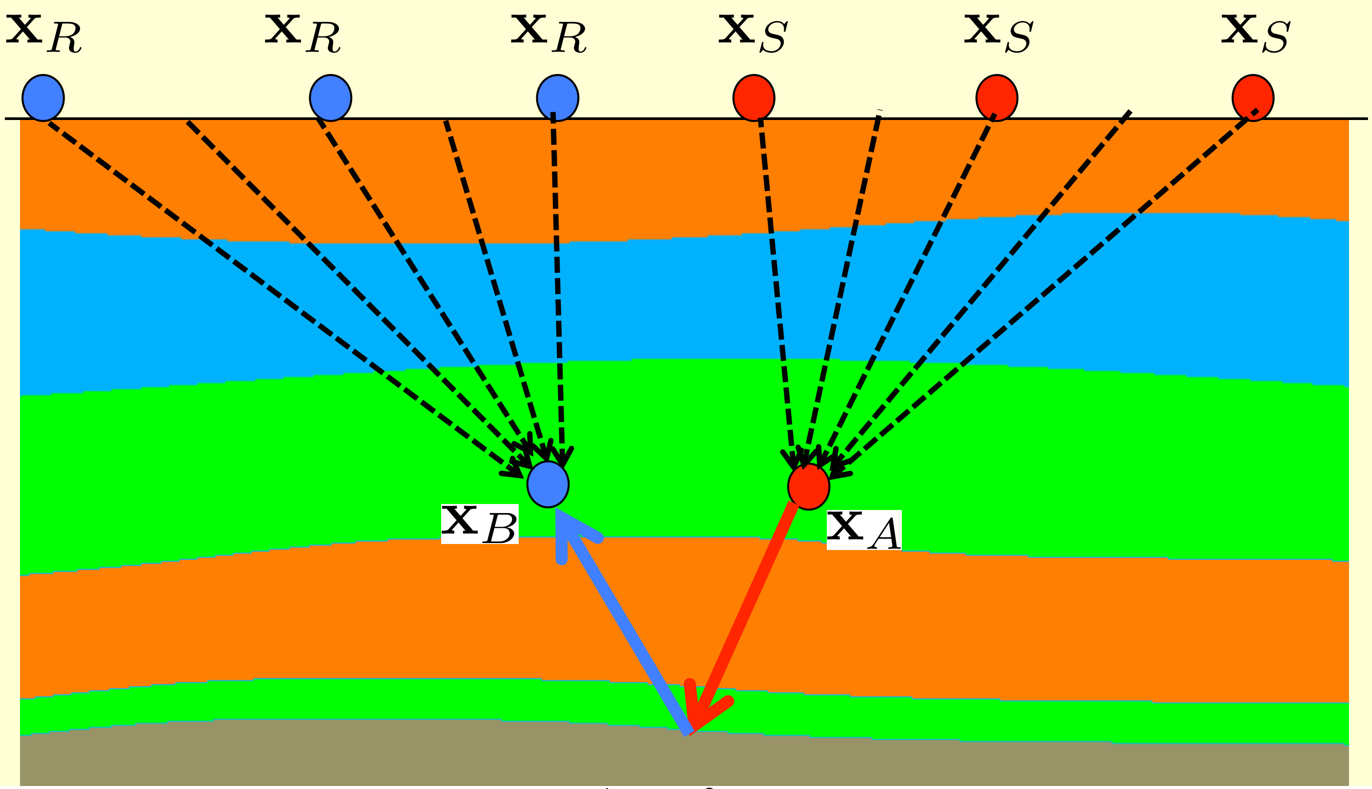

$$G(\mathbf{x}_R,\mathbf{x}_A,\omega)+G^*(\mathbf{x}_R,\mathbf{x}_A,\omega) = \Re\Big(\frac{4}{i\omega\rho}\int_{\mathbb{S}_0} G(\mathbf{x}_R,\mathbf{x}_S,\omega)\partial_3 f_2(\mathbf{x}_S,\mathbf{x}_A,\omega)\mathrm{d}^2\mathbf{x}_S\Big)$$

$$G(\mathbf{x}_B,\mathbf{x}_A,\omega)+G^*(\mathbf{x}_B,\mathbf{x}_A,\omega) = \Re\Big(\frac{4}{i\omega\rho}\int_{\mathbb{S}_0} G(\mathbf{x}_R,\mathbf{x}_A,\omega)\partial_3 f_2(\mathbf{x}_R,\mathbf{x}_B,\omega)\mathrm{d}^2\mathbf{x}_R\Big)$$

Virtual source, virtual receiver data

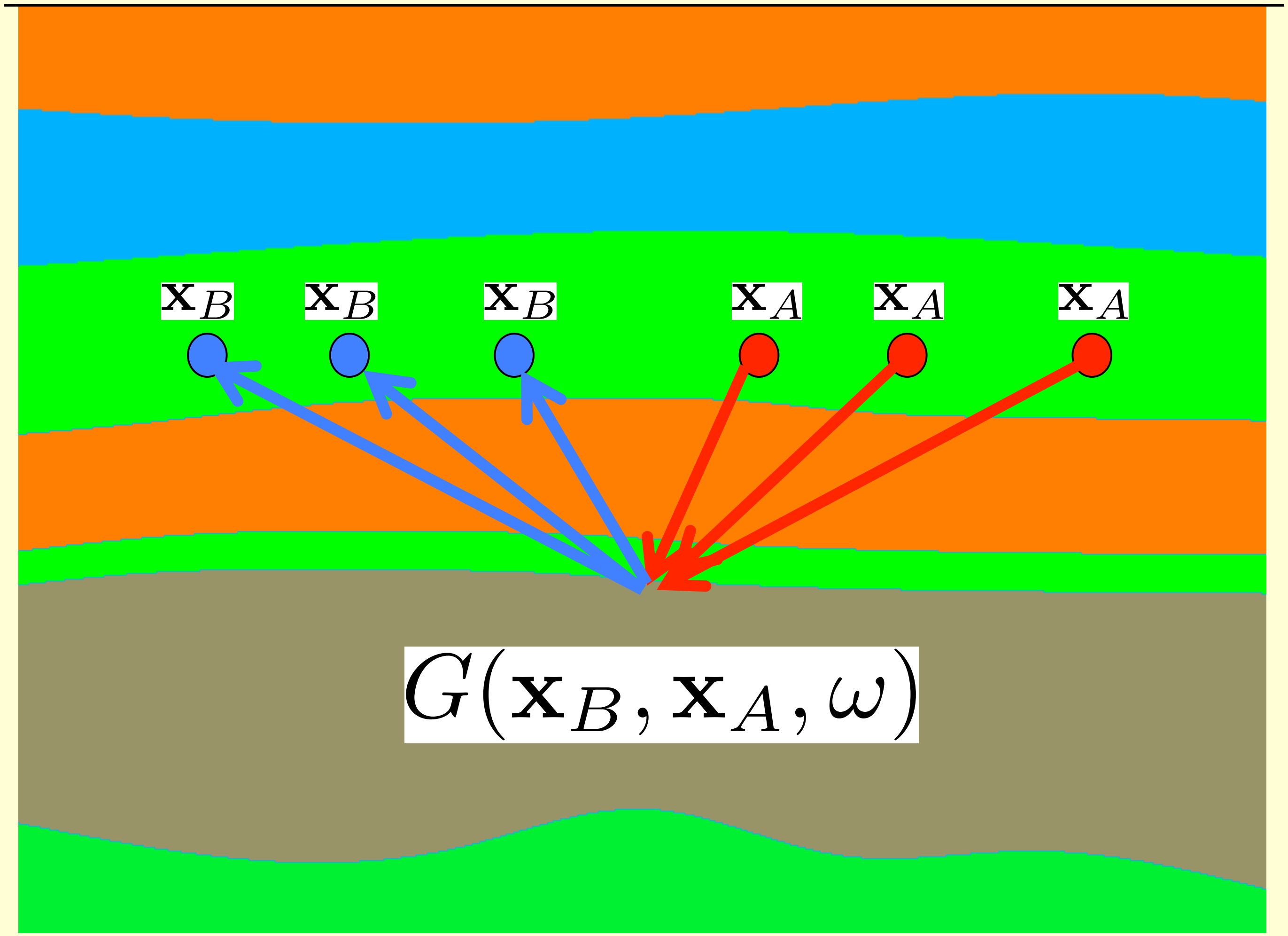

Virtual seismology:
Induced earthquake monitoring

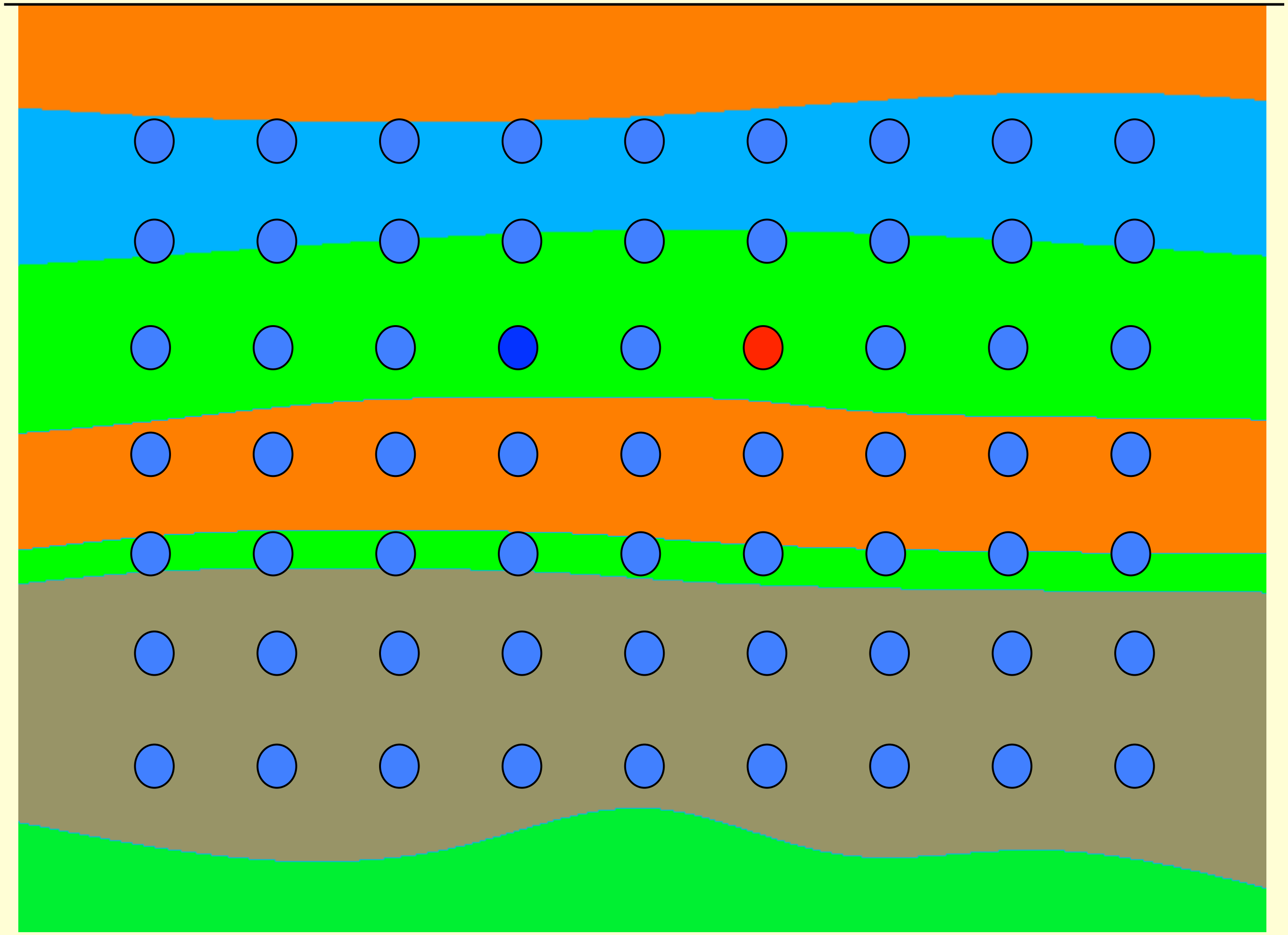

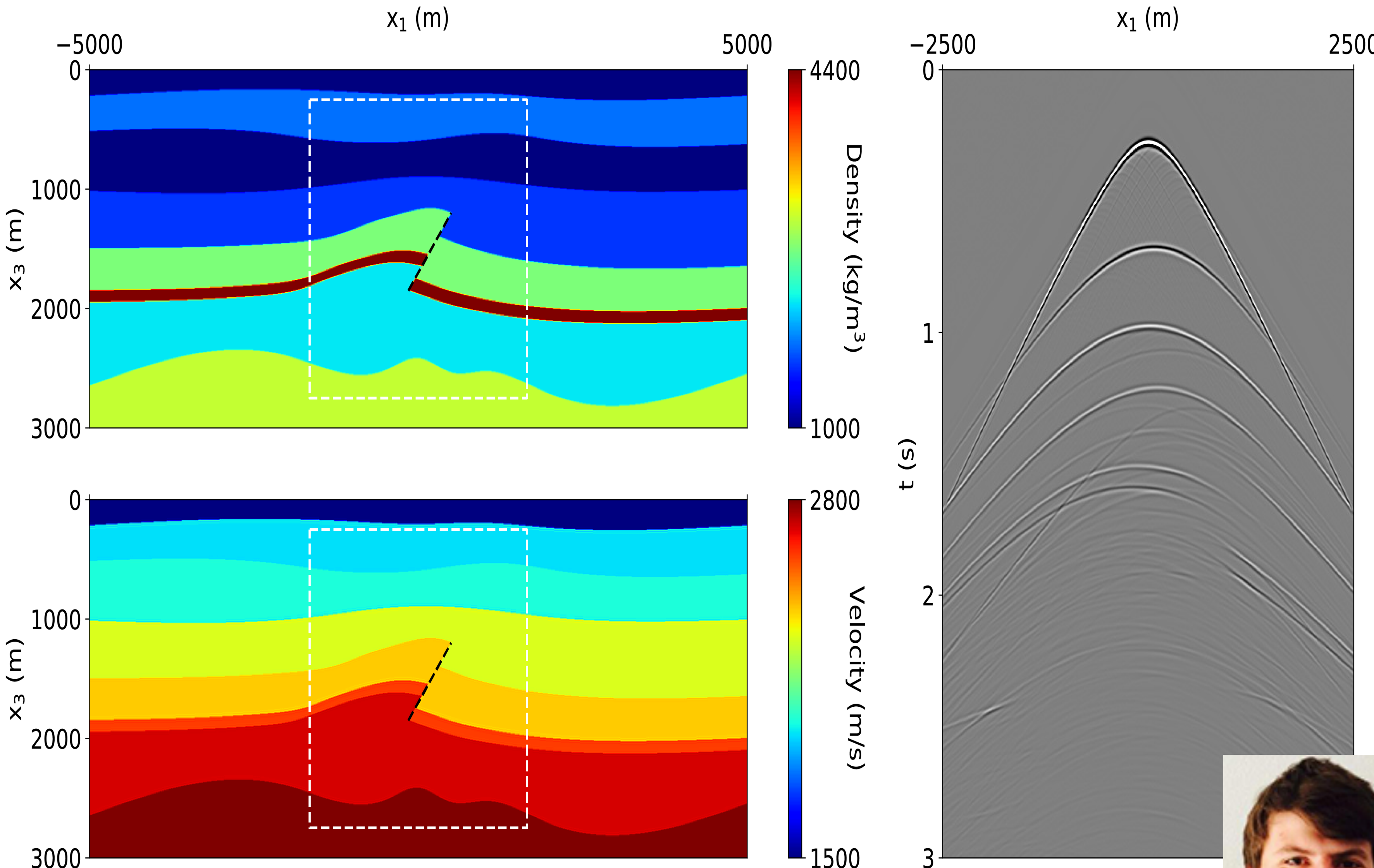
x$_1$ (m)
−5000
5000
0
1000
2000
3000
x$_3$ (m)
4400
1000
Density (kg/m^3)
2800
1500
Velocity (m/s)
−2500
2500
t (s)
0
1
2
3

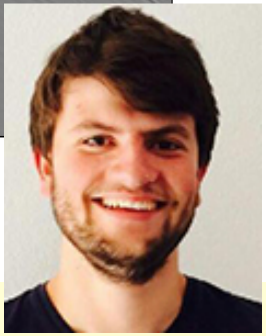

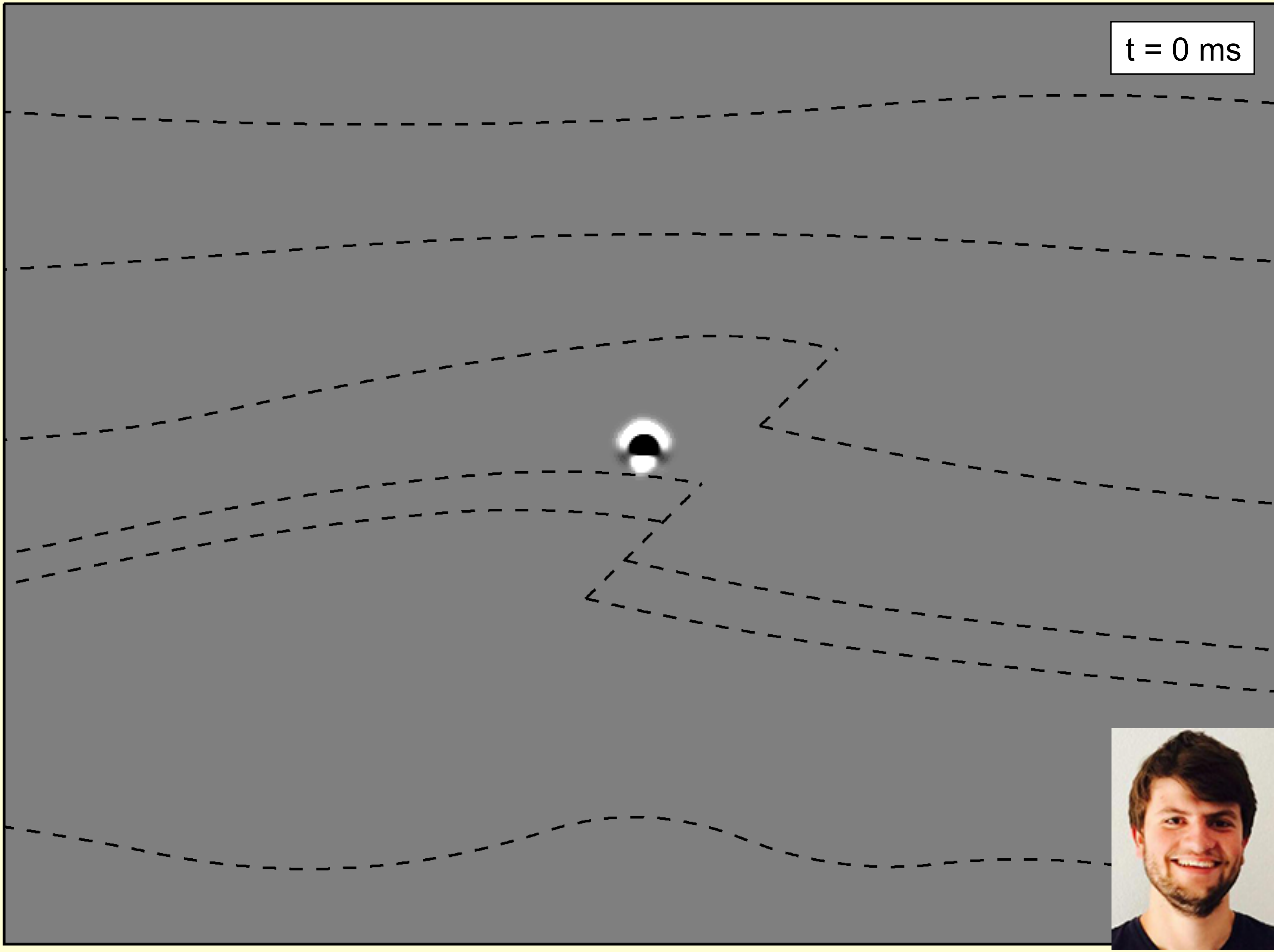
t = 0 ms

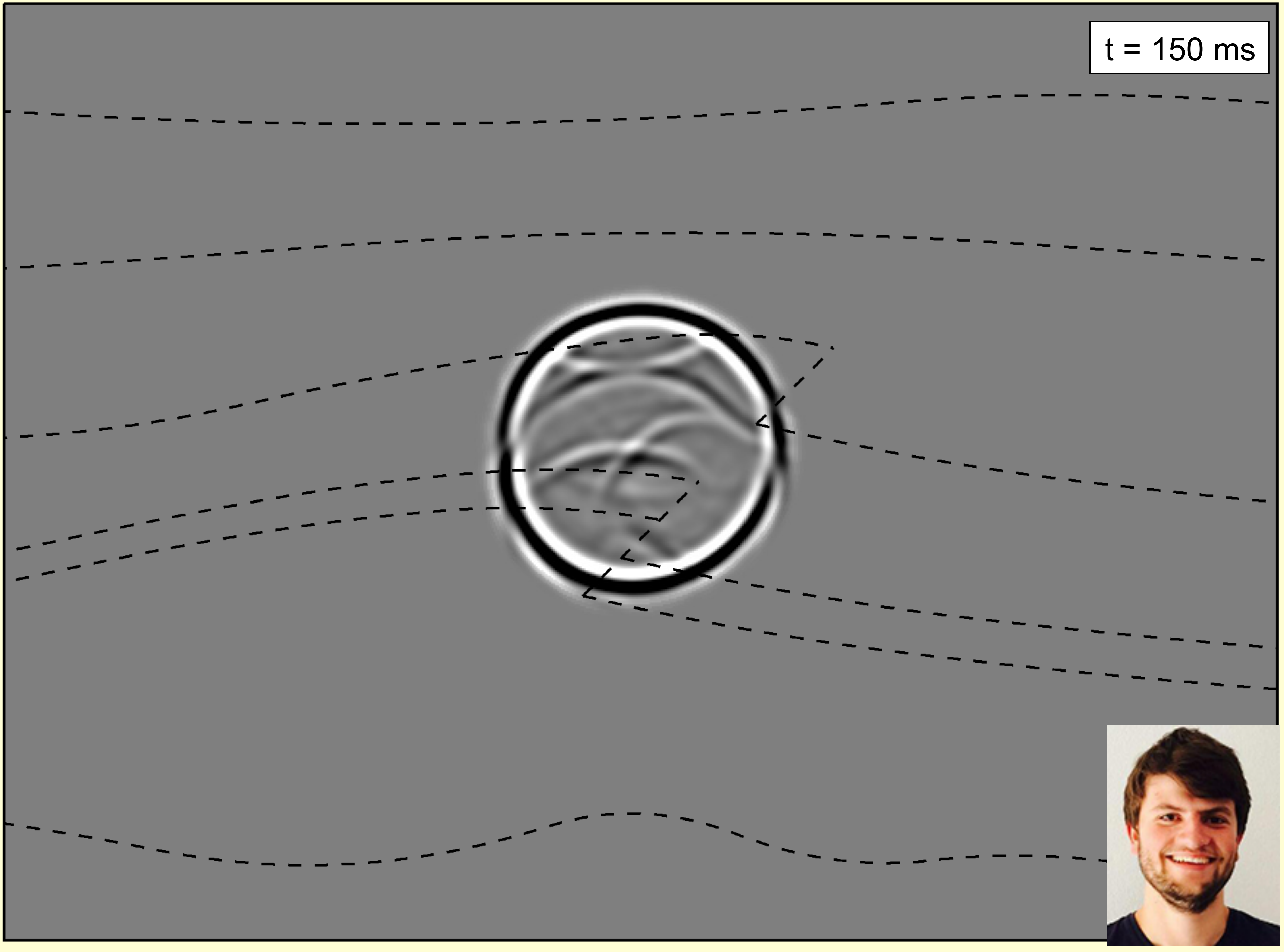
t = 150 ms

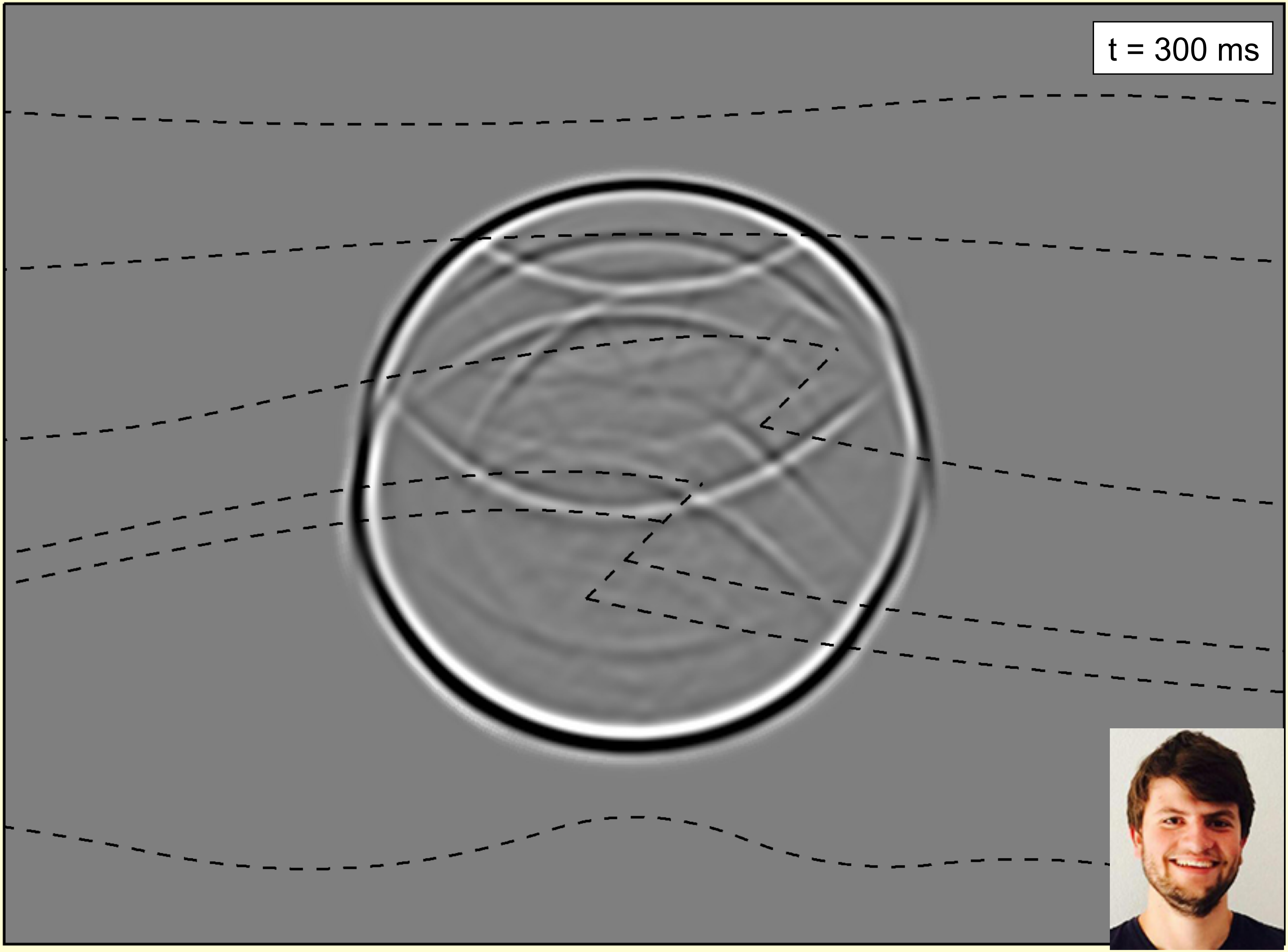
t = 300 ms

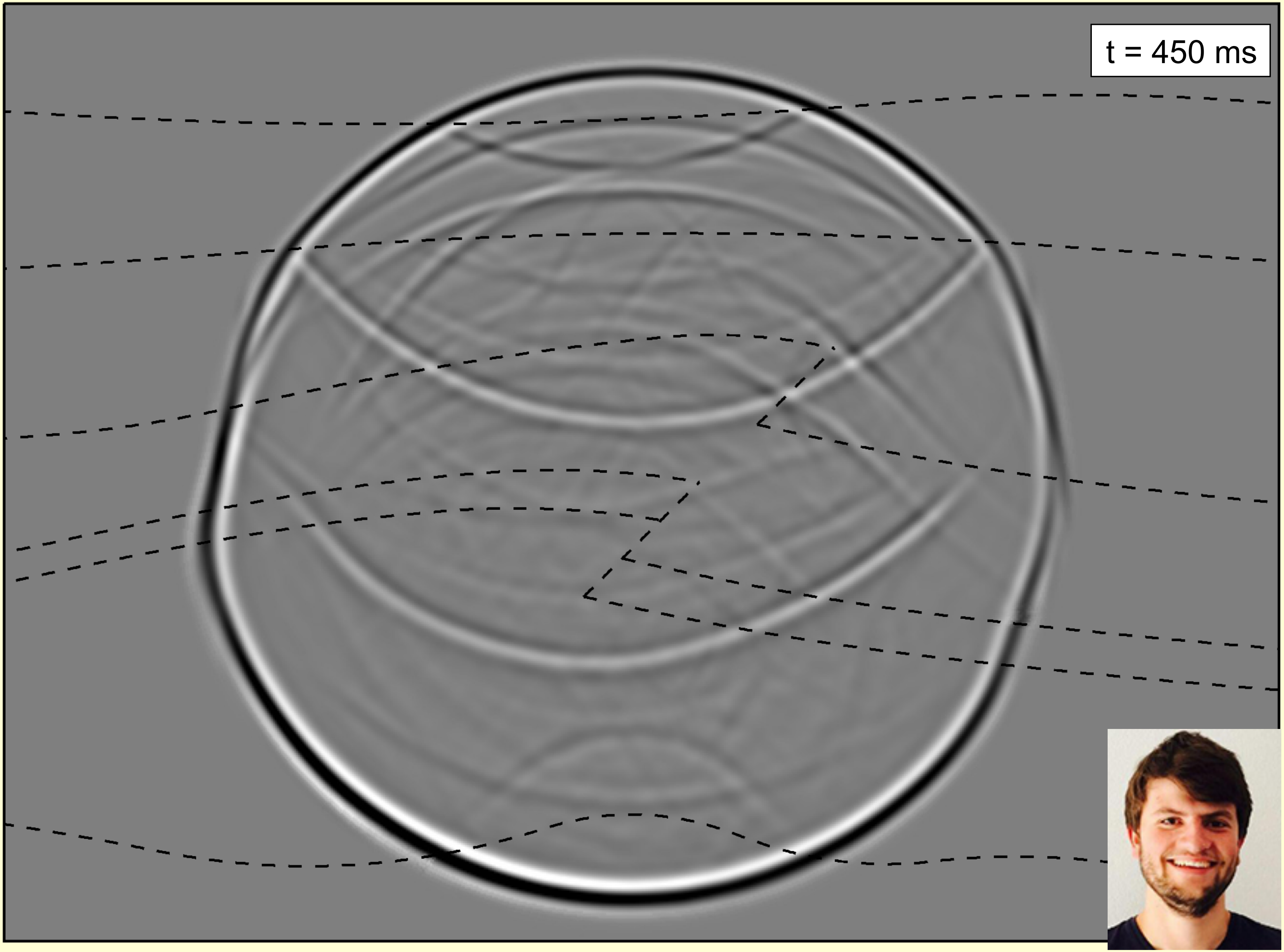
t = 450 ms

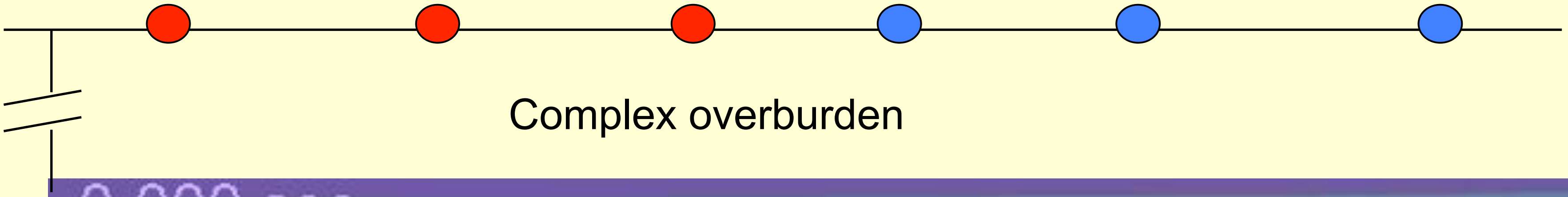

Complex overburden

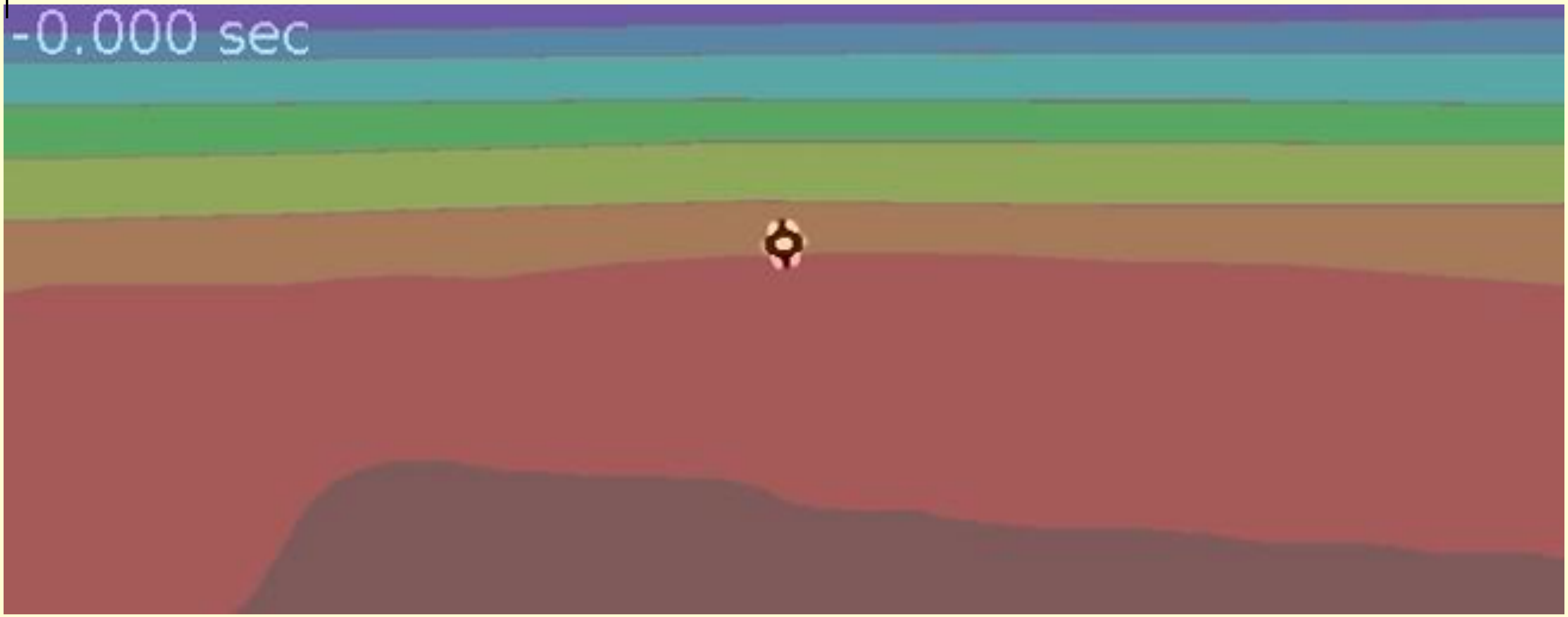

Virtual response obtained from seismic reflection data of the Vöring Basin

Joeri Brackenhoff

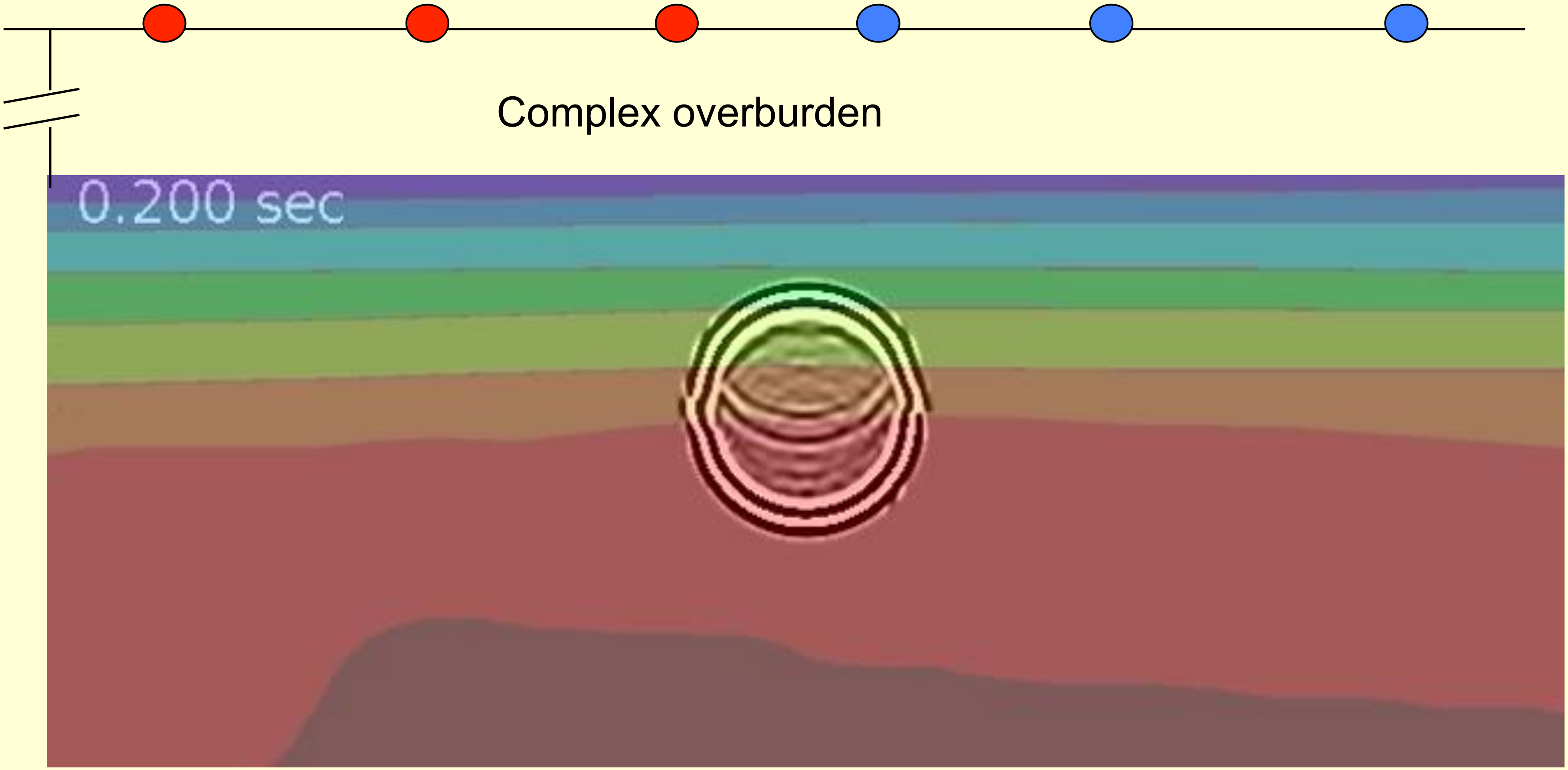

Virtual response obtained from seismic reflection data of the Vöring Basin

Joeri Brackenhoff

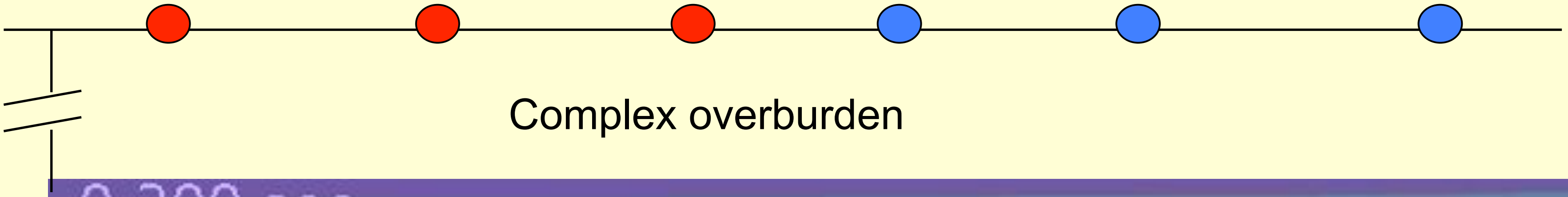

Complex overburden

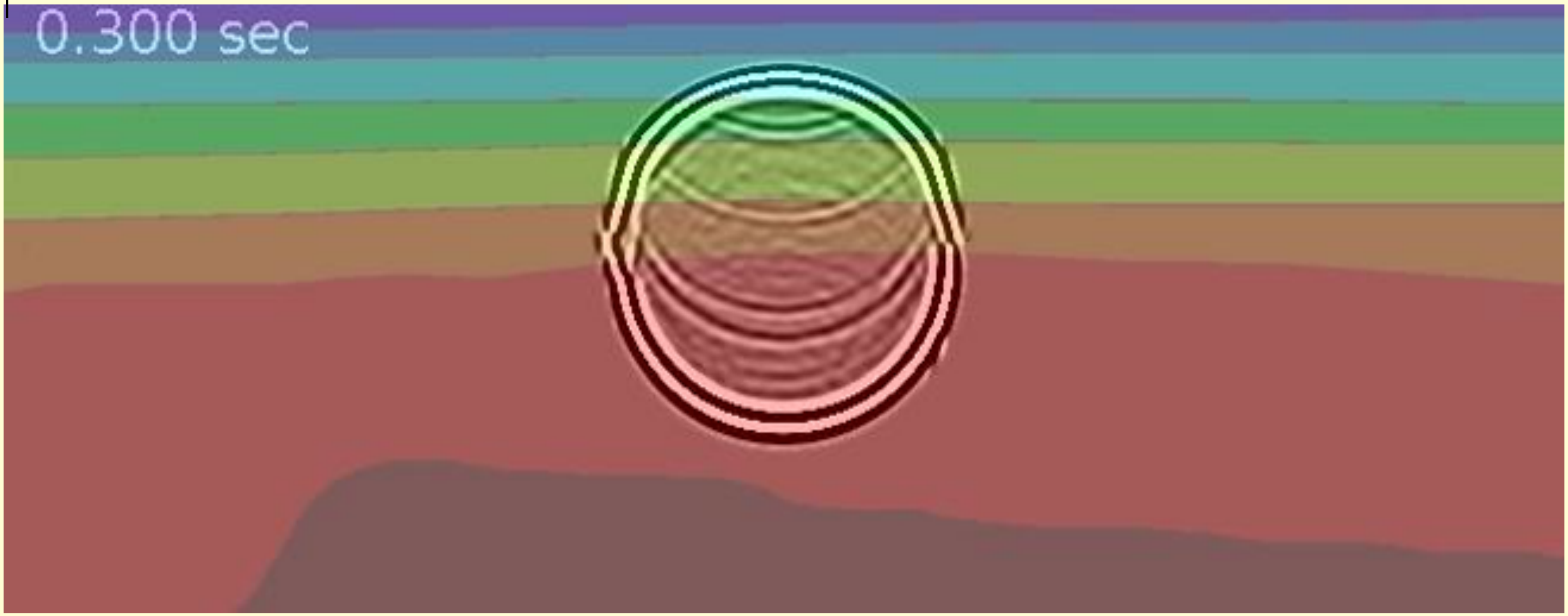

Virtual response obtained from seismic reflection data of the Vöring Basin

Joeri Brackenhoff

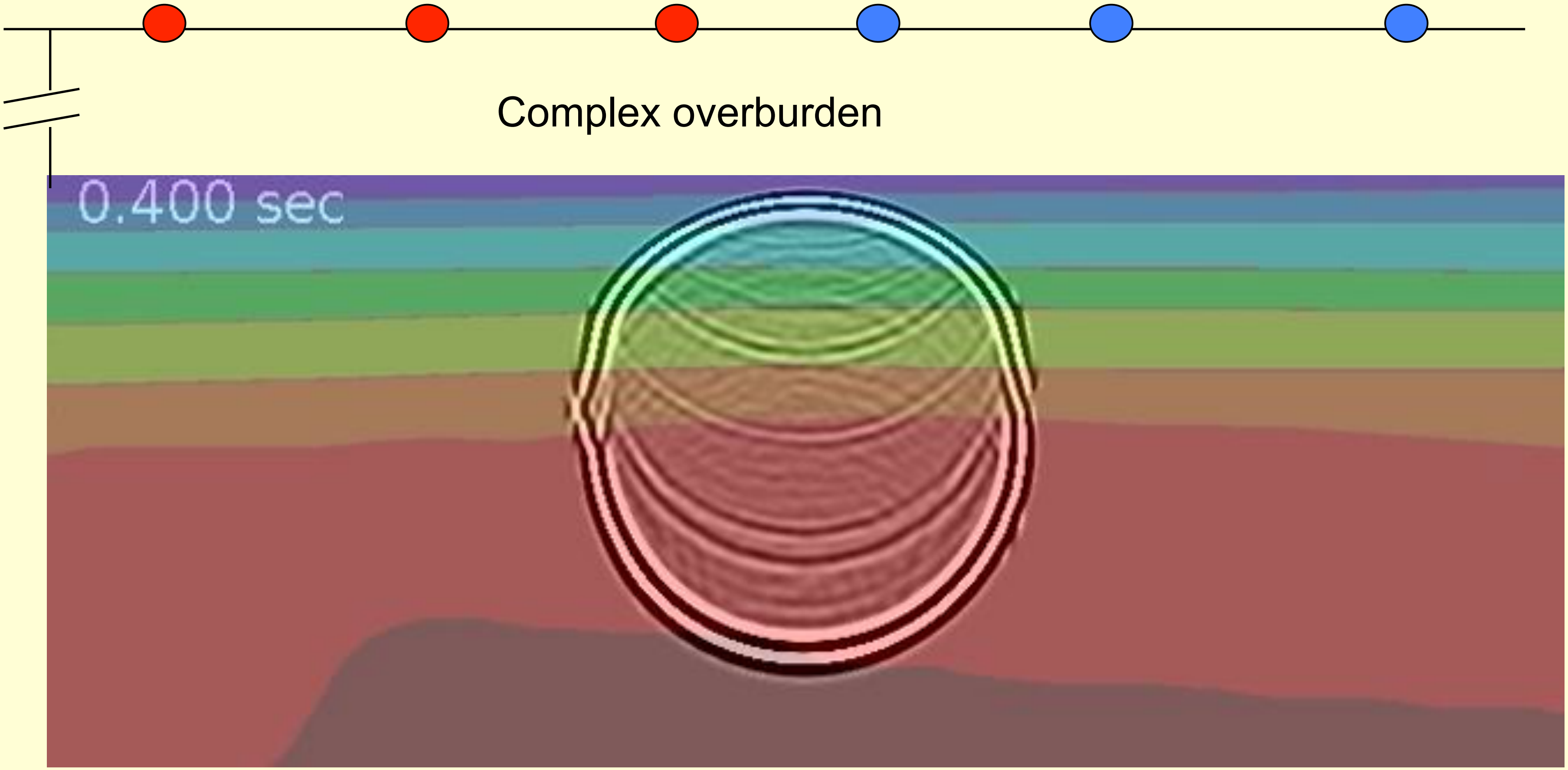

Virtual response obtained from seismic reflection data of the Vöring Basin

Joeri Brackenhoff

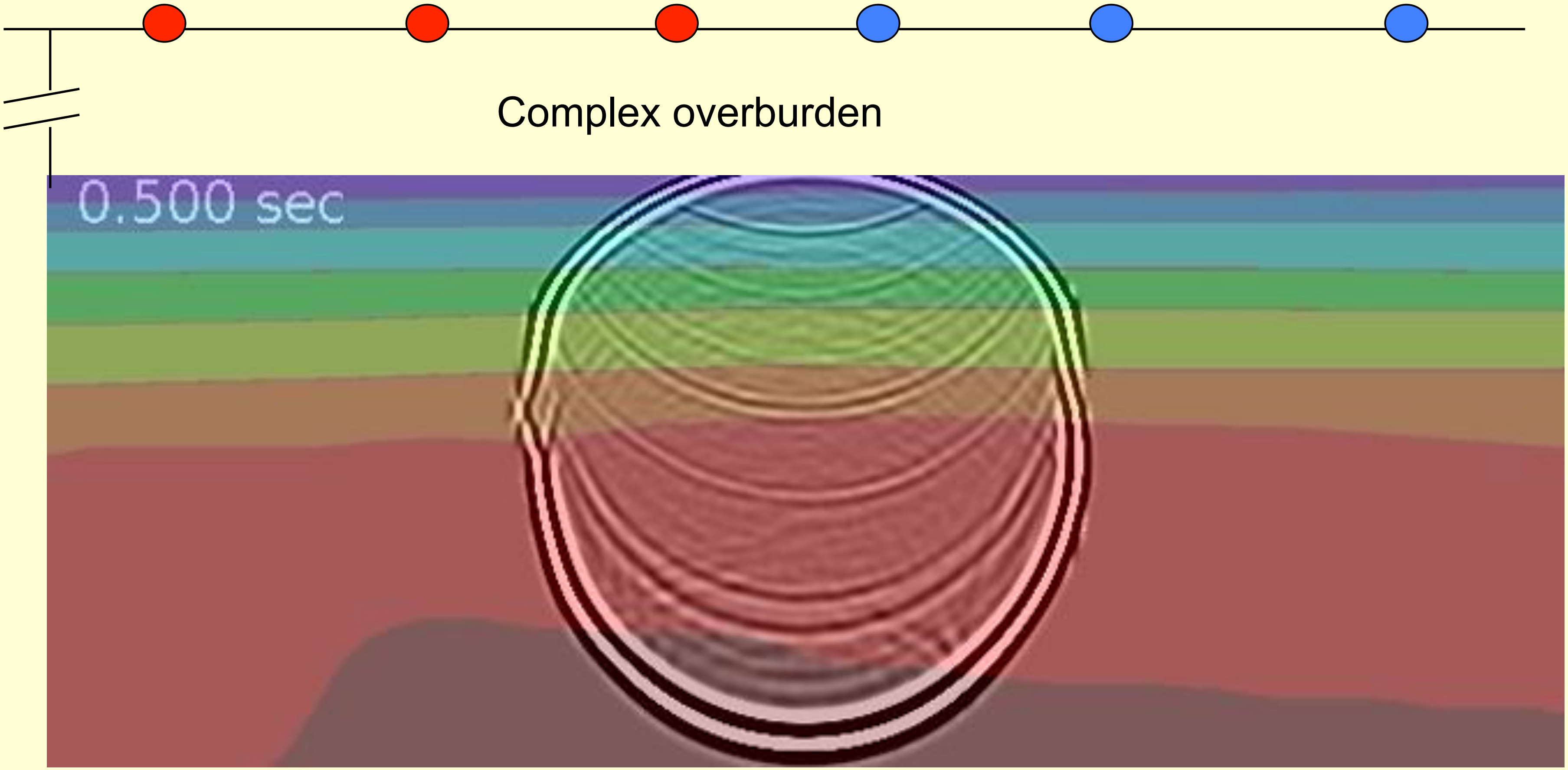

Virtual response obtained from seismic reflection data of the Vöring Basin

Joeri Brackenhoff

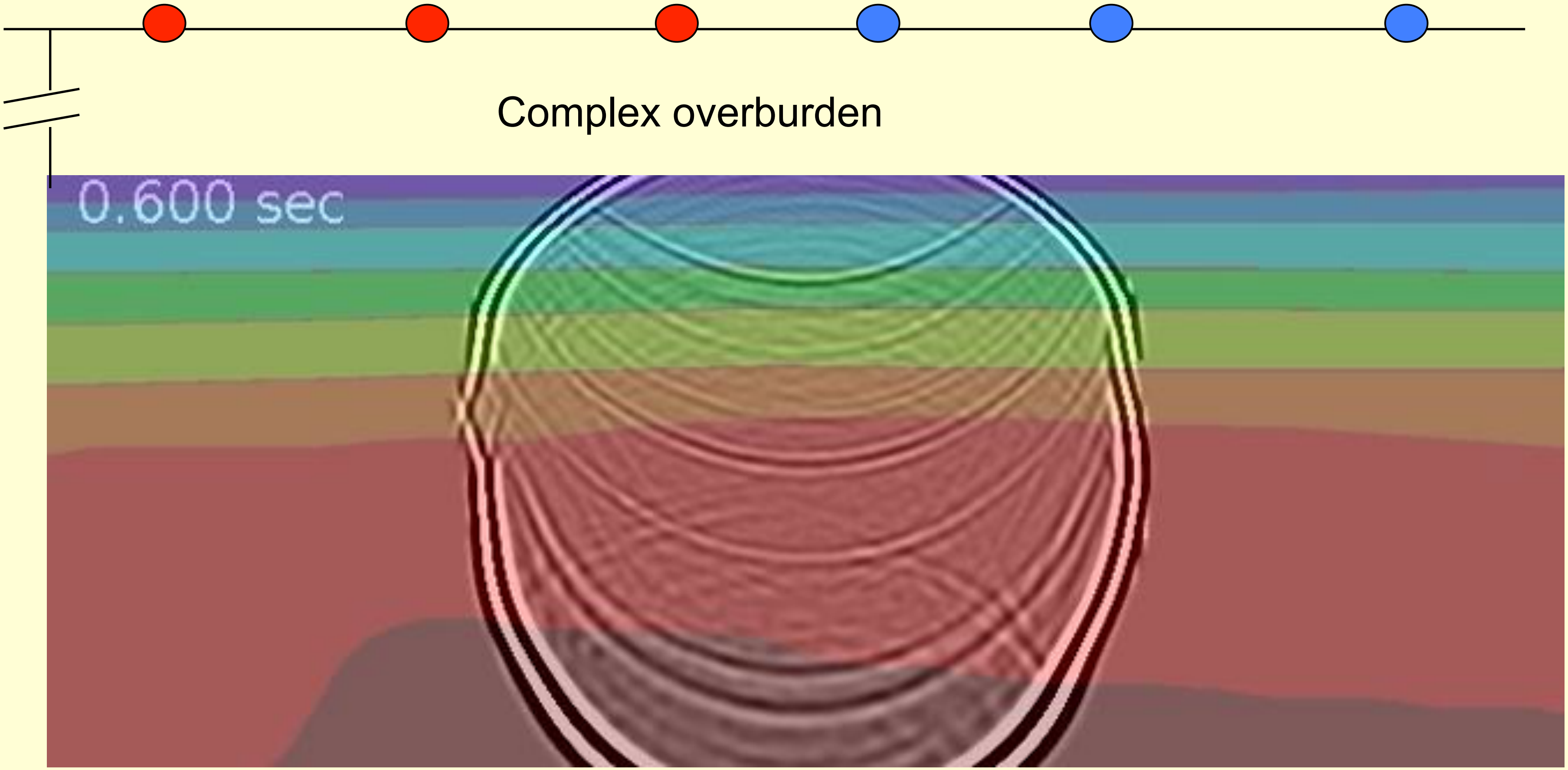

Virtual response obtained from seismic reflection data of the Vöring Basin

Joeri Brackenhoff

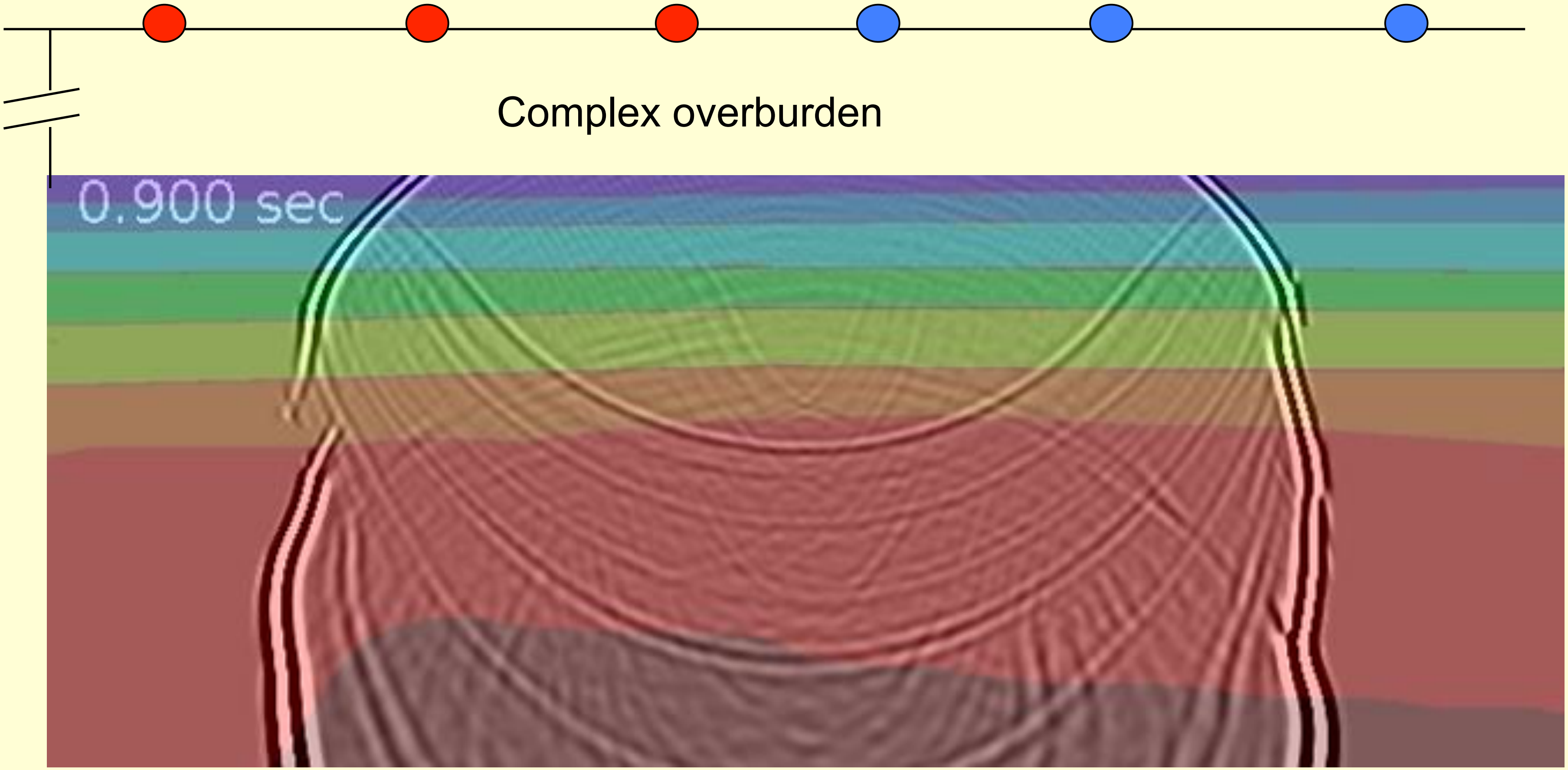

Virtual response obtained from seismic reflection data of the Vöring Basin

Joeri Brackenhoff

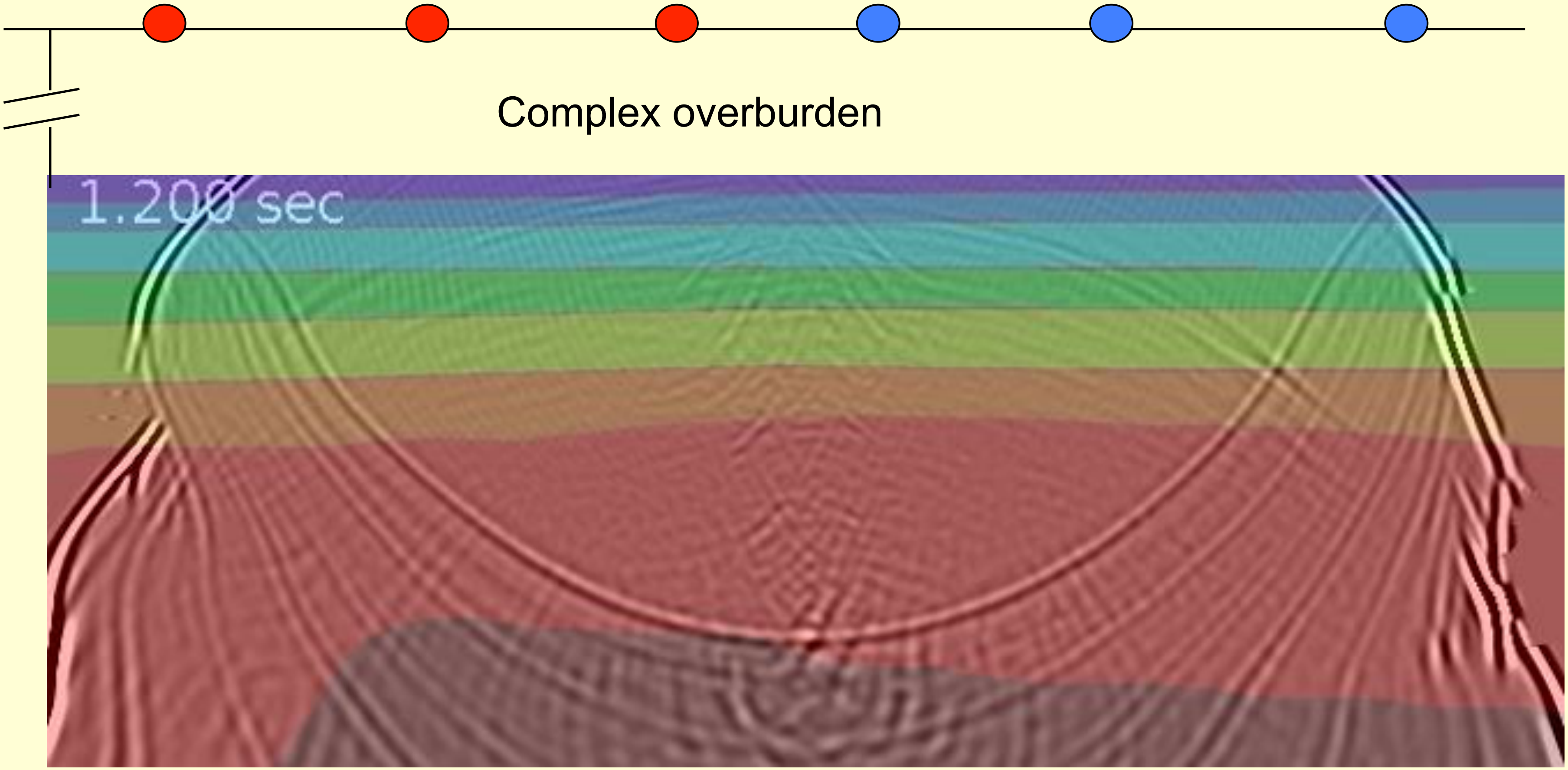

Virtual response obtained from seismic reflection data of the Vöring Basin

Joeri Brackenhoff

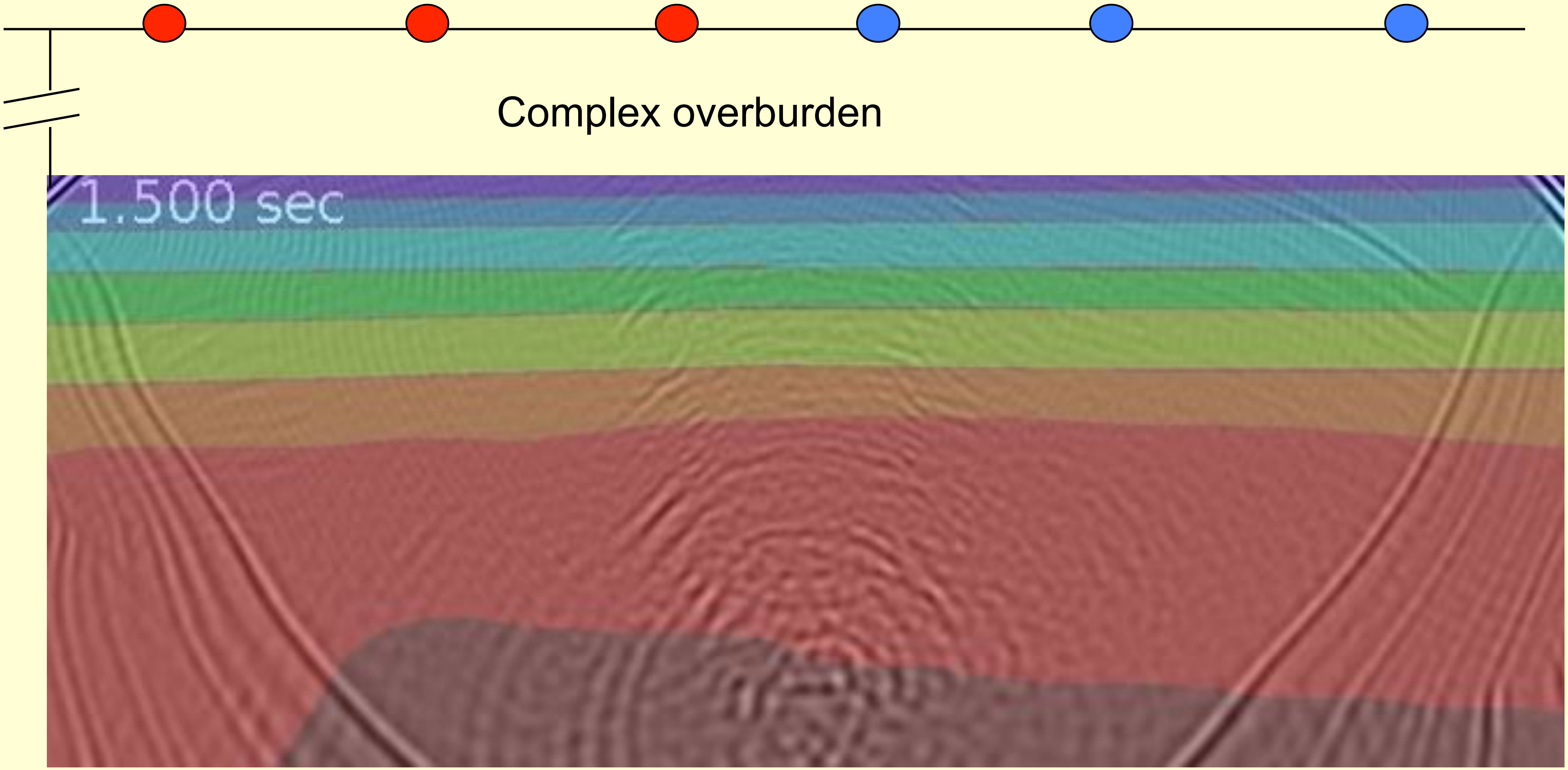

Virtual response obtained from seismic reflection data of the Vöring Basin

Joeri Brackenhoff

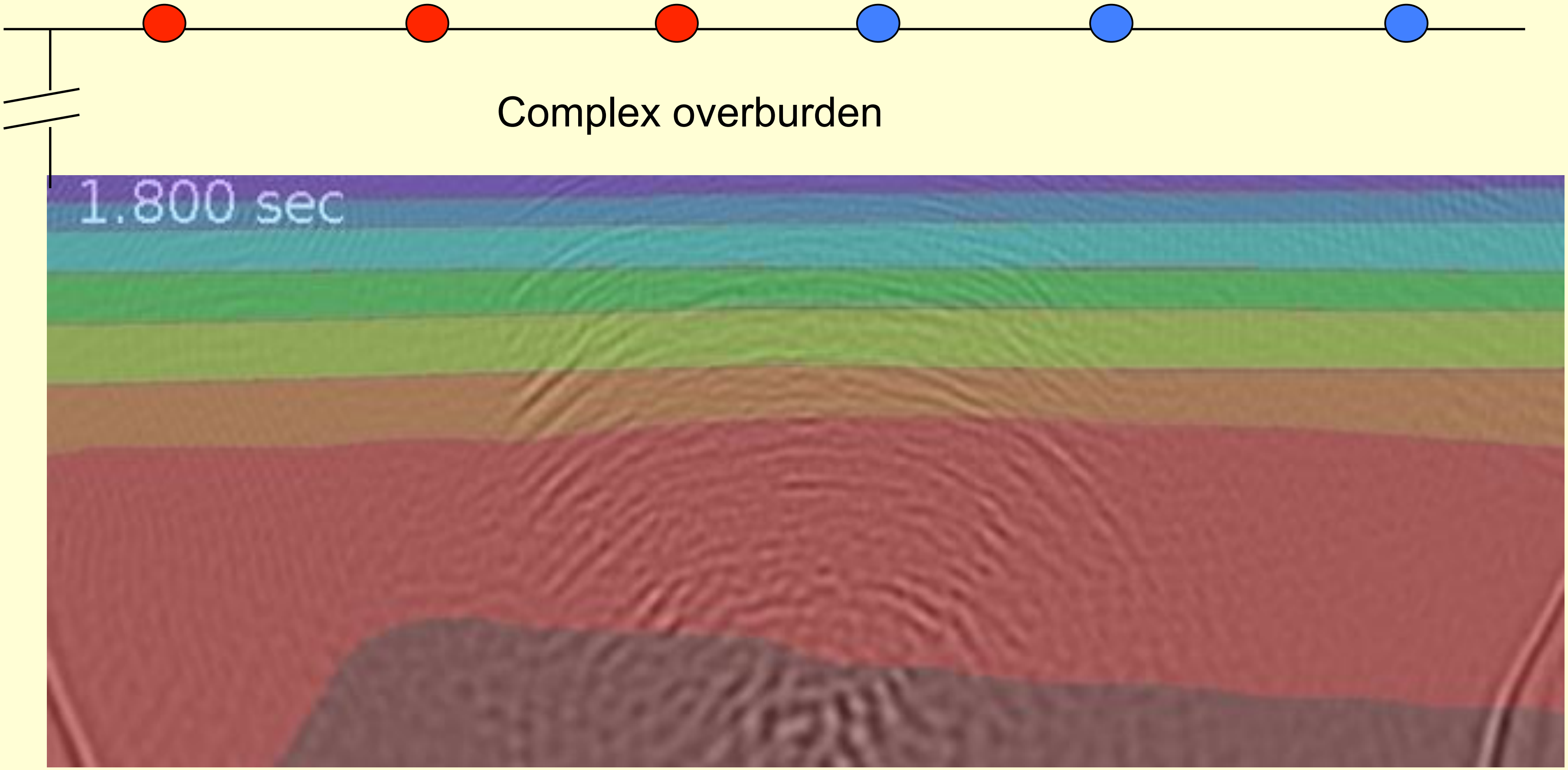

Virtual response obtained from seismic reflection data of the Vöring Basin

Joeri Brackenhoff

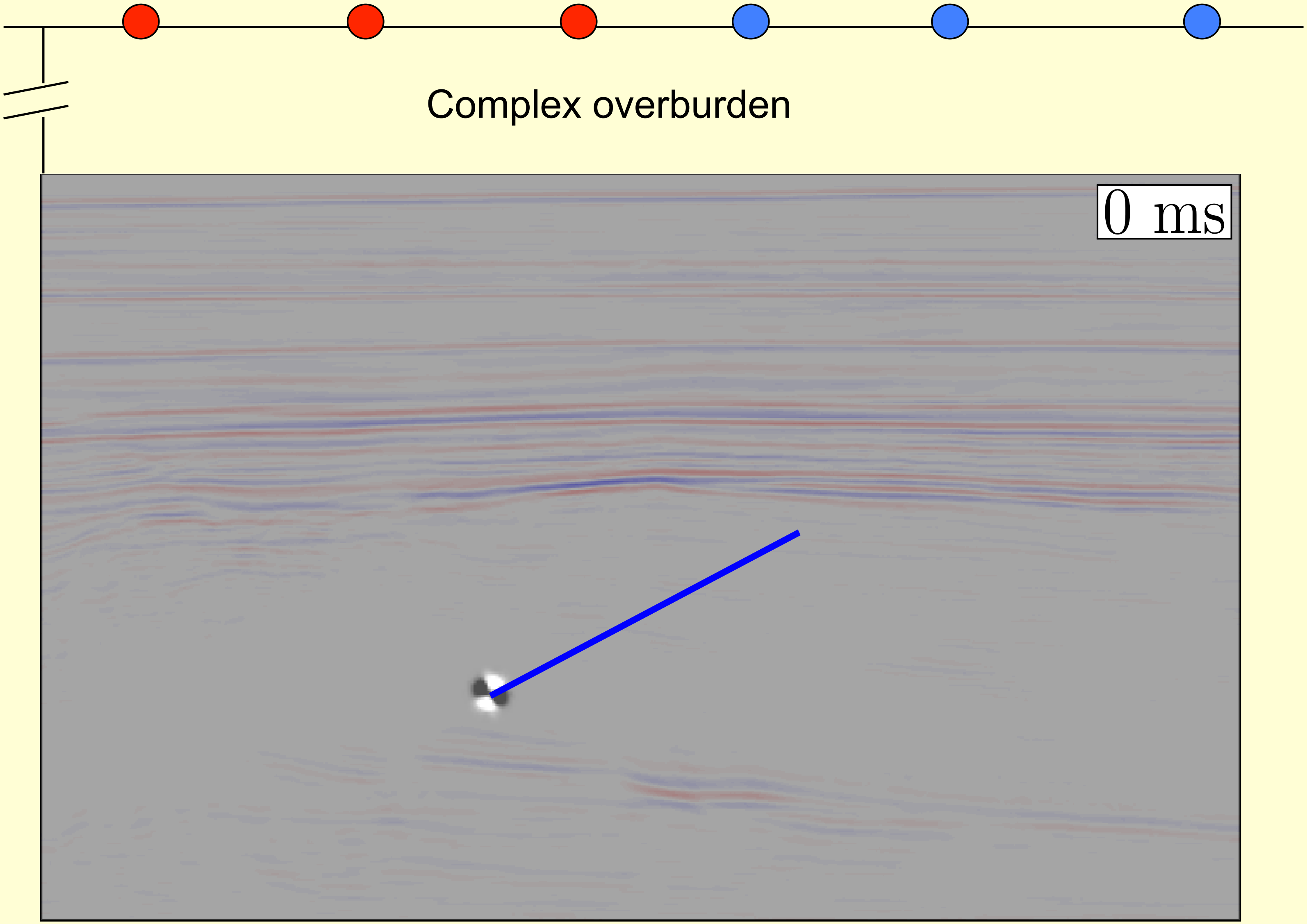

Virtual rupture (double couple source)

Joeri Brackenhoff

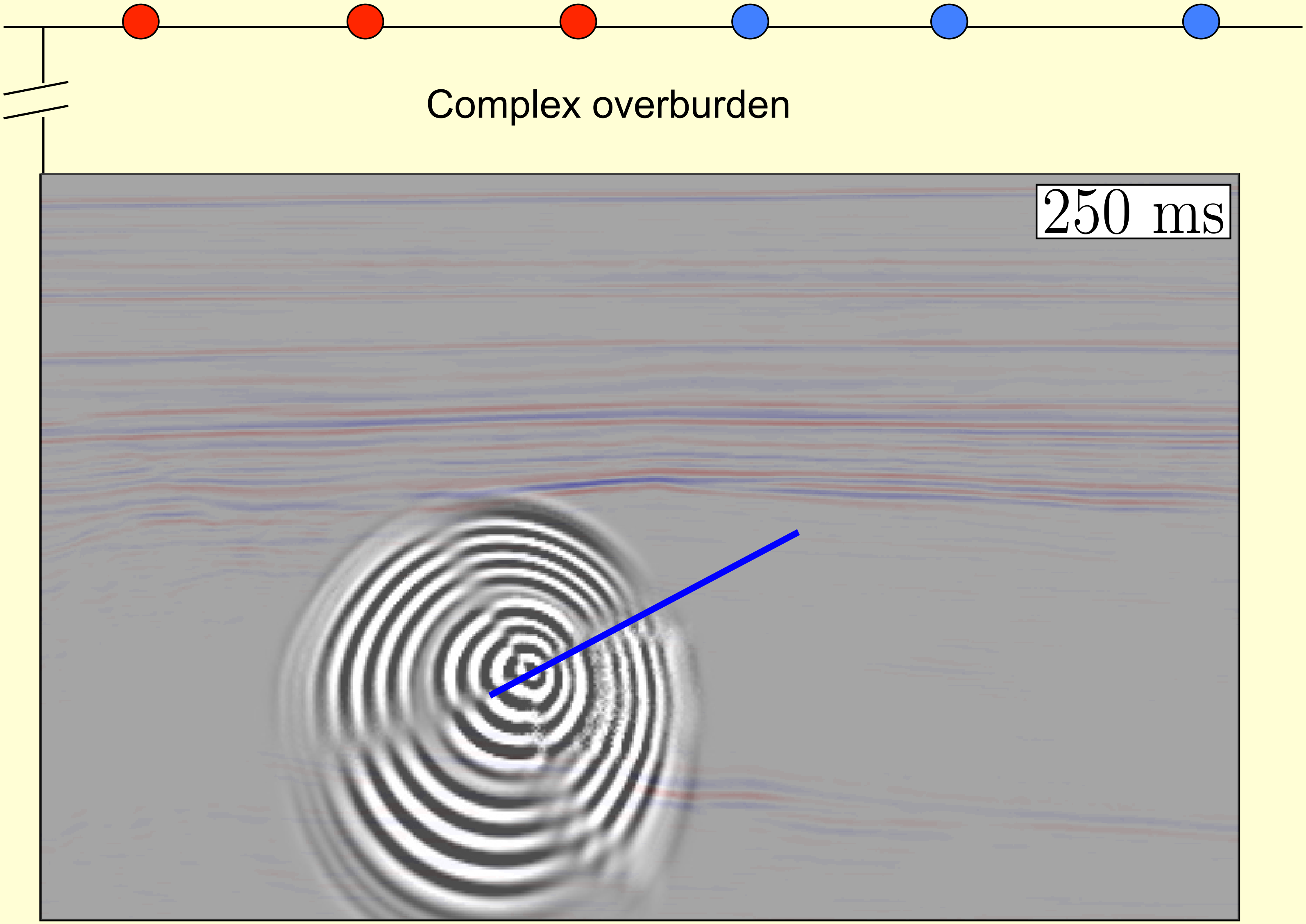

Virtual rupture (double couple source)

Joeri Brackenhoff

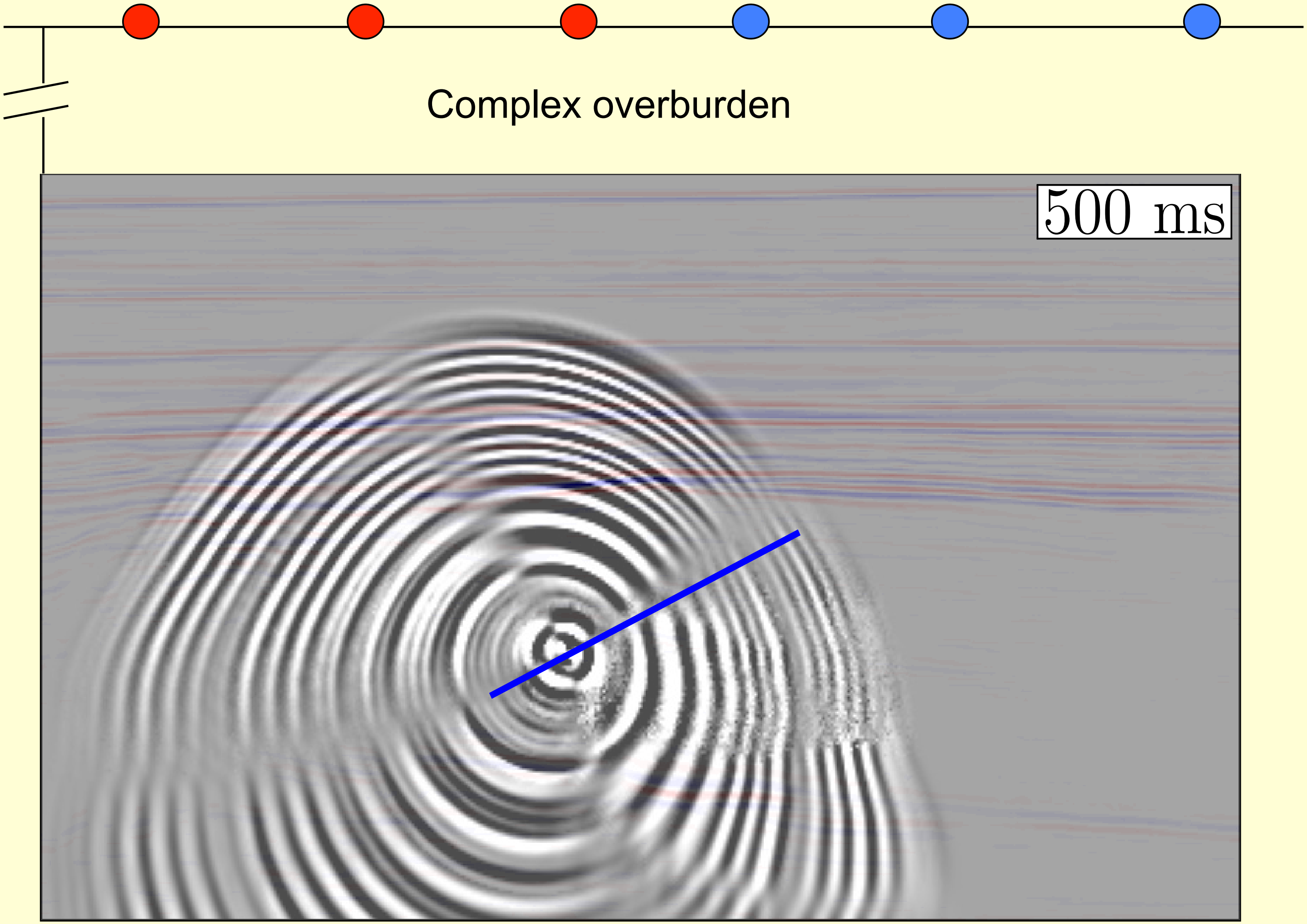

Virtual rupture (double couple source)

Joeri Brackenhoff

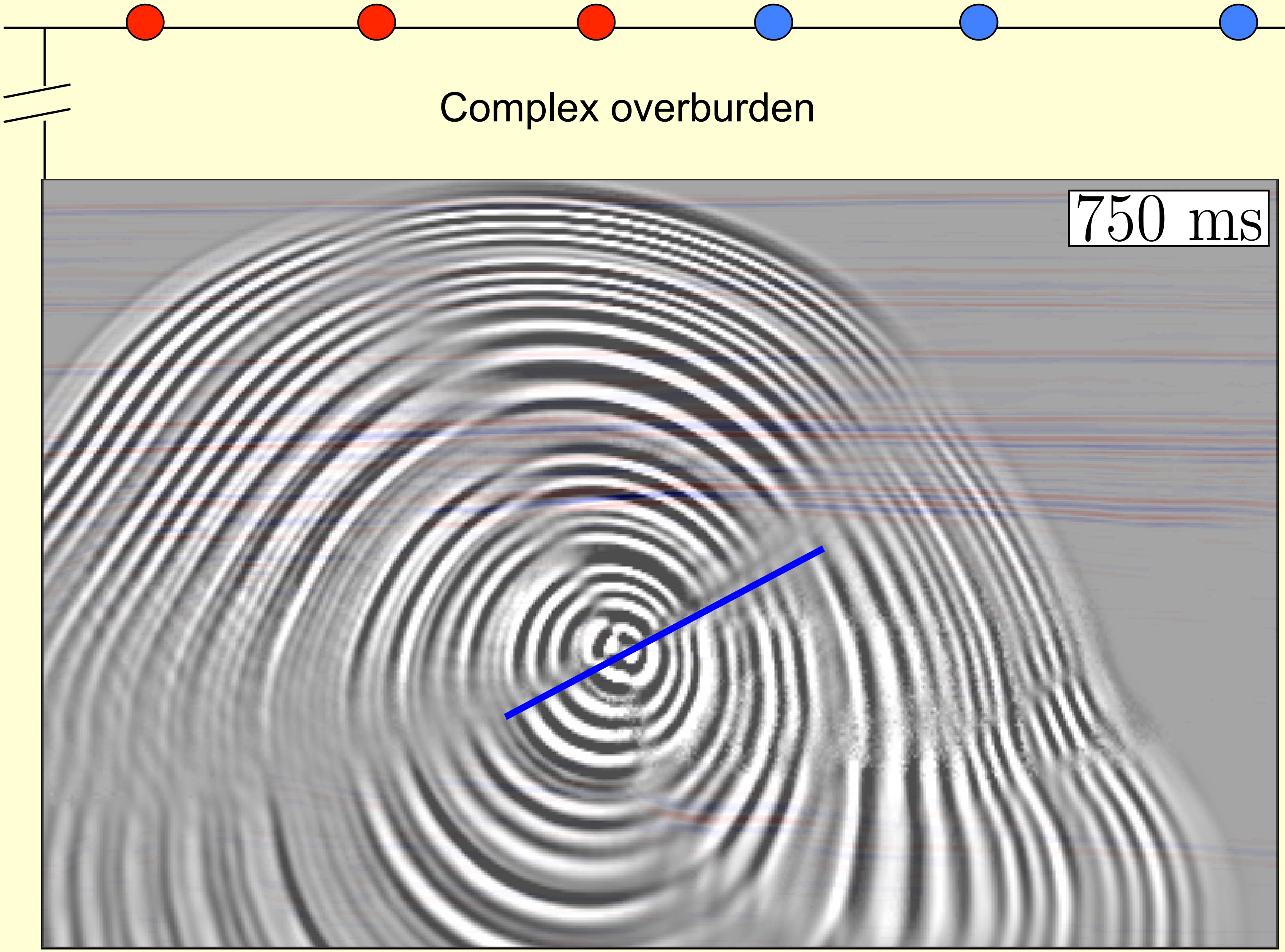

Virtual rupture (double couple source)

Joeri Brackenhoff

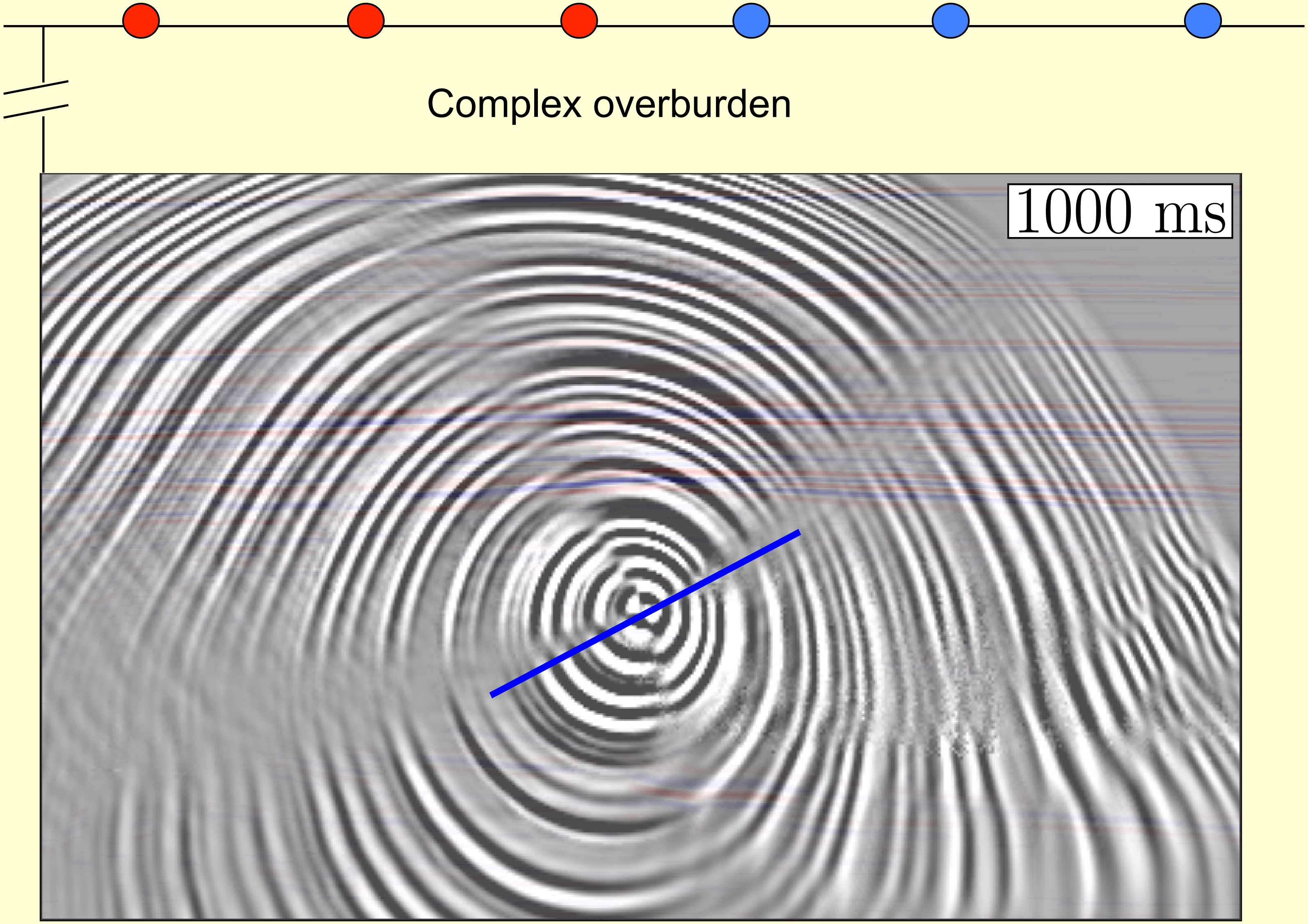

Virtual rupture (double couple source)

Joeri Brackenhoff

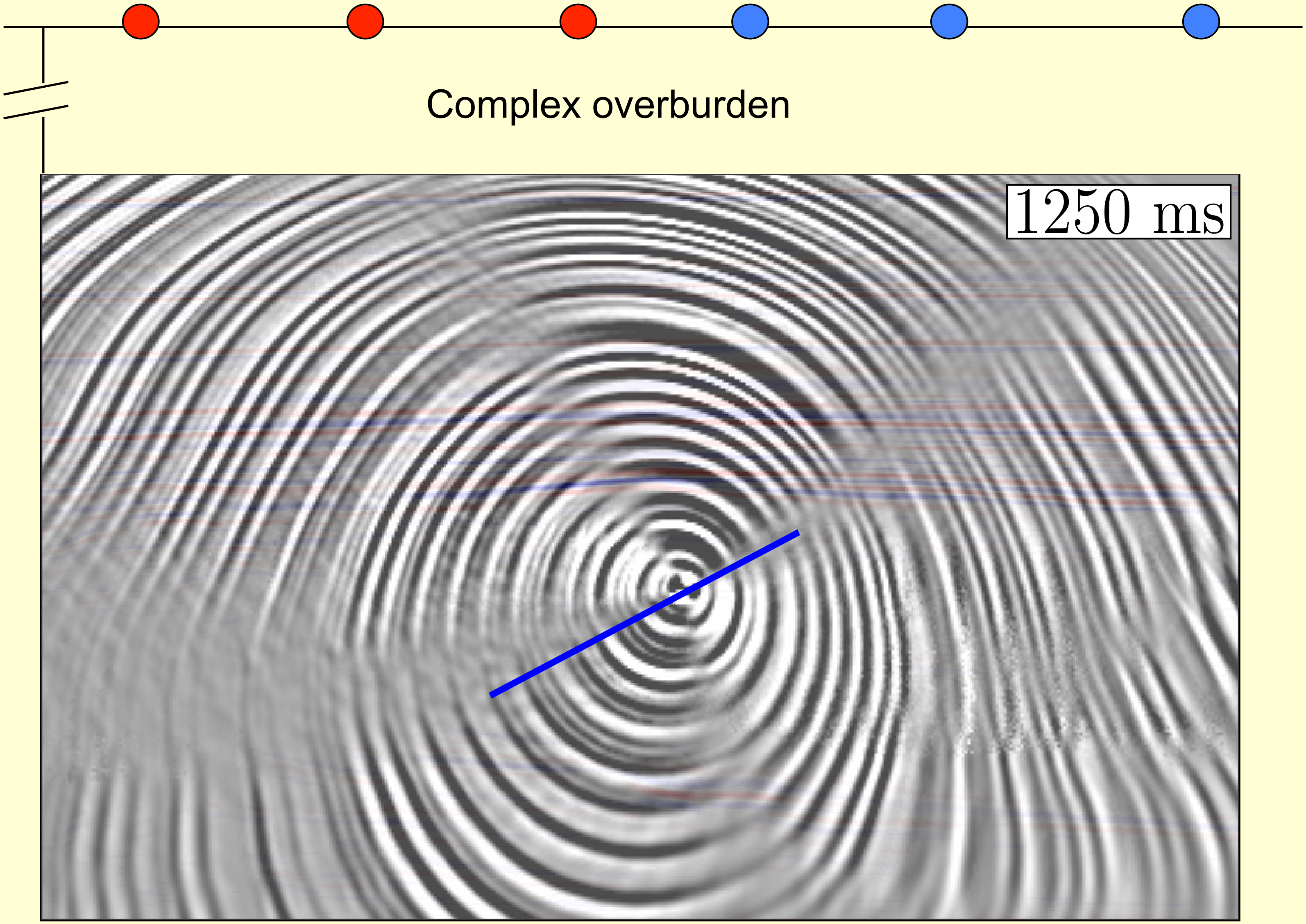

Virtual rupture (double couple source)

Joeri Brackenhoff

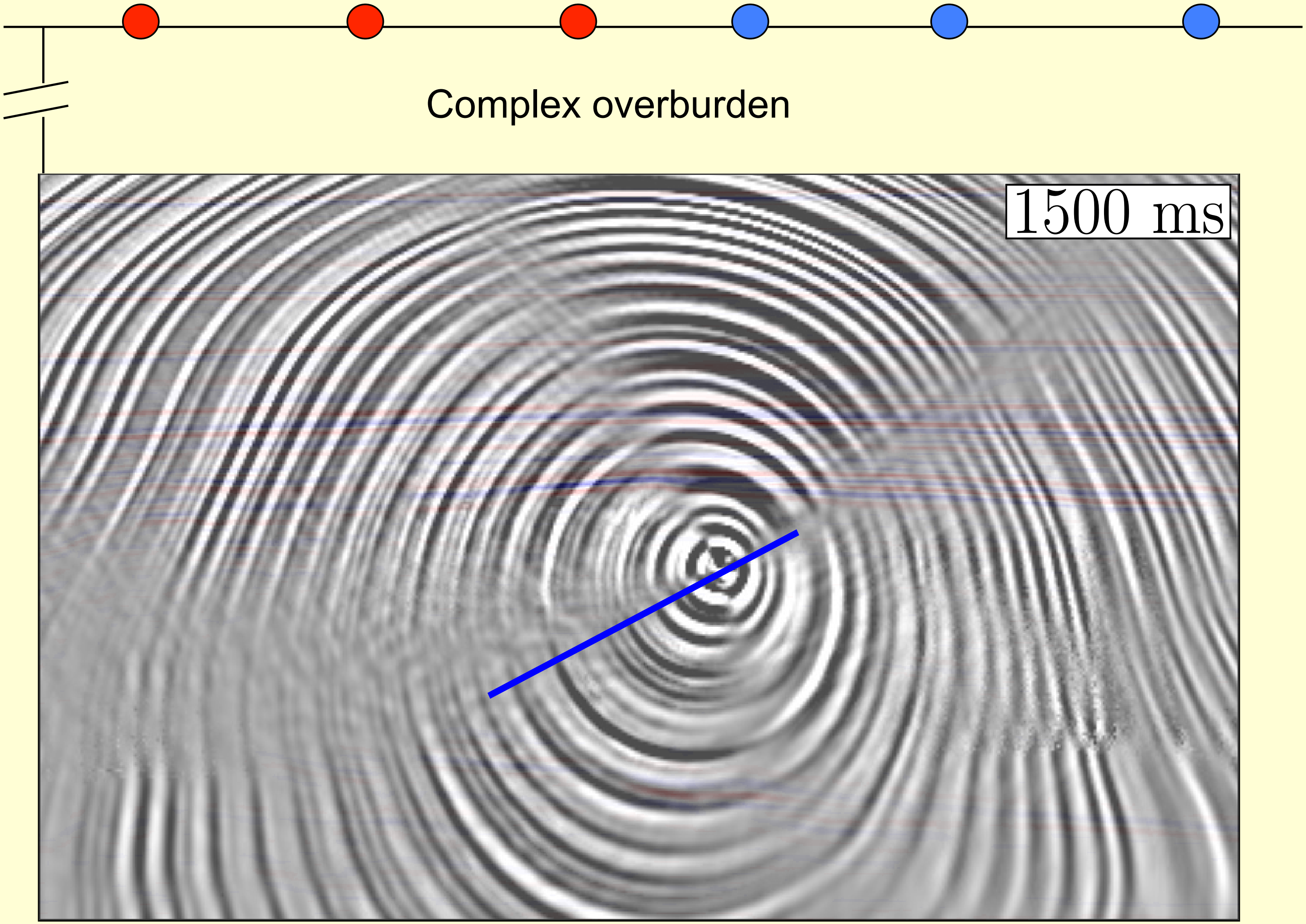

Virtual rupture (double couple source)

Joeri Brackenhoff

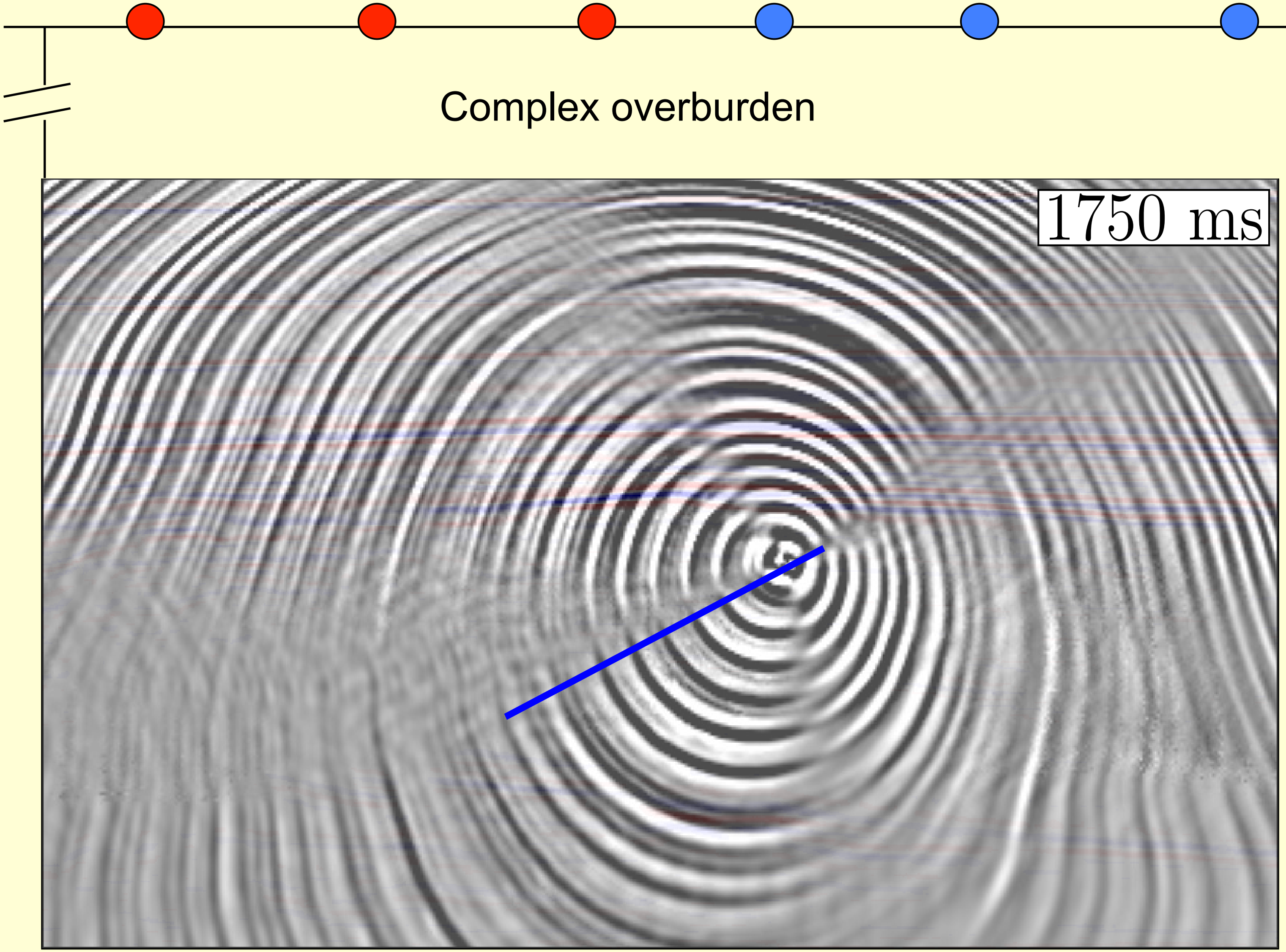

Virtual rupture (double couple source)

Joeri Brackenhoff

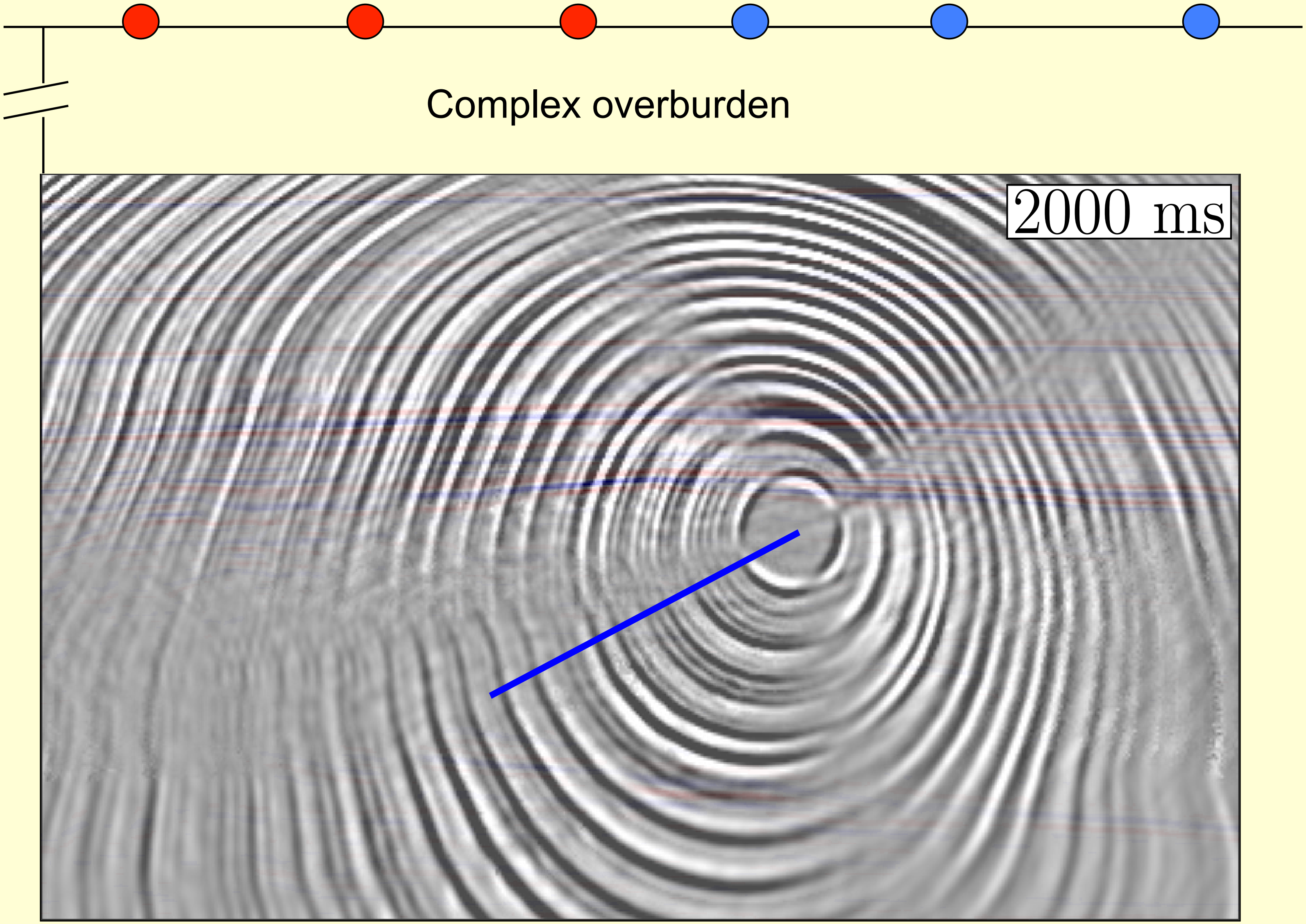

Virtual rupture (double couple source)

Joeri Brackenhoff

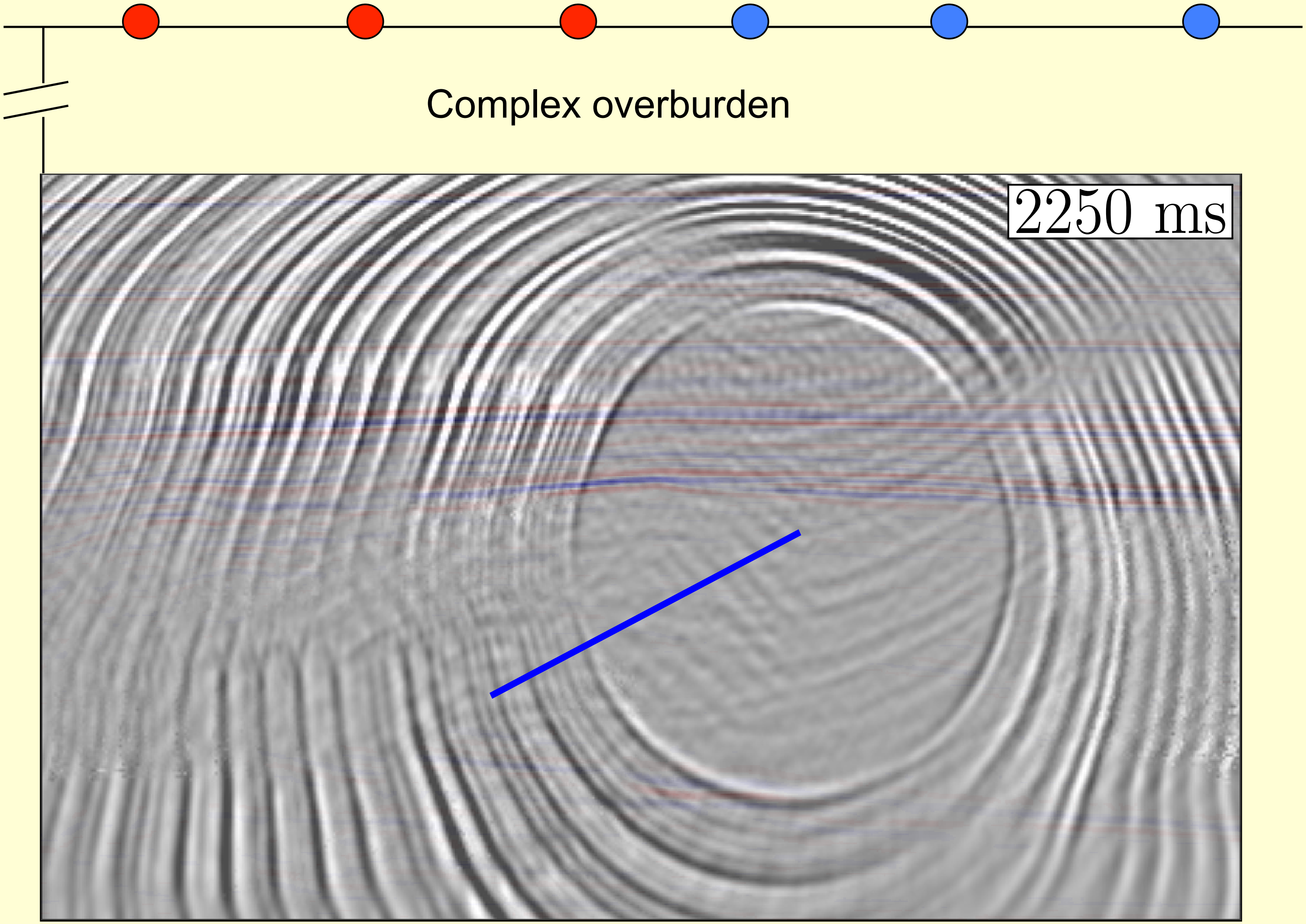

Virtual rupture (double couple source)

Joeri Brackenhoff

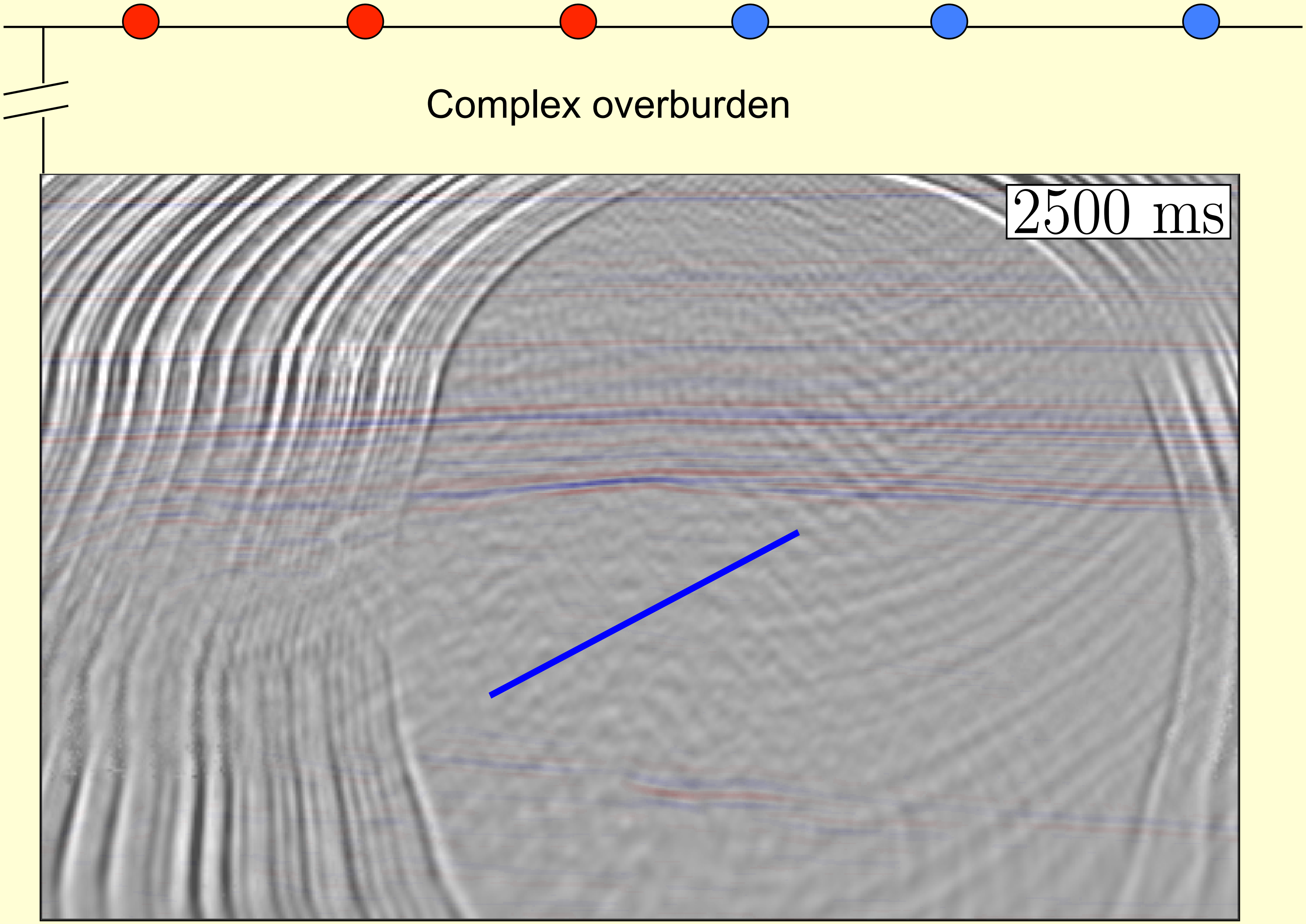

Virtual rupture (double couple source)

Joeri Brackenhoff

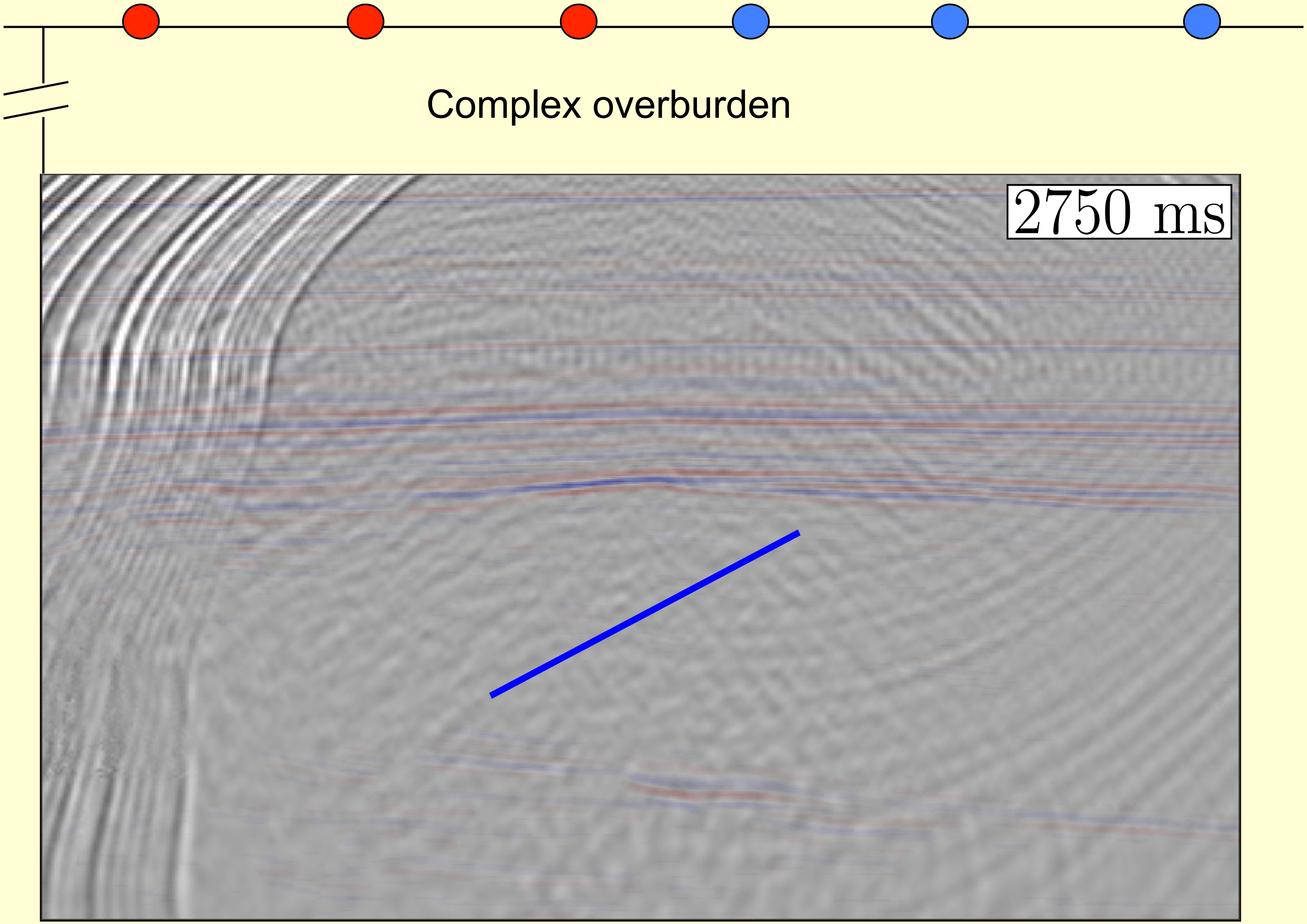

Virtual rupture (double couple source)

Joeri Brackenhoff

Take-home message:

- Classical Green's function representation: closed boundary integral

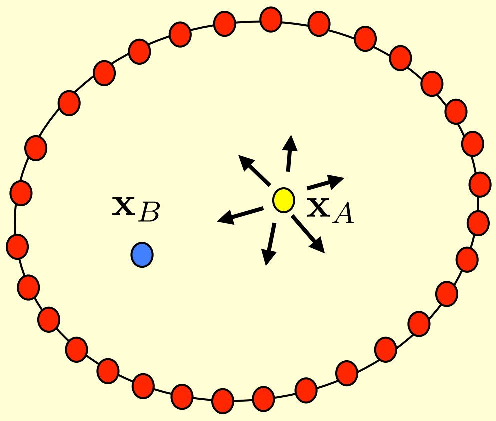

- Modified Green's function representation: single-sided integral

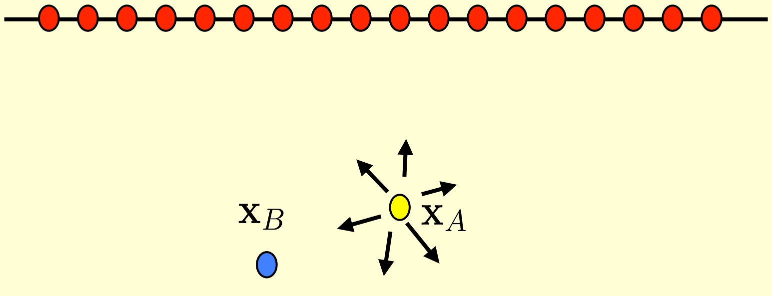

Take-home message:

- Classical Green's function representation: closed boundary integral

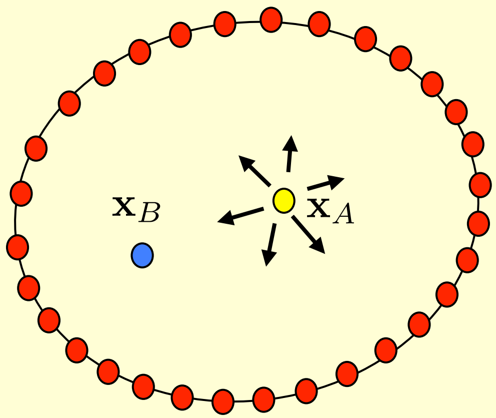

- Modified Green's function representation: single-sided integral

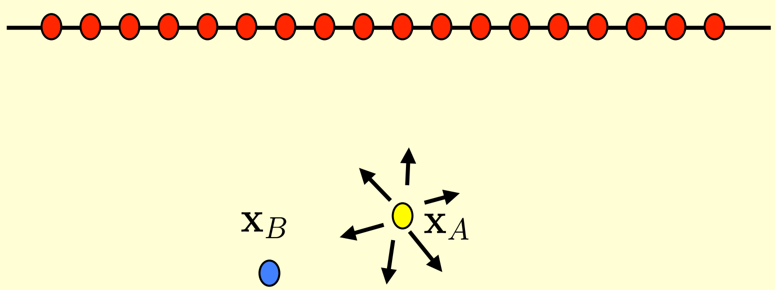

- Contains focusing functions
- Handles multiple reflections
- Modified reflection imaging
- Monitoring induced seismicity
- Etc.

Open question:

How do we deal optimally with different multiple-scattering mechanisms?

- Short-period diffusion-like multiple scattering

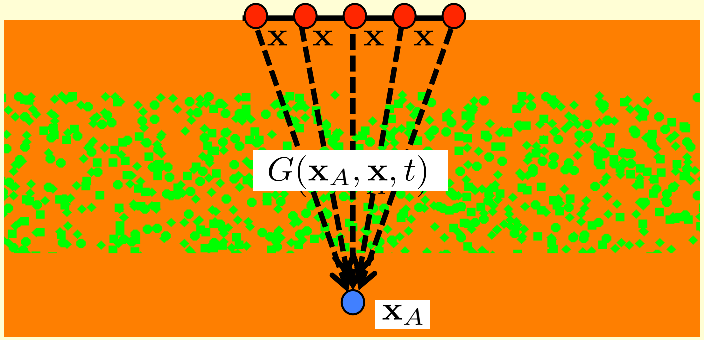

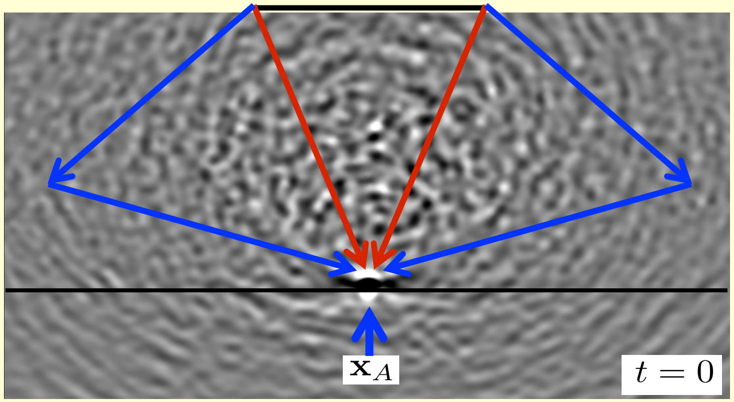

- Long-period deterministic multiple scattering

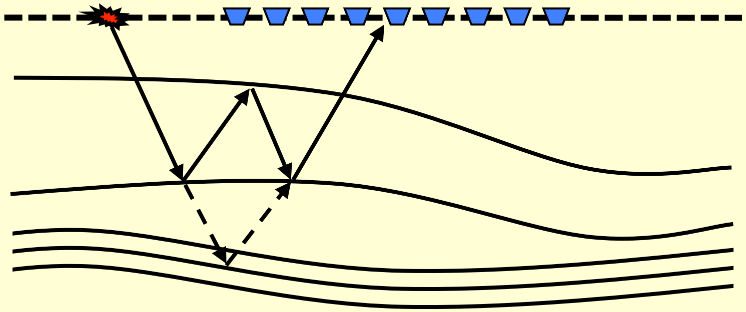

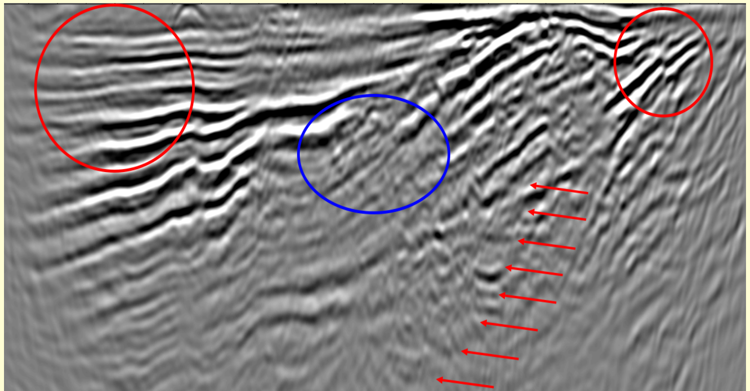

Thanks to CGG and Equinor for giving permission to use the data from the Santos Basin and the Vöring Basin, and to Shell for the cooperation on the passive data in the Lybian desert.

This research has received funding from the European Research Council (ERC) under the European Union's Horizon 2020 research and innovation programme (grant No: 742703) and from the Dutch Science Foundation

European Research Council
Established by the European Commission